

E.Stolwijk

The sheet pile behaviour for hole weakening in sheet piles



Cover photo: Van Leeuwen (n.d.) [1]
Cover photo: ArcelorMittal (2022) [2]

The sheet pile behaviour for hole weakening in sheet piles

By

Elisa Stolwijk

in partial fulfilment of the requirements for the degree of

Master of Science
in Civil Engineering

at the Delft University of Technology,
to be defended publicly on Thursday June 23, 2022 at 15.00 pm

Thesis committee:

Prof. dr. M. Veljkovic,
Dr. F. Kavoura,
Prof. dr. K.G. Gavin
Ir. R.E. van Leeuwen

TU Delft
TU Delft
TU Delft
Ballast-Nedam
Funderingstechnieken
Van Leeuwen Verankeringen
& Funderingssystemen
b.v. Ingenieursbureau
M.U.C.

Ing. M. Meeuwsen MSEng RC

This thesis is confidential and cannot be made public until June 23, 2022.

An electronic version of this thesis is available at <http://repository.tudelft.nl/>.

Preface

This thesis captures a study researching the effect of hole weakening on sheet pile behaviour and resistance by developing a model for this purpose. This thesis is written in contribution to the education Structural engineering, as part of the master Civil Engineering at the Delft University of Technology. This thesis is of interest for employees working within the foundation solutions.

The combination of soil and steel captured with finite element modelling have raised my interest for this research. Not only studying this topic, but also working with experts in the field of foundations and scientific research has been a grateful experience.

I would like to thank my committee for supporting me during this thesis. Florentia Kavoura for her weekly guidance, especially with respect to the scientific and academic approach, Mark Meeuwsen for his help and knowledge of engineering of foundations and especially sheet piles and his experiences with respect to this subject, Robbert van Leeuwen for the practical experiences and help, Milan Veljkovic for his critical view and support in case of problems and Ken Gavin for his support with respect to soil behaviour. I would like to thank all committee members and Ballast Nedam Foundation and Excavation Solutions, especially the subdepartment Van Leeuwen Verankeringen and b.v. ingenieursbureau M.U.C for their endless support, motivation and guidance through the complete thesis. Finally I would like to thank Mathieu Koetsier for the help and discussions regarding the challenges faced and my friends and family for their support.

*E. Stolwijk
Maarssen, June 2022*

Abstract

The evolution of ships requires larger depth or larger terrain loads in ports. Therefore, the existing quay walls require reinforcements. An effective way of reinforcing the structure are underwater anchors, requiring holes in existing sheet piles at the location of significant bending moment. Since this is a new area of expertise, the influence of the hole is still unknown. This report discusses a developed finite element model to study the influence of hole weakening of sheet pile and studies the influence of hole weakening on the sheet pile resistance and behaviour with the discussed model.

The 3DSSI model includes soil modelled by the subgrade reaction model (spring model) the steel sheet pile is modelled with shell elements in the finite element software DIANA FEA. The model includes both physical nonlinear and geometrical nonlinear behaviour and captures the soil-structure interaction. Also oblique bending, which is an existing phenomena of older, existing double U-sheet piles, can be captured with interface elements in the 3DSSI model. Nowadays, sheet piles are also designed using the subgrade reaction model and the sheet pile is modelled as a beam with the appropriate stiffness. The 3DSSI model is able to illustrate the 3D behaviour of the sheet pile, without having to model the soil with solid elements as well. This is beneficial with respect to calculation time.

With the 3DSSI model, the hole weakening of sheet piles can be studied. The influence of different parameters on the sheet pile resistance and behaviour is studied. The parameters studied, based on literature findings, are: hole diameter, hole location (level of the hole in depth), hole spacing (hole centre to centre distance in width), hole in-pan (compression zone) or out-pan (tension zone), sheet pile cross-section class 2 and 3 and oblique bending.

The influence of hole weakening on sheet pile behaviour and resistance is studied by finding in the parameter study for each case the load-displacement curve and from this load-displacement curve, the stiffness is derived. The load-displacement curve and stiffness curve include both steel and soil behaviour.

Resulting from the parameter study, the holes significantly reduce the sheet pile resistance and behaviour. The cases with holes in tension show less reduction in resistance and stiffness reduction. The hole diameter is also influencing the results, but the influence of hole location and hole spacing is relatively small. The failure modes are for holes in compression zone is plasticity around the hole and local buckling in the webs. For holes in tension zone, the failure mode is also plasticity around the hole, but also local buckling in the compression flange. For cases including oblique bending and holes in tension zone do not show local buckling in the compression flange, but in the compression web, due to the inclined neutral axis caused by oblique bending.

Content

Glossary.....	8
1. Introduction.....	10
1.1. Project motivation.....	10
1.2. Project definition.....	10
1.3. Research objectives.....	10
1.4. Research questions.....	11
1.5. Research method and research methodology.....	12
1.6. Scope.....	12
1.7. Thesis outline.....	13
2. Design of sheet piles.....	14
2.1. Design of sheet piles.....	14
2.2. Underwater anchor.....	14
2.3. Type of steel sheet piles.....	15
2.4. Soil models.....	16
2.4.1. Introduction.....	16
2.4.2. Earth pressure theories.....	17
2.4.3. Horizontal modulus of subgrade reaction (k_h).....	24
2.4.4. Blum's method (limit earth pressure).....	26
2.4.5. Subgrade reaction model (spring model).....	27
2.4.6. Finite element method.....	32
2.5. Plastic design.....	34
2.5.1. Blum's method for plastic design.....	34
2.5.2. Brinch Hansen.....	35
2.5.3. Windels.....	36
2.5.4. Weißenbach.....	36
2.6. Anchorage.....	37
3. Structural failure mechanisms.....	39
3.1. Existing structural failure mechanisms.....	39
3.1.1. Introduction.....	39
3.1.2. Global failure mechanisms.....	42
3.1.3. Local failure mechanism: connection anchor.....	45
3.2. Plastic design for bending moment capacity.....	48
3.2.1. Plastic behaviour in steel sheet piles.....	48
3.2.2. Yield mechanism.....	53
3.3. Oblique bending.....	55
4. Numerical modelling: 3D spring model.....	65
4.1. Numerical model: literature.....	66
4.1.1. Earth pressure theory: Müller-Breslau.....	66
4.1.2. Soil-structure interaction model: soil-spring model.....	66
4.1.3. Horizontal subgrade reaction modulus: Dutch model.....	66
4.1.4. Plastic design.....	66
4.1.5. Oblique bending.....	67
4.2. Numerical model: Soil load.....	67
4.2.1. Springs to model soil load.....	67
4.2.2. Wall friction and shear resistance of the soil.....	68
4.2.3. Oblique bending and transverse soil stiffness.....	68
4.3. Numerical model: Steel sheet pile characteristics.....	69
4.3.1. Boundary conditions.....	69
4.3.2. Top anchor.....	72
4.3.3. Oblique bending.....	73

4.3.4.	Material	74
4.3.5.	Integration layers in thickness	74
4.3.6.	Mesh (for situation without a hole).....	75
4.4.	Numerical model: Hole weakening	76
4.4.1.	Redistribution load around hole.....	76
4.4.2.	Mesh for situation with a hole	77
4.5.	Numerical model: Finite Element Analysis characteristics	80
4.5.1.	Nonlinear analysis	80
4.5.2.	Load steps	81
4.6.	Numerical model: Application	83
4.6.1.	Load increase.....	83
4.6.2.	Comparison 3DSSI model and D-sheetpiling.....	86
4.6.3.	Verification model.....	87
4.7.	Conclusion	89
5.	Design of parameter study	90
5.1.	Design of parameter study	90
5.1.1.	Research method.....	90
5.1.2.	Soil characteristics	91
5.1.3.	Sheet pile characteristics	92
5.2.	Parameters for hole weakening.....	93
5.3.	Overview parameter study.....	95
6.	Results of parameter study.....	97
6.1.	Result analysis procedure	97
6.1.1.	Failure load and failure mode	97
6.1.2.	Stiffness	98
6.2.	Results design 1.....	99
6.2.1.	Failure load and failure mode	100
6.2.2.	Stiffness	113
6.2.3.	Conclusion	114
6.3.	Results design 2.....	115
6.3.1.	Failure load and failure mode	115
6.3.2.	Stiffness	124
6.3.3.	Conclusion	125
6.4.	Comparison design 1 and design 2	126
6.5.	Results design 3.....	127
6.5.1.	Failure load and failure mode	129
6.5.2.	Stiffness	133
6.5.3.	Conclusion	134
6.6.	Conclusion	134
7.	Conclusion	136
	Discussion.....	138
	Bibliography	139
	Appendix A: D-sheet piling underwater anchor procedure	141
	Appendix B: Numerical model in DIANA FEA	144
	Appendix C: Verification model (4-point bending model)	148
	Appendix D: Oblique bending verification	152
	Appendix E: Convergence studies.....	157
	Appendix F: Parameter study	163

Glossary

A_v	Shear force area
E'_{oed}	Oedometer stiffness soil
$F_{s;Rd}$	Design local shear resistance
F_{sd}	Design local shear force
$F_{t;Rd}$	Design local tension resistance
K_0	Refer to K_n
K_a	Active earth pressure coefficient
K_n	Neutral earth pressure coefficient
K_p	Passive earth pressure coefficient
M_{Ed}	Design bending moment
$M_{c;Rd}$	Design bending moment resistance
M_{pl}	Plastic bending moment
M_u	Ultimate bending moment
V_{Ed}	Design shear force
$V_{pl;Rd}$	Design plastic shear force resistance
W_{el}	Elastic section modulus
W_{pl}	Plastic section modulus
b_f	Flange width
f_y	Yield strength
k_h	Horizontal modulus of subgrade reaction
k_x	Transverse soil spring stiffness
k_y	Lateral soil spring stiffness
p_a'	Effective active earth pressure
p_p'	Effective passive earth pressure
q_c	Cone resistance
t_f	Flange thickness
t_w	web thickness
α_{web}	Web inclination angle
β_B	Refer to β_W
β_D	Refer to β_I
β_I	Stiffness reduction factor for oblique bending
β_W	Strength reduction factor for oblique bending
γ_{M0}	Safety factor
σ'_a	Refer to p_a'
σ'_n	Effective neutral earth pressure
σ'_p	Refer to p_p'
$\sigma_{h'}$	Effective horizontal earth pressure
$\sigma_{v'}$	Effective vertical earth pressure
$\tau_{x;max}$	Maximum shear stress in the soil
φ_{pl}^U	Plastic rotation U-pile
φ_{pl}^Z	Plastic rotation Z-pile
G	Shear stiffness soil
H	Retaining height
OCR	Overconsolidation ratio
SLS	Serviceability Limit State

<i>ULS</i>	Ultimate Limit State
<i>c</i>	Cohesion
<i>r</i>	Corner radius
<i>w</i>	Deformation of the sheet pile
<i>z</i>	Level sheet pile (Depth)
α	Slope of soil-wall interface
β	Backfill slope angle
γ	unit weight of the soil
δ	Wall friction angle
ε	$\sqrt{\frac{235}{f_y}}$
ρ	Reduction factor bending moment – shear force interaction
φ'	Effective internal friction angle

1. Introduction

1.1. Project motivation

Improvement of the existing quay walls is of importance considering the competition between ports. The evolution of ships require adjustments of the ports, such as deeper bottom levels of the harbour due to larger ship draughts and higher load cases on the land due to larger equipment. Deepening the port harbours and enhancing terrain loads, increases the competitive position and enhances the revenue for the port of Rotterdam [3],[4]. Before excavating the port harbours or increase the terrain load, the quay wall resistance has to be increased. The quay wall exists of single-anchored steel sheet pile walls. To increase the resistance of these sheet pile walls, either new sheet piles with a larger cross section and/or larger embedment depth have to be installed, or the existing sheet pile wall has to be reinforced. Since installing new sheet piles is expensive, reinforcing the existing sheet piles is a viable solution. Douairi and de Gijt (2013) studied the options of upgrading existing quay walls. From their study, it appears that adding an anchor underwater is an effective way of reducing the bending moment in the sheet pile since it is the only solution reducing the span of the quay wall. Then, before placing the underwater anchor, holes have to drilled in the sheet pile at the location of the underwater anchor. Other solutions are replacing the soil in passive side with heavier soil. However, these are not as effective as adding an extra anchor. The underwater anchor provides the possibility of excavating the harbour to a greater depth and/or apply more terrain load in a cost-effective way. [5]

1.2. Project definition

Regarding the local sheet pile resistance, applying an underwater anchor exists of two important steps: drilling holes in the existing sheet pile on a location where the bending moment is significant and attaching the underwater anchors to the sheet pile at this location. The holes require a significant size of approximately 200-300 mm diameter, regarding the equipment necessary for drilling holes. This hole is always located in the flange of the sheet pile cross-section, and covers approximately 40-70% of the flange width of the sheet pile, depending also on the flange width of the sheet pile. There are still uncertainties considering these underwater anchors. One of these uncertainties is the behaviour of the sheet pile when adding an underwater anchor [5]. These uncertainties and the gap of knowledge in the behaviour of sheet piles considering the placement of underwater anchors is also identified by RoyalHaskoningDHV (2020). Weakening the existing structure with holes effects the stress distribution and the behaviour of the sheet pile and this is one of the uncertainties mentioned by RoyalHaskoningDHV (2020) [4], together with the connection of the underwater anchor to the sheet pile.

With this master thesis, the behaviour of the sheet piles when weakening the existing structure with holes will be studied. This is for now a known knowledge gap in the current calculation procedure of sheet piles in quay walls and no research can be found considering underwater anchors and hole weakening of an existing quay wall which underlines the importance of this study.

1.3. Research objectives

This thesis obtains insight into the behaviour of the sheet pile when weakening the cross section with holes at the location where the underwater anchor will be applied and the existing stresses due to the bending moment are significant. Since the quay walls are existing, they

are already loaded and subjected to a significant bending moment when the holes are made. The aim of this study is to obtain the failure modes for steel sheet piles subjected to hole weakening and study the influence of hole weakening on the capacity and behaviour of the structure. With the obtained results, an indication can be given on the resistance of a sheet pile with hole weakening with respect to the original sheet pile. Due to the great variety of possible situations regarding the hole in reality, within this master thesis the aim is to study different hole characteristics. The main objective of this research is to identify the reduction of the sheet pile capacity with hole with respect to the original situation without a hole. By studying different hole characteristics a good indication for realistic situations is given.

1.4. Research questions

This thesis aims to answer the following main research question:

What is the influence of hole weakening on the sheet pile's behaviour and resistance, before installing underwater anchors?

To answer this main research question, the following sub questions will be addressed:

1. What are the characteristics of the numerical model to obtain understanding in the sheet pile resistance and behaviour regarding the effect of hole weakening?
 - a. How can existing modelling techniques give understanding into sheet pile resistance and behaviour regarding the effect of hole weakening?
 - b. What is an appropriate modelling technique to model a sheet pile regarding the effect of hole weakening and how can this model be designed in DIANA FEA?
 - c. Which are details of the design finite element model?
 - d. How can the influence of the hole weakening on the sheet pile resistance and behaviour be studied using the designed model?
2. What is the influence of hole weakening on the resistance and behaviour of the sheet pile structure?
 - a. What phenomena will possibly have an influence on the sheet pile resistance and behaviour considering underwater anchors?
 - b. How do the hole characteristics influence the sheet pile resistance?
 - c. How do the hole characteristics influence the sheet pile stiffness?
 - d. Which variable should be considered in verification of the sheet pile structure with hole weakening?

1.5. Research method and research methodology

The main research method used for this thesis is Finite Element Modelling (FEM) with the finite element program DIANA FEA. Also desk research will be used.

For developing the model, numerical prediction and semi-empirical prediction methods are used. The desk research starts with a literature study gaining insight into the existing design options for designing a sheet pile, the plastic behaviour of sheet piles and the parameters which should be included in the model is studied with the desk research. Also, the modelling options regarding soil and soil-structure interaction will be studied. With the knowledge from the desk research, a numerical model with DIANA FEA can be designed. With the finite element model, the influence of different parameters can be determined via a parameter study and advise can be given to engineers how the hole weakening effect can be modelled and which variable are of importance. The results of the developed model can be verified with a verification model: a 4-point bending test, and models and tests from literature.

Summarizing, with a literature study a numerical model is designed. With the numerical model the influence of hole weakening on the sheet pile behaviour and resistance will be studied using a parameter study.

The hypothesis of the research is: the hole weakening of the sheet pile will reduce the sheet pile resistance and stiffness, primarily depending on the hole diameter.

1.6. Scope

The research scope is defined with the following limitations:

- Existing embedded walls made of steel sheet piles

There are several types of retaining structures. This thesis focuses on embedded walls only. The research considers existing sheet piles only which are already loaded. The sheet piles studied are steel sheet piles only.

- The considered failure mechanisms are structural failure of the steel sheet pile.

The study focuses on structural failure of the steel sheet pile and not on the geotechnical failure in the soil. It is assumed that geotechnical failure does not occur.

- The existing top anchor should not be overloaded.

For this thesis, it is assumed the capacity of the top anchor is in all cases sufficient. In practice the resistance of the top anchor and the design load have to be verified for the design situations.

- Z-shaped and double U-shaped sheet piles

The existing sheet piles considered for reinforcing with underwater anchors are Z-shaped and double U-shaped sheet piles. The existing U-shaped sheet piles are mostly double U-shaped sheet piles.

- Vertical quay walls and level ground surfaces

The research is limited to vertical quay walls. The ground surfaces are all assumed to be horizontal. This also applies to the soil layers.

- Boundary conditions: single anchored sheet piles (before applying underwater anchor)

The existing steel sheet pile walls in the existing quay wall are single anchored near the top of the sheet pile. Cantilever sheet pile walls are not of interest for this study. The initial situation is a single-anchored sheet pile wall.

- No time dependent behaviour of soil and steel included

Time-dependent behaviour of soil modelling is not studied or included in this research. Also decrease of steel quality and capacity due to corrosion is excluded from the research.

- No soil arching

Soil arching is a phenomenon which redistributes soil pressure. This behaviour is excluded for this research.

- Use of DIANA FEA

The subject is studied with the finite element program DIANA FEA.

1.7. Thesis outline

To answer the research question and meet the objectives of this thesis, first a literature study is performed on the existing considering the design of sheet piles. This is discussed in chapter 2. Chapter 3 focuses on the structural failure mechanism of the sheet pile, including plastic behaviour and oblique bending. The numerical model developed in this thesis is discussed in detail in chapter 4 and chapter 5 focuses on the design of the parameter study of the holes in sheet piles. Chapter 6 discusses the results of the parameter study and is followed by the conclusion and discussion of this thesis.

2. Design of sheet piles

This thesis focuses on the structural failure of sheet piles. However, to understand the behaviour of sheet piles and the design process, the design procedure of sheet piles is discussed. The design of sheet piles consists of soil-structure interaction. Both the soil as the steel structure are of importance and interact with one another.

2.1. Design of sheet piles

An example of a single anchored sheet pile of a quay wall is given in Figure 1. In this example, several soil layers are present and a top anchor.

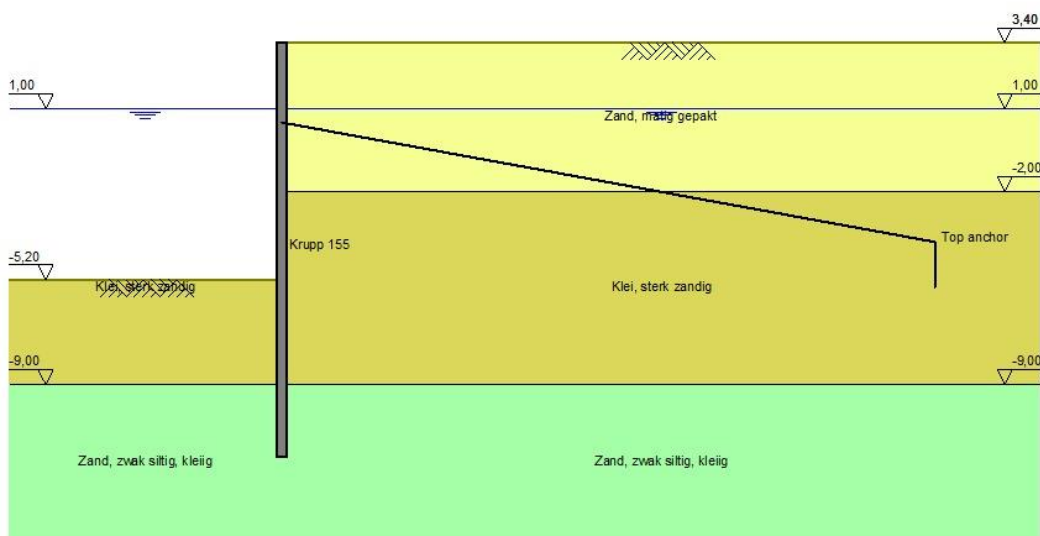


Figure 1: single-anchored sheet pile (D-sheetpiling)

The soil at the right side of Figure 1 is loading the sheet pile and pushing it towards the water side (left side). This is called the active soil pressure. The soil on the left side, is pushing back and is therefore called passive soil pressure. The anchor restrains the sheet pile near the top level of the sheet pile. The aspects of the single anchored sheet piles which need to be designed are: wall penetration depth, anchor force, wall bending moment, steel sheet pile section and the anchorage system. [6]

The advantages of anchors are a reduction of the deformation and required length and strength of the sheet pile. An anchor is mostly applied under an angle, which causes a vertical load on the sheet pile. The anchor angle makes it possible to get to the stiffer soil layers which give more resistance. The anchor and the passive resistance of the soil at the bottom of the soil act as a horizontal support for the sheet piling. The function the quay wall and the sheet pile is to retain the earth. Ships can berth to the quay wall as well. [7]

2.2. Underwater anchor

A new reinforcement method is proposed by the port of Rotterdam [8]: reinforcing the existing sheet piles with an extra anchor, which is located underwater. The anchor is connected to the existing sheet pile. When excavating the harbour, the underwater anchor acts as an extra

support and aims to keep the sheet pile at its place when deepening the harbour. The bending moment, shear force and deformation for the situation of a single anchored sheet pile and the excavated situation with underwater anchor is given in Appendix A.

Also stated by Emarah and Seleem (2016), the bending moment reduces significantly when adding an second anchor to the system at a lower depth. The optimal position for the minimum bending moment was found when placing the upper anchor at 0,30 to 0,35 of the retaining height and the lower anchor at 0,6 to 0,7 of the retaining height, depending on the soil type behind the structure. The reaction force in the lower anchor rod is always larger than the reaction force in the upper anchor rod. [9]

Considering the excavation phase, the soil behaviour is important. A minimum embedding depth is required to prevent soil behaviour such as piping. Also, the soil movement due to the propellor of the ship should be considered. Therefore, the embedding depth should be kept to a minimum of approximately 4 meters. This is taken into account when determining the finite element model.

The underwater anchors are a new area of expertise and therefore a lot is still unknown, considering both the structural and the geotechnical behaviour.

2.3. Type of steel sheet piles

Different type of sheet piles are available and applied for quay walls:

- Z-shaped sheet piles (Larssen piles) (Figure 2)
- U-shaped sheet piles (Froningham piles) (Figure 3)
- Combi-walls

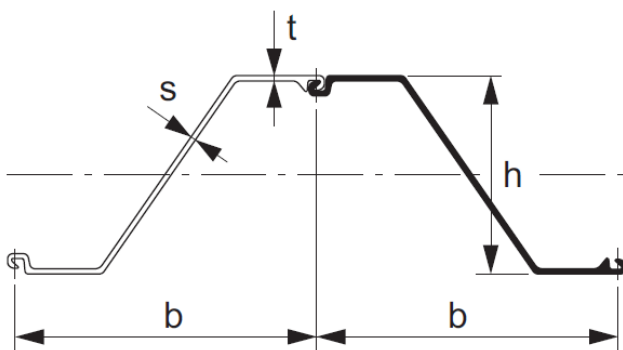


Figure 2: Z-pile cross section [34]

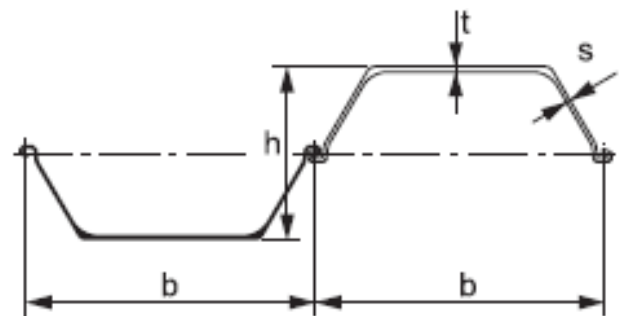


Figure 3: U-pile cross section [34]

This thesis will only focus on Z-shaped and U-shaped sheet piles. The combi-walls are not researched.

The main difference between Z-shaped profiles and U-shaped profiles is the location of the interlock. The interlocks of Z-shaped profiles are located at the outer fibre of the profile, while for U-profiles, it is located in the centre of the profile, at the neutral axis. This different position of the interlock has influence on the shear force transmission and bending behaviour. This is discussed in more detail in chapter 3.3. The U-piles existed before the Z-piles were introduced. The Z-piles were introduced due to better structural properties: higher local buckling strength and a continuous web. This results in a higher strength to weight ratio. However, in the existing

sheet pile walls, also a lot of double U-shaped sheet piles are present and therefore these type of sheet piles cannot be neglected. [10]

The sheet piles are either hot rolled or cold formed. The main differences between hot rolled and cold formed sheet piles are:

- The cross section of cold formed sections have the same thickness in both flange and web. For hot rolled sections, this is not necessarily the case.
- The interlocks of cold formed sections are looser, and also not as watertight as for hot rolled sections.
- The yield strength of cold formed sheet piles is lower than for hot rolled sections
- The cold formed sections are slender, and therefore belong mainly to cross section class 4. Explanation of cross section classification is given in chapter 3.2.1.

The interlock of hot rolled sections is different to the interlocks of cold formed sections.

The application of hot rolled and cold formed section also differs. Cold formed sheet piles are more applicable to smaller applications. For large retaining walls, mostly hot rolled sections are used. This study focuses on retaining walls for harbours and therefore the hot rolled sections are considered.

[11]

2.4. Soil models

There are different options for modelling soil. These options have different characteristics which will be discussed. The pros and cons are considered to be able to determine an appropriate soil model for the finite element model.

2.4.1. Introduction

A single anchored sheet pile can be simplified and schematized as a simple beam on 2 supports. The support at the base is depending on the embedment depth. However, modelling it as a simply supported structure is conservative and therefore acceptable, especially in predesign. For insufficient embedment depth, the wall will start rotating around the top anchor/fixed point. Increasing the embedment length will lead eventually to fully fixed sheet pile at the base, for which then also the rotation angle at the base is zero. These situations are schematized and shown in Figure 4 [12].

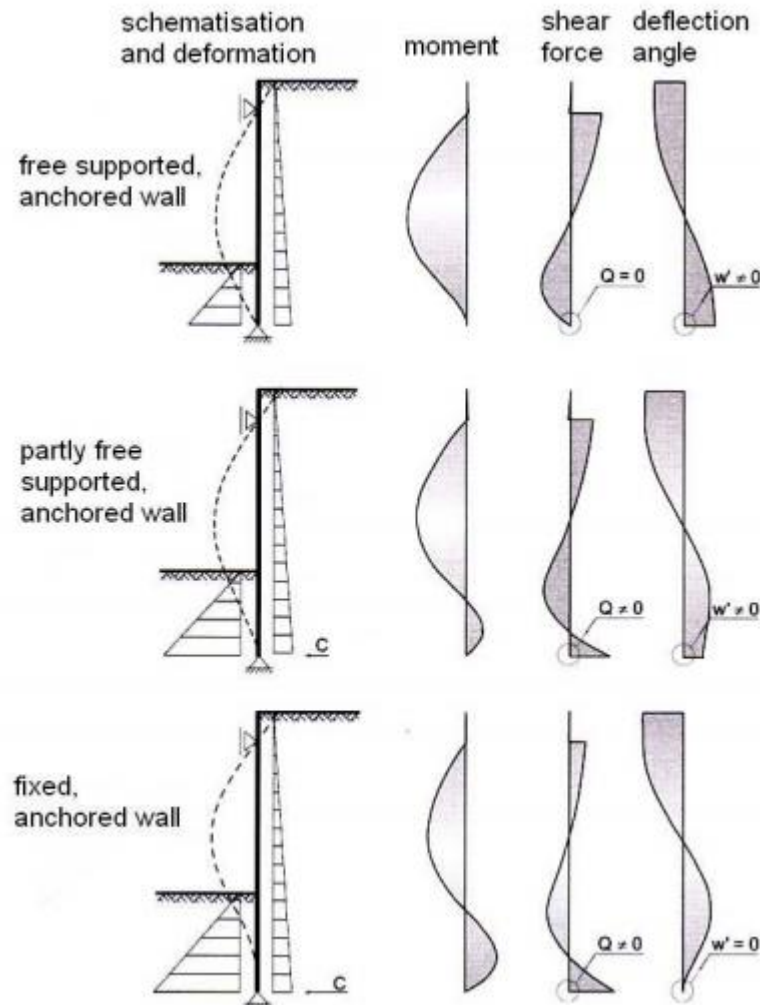


Figure 4: mechanical schematization of sheet pile structure [12]

The horizontal earth pressure of the soil is loading the sheet pile. The vertical stresses resulting in a normal force in the sheet pile are neglected.

The movement of the soil results in horizontal stresses. This results in deformation of the sheet pile which causes again deformation and ultimately failure of the soil. Compressed soil results in passive earth pressure, while relaxation of the soil results in active earth pressure. [13]

For the design of sheet piles, the slip planes should also be verified. The models used for these slip planes are of Krantz and Bishop. Other phenomena occurring in the soil which should be considered when verifying a sheet pile are for example piping and scour. These geotechnical failures are not considered in this thesis.

For determining the horizontal/lateral earth pressure of the soil acting on the sheet pile several earth pressure theories are available. These will be shortly described. Then the different possibilities of calculating retaining walls are described: Blum's method, Winkler spring method and the finite element method.

2.4.2. Earth pressure theories

To determine the lateral earth pressure on a sheet pile wall several earth pressure theories are available. The earth pressure is defined as 'the force per unit area exerted by the soil on the sheet pile structure' [14]. The earth pressure depends on several factors: soil properties,

soil-structure interaction and deformation and the influence of time on the soil strength, which is influenced by phenomena such as creep and chemical changes in the soil. The effective horizontal earth pressure is depending on the vertical effective pressure according to the equation 1:

$$\sigma_{h'} = K \cdot \sigma_{v'} \tag{1}$$

The earth pressure can be divided into two stages, the active stage and the passive stage. The active earth pressure occurs when the sheet pile moves away from the soil. In that case, the soil on the active side expands laterally which mobilizes shear resistance in the soil. This shear resistance reduces then the lateral earth pressure which is then the active earth pressure. When the soil is moving towards the soil, the soil is compressed which mobilizes the shear resistance and then increases the lateral earth pressure. This results in the passive earth pressure. When there is no movement in the soil, the neutral earth pressure is present. [14] The earth pressure depending on the deformation is shown in Figure 5 . The real soil behaviour is often simplified to as shown, with the earth pressure depending linearly on the wall deformation between the active and passive earth pressure.

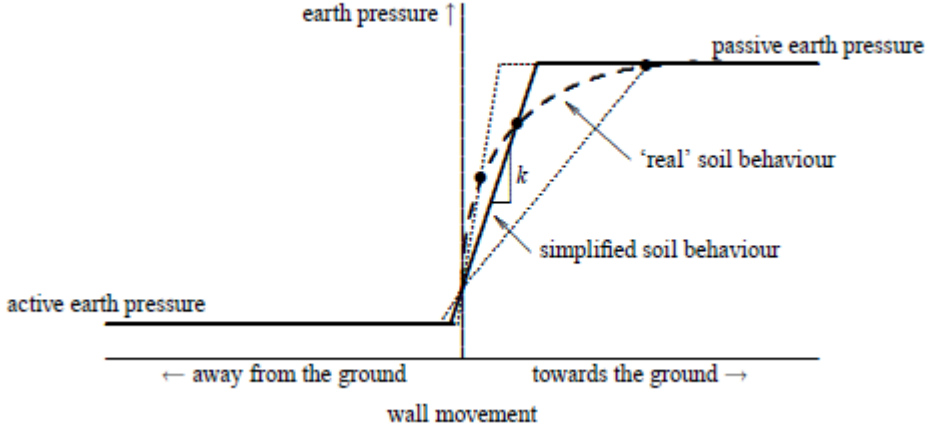


Figure 5: earth pressure and wall movement diagram [23]

How the earth pressure is distributed depends on several variables: the depth of the sheet pile, the angle of the wall and ground level, the density of the soil, stress condition, density and strength of soil, drainage conditions and the assumption of the movement of the soil and retaining structure. The latter is the most important for determining whether active, passive or neutral earth pressure occurs. The magnitude of the earth pressure is depending on wall movement relative to the soil, wall/soil placement techniques, the shear strength between wall and soil and shear strength of the soil itself, geometry of the wall, soil and groundwater and external loads. [15], [16].

The active and passive earth pressure can be calculated by the following formulas (equation 2 and equation 3) also called Bell's relationship:

$$p_a' = \gamma z K_a - 2c' \sqrt{K_a} \tag{2}$$

$$p_p' = \gamma z K_p + 2c' \sqrt{K_p} \tag{3}$$

[14] γ is here defined as the submerged weight of the soil.

The determine the active and passive earth pressure coefficients earth pressure theories are developed. The most widely used and well-known earth pressure theories are discussed.

The stiffness k is also known as the horizontal modulus of subgrade reaction and is given further elaborated in chapter 2.4.3.

Earth pressure coefficient at rest

The earth pressure coefficient at rest is also called the neutral effective earth pressure coefficient and gives a positive lateral earth pressure. The neutral earth pressure can be calculated with the neutral earth pressure coefficient according to equation 4:

$$\sigma'_n = K_n \sigma'_v \quad (4)$$

This earth pressure develops due to time-dependent behaviour of soil. Creep and swelling occur and results in a lateral earth pressure. A formula for finding the neutral effective earth coefficient is proposed by Jaky (equation 5):

$$K_0 = 1 - \sin\varphi' \quad (5)$$

Jaky's equation states that K_0 is depending on the effective internal friction angle. Experiments have shown that also the overconsolidation ratio influences K_0 . Therefore, Eurocode 7 expands Jaky's equation by including the overconsolidation ratio (equation 6):

$$K_0 = 1 - \sin\varphi' \cdot \sqrt{OCR} \quad (6)$$

There are also empirical theories for defining the neutral earth pressure coefficients. However, Jaky's equation is the most general used method and conservative and therefore this theoretical formula is used. This method is also prescribed for Dutch soils in NEN 6740 and used by the software D-sheetpiling. [17], [12], [18]

Coulomb's earth pressure theory (1776)

Coulomb was the first studying the problem of lateral earth pressure. Coulomb defines free-body diagrams of the soil bounded by soil surface, retaining wall and the failure plane, also called the soil wedge. The sliding soil wedge is considered as a rigid body. The failure plane is assumed to be planar and under an angle θ . The soil wedge is shown in Figure 6. Friction in the soil is considered by Coulomb, but the wall friction (δ) is not included. Wall friction is later introduced by Mayniel in 1908 (Figure 7) and Müller-Breslau (1906) generalized the equation for non-horizontal backfill (β) and non-vertical soil-wall interface (α) (Figure 8). The soil is assumed to be isotropic, homogeneous and cohesionless. Assumptions for all three equations are rigid soil and planar failure. [16], [19], [20]

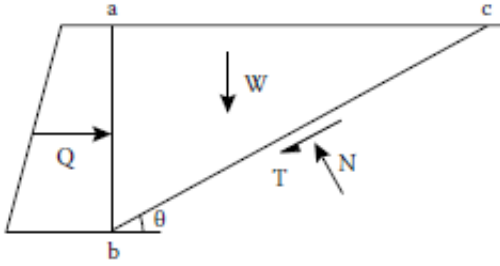


Figure 6: Force diagram Coulomb: frictional soil [16]

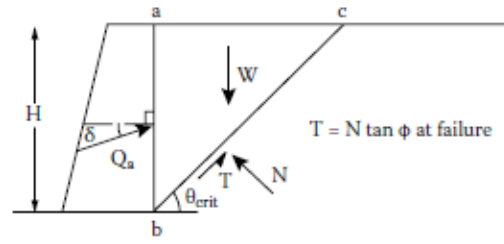


Figure 7: Force diagram Mayniel: frictional soil and wall friction [16]

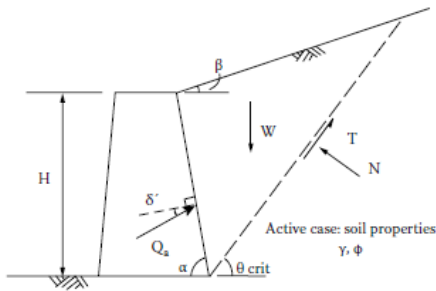


Figure 8: Force diagram Müller-Breslau: frictional soil, wall friction, backfill slope and slope soil-wall interface [16]

The total general equation for frictional soil, wall friction, backfill slope and slope of soil-wall interface is for active earth pressure coefficient (equation 7) and passive earth pressure coefficient (equation 8):

$$K_a = \frac{\sin^2(\alpha + \varphi)}{\sin^2 \alpha \sin(\alpha - \delta) \left[1 - \frac{\sin(\varphi + \delta) \sin(\varphi - \beta)}{\sin(\alpha - \delta) \sin(\alpha + \beta)} \right]^2} \quad (7)$$

$$K_p = \frac{\sin^2(\alpha - \varphi)}{\sin^2 \alpha \sin(\alpha - \delta) \left[1 - \frac{\sin(\varphi - \delta) \sin(\varphi + \beta)}{\sin(\alpha - \delta) \sin(\alpha + \beta)} \right]^2} \quad (8)$$

Summarized, the assumptions are:

- Cohesionless soil
- Homogeneous and isotropic soil
- Straight planar failure surface
- Planar ground surface
- Rigid soil

[17]

High friction angles ($\varphi > 30^\circ$) lead to a more curved shear surface which can lead to a large reduction of the passive earth pressure. Therefore, for $K_p > 6$ or $\varphi > 30^\circ$, the passive earth pressure should be calculated by a approach assuming non-linear slip surface. It is determined by CUR 166 that Coulomb's method and also Culmann's method (explained further next paragraphs) cannot be applied for $\delta \geq \frac{2}{3} \varphi$.

In D-sheetpiling Müller-Breslau's equation is limited to a maximum soil friction angle of 30° for steel sheet pilings. [21], [22]

In the Netherlands, the formula of Müller-Breslau has been extended for cohesive soils (NEN 6740). This are quite elaborate expressions, but can be simplified for assuming a vertical wall and horizontal ground level (equation 9-15):

$$\sigma'_a = K_{ca} c' + K_{\varphi a} \sigma_{v'} \quad (9)$$

$$\sigma'_n = K_n \sigma_{v'} \quad (10)$$

$$\sigma'_p = K_{cp} c' + K_{\varphi p} \sigma_{v'} \quad (11)$$

With:

$$K_{ca} = -\frac{2\cos\varphi' \cos\delta}{1+\sin(\varphi'+\delta)} \quad (12)$$

$$K_{\varphi a} = \frac{\cos^2\varphi'}{\left(\sqrt{\frac{\sin\varphi' \sin(\varphi'+\delta)}{\cos\delta}} + 1\right)^2} \quad (13)$$

$$K_{cp} = \frac{2\cos\varphi' \cos\delta}{1-\sin(\varphi'-\delta)} \quad (14)$$

$$K_{\varphi p} = \frac{\cos^2\varphi'}{\left(\sqrt{\frac{\sin\varphi' \sin(\varphi'-\delta)}{\cos\delta}} - 1\right)^2} \quad (15)$$

For the neutral earth pressure coefficient, the equation derived by Jaky (1948) is used (equation 5). [18], [23]

Rankine's theory (1857)

Rankine's earth pressure theory also describes the active and passive earth pressures. Rankine approaches the problem by deriving a solution when assuming the complete soil is in failure, where Coulomb was considering only the soil wedge in failure. The assumptions for this theory are:

- Cohesionless soil
- Homogeneous and isotropic soil
- Frictionless wall ($\delta=0$)
- Straight planar failure surface
- Planar ground surface
- Resulting force on the wall is parallel to ground surface
- Vertical retaining wall

The failure zone for Rankine's earth pressure theory for a horizontal backfill are shown in Figure 9 and the formulas in equation 16-19.

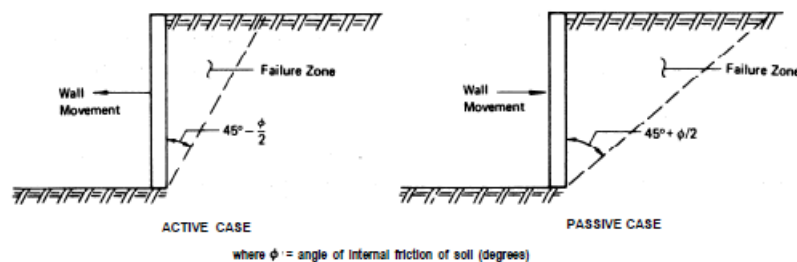


Figure 9: Rankine's failure zones for active (left) and passive (right) case [21]

[21]

$$K_a = \cos\beta \left(\frac{\cos\beta - (\cos^2\beta - \cos^2\varphi)^{\frac{1}{2}}}{\cos\beta + (\cos^2\beta - \cos^2\varphi)^{\frac{1}{2}}} \right) \quad (16)$$

$$K_p = \cos\beta \left(\frac{\cos\beta + (\cos^2\beta - \cos^2\varphi)^{\frac{1}{2}}}{\cos\beta - (\cos^2\beta - \cos^2\varphi)^{\frac{1}{2}}} \right) \quad (17)$$

These formula can be simplified for a level embankment ($\beta=0$):

$$K_a = \frac{1 - \sin(\varphi)}{1 + \sin(\varphi)} \quad (18)$$

$$K_p = \frac{1 + \sin(\varphi)}{1 - \sin(\varphi)} \quad (19)$$

Since a frictionless wall is assumed, Rankine's earth pressure is only correct for a zero embankment slope or a negative embankment slope. This theory is best applied for determining earth pressures within soil masses on a vertical plane.

For determining the earth pressure directly against the wall, Rankine's earth pressure theory is not recommended. [16], [21]

Culmann (1866)

Culmann's method is based on Coulomb's method. Culmann's method is applicable for non-horizontal soil surfaces and surcharges. The method is based on the equilibrium of the following forces: Q: pressure on the sheet pile, W: Weight of the sliding soil mass, B: surcharge load, T: friction along straight slip surface, N: normal reaction of soil. This is for both the active and the passive side (Figure 10 and Figure 11). [22]

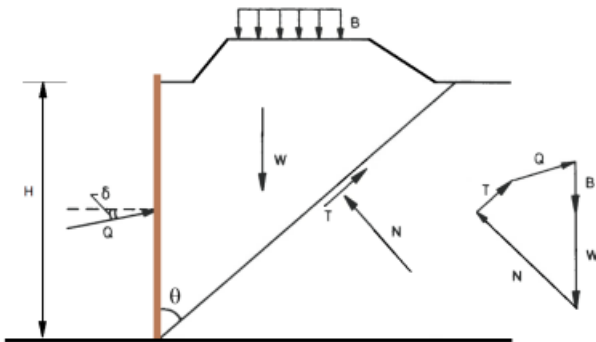


Figure 10: Culmann active case [22]

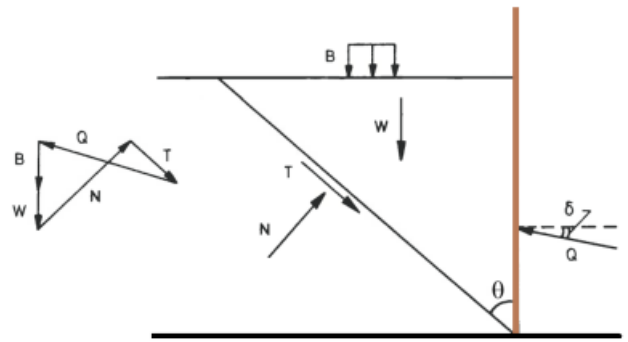


Figure 11: Culmann passive case [22]

By horizontal and vertical force equilibrium equations the horizontal active and passive force Q_h can be determined. The angle θ is determined iteratively, until the angle is found with the maximum active force and minimum passive force; thus the worst case scenario. Then the earth pressure coefficients can be determined for points along the height of the sheet pile. this procedure is shown in Figure 12.

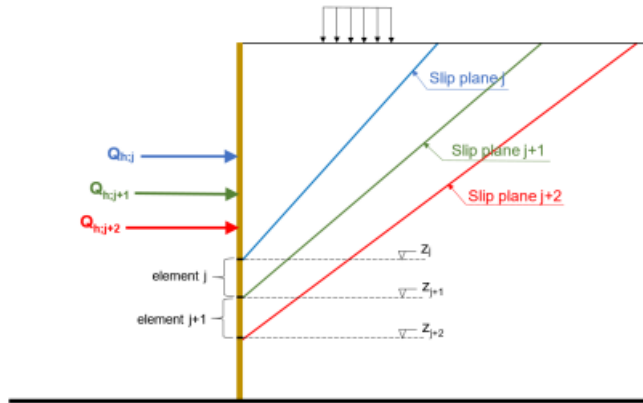


Figure 12: Iterative procedure [22]

The formula for finding the earth pressure coefficient for an arbitrary element, element j , is given in equation 20:

$$\lambda_j = \frac{\sigma_{h,j+1}}{\sigma'_{v,j+1}} = \frac{Q_{h,j+1} - Q_{h,j}}{(z_j - z_{j+1})\sigma'_{v,j}} \quad (20)$$

Also the sign of δ in the equations, positive or negative, implies some assumptions. The most common situation is a positive δ which assumes:

- Soil is settling more than sheet pile wall when calculating K_a
- Soil is settling less than sheet pile wall when calculating K_p

[22]

Culmann is a graphical method which can be used to find the earth pressure by hand. This is not explained in further detail. Culmann's method is based on Coulomb's method and also assumes planar failure surfaces. Therefore this method is also not applicable for large internal friction angles ($\phi > 30^\circ$) and large wall friction angles ($\delta \geq \frac{2}{3}\phi$).

Kötter

Kötter also provides an earth pressure theory to determine the earth pressure coefficients. The main difference between Kötter and Coulomb's theory is failure plane. Kötter's theory is based on a curved failure surface, where Coulomb's theory is based on a plane failure surface. The assumptions summarized for Kötter's earth pressure theory are:

- Curved failure surface
- Cohesionless soil
- Homogeneous soil
- Weightless soil

Again the sign of δ in the equations, positive or negative, implies some assumptions. The most common situation is a positive δ which assumes:

- Soil is settling more than sheet pile wall when calculating K_a
- Soil is settling less than sheet pile wall when calculating K_p

Kötter's equations for finding the active and passive earth pressure are again according to Bell's equations (equation 21-23):

$$\sigma'_a = K_a \sigma'_v - 2c\sqrt{K_a} \quad (21)$$

$$\sigma'_n = K_n \sigma'_v \quad (22)$$

$$\sigma'_p = K_p \sigma'_v + 2c\sqrt{K_p} \quad (23)$$

For the neutral earth pressure coefficient again Jaky's equation is used. The active and passive earth pressure coefficients are given in equation 24 and equation 25:

$$K_a = \frac{1 - \sin \varphi' \sin (2\alpha + \varphi')}{1 + \sin \varphi'} e^{\left(-\frac{\pi}{2} + \varphi' + 2\alpha\right) \tan \varphi'} \quad (24)$$

$$\alpha: \cos(2\alpha + \varphi' - d) = \frac{\sin \delta}{\sin \varphi'}$$

$$K_p = \frac{1 + \sin \varphi' \sin (2\alpha - \varphi')}{1 - \sin \varphi'} e^{\left(+\frac{\pi}{2} + \varphi' - 2\alpha\right) \tan \varphi'} \quad (25)$$

$$\alpha: \cos(2\alpha - \varphi' + d) = \frac{\sin \delta}{\sin \varphi'}$$

[22], [23]

2.4.3. Horizontal modulus of subgrade reaction (k_h)

To determine the earth pressure diagrams, also the horizontal stiffness k_h of the earth pressure diagrams has to be known. There are 2 methods known to determine the horizontal modulus of subgrade reaction (k_h): Terzaghi's method and Ménard's method. These methods do not take into account the deformation in the soil. There are experimental data for Dutch soils which are also used.

Terzaghi's method

Terzaghi provides the following method for finding the horizontal modulus of subgrade reaction (equation 26 and equation 27).

For $u > 0.0002D$

$$k_h = L_h \frac{z}{D} \quad (26)$$

For $u \leq 0.0002D$

$$k_h = L_h' \frac{z}{D} \quad (27)$$

L_h is a constant depending on the density and unit weight of the soil, u the horizontal displacement of the sheet pile wall and D the depth of the toe of the sheet pile wall below the ground level at the regarded site of the wall, z the depth of the point beneath ground level.

The value for the constant L_h is depending on the relative void ratio (R_e), cone resistance (q_c) and void ratio (e).

The constant L_h is underestimated and is only applicable for normally consolidated sands. For excavating different equations are given, since the horizontal pressure does not reduce proportional to the vertical pressure. Also for clay different equations can be found in CUR 166. Terzaghi's method does not take into account in the deformation of the soil when determining the horizontal modulus of subgrade reaction. [7], [24]

Ménard's method

Ménard proposes equation 28 for calculating the horizontal modulus of subgrade reaction:

$$k_h = E_M \left(\alpha \frac{a}{2} + 13(9a \cdot 10^{-4})^\alpha \right)^{-1} \quad (28)$$

With α as the rheological coefficient which can be found by reading the table, depending on the soil type and consolidation of the soil. a is the length in meters, and for a freely supported wall equal to the length of the sheet pile wall below ground surface on the low side (D). For clamped walls, a is equal to $2/3D$. E_M is the young's modulus determined by Ménard's pressuremeter test. Similar to Terzaghi's method, Ménard does not consider the deformation of the soil when determining the horizontal modulus of subgrade reaction. [7], [24]

Dutch model

For the Netherlands data from measurements are used to determine the horizontal modulus of subgrade reaction method. The table with the values for horizontal subgrade reaction modulus determined for Dutch soils is given in Figure 13. These values can be used in combination with the spring model as shown in Figure 14. The Dutch model includes three intervals with three stiffnesses / horizontal modulus of subgrade reaction and thus the deformation of the soil is taken into account which is not the case for Terzaghi's and Ménard's method. Figure 14 is discussed further in chapter 2.4.5 .

[7], [24]

		$k_{h,1}$ [kN/m ³]		$k_{h,2}$ [kN/m ³]		$k_{h,3}$ [kN/m ³]		
		1) $p_0 < p_h < 0.5 p_{ea,h;p,rep}$		0.5 $p_{ea,h;p,rep} < p_h < 0.8$		0.8 $p_{ea,h;p,rep} < p_h < 1.0$		
		1 ²⁾	2 ³⁾	1 ²⁾	2 ³⁾	1 ²⁾	2 ³⁾	
Sand:	q_c [MPa]							
	loose	5	12,000	27,000	6,000	13,500	3,000	6,750
	moderate	15	20,000	45,000	10,000	22,500	5,000	11,250
dense	25	40,000	90,000	20,000	45,000	10,000	22,500	
Clay:	f_{undr} [kPa]							
	soft	25	2,000	4,500	800	1,800	500	1,125
	moderate	50	4,000	9,000	2,000	4,500	800	1,800
stiff	200	6,000	13,500	4,000	9,000	2,000	4,500	
Peat:	f_{undr} [kPa]							
	soft	10	1,000	2,250	500	1,125	250	560
moderate	30	2,000	4,500	800	1,800	500	1,125	

- 1) the values in this column can be used for active soil pressure $P_{ea,h;p,rep}$
 - 2) characteristic value of the low average if a low spring constant is unfavourable
 - 3) characteristic value of the high average if a high spring constant is unfavourable
- p_0 is the neutral soil pressure in [kN/m²]
- $p_{ea,h;p,rep}$ is the characteristic value of the maximum horizontal soil pressure for (passive) stress increase in [kN/m²]
- p_h is the maximum horizontal pressure in [kN/m²] for the course of the modulus of subgrade reaction

Figure 13: Dutch model: horizontal modulus of subgrade reaction [24]

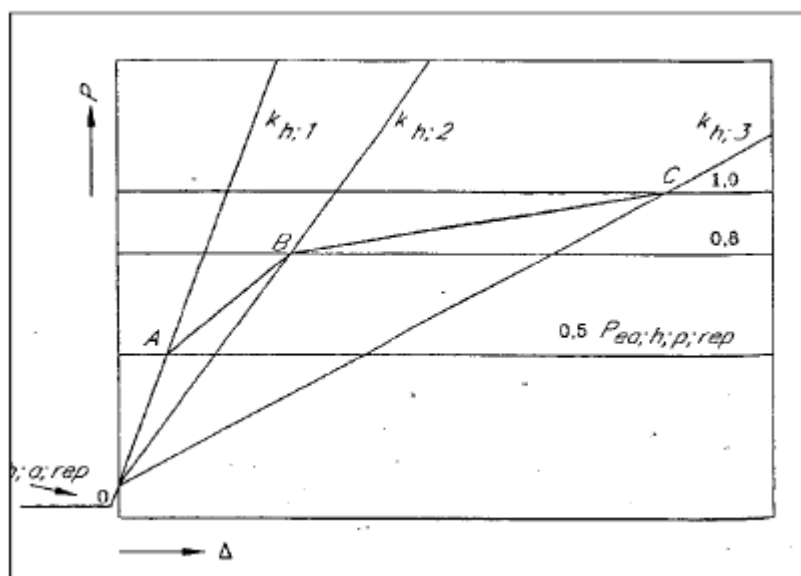


Figure 14: Dutch model: soil stiffness depending on deformation [24]

2.4.4. Blum's method (limit earth pressure)

Blum's method is a hand calculation method which has been used since 1931. Blum's method aims to determine the required embedment length of the sheet pile.

The main assumption of Blum's method is the limit earth pressure and Rankine's earth pressure model; the soil pressure is either calculated as minimum active or maximum passive earth pressure and thus only the plastic areas on the soil diagram are considered [25]. This results in the following soil pressure distribution (Figure 15). The embedment depth of the pile should be long enough to have a balance in horizontal forces and bending moment [12]. Blum's method is an analytical method schematizing a statically undetermined structure into a statically determined structure. The passive soil resistance acts as a support in the soil. The passive soil resistance and the anchor are simulated as supports for the sheet pile, which is then simulated as a beam on these supports. Blum's method is not accurate for determining the deformations of the sheet pile and soil. [25]

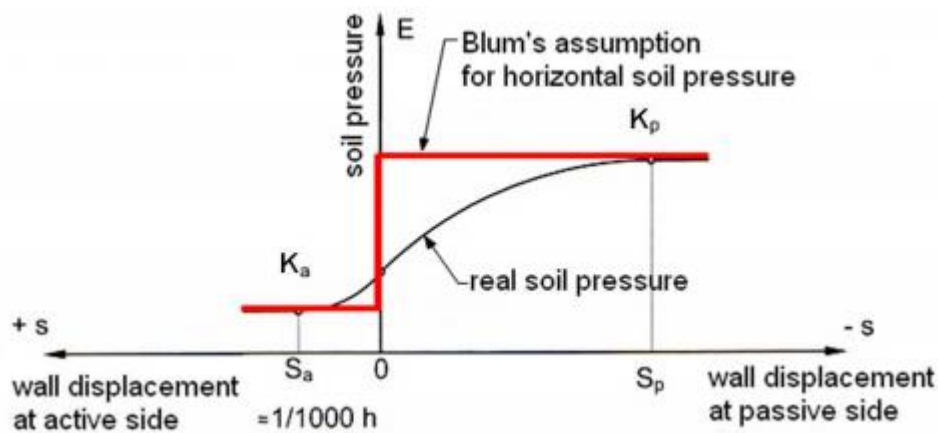


Figure 15: Blum's method: soil pressure [12]

The method of Blum for single-anchored sheet piles is schematized according to the following manner (Figure 16):

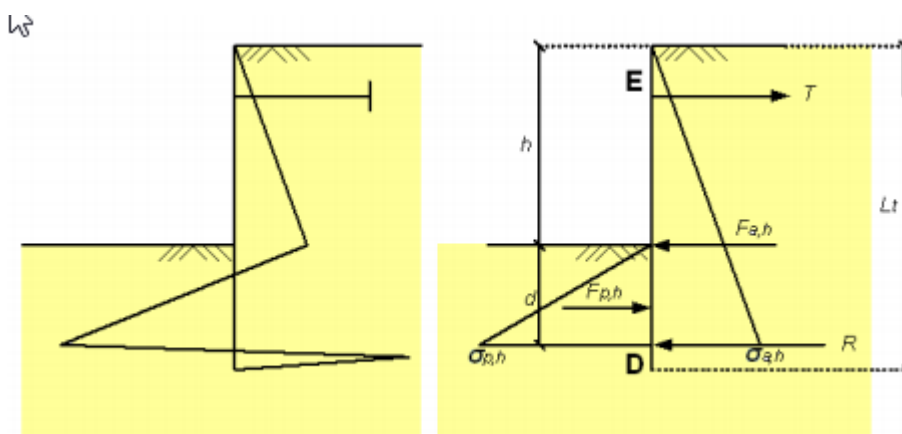


Figure 16: Blum's schematization [12]

The principal of Blum's method is a sheet pile clamped at the toe, but with a bending moment of zero at the toe of the sheet pile and a shear force R. The shear force R simulates the soil pressure on the sheet pile beneath R. To ensure that this shear force can actually occur, the computed embedded depth should be increased by 20%. There are now 3 unknowns: T

(anchor force), R (substitute force which simulates the horizontal soil pressure), and d (embedded depth). To be able to solve the problem, an additional criteria is needed. Therefore, the displacement at the location of the anchor is set to zero. The equilibrium equations for solving the unknowns T, R and d are then: zero displacement at location of the anchor, zero bending moment at the toe of the sheet pile (point D) and horizontal force equilibrium [12].

Blum's method does not take into account the earth pressure redistribution of the soil such as the arching effect of the soil. To account for redistribution, it is allowed to reduce the active effective earth pressure by 33% and increase the anchor force by 15%. This is only true for sheet piles driven in the soil, and may not be applied to sheet piles which are backfilled. [12], [25]

Blum's method uses the fixed earth support method with the following characteristics: flexible sheet pile and fixed at the toe. This method requires a large penetration depth.

Assumptions are:

- Pile embedded deep, no deflection or angle/rotation at the base. There is an inflection point in the sheet pile.
- Inflection point: change in curvature, zero moment at inflection points.

Blum's method is used for preliminary calculations estimating the embedded depth and sheet pile properties, but is not able to take into account the following phenomena:

- Deformation of soil and sheet pile
- Pre-tensioning of anchors
- Constructions with more than one anchor
- Different construction phases
- Overconsolidation

A very important disadvantages are the inaccurate deformations resulting from Blum's method. [7]

2.4.5. Subgrade reaction model (spring model)

The subgrade reaction model is a spring supported beam method. This spring supported beam method had originally been derived by Winkler for beams elastically supported on soil to simulate a train rails. Therefore a beam on an elastic foundation is also called a Winkler spring beam.

The subgrade reaction model is a spring supported beam method, which simulates the soil with many discrete spring (Figure 17). The sheet pile is modelled as a beam with a unit width. The basic differential equation for the Winkler beam spring model is given in equation 29:

$$EI \frac{d^4 w}{dx^4} + k(x, w) \cdot w = f(x) \quad (29)$$

The general assumptions for the beam theory are applicable. The assumptions are:

- Euler-Bernoulli: 'plane cross sections remain planar and normal to the beam axis in a beam subjected to bending' [26]
- Hooke's law: $\sigma = E \epsilon$
- Normal forces are small and do not contribute to the displacement
- Angular displacements are small
- Springs are uncoupled

This equation exists of three parts:

$EI \frac{d^4w}{dx^4} \sim$ rigidity of the beam

$k(x) \cdot w \sim$ elastic foundation / soil reaction (earth springs)

$f(x) \sim$ external loads (for example: external line loads, water pressure, initial anchor force..)

The strain of the subsoil determines the soil pressure. Springs do not interact and therefore nonlinear behaviour such as arching is not included in this model. The springs in the subgrade reaction model can be active, passive and neutral. The characteristic for each spring based on soil as an elastoplastic material is given by Figure 18. A transition area between fully active and fully passive earth pressure is considered with a linear relation between stress and displacement between the plastic zones.

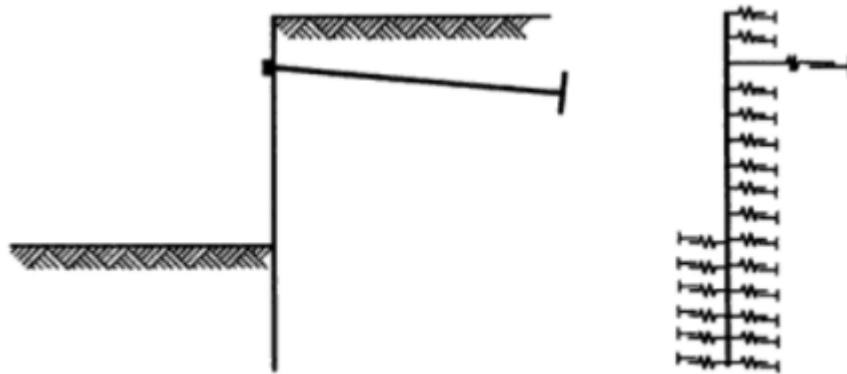


Figure 17: subgrade reaction model

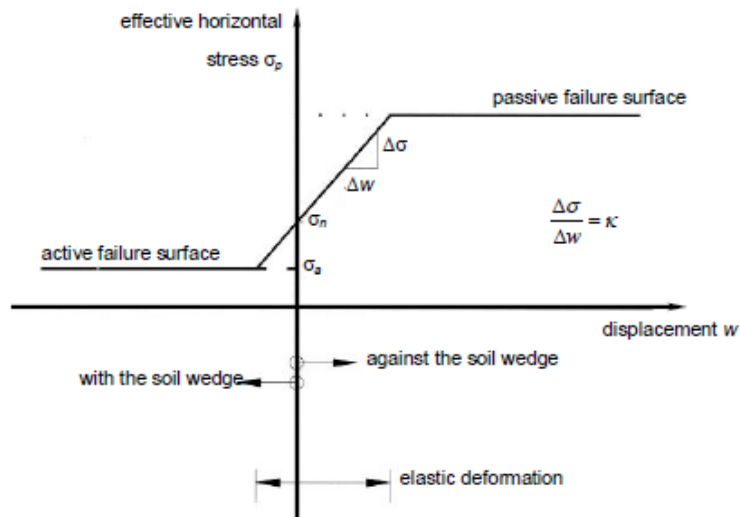


Figure 18: bilinear spring characteristic; stress deformation diagram soil [24]

When the sheet pile moves away from the soil, the soil is in active state. The sheet pile moving towards the soil results in a passive soil pressure. In between $w_{pl;a}$ and $w_{pl;p}$ the soil is assumed to behave linear with stiffness k (also indicated as k_h), which is known as the Winkler spring constant, horizontal modulus of subgrade reaction or subgrade modulus (dimensions: force / area / displacement; FL^{-3}). The methods to derive k_h are elaborated in chapter 2.4.3. The general spring model with stress-deformation properties is given in Figure 18. The values for

σ'_a , σ'_p and σ'_n can be determined by applying one of the earth pressure theories described in chapter 2.4.2 and have to be calculated for every spring. For a certain depth z with the earth pressure coefficients the passive, active and neutral earth pressure can be calculated. With the horizontal modulus of subgrade reaction the displacements $w_{pl;a}$ and $w_{pl;p}$ can be calculated and each spring can be assigned its spring characteristics.

The horizontal earth pressure is thus given in the spring characteristic and depending on the deformation of the sheet pile. Depending on the displacement, the earth pressure has thus a value between the active and the passive earth pressure. When the sheet pile moves against the soil equation 30 is applicable:

$$\sigma'_h = \sigma'_n + k_h w \leq \sigma'_p \quad (30)$$

And when the soil moves from the soil equation 31 is applicable (with the soil wedge; Figure 18):

$$\sigma'_h = \sigma'_n - k_h w \geq \sigma'_a \quad (31)$$

The spring supported simple beam method has the following characteristics:

- User friendly
- Simple schematization of soil pressure
- Soil-structure interaction on front wall
- Not applicable for complex quay walls, for example with relieving platform, or inclined quay walls
- Short calculation time
- Construction stages, pre-tensioning of anchors, over consolidation and multi-layered soil can be accounted for.
- The deformations of both soil and sheet pile are considered

The spring model gives an accurate estimation of the displacement and deformation of the wall, shear force distribution, bending moment distribution and anchor force(s). However, the soil movements are not accurately estimated. Therefore, this model cannot be used for determining the influence of soil movement on adjacent buildings.

[7], [22], [24],[27], [28],[16]

Calculation procedure

The spring model is applied for 2D calculations. The sheet pile is considered as a beam with the stiffness and strength properties of the sheet pile for a unit width. The springs are assigned the characteristics of the soil and the characteristics are thus also depending on the depth. Due to the soil pressure simulated by the springs and the stiffness of the sheet pile, deformations occur. Due to these deformations the soil pressure changes to a more active or more passive soil pressure, depending on whether the sheet pile moves away from the soil or towards the soil. By adjusting the soil pressure, calculating the new deformation and repeating this eventually the soil pressure on the sheet pile can be calculated. The soil pressure and deformation are found when the earth pressure simulated by the springs corresponds with the displacements and vice versa. This iterative calculation procedure is given in Figure 19.

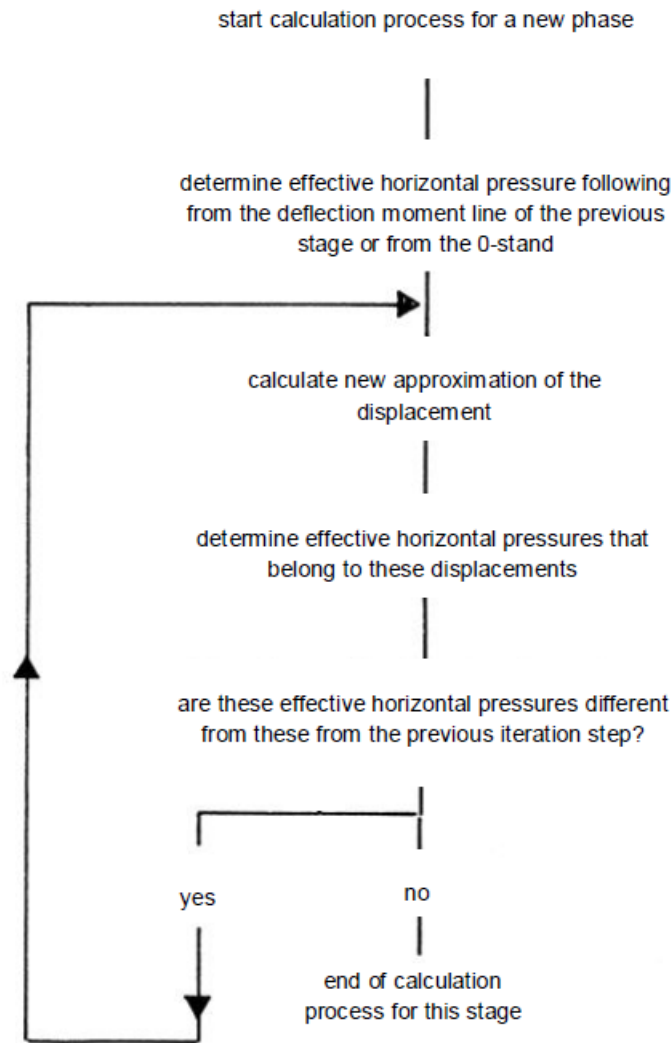


Figure 19: calculation procedure spring model [24]

[7], [22], [24]

D-sheetpiling

The software D-sheetpiling uses the subgrade reaction model. For D-sheetpiling also the calculation method for finding the earth pressure can be chosen. D-sheetpiling offers the options of inserting the earth pressure coefficients manually or calculating them by Müller-Breslau or Kötter. [12]

The structural resistance checks included in this approach are checking of the bending moment, shear force, normal force and deformations. [27]

Construction stages

The spring model is able to take into account different construction stages and including the history of the sheet pile with respect earlier construction stages. To change construction stages, the spring characteristics are updated for the new situation. For filling the soil, the change in the spring characteristics is drawn in Figure 20. For excavating similar approach is used, but the spring characteristic moves down with $\Delta\sigma$.

It is assumed that the increase in earth pressure due to filling of the soil (or the decrease in earth pressure due to excavating of the soil) is equal to the difference in neutral earth pressure before and after excavating as given in equation 32:

$$\Delta\sigma = \sigma_h^* - \sigma_h = K_0\Delta\sigma_v \quad (32)$$

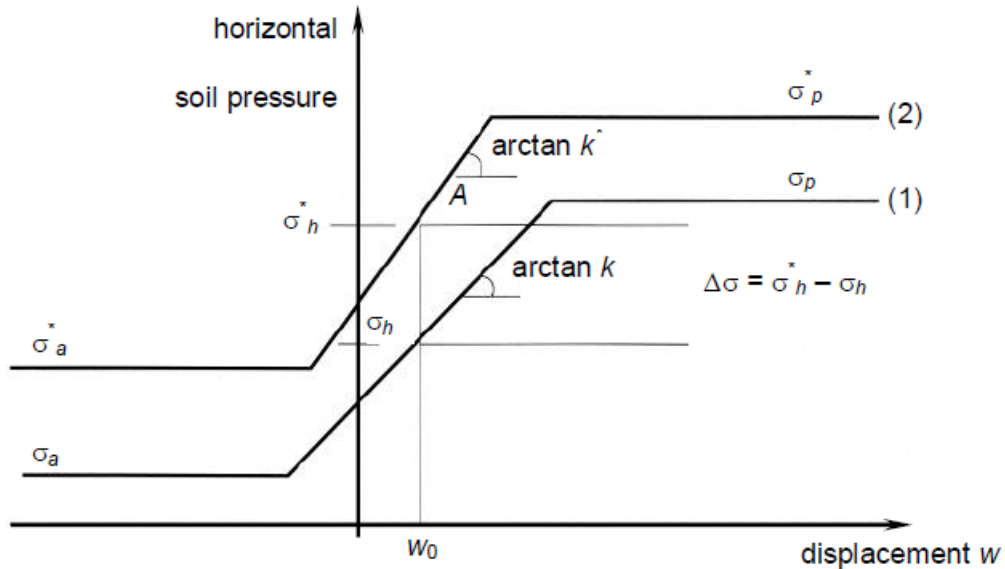


Figure 20: Alternation spring characteristic for filling soil [24]

The new horizontal earth pressures can be calculated with the new horizontal modulus of subgrade reaction: k^* and w_0 , the original wall displacement before filling or excavating. The horizontal modulus of subgrade reaction only changes due to the following:

- Arching effect
- Presence of a slope
- During excavation, the subgrade reaction modulus is slightly reduced. This effect is very small and therefore generally neglected, also by software such as D-sheetpiling.

Assuming a constant horizontal modulus of subgrade reaction, the new spring characteristics are calculated. This method is used for the numerical model as described in chapter 4. [7], [22], [24]

Dutch spring characteristic

For the Dutch soils, the spring characteristic is defined multilinear. This is already shortly described in chapter 2.4.3. The elastic range of the spring model is divided into 3 parts with different stiffnesses (horizontal modulus of subgrade reaction): $k_{h,1}$, $k_{h,2}$, $k_{h,3}$ (Figure 21). The stiffnesses are given by CUR 166, based on experimental data. These are discussed in chapter 2.4.3, Figure 13.

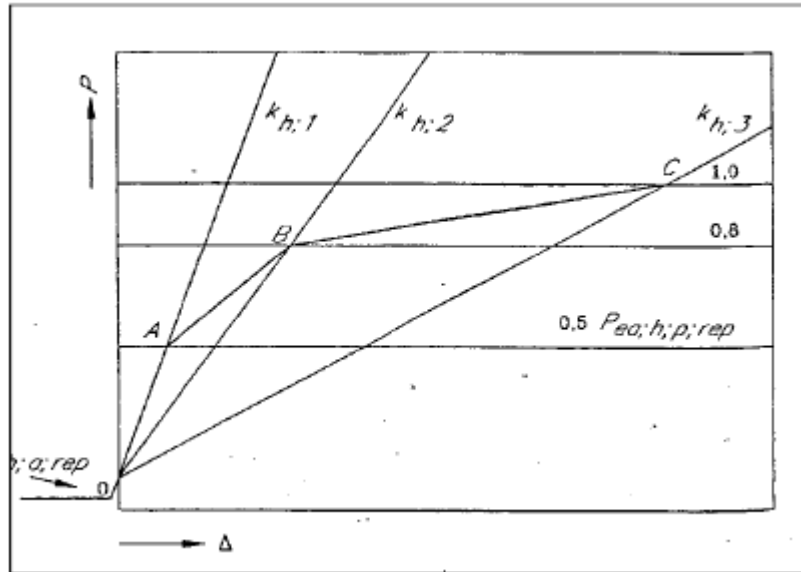


Figure 21: Dutch spring characteristic [24]

[7], [22], [24]

2.4.6. Finite element method

Earth retaining walls with sheet piles can also be modelled using finite element software. The finite element model has the following characteristics:

- Complicated (not user friendly)
- Soil and structure are calculated more accurately (interaction taken into account as well)
- Different design verifications possible with one model
- More complex designs of quay walls are possible to calculate

In a finite element analysis, the properties of the soil are calculated by using the relation between the stress and the displacement. The finite element method can also perform 3D calculations and dynamic loads.

The different constitutive models for the soil in the finite element method are:

- Mohr-Coulomb: the Mohr-coulomb models considers soil behaviour from linear-elastic to perfectly plastic. This model is mostly used for first analysis.
- Hardening Soil Model: This model uses also the Mohr-Coulomb failure criteria, but the soil stiffness is extended with shear and compression hardening and the stress-dependency of the stiffness modulus. It can also take into account pre-consolidation and the unloading and reloading behaviour. This model is mostly used for the calculation of retaining structures.
- Hardening Soil Small Strain model: This model is an extension of the hardening soil model. It takes into account increased stiffness at small strains. This is also used for retaining structures.
- Soft Soil Creep Model: this model takes into account creep behaviour of the soil, which is mainly of importance for soft soils. This model should be used when time dependent behaviour is dominant. This is mainly when soft soils are present.

[27]

The finite element method is able to not only calculate the movement of the sheet pile, but also the movements in the soil near the sheet pile and in front or behind the sheet pile wall. Therefore, the finite element method is primarily used for studying the soil deformation which could influence objects near the retaining wall, for example adjacent buildings. Also, for expensive sheet pile walls the finite element method is of interest. Since the finite element method takes can take into account arching and soil-structure interaction, a better and optimal design can be made. Finally, for situations where the assumptions for the spring model and Blum model are not applicable to the situation, a finite element model is made. [7], [24]

2.5. Plastic design

There are different methods to describe the plastic design of steel sheet piles regarding the geotechnical behaviour. The classical methods are: Brinch-Hansen, Windels and Weißenbach. Blum’s method is generally not used for plastic design. However, Blum’s method is used for plastic design by Kort (2002) and this is also discussed. These methods assume that the plastic rotation capacity of the steel sheet pile is unlimited. However this is not reality since the rotation capacity is depending on the web and flange slenderness. The theory of the rotation capacity of steel sheet piles is explained in chapter 3.2 [23].

2.5.1. Blum’s method for plastic design

Blum’s method is hand calculation method for designing a sheet pile retaining wall. This is explained in more detail in chapter 2.4.4. Blum’s method is explained for plastic design by Kort (2002). The assumptions are an infinitely stiff wall with zero to a maximum of 2 plastic hinges. The concentrated force simulating the earth pressure jump is not applied in this example.

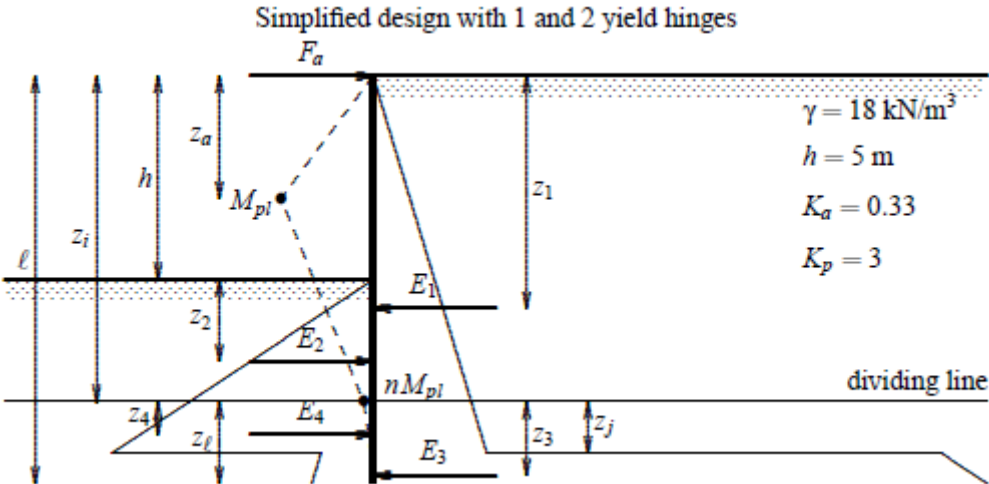


Figure 22: Blum’s sheet pile wall theory [23]

According to Figure 22, the plastic moment occurs in the graph at a depth of z_a . The fixity in the ground is indicated by the symbol n , for which $n=0$ is a free earth support and $n=1$ is a fully fixed earth support. The assumed wall movement is shown with a dashed line. The choice of the wall movement indicated a plastic hinge at z_a and a fixed moment at z_i . To create a fixity at z_i , the sheet pile in reality must be longer than length z_i , because the bending moment at the toe of the sheet pile must be zero. The earth pressure distribution can be derived from the wall movement. At z_j a jump between passive and active earth pressure is shown, known as the earth pressure jump. At the plastic hinge the shear force equal zero. Therefore, the jump between passive and active earth pressure is always located beneath the second plastic hinge. By equilibrium equations the length of the sheet pile, the location of the plastic bending moment z_a , the anchor force and the occurring bending moment can be calculated.

2.5.2. Brinch Hansen

The Brinch Hansen method is also known as the Danish method. The Brinch-Hansen method differs from the Blum method. Brinch-Hansen's method is not based on Rankine's method, but based on the failure mechanism of the soil, which is determined with the chosen wall movement. Brinch Hansen assumes a rigid wall which rotates about one or more points. Within the wall, yield hinges can develop, but between the yield hinges the wall is rigid. The failure mechanisms possible in the Brinch-Hansen method are: line ruptures, zone ruptures and composite ruptures. Line rupture illustrates a failure in a thin plastic zone and zone rupture assumes the whole zone above the rupture line is in failure. Composite rupture combines line

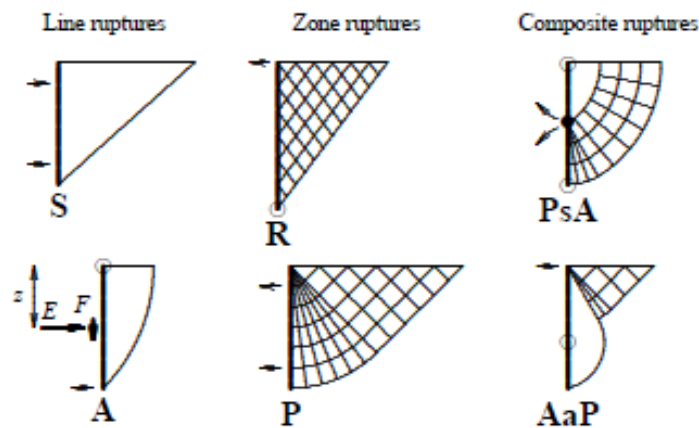


Figure 23: rupture figures Brinch Hansen [23]

rupture and zone rupture. The soil between the wall and the failure line is assumed to be rigid. These rupture figures are given in Figure 23. The hinges are illustrated with black dots and the rotation axis with open white dots. [23]

Based upon these rupture figures, the horizontal and vertical resulting earth pressure forces E and F and the location of these earth pressure z , are determined. The rupture figure is indicated by the designer and based upon the chosen wall movement. For a propped wall, the following wall movements are possible (Figure 24). Assumed is stable anchoring and the failure is depending on the penetration depth of the sheet pile wall.

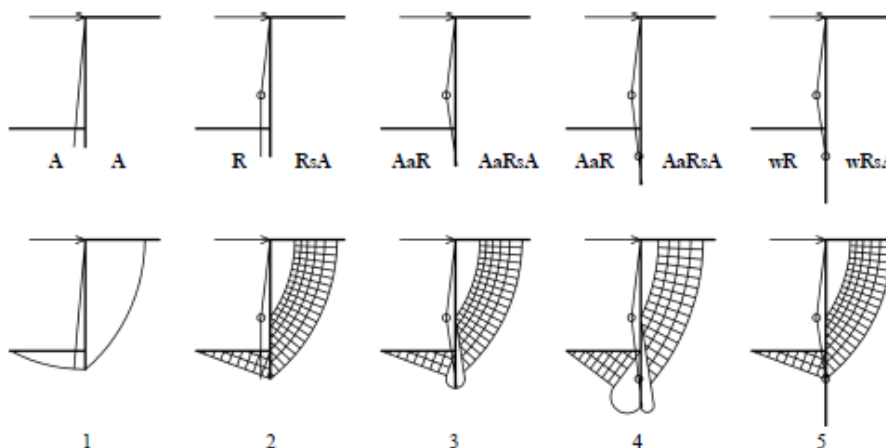


Figure 24: wall movements and rupture figures Brinch Hansen [23]

The wall displacements are shortly discussed. The walls are ordered for each number to have a longer penetration depth. For number 1, the wall rotates about the anchor and a free earth

support is considered. Number 2 consists thus of a slightly longer sheet pile which makes it possible to generate a plastic hinge at the location of the maximum bending moment. The earth pressure can be redistributed due to the longer sheet pile and therefore a combination of circular and Rankine's pressure zone is found. For number 3 the length of the sheet pile is long enough to result in a partially fixed sheet pile wall in the ground. The earth pressure can again redistribute which results in two circular rupture figures. Number 4 is able to generate a plastic moment at the location of the fixed bending moment. Increasing the length of the wall even more as done for number 5 does not influence the wall movement more. Determining the rupture figures and calculating the earth pressure is generally performed by computer programs. [23], [29]

2.5.3. Windels

Windels has developed a model based on pile supported on multiple levels. The extreme bending moments are located at the position of the struts and in the spans between two struts. According to the plasticity calculations in structural mechanics, in case the spans are loaded by a distributed load, the extreme bending moments are $M_{pl} = \frac{1}{16} \sigma l^2$. For sheet piles, the load is then equal to the average earth pressure between the spans. The lower part of the sheet pile is analysed with Blum's method. Again, due to earth pressure redistribution, the bending moment is reduced and the strut force increased. Windels approaches the cross section resistance of the sheet pile similar to the cross section resistance of a I-section, considering plastic bending and bending, shear force, normal force and bending and shear force interaction by von Mises and normal force and bending moment interaction. This however, does not take into account geometric instability, such as local buckling. [23]

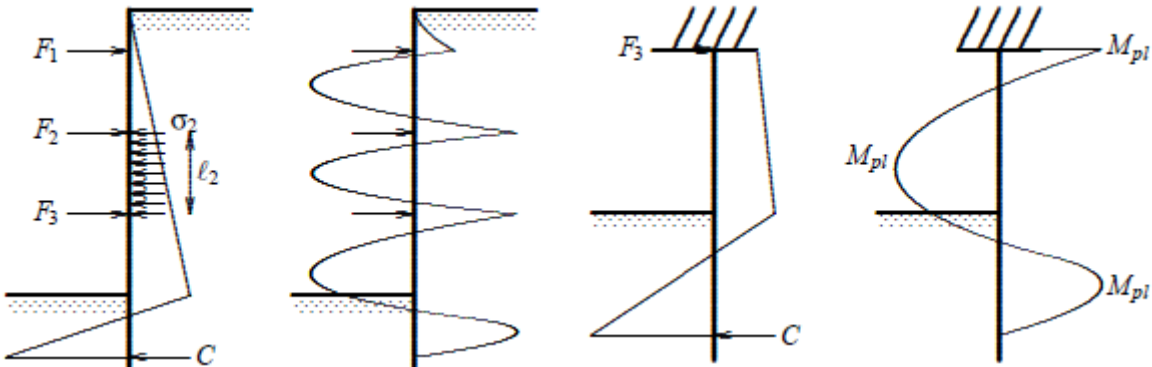


Figure 25: Windels' sheet pile wall theory [23]

2.5.4. Weißenbach

Weißenbach is based on Windels' theory. The difference between Windels' and Weißenbach's theory is the shape of the earth pressure. Windels assumes a different earth pressure distribution, which is shaped trapezoidal that takes into account the redistribution of earth pressure (Figure 26). Also, Windels take the geometrical instability of flange buckling into account. To prevent local buckling of the compression flange, the minimum thickness of the flange is prescribed:

$$\begin{aligned}
 f_y = 370 \text{ N/mm}^2 & \quad \rightarrow \quad t_f \geq \frac{b_f}{34} \\
 f_y = 520 \text{ N/mm}^2 & \quad \rightarrow \quad t_f \geq \frac{b_f}{28}
 \end{aligned}$$

In practice, many sheet pile types do not fulfil these requirements.

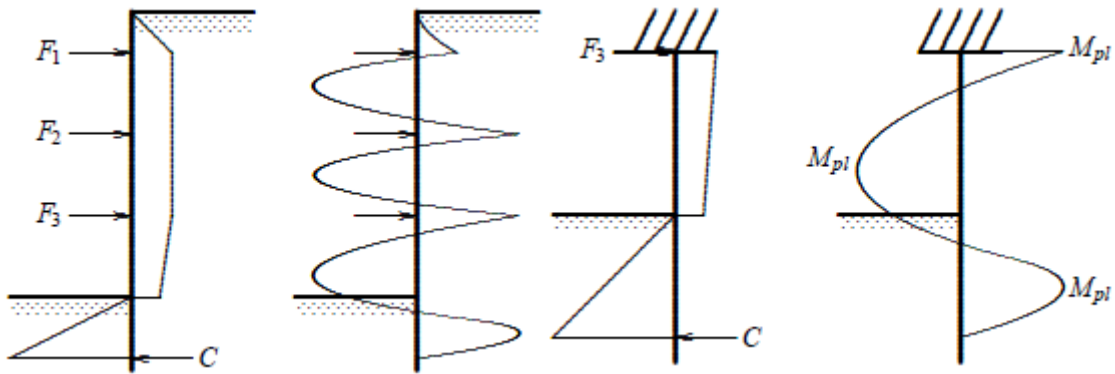


Figure 26: Weißenbach's sheet pile wall theory [23]

It is of importance to notice, that Weißenbach assumes for the given rules for the minimum flange thickness in relation to the flange width and steel grade, no geometrical instability occurs and unlimited rotation capacity is considered. However, in reality, this might not be the case and the rotational capacity can be limited. Therefore, for the rotation capacity and plastic design of steel sheet piles, more research is performed in the study of Sedlacek et al [30] and explained in chapter 3.2. [23]

2.6. Anchorage

The single-anchored sheet piles in quay walls are anchored near the top of the sheet pile. There are several options for connecting the anchor to the sheet pile wall: an anchor plate or a waling in front or behind the wall. These options are shown in EN 1993-1 part 5. The options are shown in Figure 27, Figure 28 and Figure 30.

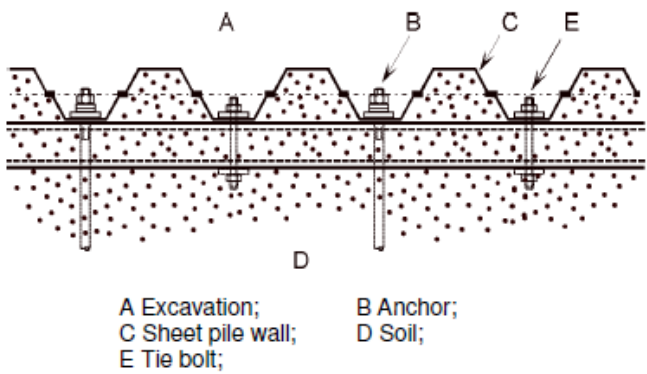


Figure 27: anchoring with waling behind sheet pile wall (EN 1993-1 part 5); not possible for underwater anchors [11]

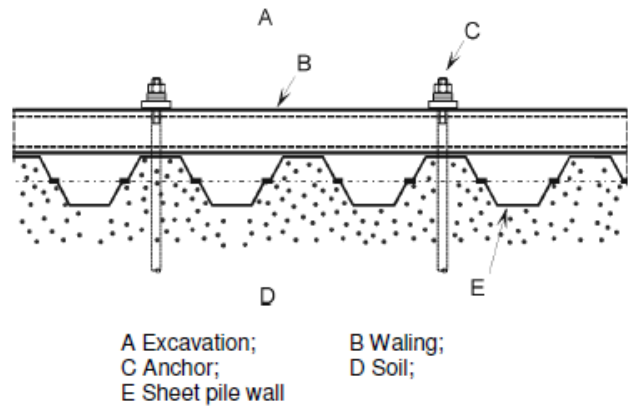


Figure 28: anchoring with waling in front of sheet pile wall [11]

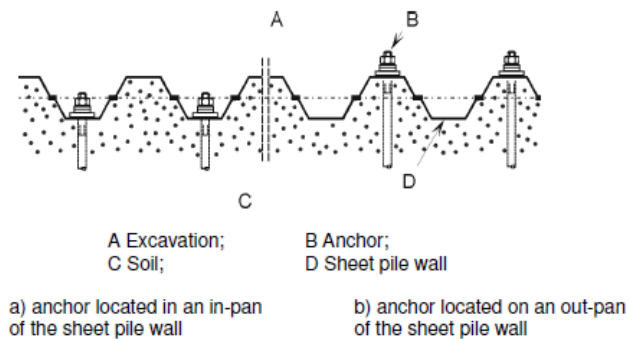


Figure 30: anchoring without waling (left: in-pan, right: out-pan) [11] (nen-en1993-1-5)

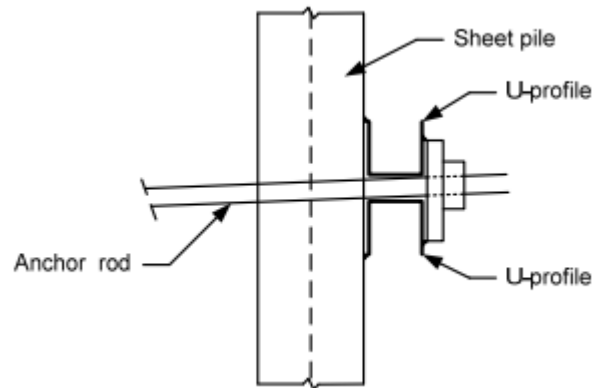


Figure 29: wale with anchor connected to sheet pile 5] (manual hydraulic structures)

For the procedure of reinforcing existing sheet pile walls with underwater anchors, the waling cannot be applied behind the wall (in the soil), since it is an existing sheet pile wall. An illustration of an waling to sheet pile connection with an anchor is given in Figure 29. Further details about the design calculation for these connection are given in Eurocode 3 – design of steel structures - part 5: piling. In CUR-publicatie 166, the anchor is verified. The components verified are the anchor rod, waling or anchor plate and grout body. CUR – publicatie 166 does not consider the behaviour of the sheet pile at the location of the connection.

Anchors can be assumed to be either completely rigid or flexible. A rigid anchor acts as a lateral support preventing any lateral deformation at all. Rotation is not prevented by an anchor. An anchor can also be more flexible. Then some movement at the location of the anchor is possible.

CUR 166 also gives an approach for modelling the anchor as a spring. The anchor is modelled as a spring with the characteristics of the rod: modulus of elasticity, cross sectional area, length of the anchor. The lower limit boundary is a zero force, so no compression can occur in the anchor. The upper limit boundary is the ultimate tension force of the anchor rod. The prestress force can be either included in the spring characteristics, or added as an horizontal force on the sheet pile wall at the location of the anchor. [24]

3. Structural failure mechanisms

Sheet piles in quay walls experience different type of loads: water pressure, soil pressure, anchor forces, terrain loads, crane loads etc. These loading types lead to internal forces in the steel sheet pile wall.

In the Netherlands, the guiding design rules for steel sheet piles are Eurocode 3 part 5: piling, CUR - publicatie 166 and Handbook of quay walls.

3.1. Existing structural failure mechanisms

The structural failure mechanisms are of interest to interpret the behaviour of the steel sheet pile.

3.1.1. Introduction

CUR - publicatie 166 and Handbook of quay walls both provide a fault tree. This fault tree provides the verifications to be carried out when designing a quay wall. Distinction is made between Ultimate Limit State (ULS) and Serviceability Limit State (SLS). The fault tree in handbook of quay walls is based on a quay wall with a superstructure, while the fault tree in CUR 166 is based on a single-anchored sheet pile. This fault tree is given in Figure 31.

In general, there are four failure mechanisms for quay walls:

- Failure of sheet pile
- Failure due to too high ground water flow
- Loss of stability
- Failure of anchorage system / support

[24], [31]

The structural failure of researched this thesis is yielding or failure of the profile of the steel sheet pile. This is included in the failure trees of CUR 166 and handbook of quay walls (Figure 32).

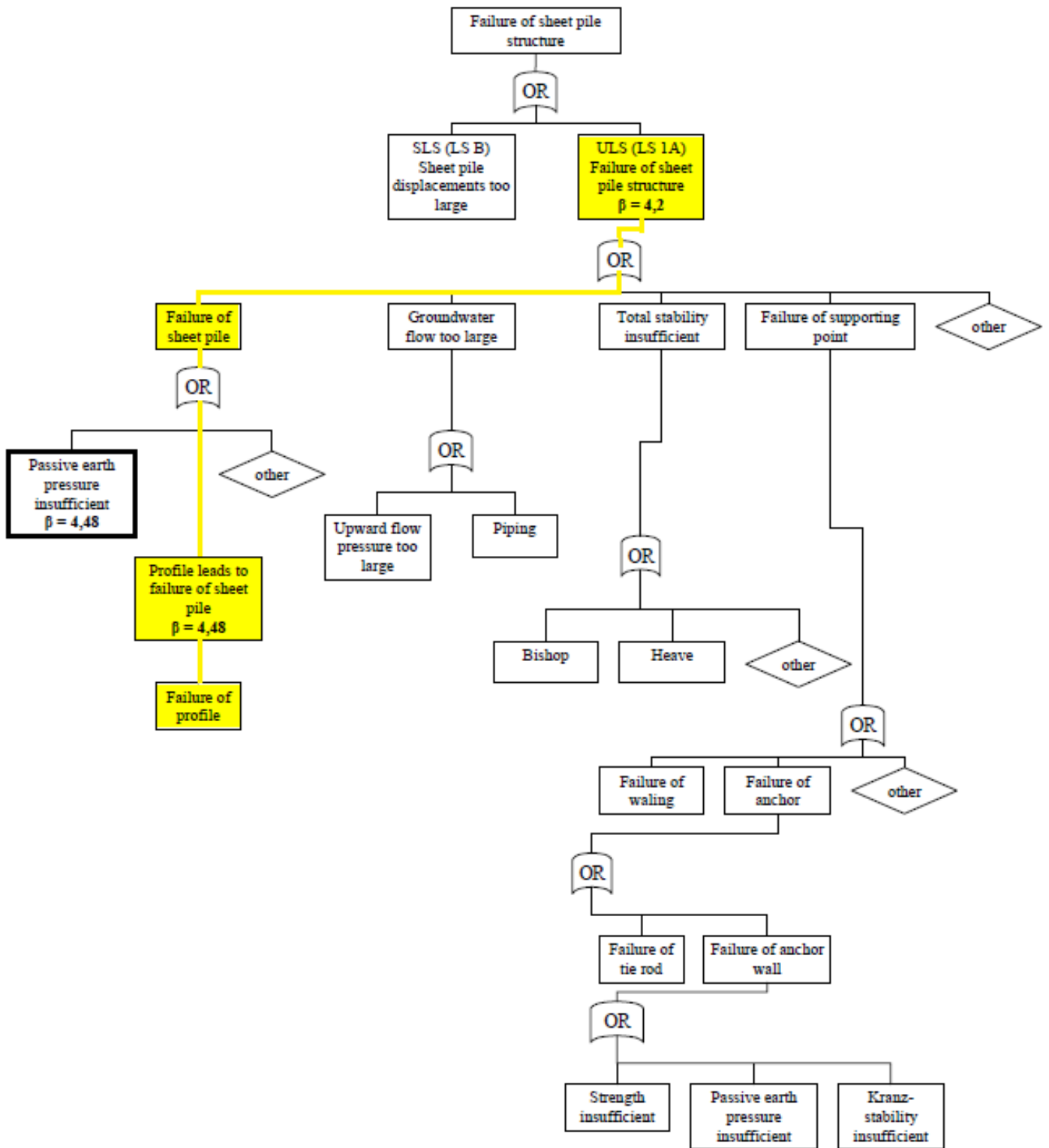


Figure 31: Fault tree CUR publication - 166 [24]

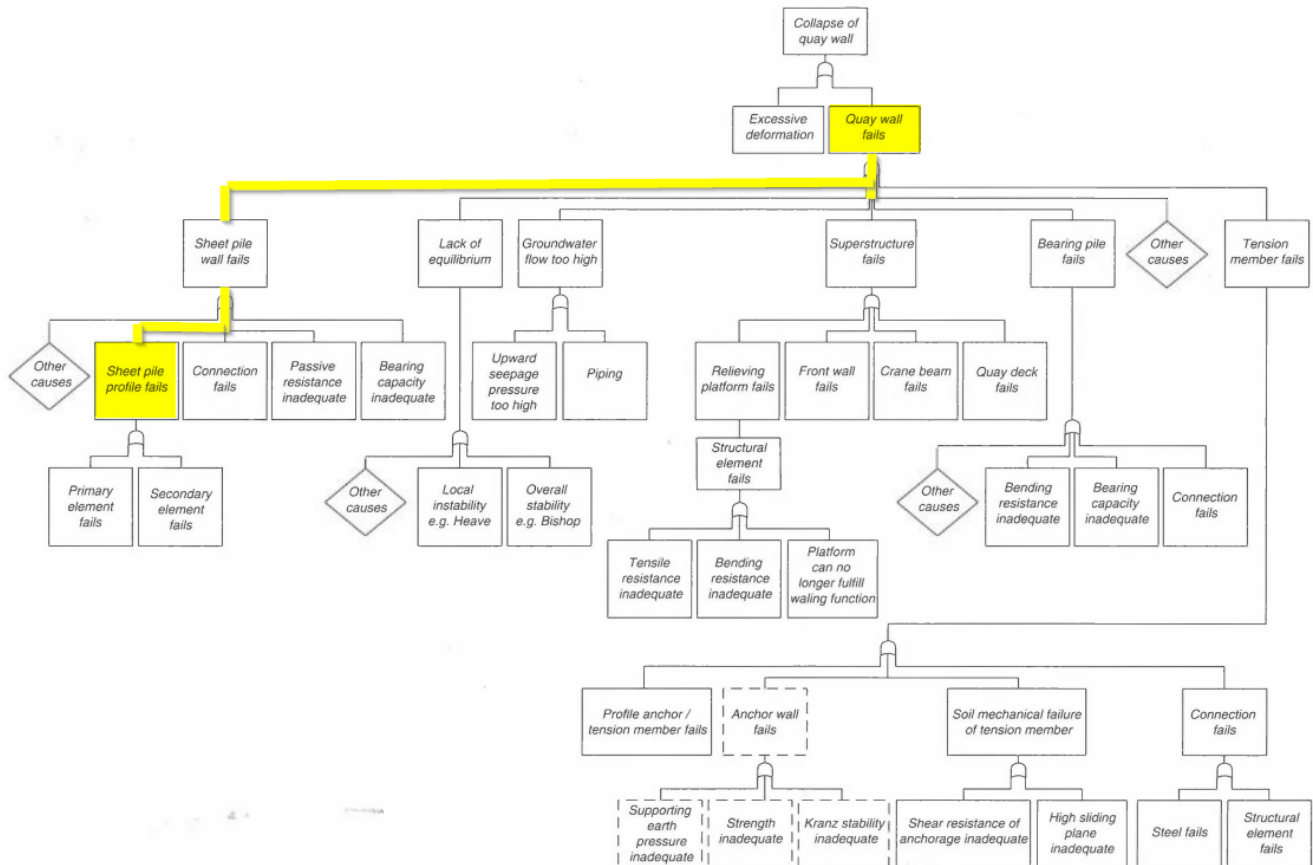


Figure 32: Fault tree handbook of quay walls [27]

The structural failure mechanisms of interest for structural failure are thus the sheet pile wall failure, specified as the profile failure. The failure mechanisms mentioned in Eurocode 3, part 5 are also subdivided in ultimate limit state and serviceability limit state criteria. This norm only includes structural failure of the steel sheet pile. Eurocode 3 part 5 divides the ultimate limit state criteria into the following:

- Soil failure resulting in failure of the structure
- Structural failure
- Combination of soil failure and structural failure

The structural failure for retaining walls can be subdivided into the following failure modes:

- Bending and/or axial force
- Overall flexural buckling
- Local buckling (due to bending)
- Local failure, at the location of the load application (of the anchor force)
- Fatigue

For the serviceability limit state of the retaining walls, the criteria are deformation limits:

- Limited deformation for the serviceability of the retaining wall
- Limited horizontal displacement, vertical settlements and vibrations for the serviceability of the structures near the retaining wall.

For the serviceability limit state an additional criteria is no plastic deformations and no yielding will occur at the serviceability loading, or it has to be shown that it will not lead to an ULS. The difference in SLS and ULS is shown in Figure 33.

[32]

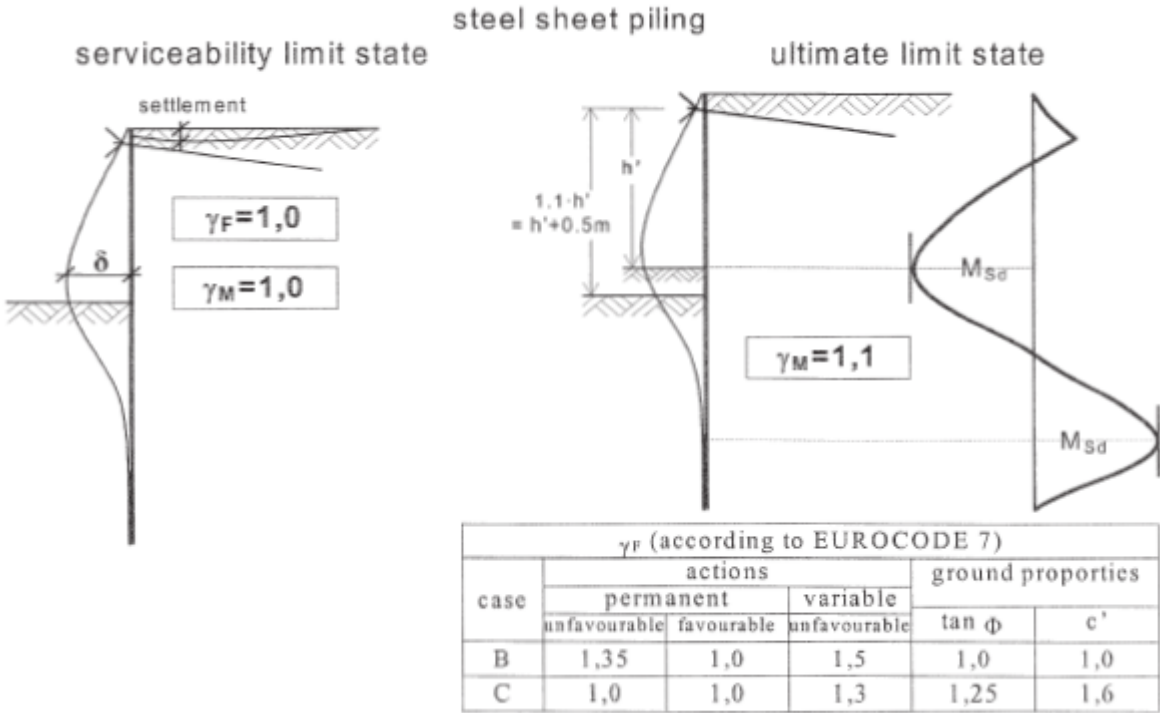


Figure 33: SLS and ULS [30]

3.1.2. Global failure mechanisms

The global failure mechanisms for the ultimate limit state are thus bending and / or axial force, overall flexural buckling and fatigue. Since this thesis focuses on the bending failure, flexural buckling and fatigue are not further discussed.

Bending failure

The bending moment capacity is very important verification for sheet piles, since sheet piles are mainly loaded in bending due to earth and water pressure. For bending failure, nowadays not only the elastic bending moment capacity is used, but based on the cross section classification, plastic bending moment capacity can be used.

The behaviour of a sheet pile is studied by Sedlacek et all (2001) by a 4-point bending test. It is found that the bending moment can also influence local behaviour, such as local buckling in the flange due to bending. For the relation between elastic and plastic capacity of a steel sheet pile it was found that the plastic cross-section capacity is approximately 15% more than the elastic cross-section capacity (equation 33):

$$W_{pl} \approx 1,15W_{el} \tag{33}$$

However the plastic capacity is also related to the rotation capacity and cross section classification. This is further discussed in chapter 3.2 .

The bending capacity is influenced by the occurring shear force and/ or axial force at the same position.

If no shear or axial force is available, the failure criteria is given in equation 34:

$$M_{Ed} \leq M_{c;Rd} \quad (34)$$

The bending moment capacity is also depending on the type of sheet pile: U-shaped profile or Z-shaped profile. The shear resistance of the interlocks influence the bending moment capacity of the sheet pile. This is in the current design verifications included by the factor β_B . For Z- sheet piles, and triple U-piles, there is no reduction due to a possible lack of shear force transmission. For single and double U-piles a possible the bending moment resistance is reduced. The phenomena causing this reduction factor is called oblique bending. This is further discussed in chapter 3.3.

The design verifications of the bending moment are based on analytical model and tests. The design rules for the bending moment depend thus on the cross section classification, which determines the plastic or elastic resistance, the phenomena oblique bending and the interaction with shear force and axial force. [30], [32]

Shear force resistance (webs)

The webs of the sheet piles should be designed such that the shear force does not exceed the shear force resistance. This procedure is similar to the verification of shear resistance of I-shaped girders, as prescribed in EN 1993-1-1. The verification is given in equation 35-37:

$$V_{Ed} \leq V_{pl;Rd} \quad (35)$$

$$V_{pl;Rd} = \frac{A_v \cdot f_y}{\sqrt{3} \cdot \gamma_{M0}} \quad (36)$$

With:

$$A_v = t_w (h - t_f) \quad (37)$$

Besides the shear force resistance verification, also shear buckling has to be considered. The shear buckling is obtained by first calculating the slenderness for the web. Then the procedure of EN 1993-1-1 for shear buckling can be used to determine whether the shear buckling resistance is larger than the shear force in the web [32]. Generally, the shear force verification is not governing in the design of a sheet pile.

The interlocks influence the shear resistance as well. This is discussed in the next chapter (chapter 3.3).

Interaction bending moment and shear force

The shear force and bending moment can interact. When exceeding 50% of the plastic resistance limit of the sheet pile, the bending moment capacity reduces [32]. For the combination of shear force and bending moment, the VON MISES yield criterion is applicable (equation 38).

$$\sigma_1^2 + 3\tau^2 = f_y^2 \quad (38)$$

From this criteria, the bending moment and shear force interaction can be derived. Rewriting this formula to obtain the reduced yield stress results in equation 39:

$$f_{y;v} = f_y \cdot \sqrt{1 - \frac{3\tau^2}{f_y^2}} \quad (39)$$

The formula for the reduces plastic moment resistance is then proposed by Heyman and Dutton (equation 40):

$$M_{pl;V} = M_{pl} - W_{pl;V} \cdot f_y \cdot \left(1 - \sqrt{1 - \left(\frac{V}{V_{pl}}\right)^2}\right) \tag{40}$$

[30]

The bending moment – shear force interaction formula from Heyman and Dutton (equation 40) is shown in Figure 34.

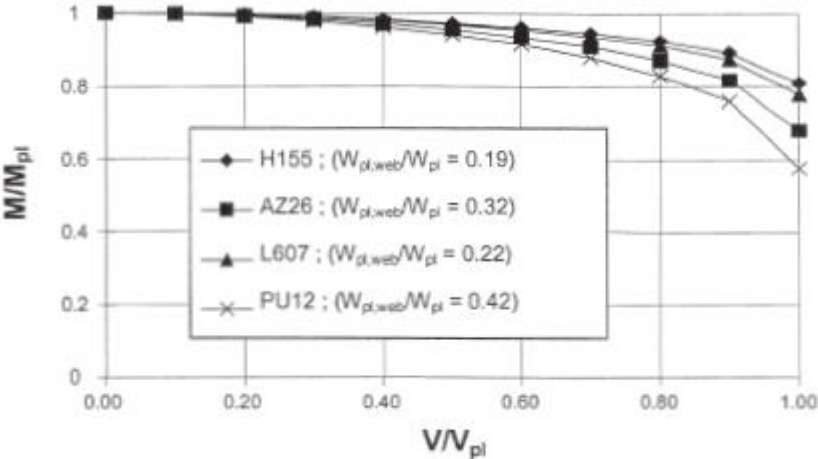


Figure 34: M-V interaction of steel sheet profiles according to Heyman and Dutton [30]

For shear forces under the 50%, the M-V (shear fore – bending moment) interaction is neglected. The interaction formula is still safe sided, since the hardening of steel is neglected in this model. [30]

The Eurocode 3 part 5 also considers a reduction of the bending moment resistance due to shear force. A reduction is applied similar to the reduction for I-girders in Eurocode 1993-1-1 (equation 41):

$$M_{pl;V} = M_{pl} - \left(\frac{2 \cdot V}{V_{pl}} - 1\right)^2 * M_{pl;web} \tag{41}$$

The interaction formula propose by Heyman and Dutton is compared to the interaction formula of Eurocode 3 part 1.1. The differences are mostly smaller than 5%. For cross sections with a large web to total area ratio, the difference can increase to 10%. (Figure 35) [30]

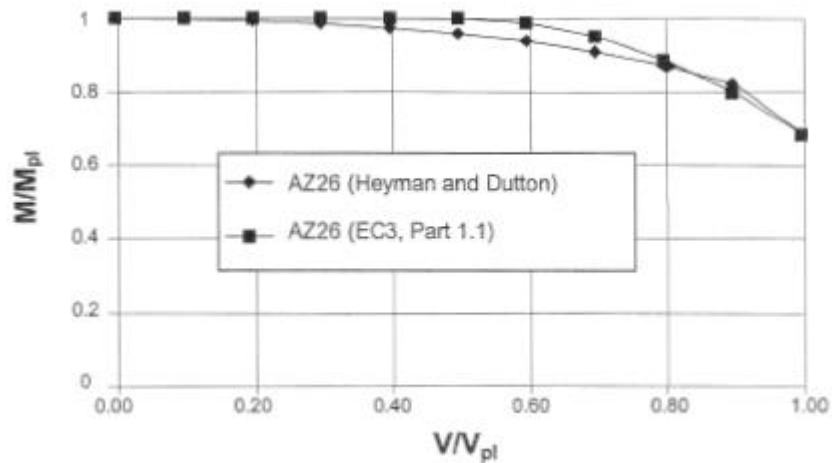


Figure 35: comparison interaction formulas Eurocode and Heyman and Dutton [30]

The bending moment - shear force interaction formula for sheet piles given in Eurocode 3 part 5 is equal to the bending moment-shear force interaction of EC 3 part 1.1 which is given as an alternative of calculating the bending moment – shear force interaction resistance for I profiles with identical flanges and bending around the strong axis. The bending moment-shear force interaction formula is given in equation 42 and 43.

$$\rho = \left(\frac{2V_{Ed}}{V_{pl,Rd}} - 1 \right)^2 \quad (42)$$

$$M_{V,Rd} = \left[\beta_B W_{pl} - \frac{\rho A_v^2}{4t_w \sin \alpha_{web}} \right] \frac{f_y}{\gamma_{M0}} \quad (43)$$

[30], [32]

3.1.3. Local failure mechanism: connection anchor

Local failure is verified for sheet piles at the connection of the anchor by an anchor plate or waling to the sheet pile. The anchor plate or waling introduce local forces in the sheet pile. Besides the local introduction force of the anchor, there is also the local force in combination with the global bending moment which should be considered.

Anchor plate

The formula for these connections are based on test results and analytical formula. However, phenomena such as the vertical component of the anchor force, and the hole for the anchorage, are not included in these tests and design formula. The test set-up is given in Figure 36.

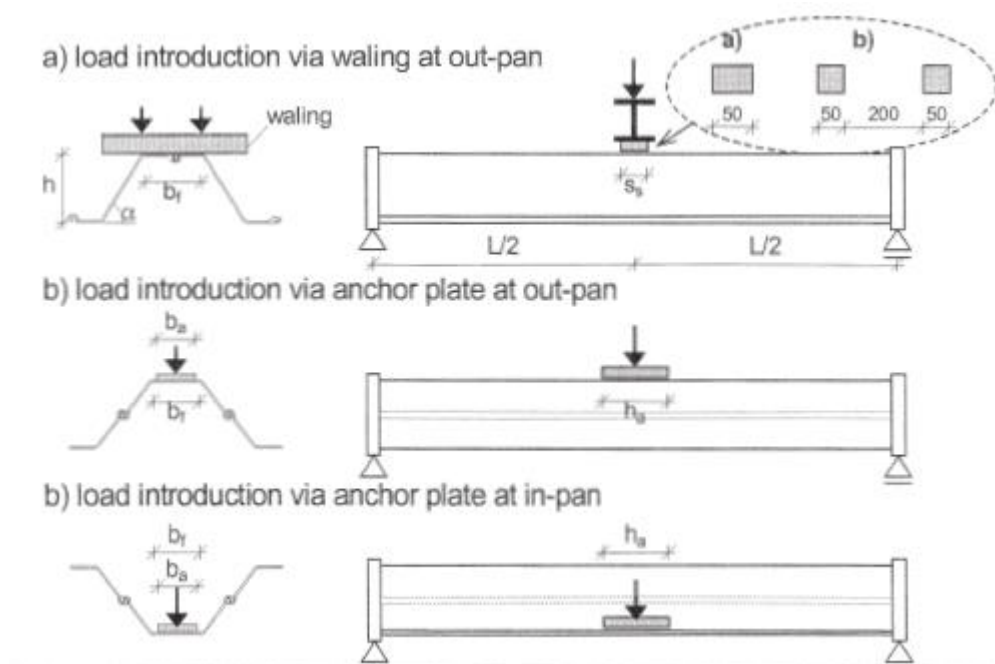


Figure 36: Test set-up for anchor force introduction

The connection of the anchor plate to the sheet pile is governed by a yield mechanism in the flange or the maximum tension resistance in the webs. To prevent a yield mechanism occurring in the flange, a ratio of b_a (anchor plate) to b_f (flange width) ≥ 0.8 is prescribed. Then the design is governed by the tension resistance in the webs and local shear force design check:

The local shear force design check (equation 44):

$$F_{sd} \leq F_{s;Rd}$$

$$F_s = 2 (h_a + b_a) * t_f * \frac{f_y}{\sqrt{3}} \quad (44)$$

The local tension force design check (equation 45):

$$F_{sd} \leq F_{t;Rd}$$

$$F_t = 2 * l * t_w * f_y ; l = h_a \quad (45)$$

F_{sd} is the force introduced via the anchor or waling bolt. [30]

Waling

For the load introduction via a waling, there are three main phenomena determined to influence the capacity for the local force introduction:

- Buckling failure of the webs
- Bending failure of the webs; the radius of the corner between the web and flange causes an eccentric load
- Interaction of local failure (the above mentioned buckling and bending failure) and global bending

Tests, finite element modelling and design formula based on the design formulas of Lagerqvist are considered. Lagerqvist gives design formula for concentrated loads in webs of welded and hot rolled beams. Lagerqvist proposed for the resistance of the web against compression load.

The corner radius also has influence on the local force introduction. The list of equations prescribed to calculate the maximum buckling force of the web can be found in Eurocode 3 part 5 ([32]). [30]

3.2. Plastic design for bending moment capacity

Steel can take stresses up to the yield stress, without showing permanent deformation. The capacity of the steel above the yield stress can be used, however, then permanent deformation will occur.

3.2.1. Plastic behaviour in steel sheet piles

Plastic bending of sheet piles has been introduced to fully optimize the available steel in the cross section. The available plastic capacity depends on the rotation capacity of the cross section. The definition of the rotation angle is given in Figure 37 [32]. The calculation of the resistance of steel sheet piles is a limit state design approach. Important aspects of the limit state design principles are whether the plastic hinges in the steel sheet pile are safe and whether the plastic deformation is not exceeding the limits. The plasticity is only allowed in ULS and not in SLS. The plastic bending moment capacity is in general approximately 15% higher than the elastic bending moment capacity. [30], [33].

Plastic bending moment capacity and rotation capacity

The plastic bending moment capacity is when the full cross section is yielding (f_y), while the elastic bending moment capacity is identified as when the outer fibres start yielding. Due to hardening, it is possible for the cross section to have an even higher bending moment capacity than M_{pl} . However, increasing the rotation even more, will lead to local buckling in the cross section's compression zone at the location of the maximum bending moment and a reduction of the resistance up to zero. For calculations, it is assumed that the plastic rotation does not lead to hardening, and thus no increase above the plastic moment capacity is included. The rotation capacity of the sheet piles depend on the cross section classification, explained below. [33]

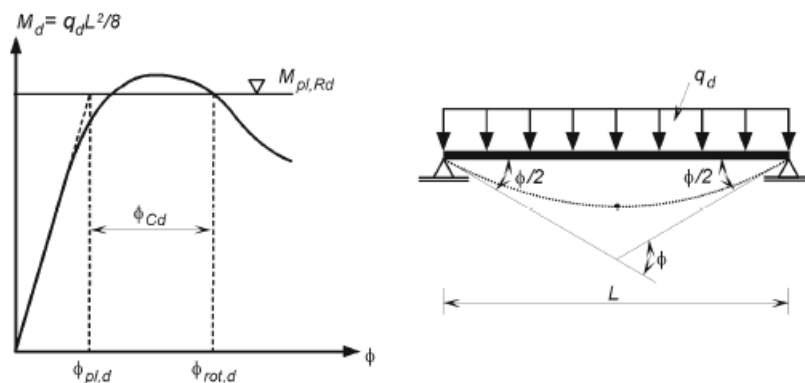


Figure 37: Definition of rotation angle (Eurocode 3 part 5) [32]

Cross section classification

The cross section classification depends on the rotation capacity of the cross section. Similar to EN 1993-1-1, the cross sections are classified into 4 classes. These cross section classes are identified by the web-slenderness. The bending moment-rotation diagram for the four different cross-section classes is shown in Figure 38. The four cross section classes are:

1. Cross section class 1: cross section class 1 has sufficient rotation capacity to resist the plastic bending moment capacity of the cross-section in plastic design.
2. Cross section class 2: cross section class 2 is able to resist the plastic bending moment capacity of the cross-section in elastic design.

3. Cross section class 3: in cross section class 3, it is not allowed to calculate with the plastic resistance. The elastic bending moment capacity of the cross-section is the resistance of the cross section. This since only partial plastification can occur, and then buckling will occur.
4. Cross section class 4: the elastic moment is not reached for cross section class 4, due to local buckling which occurs in the elastic range.

[27], [34]

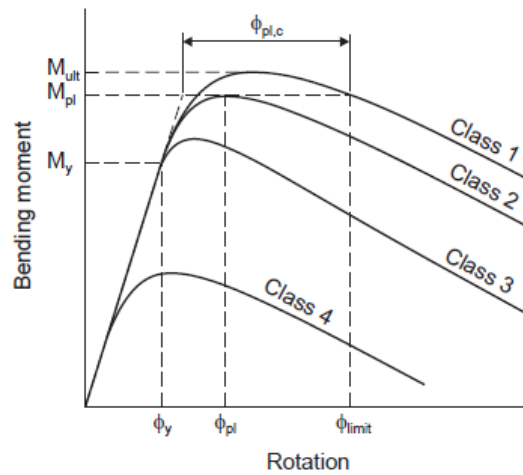


Figure 38: bending moment - rotation capacity diagram with cross section classes [34]

The specific stress distribution possible for each cross section class is given in Figure 39.

behavior of a sheet piling section			
determination of effects of actions	Elastic	Elastic	Plastic
load capacity of cross-section	Elastic 	Plastic 	Plastic

Figure 39: stress distribution and cross section class [30]

To determine these cross section classes tests are performed. 4-point bending tests and 3-point bending tests. The results showed lower rotation capacity for the 4-point bending test, due to influence of the load stiffeners. The load stiffeners have an influence on the local buckling behaviour [30]. The relationship between the rotation capacity and the flange slenderness is given by Bourne-Webb et al (2007) [33].

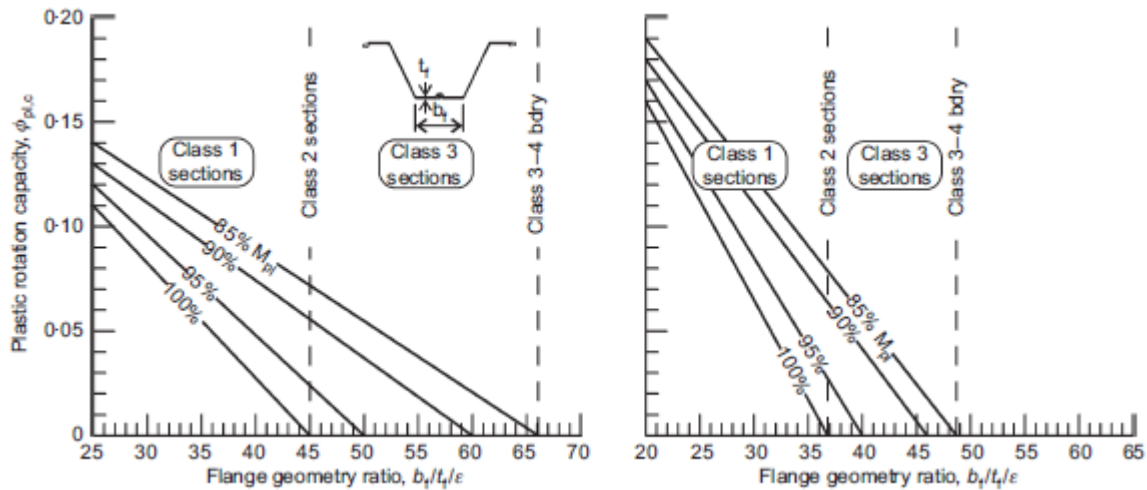


Figure 40: plastic rotation and flange geometry (left: z-piles, right: u-piles) [33].

Derivation of design formula

The derivations of the cross section classifications are based on 3-point and 4-point bending tests. The moment distribution of the 4-point bending test is more similar to the moment distribution of the sheet pile in between the moment zero points. Where the loads are applied, stiffeners are applied. Different type of stiffeners are applied, as shown in Figure 41 (a), (b) and (c). Also, different interlock types are included for the U-profiles in the tests: welded, free, and crimped. [30]

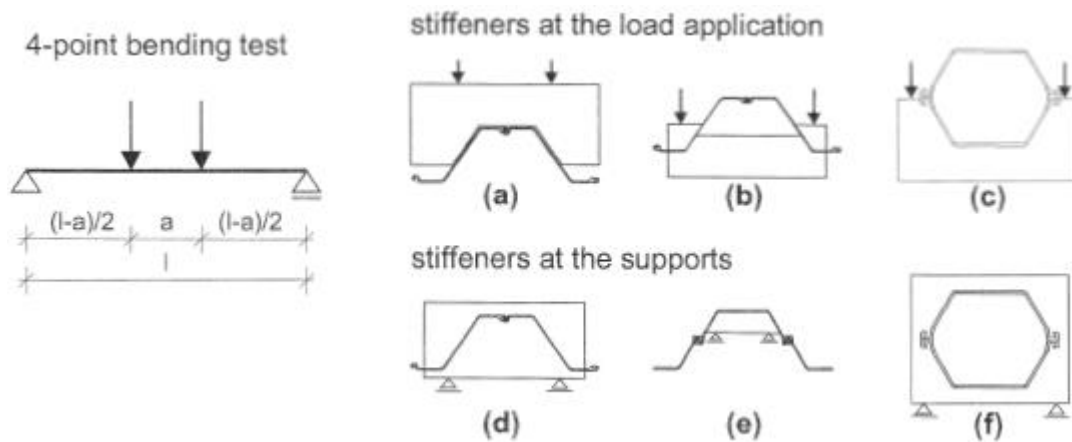


Figure 41: stiffeners at location of loads and supports [30]

From the bending tests, the following can be concluded. Firstly, the distinction between U and Z-profiles should be made. The interlock located in the flange of Z-sections increases the stiffness of these sections. Secondly, the type of interlock for U-profiles is of importance. The welded interlocks assume to have full shear transfer, while crimped interlocks only have partial shear transfer. This influences the resistance of the sheet piles. [30]

Researched is the influence between the moment capacity and the slenderness of the flange, as described at cross section classes. The obtained relationship is linear, and can be described as in equation 46 and 47 for respectively Z-shaped profiles and U-shaped profiles with welded interlocks (full shear force transmission) [30]:

$$\frac{M_{uZ}}{M_{pl}} = f_Z\left(\frac{b}{t}\right) = -0.005 * \frac{\frac{b_f}{t_f}}{\varepsilon} + 1.2 \quad (46)$$

$$\frac{M_{uU}}{M_{pl}} = f_U\left(\frac{b}{t}\right) = -0.011 * \frac{\frac{b_f}{t_f}}{\varepsilon} + 1.405 \quad (47)$$

The moment capacity reduces with the slenderness of the flange. This relationship is also plotted in graphs:

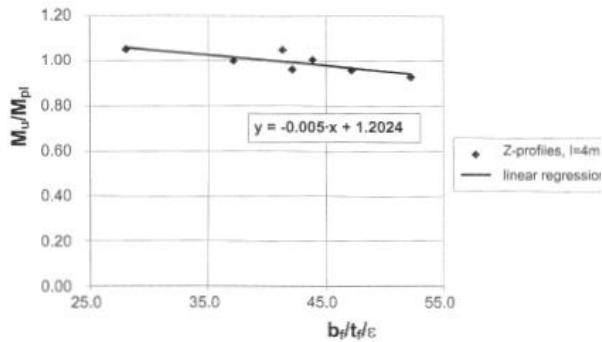


Figure 42: relationship Z-profile M_u/M_{pl} and slenderness flange [30]

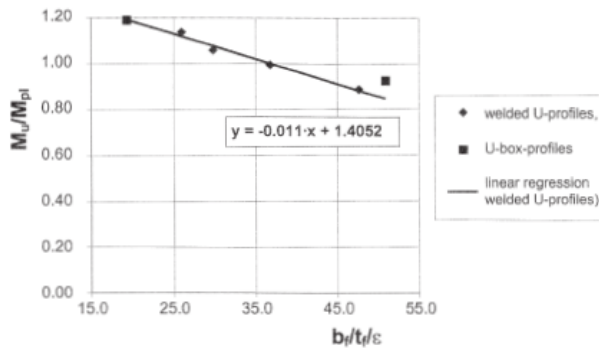


Figure 43: relationship U-profile M_u/M_{pl} and slenderness flange [30]

Based on this relationship, the boundaries for the cross section classes can be determined. However, this can also be done based on the moment rotation capacity. Based on the bending moment capacity, the boundaries are:

- Boundary class 2 to 3: $M_{ud}/M_{pl} = 1$
- Boundary class 3 to 4: $M_{ud}/M_{pl} = 1/1.15$

Tests for finding the correlation between the plastic rotation and slenderness for U-shaped profiles (with welded interlocks) and Z-shaped profiles, are also performed. The results found by Sedlacek et al and the correlation prescribed in the Eurocode 3 part 5 based upon these results are given in Figure 44, Figure 45, Figure 46 and Figure 47.

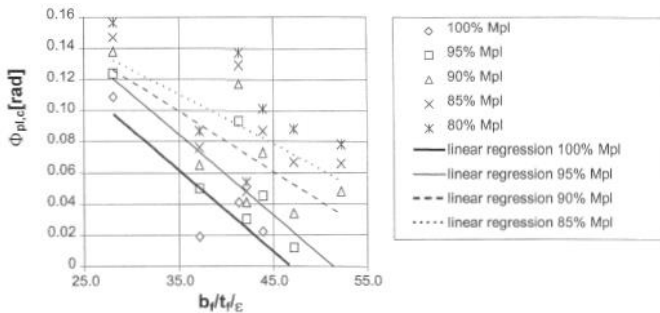


Figure 44: relationship Z-profile plastic rotation and slenderness flange [30]

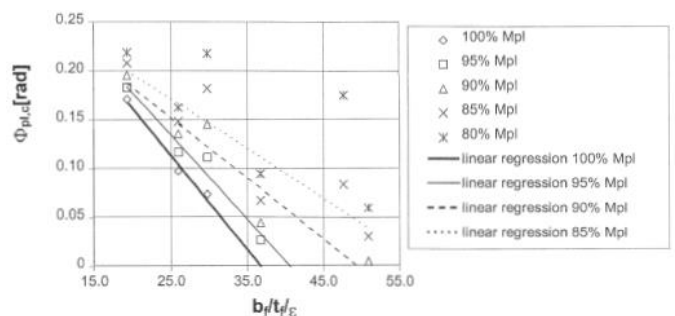


Figure 45: relationship U-profile plastic rotation and slenderness flange [30]

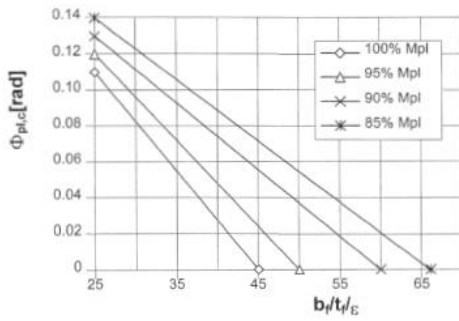


Figure 46: graphs to determine rotation capacity for Z-profiles according to Eurocode 3 part 5 [30]

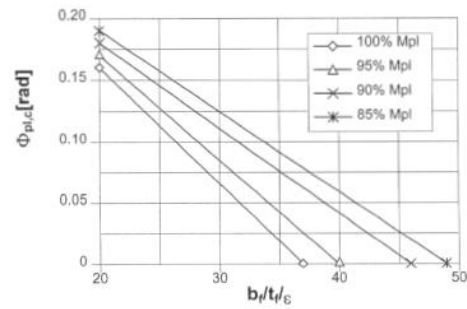


Figure 47: graphs to determine rotation capacity for Z-profiles according to Eurocode 3 part 5 [30]

The scatter in these results (Figure 44 and Figure 45) is much larger than the results from the bending moment capacity study (Figure 42 and Figure 43).

Thus, the cross section classification and the boundaries between the different cross section classes is based upon the tests and numerical analysis for the correlation between M_u/M_{pl} and the flange slenderness and the correlation between the rotation capacity and the flange slenderness. Then the following boundary's between the different cross section classes are defined (Figure 48) [30], [32]:

Classification		Z-profile	U-profile				
Class 1		- the same boundaries as for class 2 apply - a rotation check has to be carried out					
Class 2		$\frac{b/t_f}{\epsilon} \leq 45$	$\frac{b/t_f}{\epsilon} \leq 37$				
Class 3		$\frac{b/t_f}{\epsilon} \leq 66$	$\frac{b/t_f}{\epsilon} \leq 49$				
$\epsilon = \sqrt{\frac{235}{f_y}}$	f_y [N/mm ²]	240	270	320	355	390	430
	ϵ	0,99	0,93	0,86	0,81	0,78	0,74

Figure 48: Boundaries cross section classification (Eurocode 3 part 5) [32]

Studied influencing parameters

The influence of several parameters are determined using the finite element study for the bending moment resistance and rotation capacity. The studied parameters are:

- Imperfections

The geometrical imperfections are expected to influence the bending moment-rotation curve. The Z-profiles are more sensitive to imperfections than U-profiles. For Z-profiles, the influence of the imperfections is noticed after reaching the maximum bending moment, thus in the

decreasing section of the bending moment – rotation diagram. For U-profiles, the influence is mainly visible at the maximum bending moment, which is decreased due to the imperfections. However, this effect is quite small. The difference of the influence of imperfections is derived on the influence of web slenderness. The webs of U-sheet piles are strengthened by the interlocks which reduces the influence of the web slenderness.

- Span length

The maximum bending moment resistance is independent of the span length, it is a cross section characteristic. The plastic rotation is also not dependent on the cross section resistance. However, the tests show a small difference between a span length of 4 meters and a span length of 6 meters, latter with a lower maximum moment capacity and rotation capacity. This behaviour could be explained with phenomena such as horizontal deflection and/or twisting, or the different test set-ups, since the tests are performed at different laboratories.

- Loading

Different type of loadings are researched: constant, 4-point bending tests with different distances between the loading. Again, since the bending moment resistance and rotation capacity are a cross section characteristic, they are independent of the loading type.

- Flange and web slenderness

For Z-profiles, the bending moment-rotation curve depends on the slenderness in the instable branch (after reaching the maximum). An increasing slenderness results in a decreasing rotation capacity. The influence of the web slenderness is larger than the influence of the flange slenderness. This is due to interlock in the flange.

For U-profiles, the web and flange slenderness are of less influence in the plastic, instable branch.

- Web angle

The web angle appeared to have no influence on the bending moment-rotation diagram.

- Yield strength

The yield strength has a significant influence on the bending moment capacity. An increasing yield strength results in a decreasing rotation capacity.

[30]

3.2.2. Yield mechanism

To determine the rotation capacity formulas are derived from yield lines for cross section class 2 to 4. At a certain maximum bending moment, depending on the cross section characteristics and cross section classification, the compression flange starts to buckle. This is called local buckling of the compression flange. During testing of the sheet piles, the buckling shapes obtained are shown in Figure 49 and Figure 50.

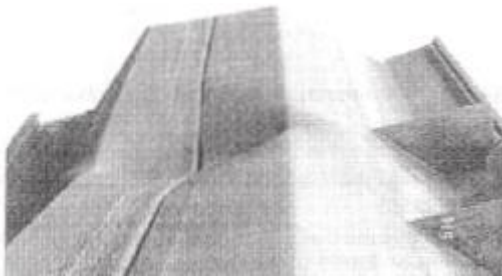


Figure 49: buckling shape Z-profile [30]

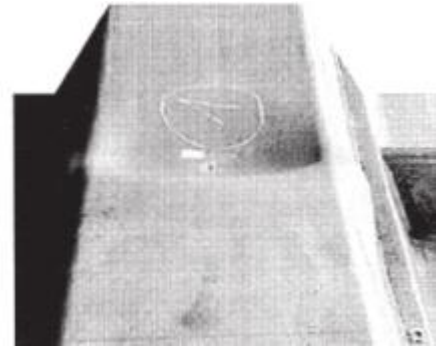


Figure 50: buckling shape U-profile [30]

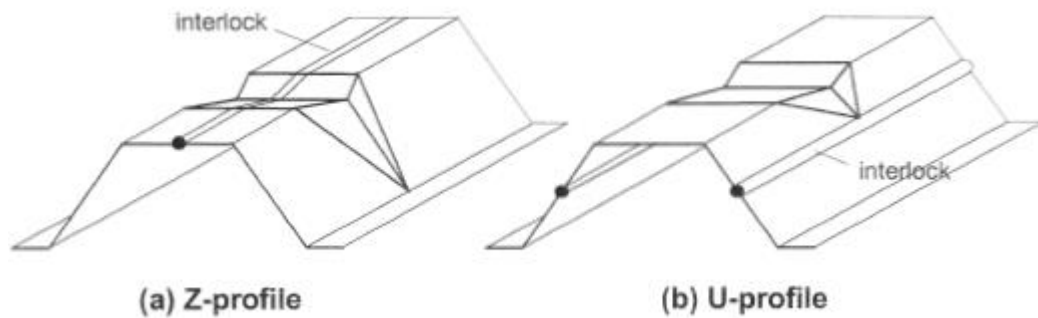


Figure 51: yield line models [30]

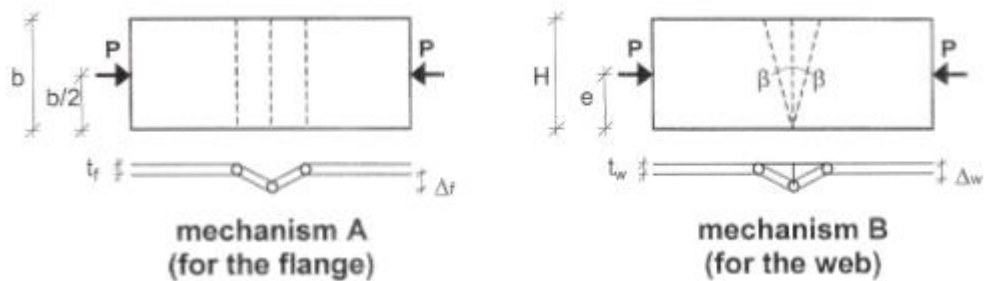


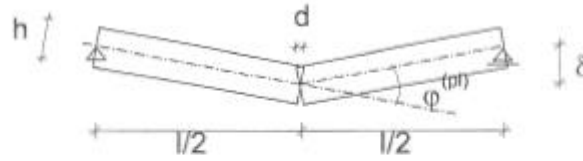
Figure 52: mechanisms for flange and web for derivation analytical formulas [30]

The yield lines for Z-profiles and U-profiles are schematized in Figure 51.

The assumption of a yield line model is that the plasticity is concentrated in the yield lines. All other parts remain rigid and straight.

The analytical formulas for the yield line mechanism can be derived. This derivation is based on the mechanism for the web and the flange (Figure 52). These formulas are then simplified. To determine rotation capacity, rigid body deformations are assumed. This is shown in Figure 53.

Elevation view



Sectional view of buckling in the flange

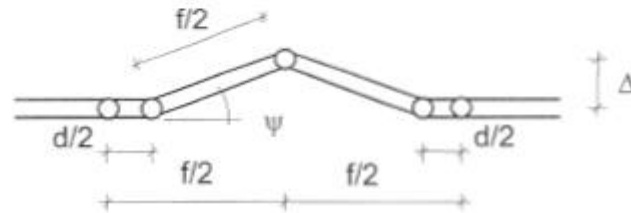


Figure 53: rigid body deformations [30]

Based upon these mechanical schemes and the derivation described in Sedlacek et al [30] the plastic rotation can be calculated for a certain bending moment (generally the plastic bending moment). The formulas derived are given in equation 48-52:

For Z-piles:

$$\varphi_{pl}^Z = \frac{0.4F_{y;f}t_f + 0.6F_{y;w}t_w}{\frac{M_{pl}}{a} - 0.5F_{y;f}h - 0.15F_{y;w}h} \quad (48)$$

For U-piles:

$$\varphi_{pl}^U = \frac{0.2F_{y;f}t_f + 0.15F_{y;w}t_w}{\frac{M_{pl}}{a} - 0.5F_{y;f}h - 0.29F_{y;w}h} \quad (49)$$

With:

$$F_{y;f} = bt_f f_{y;f} \quad (50)$$

$$F_{y;w} = \frac{h}{\sin \alpha} t_w f_{y;w} \quad (51)$$

$$a = 1.25 \frac{t_f}{t_w} \quad (52)$$

These equations are valid for $0.03 \text{ rad} \leq \varphi_{pl} \leq 0.2 \text{ rad}$. [30]

3.3. Oblique bending

The resistance of a sheet pile can be reduced to the phenomena oblique bending. Oblique bending occurs only for U-shaped profiles due to reduced shear force transmission in the interlocks. The interlocks and the phenomena oblique bending are discussed.

Interlock effect

The interlock effect is only of concern for U-shaped profiles and not for Z-shaped profiles. The shear resistance is at its maximum at the position of the interlock of U-shaped sheet piles and therefore the shear force transmission is of importance for the stiffness and capacity of the

sheet pile wall. The shear resistance which can be transferred by the interlocks is identified as the interlock resistance. The interlocks can transfer the shear resistance when the interlocks are connected in one of the following manners:

- Welding the interlocks together
- Crimping the interlocks

The crimping of the interlock will lead to partial shear connection (reduced modulus action; RMA) and welding to full shear connection. Only partial connection is possible due to the displacement of the interlocks, which is caused by the loading. Then, the partial connection is depending on the number of crimping points, and the deformation behaviour depends on the partial connection.

The interlock resistance influences thus the flexural stiffness. However, determining the exact stiffness is difficult, and therefore the two boundaries are mostly considered:

- No transmission of shear forces (0%)
- Full transmission of shear forces (100%)

[35]

No shear force transmission results in a reduction of the stiffness of 30%. Then the moment of inertia is reduced to the moment of inertia of a single sheet pile. This is also shown in Figure 54). While for full transmission, no reduction on the stiffness occurs. The study of Vanden Berghe et al (2001) [36] aims to provide a relationship, which can be used further in FEM models when determining for example sheet pile behaviour. Pull-out tests are performed. From this tests, it can be concluded that the interlock resistance is mostly depending on the installation method and the soil behaviour during installation. This is for placing new sheet piles, and cannot be optimized for underwater anchors procedure. [36]

Oblique bending

The bending stiffness is reduced due to oblique bending. Oblique bending means bending in two directions. This phenomena only occurs at U-shaped profiles due to the reduced shear resistance transmission in the interlocks which are not welded or crimped together. The U-shaped profile has an asymmetric cross section with the interlocks located at the position of the maximum shear force. A double U-profile means that each two U-shaped profiles are connected together by crimping or welding the interlocks. This is the most applied composition used in older, existing sheet piles. Double U-profiles are thus placed in pairs. The interlocks are welded or crimped at the fabric, and the interlocks between two double U-profiles are untreated and described as free interlocks. Slip will occur in the free interlocks. A double U-profile composition forms a new profile, with an asymmetric cross section. The neutral axis rotates, as shown in Figure 54(b). Then, the earth and water pressure results in lateral (out-of-plane) and transverse (in-plane) directions. The rotation of the neutral axis results in a smaller effective height; a smaller distance between the neutral axis and the outer fibre of the sheet pile reducing the bending stiffness and strength. This phenomenon is in literature defined as oblique bending. When all interlocks are welded or crimped together there is no rotation of the neutral axis and therefore no oblique bending. This is shown in Figure 54 (c). For Z-shaped sheet piles the interlocks are not located on a position where the shear stresses are transferred. Therefore, the neutral axis for Z-shaped sheet piles does not rotate and no oblique bending has to be considered for Z-shaped sheet piles (Figure 54 (d)). In case the U-shaped profiles are not crimped or welded together (all interlocks are free), the neutral axis is equal to the neutral axis of a single U-shaped profile (Figure 54 (a)).

[37] [38]

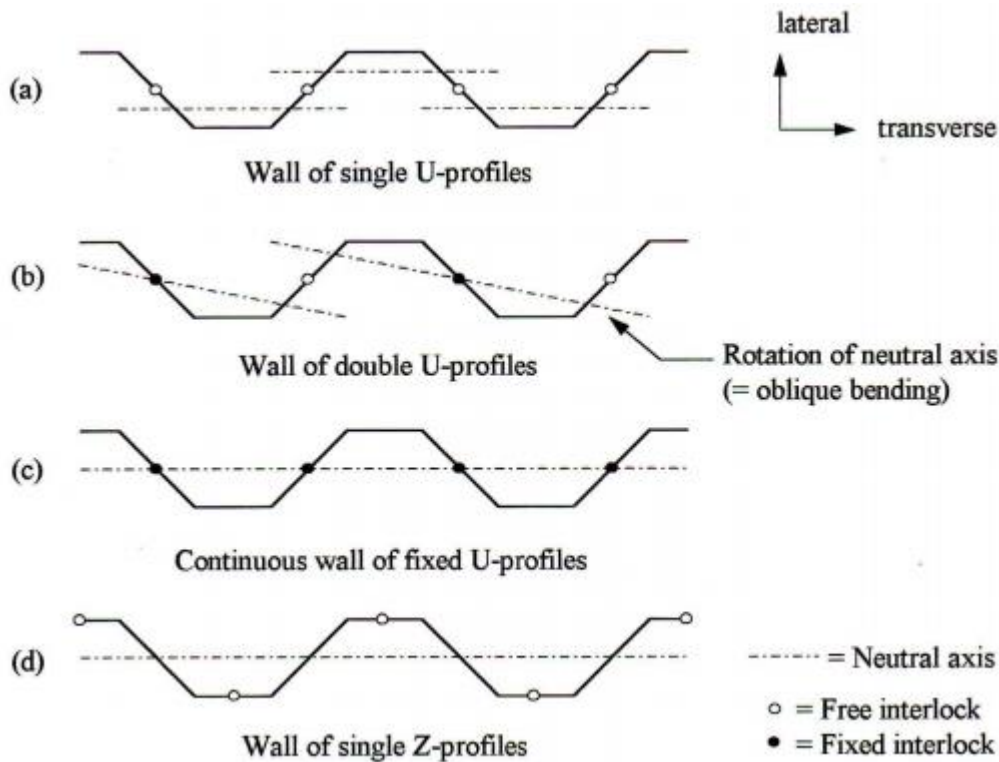


Figure 54: oblique bending [37]

Oblique bending is studied by performing tests, analytical derivations, subgrade reaction models verified with 3D finite element models.

Phenomena influencing oblique bending

Kort (2002) [23] proposes a simplified method to find the reduction factors for oblique bending. These are derived from a subgrade reaction model. The factors derived are the reduction factors for the displacement, β_I (equation 53), and the maximum normal bending stress, β_W (equation 54). It is studied that using these factors result in accurate displacement and bending moment graphs for sheet piles compared to calculations for which oblique bending is included by taking into account bending in two directions. [23]

$$\beta_I = \frac{w_{y,max;normal}}{w_{y,max;oblique}} \quad (53)$$

$$\beta_W = \frac{f_{y;normal}}{f_{y;oblique}} \quad (54)$$

This study performed by Kort (2002), the 3D study of Van Duijnen and the tests performed in Rotterdam form the basics of the design rules of CUR 166 regarding oblique bending. Not only the interlocks influence the oblique bending behaviour. The factors influencing the oblique bending are:

- Shear resistance of the soil / Soil type

When the sheet pile moves in transverse direction, the soil has to move in that direction as well. This movement is restrained by the shear resistance of the soil. Also due to wall friction between soil and sheet pile, the movement in length direction is hampered by this wall friction. The wall friction also depends on the soil type.

- Lateral supports

Lateral supports increase the shear force in the sheet pile at that location. This then results in an increase in the normal force in the interlocks and increase of friction capacity of interlocks. Moreover, the lateral supports reduces the lateral curvature and therefore also the transverse curvature.

- Transverse supports or a capping beam

A transverse support reduces the transverse bending and therefore reduces the oblique bending.

- Soil particles in the interlock

Soil particles in the interlocks increase the interlock friction capacity of the interlock.

- Fixation of interlocking during excavation

Fixation of interlocking reduces the possibility of transverse bending.

- Lubrication of interlocks

Lubrication of interlocks reduces the interlock friction capacity. Therefore lubrication of interlocks increases oblique bending.

- Straightness of piles and the sequence of installation

The installation technique influences the deviations of the sheet pile. These deviations influence the shear resistance of the interlocks.

[23]

Most of these factors are also considered by CUR 166 [24]. Also Eurocode 3 part 5:piling [32] considers oblique bending. An impression on the deformations of the sheet pile in transverse direction for several cases is given in Figure 55. The horizontal fix results in the whole sheet pile moving except the points of the horizontal fix. Slipping in the free interlocks can occur. A capping beam impedes rotation at the top of the sheet pile and also prevents slip at the capping beam level. For welded interlocks, almost no slip can occur in the welded upper half of the sheet pile. Therefore for this case, the upper half of the sheet pile is straight. [37].

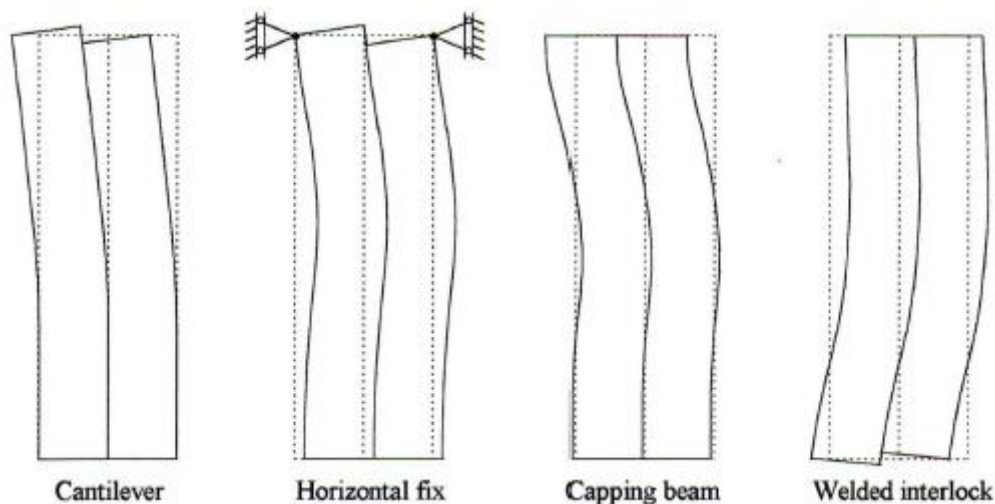


Figure 55: deformation of sheet pile in transverse direction for several cases [37]

Oblique bending tests

Before determining the subgrade reaction model for oblique bending, the oblique bending is studied without including soil behaviour, by a 4-point bending test and modelling this 4-point bending test in a finite element model. These tests and models are described in the papers of Aukema and Joling (1997) [39], Kort (2002) [23] and Sedlacek et al (2001) [30] and are performed to give insight into the reduction of the moment of inertia and the section modulus. Aukema and Joling (1997) and Kort (2002) have extended their research by also studying the oblique bending with a finite element model including 3D soil elements. Sedlacek have performed tests with including a sheet pile loaded with sand. [23], [30], [39]

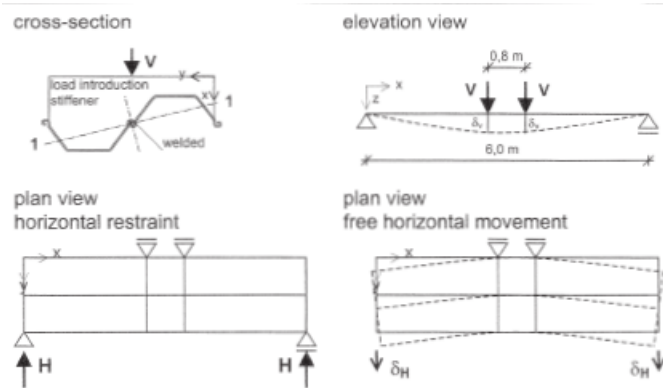


Figure 56: 4-point bending test to study oblique bending [30]

The 4-point bending tests are modelled with double PU8 profiles. The span length is 6.0 meters and the distance between the loads is 0.8 meters. The tests are performed for a restraint sheet pile; horizontal deformation and thus oblique bending is prevented, and for a unrestraint sheet pile. The two situations are shown in Figure 56 [30]. Stiffeners are located at the position of the load introduction.

Findings of the tests are for unrestraint bending:

- The ratio horizontal deflection to vertical deflection is equal in elastic and plastic range.
- The moment of inertia reduces to 50-60% of the moment of inertia assuming restraint bending.

The test is also performed by Sedlacek et al (2001) by loading the sheet pile with sand (Figure 57). The results were similar to the 4-point bending tests. The sheet pile loaded with sand showed similar deflection in the profile as for the 4-point bending test; bending about the inclined main axis. Sedlacek et al concluded based on this test that the friction in the free interlocks has a negligible effect on the moment of inertia and section modulus. Also, the shear resistance of the soil was studied. Since the sheet pile with oblique bending moves in transverse direction, this could be prevented by the shear resistance in the soil. However, the measurements showed a shear deformation in the soil and no horizontal reaction forces from the shear resistance of the soil was measured. This test could thus not prove a positive effect of interlock friction and soil shear resistance which reduce oblique bending. [30]

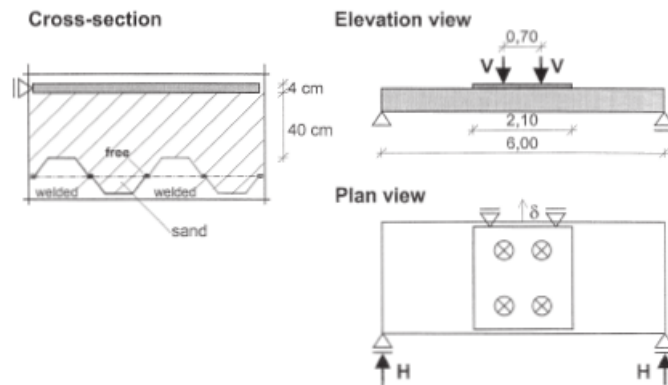


Figure 57: oblique bending test including sand [30]

Subgrade reaction model for oblique bending

According to Kort (2002), the subgrade reaction model can be extended for oblique bending by including transverse springs, representing the shear resistance of the soil.

The subgrade reaction model is largely similar to the subgrade reaction model as elaborated in chapter 2.4.5. The springs in lateral direction are similar, denoted as k_y in Kort's subgrade reaction model (Figure 59). The spring k_x simulates the shear strength of the soil. Due to the inclined neutral axis, the sheet pile does not only move in lateral (y -) direction, but also in transverse (x -)direction. This movement in transverse direction is partly restrained due to the soil resistance of the soil, which is captured in spring stiffness k_x . The spring model for this spring is given in Figure 59 and also the elasto-plastic spring stiffness k_y which is discussed in chapter 2.4.5. is given (Figure 58). The maximum shear resistance which can be mobilized is depending on the cohesion and the lateral earth pressure (equation 55) and the shear stiffness can also be calculated (equation 56).

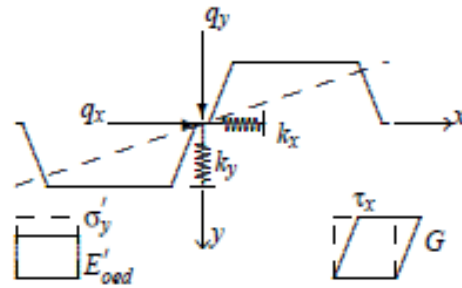


Figure 59: subgrade reaction model for oblique bending [23]

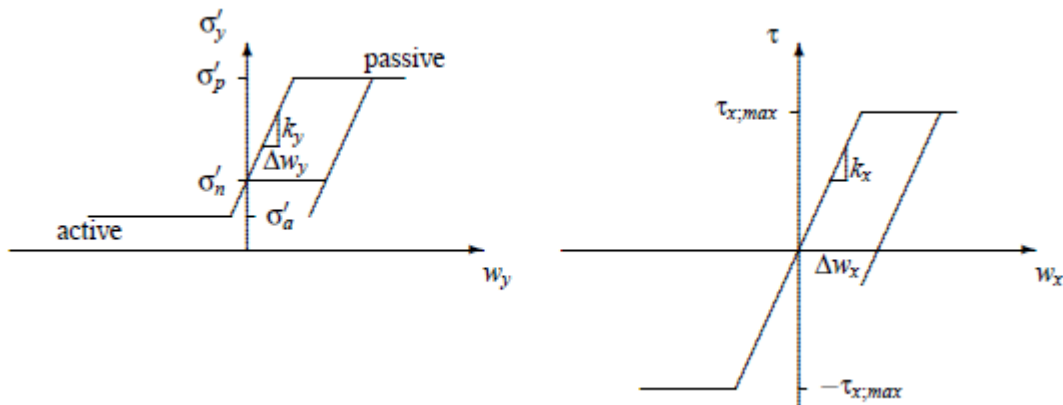


Figure 58: spring model for lateral and transverse springs [23]

$$\tau_{x,max} = c' + \sigma'_y \tan \phi' \quad (55)$$

$$\frac{k_x}{k_y} = \frac{G}{E'_{oed}} = \frac{1-2\nu'}{2-2\nu'} \quad (56)$$

The influence of the shear springs on oblique bending has been studied by this subgrade reaction model. It is found that the influence of the shear springs and thus the shear resistance of the soil is 5-10%.

The oblique bending can also be influenced by friction in the interlocks. Interlock friction occurs in the free interlocks, due to soil particles intruding in the interlocks. An infinite friction interlock results means that transverse bending is completely restrained, while a friction interlock of 0 kN/m³ means that transverse bending is not restrained. The friction in the interlocks hampers transverse bending. The interlock friction is modelled by Kort (2002) by again using springs.

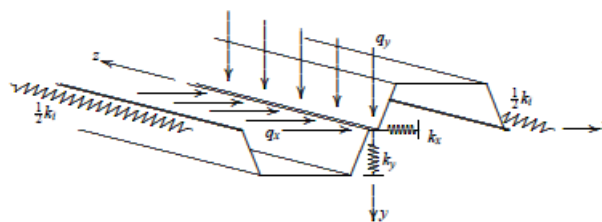


Figure 60: subgrade reaction model for oblique bending with interlock springs [23]

These springs are shown in Figure 60. The derivation of the spring characteristics are not elaborated, but can be found in Kort (2002). [23]

Kort also studies the interlock friction based on experiments performed by Juaristi and Vanden Berghe [36]. This phenomenon is studied by Juaristi and Vanden Berghe [36], by performing experiments. The tests are performed by driving two sheet piles into a sand tank. The force-displacement relationship was then measured by a pull-out test. It was found that the interlock friction depends on the factors: dimensions and shape of the interlocks and the grain size. Resulting from the load-displacement tests are the stiffness of the springs k_i . These are given in Figure 61. [23], [36]

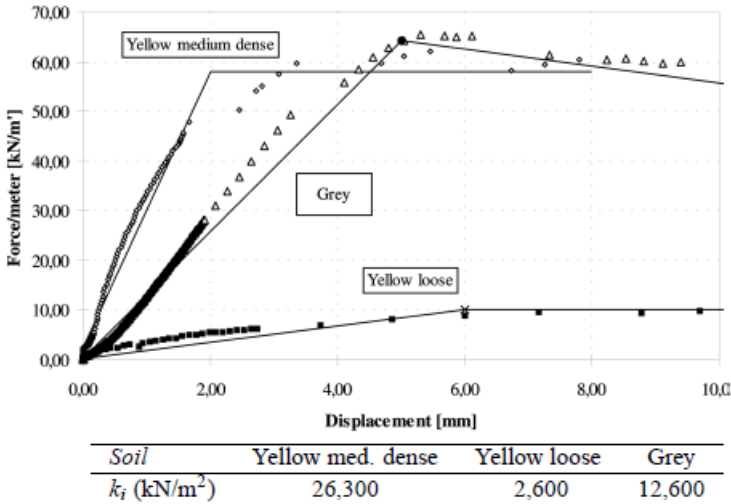


Figure 61: interlock friction found by performing tests [36]

The influence of the spring stiffness of interlock friction on the oblique bending is studied by a three point bending test (Figure 62). From this figure, it can be obtained that from a stiffness of 100.000 kN/m² the spring stiffness significantly influences the reduction factor for oblique bending. From the study of Juaristi and Vanden Berghe a maximum stiffness is found for medium dense sand of 26.300 kN/m². For less stiff soil types such as clay and peat, the interlock friction stiffness will be significantly lower. The range of the spring stiffness caused by interlocking have thus a minimal influence on the deflection. For a spring stiffness of 25000 kN/m², the reduction factors increase for β_l and β_w by respectively 0.03 and 0.07. [23], [36]

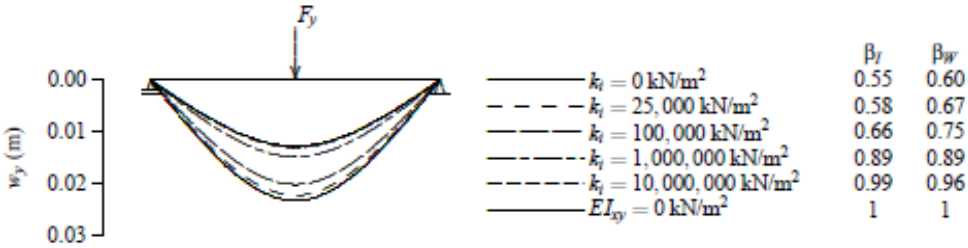


Figure 62: influence of interlock spring stiffness on vertical deflection of a three-point bending test [23]

Calculation procedure for oblique bending

The oblique bending is now calculated as a reduction factor on the bending stiffness and bending strength. For the bending stiffness, the moment inertia is reduced with a factor β_I and the elastic section modulus is reduced with factor β_W . These factors are determined by the following relationship given in equation 57 and equation 58:

$$\beta_I = \frac{w_{y,max,normal}}{w_{y,max,oblique}} \quad (57)$$

$$\beta_W = \frac{f_{y,normal}}{f_{y,oblique}} \quad (58)$$

The oblique bending characteristics found by Kort (2002), CUR 166 and are compared for single anchored sheet pile walls. In the Netherlands, CUR 166 is used to determine the reduction factor for oblique bending. The reduction factors of CUR 166 are based on the study of the sheet pile of Kort (2002) and measurements of tests in Rotterdam [23], [24]. This is elaborated in Table 1.

Table 1: oblique bending reduction factor coefficients

Influencing factor	Kort (2002) [23]		CUR 166 [24]
	$\beta_{I,0}$	$\beta_{W,0}$	$\beta_{I,0}$ and $\beta_{W,0}$ (in CUR 166 as respectively $\beta_{D,0}$ and $\beta_{B,0}$)
Min β factor for single anchored walls*	0.55	$\frac{I_{xx}I_{yy} - I_{xy}I_{yx}}{-I_{xy}x + I_{xx}y} \frac{h}{2I_{yy}}$	0.55 $\frac{I_{xx}I_{yy} - I_{xy}I_{yx}}{-I_{xy}x + I_{xx}y} \frac{h}{2I_{yy}}$
	$\Delta\beta_I$	$\Delta\beta_W$	$\Delta\beta_I$ and $\Delta\beta_W$ (in CUR 166 as respectively $\Delta\beta_D$ and $\Delta\beta_B$)
Factors influencing oblique bending			
• Soil type / shear strength of soil			
Shear strength of soil (factors also depending on cohesion)	1. 0 ($q_c \leq 20$ MPa) 0.05 ($q_c \geq 20$ MPa)	1. 0 ($q_c \leq 20$ MPa) 0.10 ($q_c \geq 20$ MPa)	1. 0.05 ($q_c \leq 5$ MPa) 0.10 ($5 < q_c \leq 15$) MPa) 0.15 ($q_c > 15$ MPa)
Restrains / anchors			
Lateral restraint	-	-	2. 0 (no support) 0.05 (support) 0.15 (>1 support)
Restraint in transverse direction (X) (in case of 0 lateral supports)	2. 0 (no support) 0.10 (simply supported) 0.10 (weld or capping beam)	2. 0 (no support) 0.05 (simply supported) 0.05 (weld or capping beam)	3. 0 (no support) 0.05 (1 support)
Restraint in transverse direction (X) (in case of 1 lateral support)	3. 0.05 *Weld or capping beam at top	3. 0.10 *Weld or capping beam at top	
Restraint in length direction (Z)	-	-	4. 0 (no restraint) 0.05 (restraint)
• Installation method and interlock friction			
Soil in interlock	A. 0 (lubricated interlock and/or $q_c < 20$ MPa)	A. 0 (lubricated interlock and/or $q_c < 20$ MPa)	5. 0 (no sand present above water level)

	0.05 ($q_c \geq 20$ MPa)	0.05 ($q_c \geq 20$ MPa)	0.10 (sand present >5m above water level (so at least 5 m of dry sand))
Treatment of driving interlocks	B. 0 (lubrication) 0.20 (welded during excavating)	B. 0 (lubrication) 0.20 (welded during excavating)	6. 0 (pushing and/or lubricated interlocks) 0.10 (vibrating or driving; non-lubricated)
Installation technique	C. 0 (pushing or lubricated interlocks) 0.10 (vibrating or driving)	C. 0 (pushing or lubricated interlocks) 0.15 (vibrating or driving)	
*calculations according to coordinate system applied in Kort (2002) (Figure 60)			

For a single propped wall, the oblique bending reduction factors can be calculated in the following manner propped by Kort (2002) (equation 59-62):

$$\beta_I = \beta_{I;0} + \sum_{i=1}^3 \Delta\beta_{I,i} + \max(\Delta\beta_{I,A}, \Delta\beta_{I,B}, \Delta\beta_{I,C}) \leq 1.00 \quad (59)$$

$$\beta_W = \beta_{W;0} + \sum_{i=1}^3 \Delta\beta_{W,i} + \max(\Delta\beta_{W,A}, \Delta\beta_{W,B}, \Delta\beta_{W,C}) \leq 1.00 \quad (60)$$

And as prescribed by CUR 166:

$$\beta_I = \beta_D = \beta_{I;0} + \sum_{i=1}^6 \Delta\beta_{I,i} \leq 1.00 \quad (61)$$

$$\beta_W = \beta_B = \beta_{W;0} + \sum_{i=1}^6 \Delta\beta_{W,i} \leq 1.00 \quad (62)$$

4. Numerical modelling: 3D spring model

To study the procedure of underwater anchors a numerical model is made with the finite element program DIANA FEA. This chapter answers the sub question:

1. What are the characteristics of the numerical model to obtain understanding in the sheet pile resistance and behaviour regarding the effect of hole weakening?

A new type of modelling is designed, based upon existing theories. The numerical model design is based on the literature study described in chapter 2 and 3. The applied theories in the numerical model are addressed again in chapter 4.1.

Modelling of a sheet pile retaining wall includes two aspects: Modelling of the soil load and modelling of the steel sheet pile. The developed model is a 3D soil and structure interaction model based on 1D springs and 2D shell elements and will be addressed as the '3DSSI model' (3D Soil and Structure Interaction model). Impressions of the model is given in Figure 64 and Figure 63 and more detailed in Appendix B including detailed input in DIANA FEA.

The 3DSSI model expands the subgrade reaction model, which is normally used in 2D calculation programs such as D-sheetpiling, to 3D. This is not introduced before in designing manuals such as CUR 166 [24] or the handbook Quay walls [27]. The thesis of Kort (2002) [23] already studies the possibilities of the subgrade reaction model for oblique bending and plasticity. However, the sheet pile is still modelled as a beam. The 3DSSI model is thus unique for modelling a sheet pile in 3D with the subgrade reaction method.

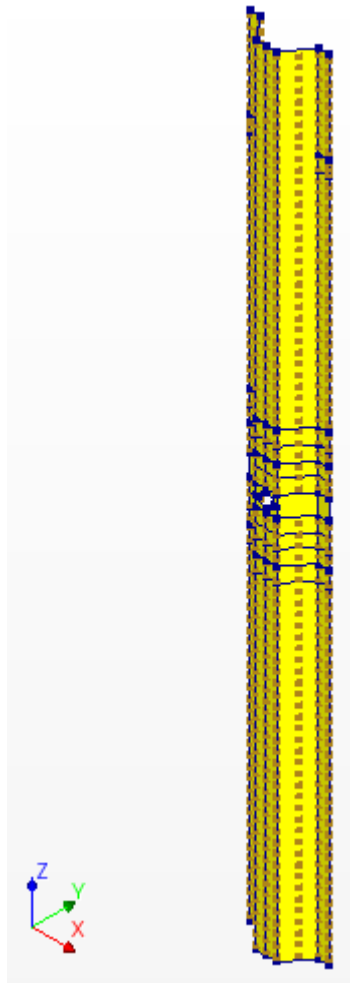


Figure 64: 3DSSI model (1)

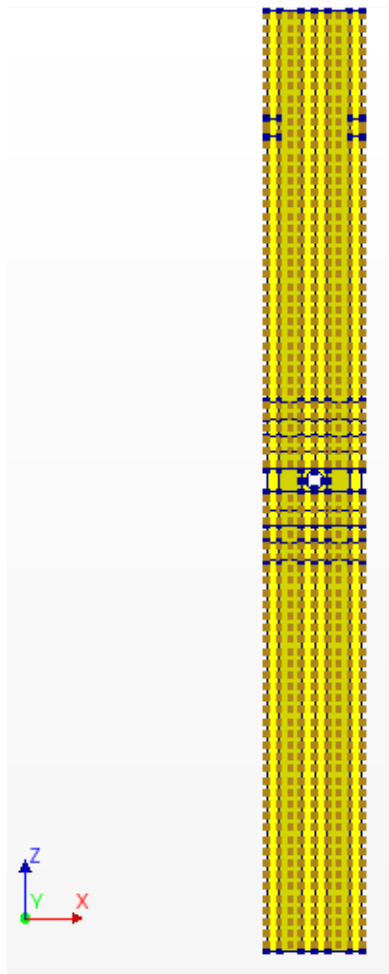


Figure 63: 3DSSI model (2)

4.1. Numerical model: literature

The literature is given in chapter 2 and chapter 3. From the different theories discussed, the most appropriate are chosen as input for the numerical model. This is shortly discussed in this paragraph.

4.1.1. Earth pressure theory: Müller-Breslau

The earth pressure theory applied in the 3DSSI model is the theory of Müller-Breslau. This theory is based on Coulomb's earth pressure theory. Müller-Breslau includes frictional soil, wall friction, backfill slope and slope soil-wall interface. The formulas of Müller-Breslau are extended in the Dutch design codes for cohesive soils. Müller-Breslau is chosen above Rankine's theory, since Rankine's theory is not accurate for determining the earth pressure directly against a wall. Also, Kötter is an earth pressure theory. Kötter is more accurate for larger friction angles: $\varphi > 30^\circ$. For friction angles below 30° Müller-Breslau is considered accurate by design regulations. Therefore, Müller-Breslau is used.

The neutral earth pressure is specified by Jaky's equation (Equation 5, chapter 2.4.2) This is a conservative method of determining the earth pressure and therefore also generally applied and prescribed in Eurocode 7.

4.1.2. Soil-structure interaction model: soil-spring model

To model the soil-structure interaction the soil spring model is used. The spring model is a common method used to determine internal forces and deformations in the sheet pile. This method is also applied in the 2D software D-sheetpiling. Also, the soil can be modelled in FEM with volume elements. Modelling the soil in FEM is very time consuming for the purpose of this study and is mainly used studying other phenomena, such as the deformation of adjacent buildings, than the forces and sheet pile behaviour. This is explained in more detail in chapter 2.4.6. The third method discussed is Blum's method. However, this is not an accurate method determining the internal forces and deformations of the sheet pile and therefore not included. The soil spring model is thus an appropriate and time-efficient manner for modelling the soil pressure on a sheet pile.

4.1.3. Horizontal subgrade reaction modulus: Dutch model

Determining the spring characteristics, the earth pressure theory of Müller-Breslau is used as described in chapter 2.4.2. For the horizontal subgrade reaction modulus, the Dutch model is used. This model is based on measurements of the Dutch soil. Moreover, the Dutch model takes into account the deformation of the soil, which is not included by Terzaghi or Ménard's method.

4.1.4. Plastic design

As described in chapter 3.2 the available plastic capacity is depending on the cross-section classification. Since it is expected that hole weakening is influencing this plastic capacity, the load will be increased up till the ultimate failure and the ultimate capacity of the sheet pile, exceeding the elastic limit. In chapter 3.2.1 the plastic design depending on the cross-section classification is discussed elaborately. Also, it is allowed to design sheet piles of cross-section class 1 and 2 with the plastic bending moment. The influence of hole weakening is therefore researched including the plastic behaviour. Also hole weakening for different cross-section

classes: cross-section class 2 and cross-section class 3 is studied. Cross section class 1 and 4 are less common and therefore not studied [34].

4.1.5. Oblique bending

As discussed in chapter 3.3, oblique bending occurs in existing double U-sheet piles. Since the influence of the oblique bending on the deformation and maximum load is significant, the oblique bending cannot be neglected. In general, oblique bending is incorporated using reduction factors. However, since this reduction factor does not give insight into the sheet pile behaviour in 3D regarding the interaction of hole weakening and oblique bending, a more appropriate modelling approach are interface elements. Therefore, as described in chapter 3.3 and Appendix D, the interface elements are designed in the free interlocks to simulate the oblique bending. Understanding the sheet pile behaviour for the combination of hole weakening and oblique bending is then possible. The interface element contains an axial degree of freedom to simulate the slip along the interlocks.

4.2. Numerical model: Soil load

In this chapter it is discussed how the soil model is realised in the 3DSSI model.

4.2.1. Springs to model soil load

The soil model determines the load on the sheet pile, depending on the deformation of the sheet pile. Therefore, soil-structure interaction is of importance determining the soil load and deformation of the sheet pile.

As described in chapter 4.1 the subgrade reaction model, using Müller-Breslau and the Dutch model to define the spring characteristics, is used in the 3DSSI model. The sheet pile is modelled in 3D and loaded by the springs from the subgrade reaction model. The springs are uncoupled.

The stiffness of the springs depend on the depth of the soil represented by the springs. Therefore, a python a loop is created to model the springs over the height of the sheet pile and assign the correct spring characteristics, depending on the depth of the spring with respect to the soil surface. The resulting pressures (kN/m^2) are multiplied with the area the spring is covering, to determine the soil load (kN). The springs are located every 200 mm width and height, covering a square area of the sheet pile. A convergence study has been performed to determine the distances between springs. This is shown in Appendix E. Based on this analysis, a centre to centre distance between the springs of 200 mm is chosen.

It is assumed that the water pressure on both sides of the sheet pile are equal. Therefore, these are not included as an additional load in the model.

For this thesis, the earth pressure theory of Müller-Breslau is applied with assuming a vertical wall and horizontal ground level. Then the equations 9-15 given in chapter 2.4.2 are applicable. The neutral earth pressure coefficient is then given by Jaky's equation (equation 5, chapter 2.4.2).

The spring forces (thus the soil load) depend on the deformation. To determine the equilibrium between the spring forces and the deformation of the sheet pile an iterative calculation procedure is necessary. This calculation procedure is given in Figure 65. This calculation procedure is followed in D-sheetpiling and also in the 3DSSI model.

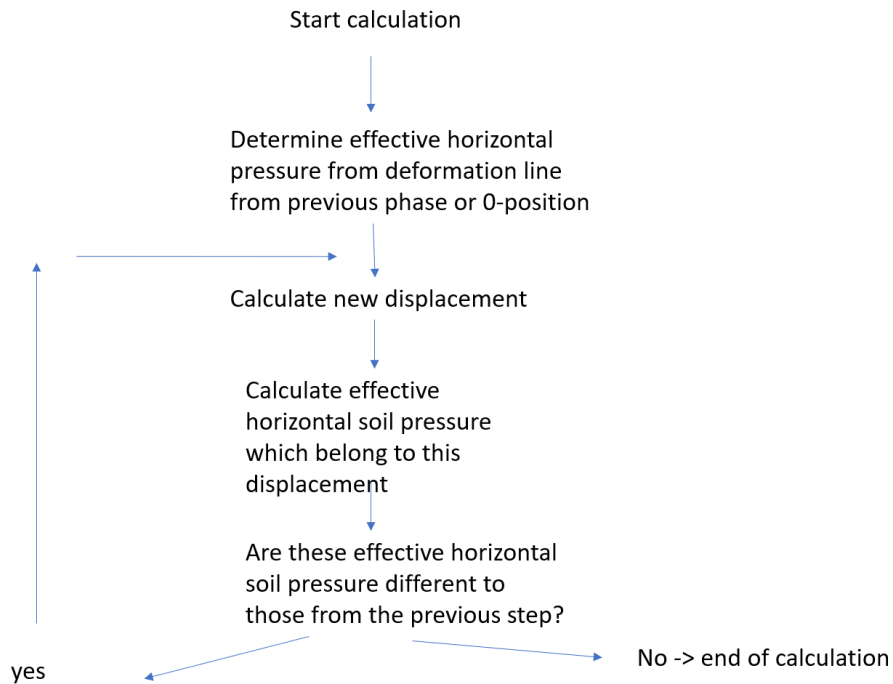


Figure 65: subgrade reaction model calculation procedure

4.2.2. Wall friction and shear resistance of the soil

The wall friction is neglected for the numerical model proposed in this thesis. Now, the vertical stresses introduced by the anchor are transferred completely to the support at the toe of the sheet pile and are not partly taken by wall friction and shear resistance of the soil. To find a significant influence of the wall friction, stiff soils and significant movement in axial direction are necessary. The wall friction depends on the shear stiffness of the soil and the difference in settlement of the ground and the sheet pile. In sheet pile calculation program D-sheetpiling wall friction is only considered for the vertical equilibrium verification of the sheet pile: vertical equilibrium is calculated by considering the vertical forces such as the vertical component of the anchor force, the vertical forces produced by the wall friction on active and passive side and the vertical toe capacity. In the designed numerical model it is assumed all wall friction is transferred to the toe of the sheet pile. This is a conservative assumption. It is assumed that in all design cases this friction is sufficient to assume zero displacement at the toe of the sheet pile.

4.2.3. Oblique bending and transverse soil stiffness

The transverse soil stiffness or shear resistance, as discussed in chapter 3.3 and represented in Figure 58 and Figure 59, present in case of oblique bending, is also neglected in the numerical model. The influence found by the study of Kort (2002) was small: 5%. In the design regulations of CUR 166 an influence of 15% is defined, but only for very stiff soils. Including the shear springs as defined by Kort (2002) (Figure 58) requires a difficult iterative procedure, since the shear spring characteristics depend on the lateral spring forces. Neglecting the shear spring is conservative and as found by Kort (2002), the influence using the subgrade reaction method is lower than 5%. Therefore the shear stiffness/transverse soil stiffness is neglected. [23], [24].

4.3. Numerical model: Steel sheet pile characteristics

The steel sheet pile is modelled with shell elements. These shell elements are given the thickness of the sheet pile flange and sheet pile web and are divided into 3 layers in the thickness. Shell elements are suitable for modelling plate and shell structures. The model does not include the additional steel in the corner radii and the interlocks. This is shown in the top view of the model in Figure 66 for a Z-profile. The shell elements are modelled in the centre line of the cross-section (Figure 67). For the U-profile, similar is shown in Figure 68 and Figure 69. The coordinate system is defined as z-axis in axial direction, y-axis in lateral direction and x-axis in transverse direction (similar to the coordinate system used by Kort (2002) (Figure 60). The model in full detail and the input in DIANA FEA is given in Appendix B. [23]

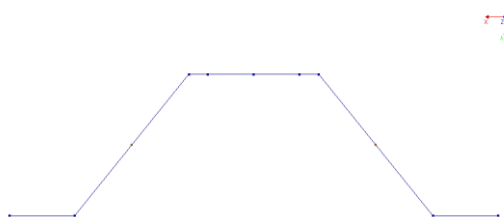


Figure 66: Cross-section AZ23-800 3DSSI model

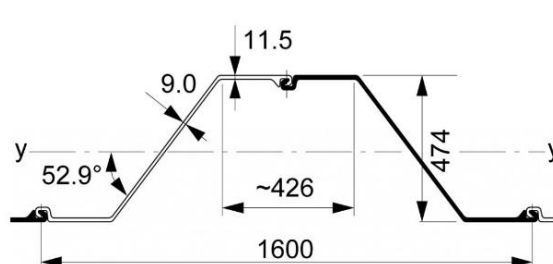


Figure 67: Cross-section AZ23-800, ArcelorMittal [44]

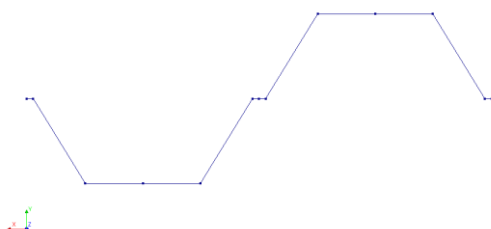


Figure 68: Cross-section PU22 3DSSI model

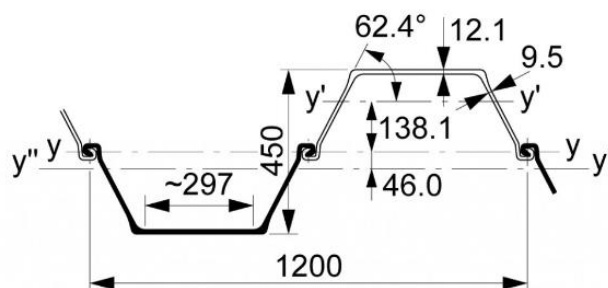


Figure 69: Cross-section PU22, ArcelorMittal [40]

4.3.1. Boundary conditions

For the boundary conditions supporting the sheet pile in z-direction, several options have been considered. This is performed to find the most representative boundary condition and model the sheet pile behaviour as accurate as possible. All considered options are supporting the sheet pile at the toe. Since the shear resistance and wall friction of the soil is neglected, it is assumed all vertical forces acting on the sheet pile are transferred to the toe of the sheet pile. In reality, partly these vertical forces are taken up by the soil along the sheet pile by wall friction and shear resistance. The assumption all vertical forces are transferred to the toe is a conservative assumption.

1. Boundary condition 1: Eccentric support in z-direction over one flange of the sheet pile at the toe of the sheet pile. (Figure 70)
2. Boundary condition 2: Support in z-direction over complete toe of the sheet pile. (Figure 71)
3. Boundary condition 3: Support in z-direction in the centre of gravity of the sheet pile. (Figure 72)
4. Boundary condition 4: Support in z-direction which can only take up compression force. (Figure 73)

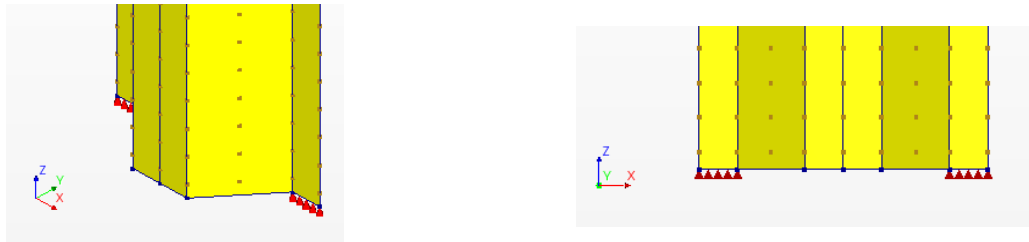


Figure 70: Boundary condition: 1 3D view and front view

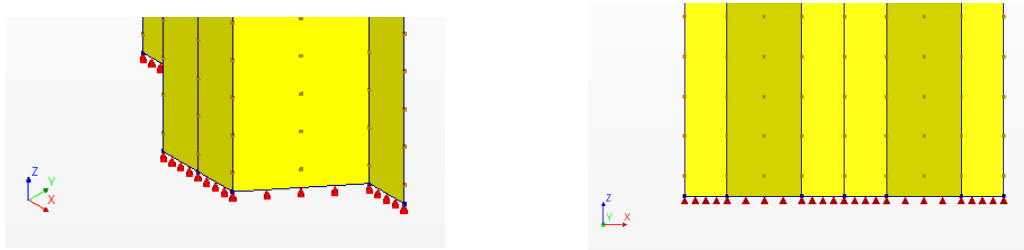


Figure 71: Boundary condition: 2 3D view and front view

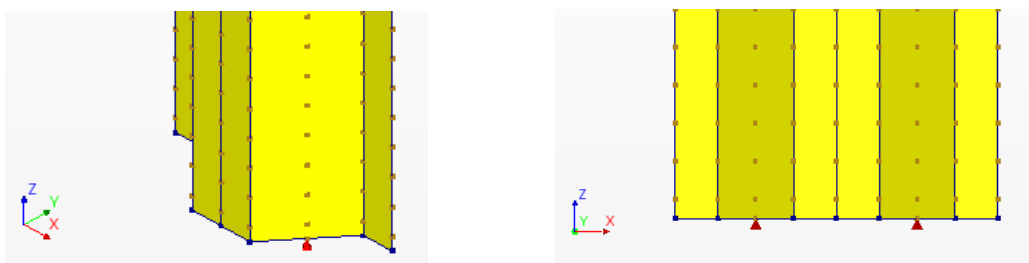


Figure 72: Boundary condition 3: 3D view and front view

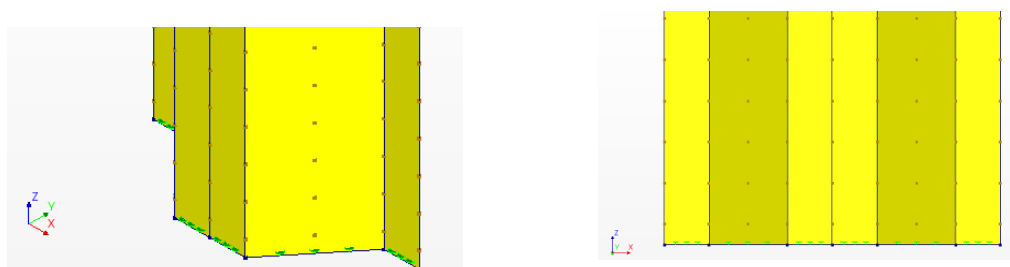


Figure 73: Boundary condition 4: 3D view and front view

The deformation of the sheet pile over the height is plotted to study the influence of the boundary conditions on the sheet pile behaviour.

The boundary conditions are studied for a realistic design which will also be used in the parametric study: a sheet pile AZ23-800 with a total length of 16 meters, an anchor on level -2m, a retaining height of 9m and an embedment depth of 7 meters. For more details on this design, refer to chapter 5.

For the boundary conditions, it is found that boundary condition 3 provides numerical problems. The support in the centre of gravity are two nodal supports, resulting in large forces and plasticity at the load introduction of the support. For a more fictitious design with a large sheet pile: AZ27-800 and a large embedment depth of 11 meters, a result could be found for boundary condition 3. With this design, the sheet pile is completely clamped into the soil (approximately zero rotation and displacement at the toe of the sheet pile) and the support has less influence on the sheet pile behaviour and rotation at the toe of the sheet pile. The deformation in z-direction and local plasticity at the nodal support are shown in respectively Figure 75 and Figure 74. Summarizing, due to the numerical problems and the large plasticity at the nodal supports, boundary condition 3 is not a suitable boundary condition.

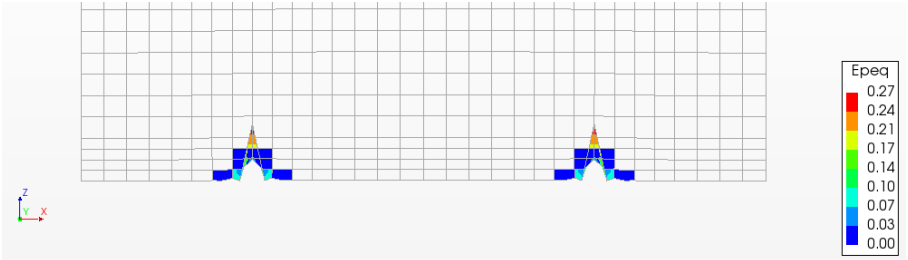


Figure 74: local plasticity at support BC3

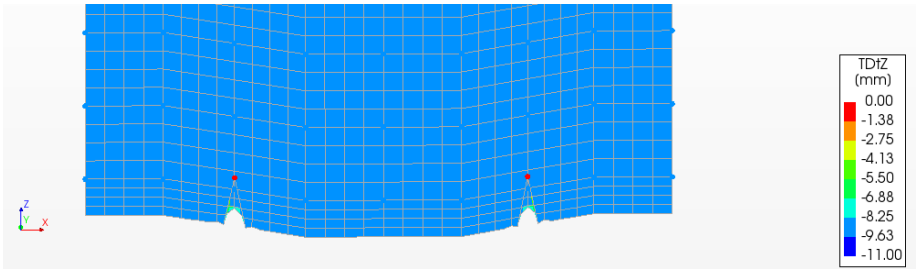


Figure 75: Deformation at support BC3 in z-direction

Boundary condition 4 consists of a support only taking up compression force. However, due to the neglect of shear resistance of the soil, the soil load on the sheet pile is applied in lateral direction. This results, due to the deformation of the sheet pile also into vertical stresses in the sheet pile which are conservatively assumed to be transferred to the toe of the sheet pile and not (partly) taken by the shear resistance. However, this can in some design cases result in tension at the toe of the sheet pile. Therefore, boundary condition 4 is also not a suitable solution for all designs.

Boundary condition 2 supports the sheet pile of the complete toe of the sheet pile. The complete shear resistance is thus transferred to the toe of the sheet pile. Due to the shape of

the sheet pile, within the support a lever arm in y-direction is created. This results in a clamped support of the sheet pile at the toe. This is in reality not the case, since rotation can occur at the toe of the sheet pile. This rotation influences the deformation significantly as observed in Figure 77. Boundary condition 2 is due to this clamped support not a conservative approach.

Boundary condition 1 is compared to boundary condition 2 more conservative, since rotation can occur. Boundary condition 1 allows rotation at the toe of the sheet pile and the shear resistance is assumed to be transferred to the toe of the sheet pile. Therefore, boundary condition is conservative and applied in the model. The support is located at the active side, this results in the largest rotation at the sheet pile and the most conservative results.

The deformation plots for the different boundary conditions are shown in Figure 76. Figure 77 shows the deformation plot with larger loads, resulting in a larger rotation at the toe of the sheet pile, which is prevented by boundary condition 2. Also, for a situation with compression at the toe of the sheet pile, boundary condition 4 and 1 give very similar results.

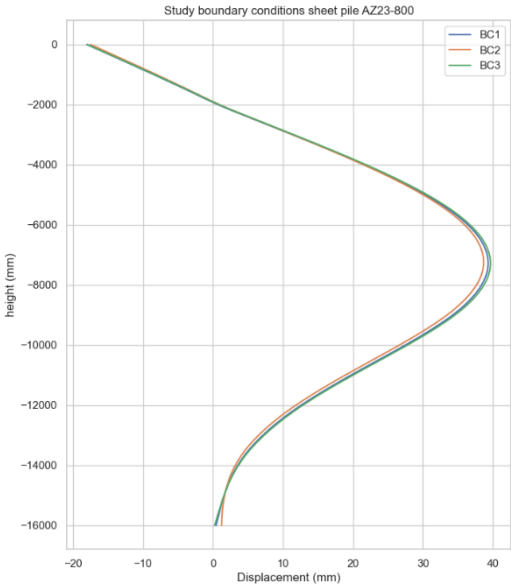


Figure 76: Deformation over height for BC1, BC2 and BC4

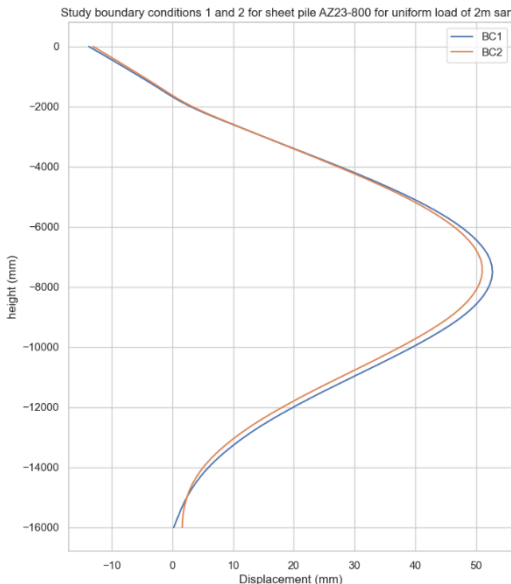


Figure 77: Deformation over height for BC1 and BC2

Each sheet pile is supported by another sheet pile in transverse direction. Therefore the sheet pile only moves in lateral direction. This is different for the phenomena oblique bending, which is explained later. For Z-piles, the boundary conditions on the edges of the sheet pile along the axial axis are defined with a zero displacement in transverse (x-)direction and also a rotational restraint around z-axis. This results in uniform global displacements along the width (transverse direction) of the sheet pile in lateral, transverse and axial direction.

4.3.2. Top anchor

The anchor is modelled as a linear stiff spring on the steel sheet pile. To distribute the force produced by the spring, an anchor plate is defined with linear elastic material properties. The anchor plate has the dimensions similar to regularly used anchor plates: 300mm height and the width is equal to flange width. Generally, the anchors are applied under angle. A common used angle for anchors is 45 degrees, which is also applied in this design. The stiff spring is

based on the assumption of a rigid anchor and during all load cases the anchor is designed such that the displacement of the sheet pile at the location of the top anchor is zero. The stiff spring is in all situations an anchor force corresponding with the situation. This is thus modelled by modelling a rigid boundary spring under an angle of 45 degrees in the 3DSSI model.

4.3.3. Oblique bending

For double U-profiles, as described in chapter 3.3 and chapter 4.1.5, oblique bending is of importance for finding the bending moment resistance and sheet pile behaviour. Therefore oblique bending is modelled. To verify the model, the 4-point bending tests performed by Sedlacek et al (2001) [30] and Aukema and Joling (1997) [39] are reproduced with DIANA FEA. Then, the results from a model including 3D soil elements produced by Aukema en Joling are compared to verify the oblique bending model. This is documented in Appendix D.

The oblique bending model for single anchored double U-profiles is, compared to the model for Z-piles, extended with interface elements in the free interlocks. This interface element is defined with a zero shear stiffness in axial direction. Interlock friction is therefore neglected. Based on research as described in chapter 3.3 the interlock friction only had a small influence on the bending moment capacity. Study on the deflection of a 4-point bending test found an influence of 3-7% and the design rules take into account 5% less reduction on the stiffness and strength in case of soil particles in the interlock which cause interlock friction. This influence is thus small and neglected in the finite element model designed in this thesis. The studied phenomena discussed in chapter 3.3 can only increase the resistance of the sheet pile. Assuming a zero shear stiffness in axial direction in the free interlocks is the most conservative assumption.

Due to the oblique bending behaviour, the chosen boundary conditions on the edges of the sheet pile, supporting the sheet pile in x-direction and rotational around z-axis, for symmetry conditions, are not completely applicable anymore. Therefore, to minimize the influence of these boundary conditions, a wider model is made, with nine U-sheet piles. It can be seen that now for the middle sheet piles, the deformations are not changing anymore and the influence of the boundary conditions is not noticeable. Due to these boundary conditions, only the middle 2 sheet piles, forming one double sheet pile are considered for the study and the results, showing the oblique bending behaviour of the sheet pile correctly (Figure 79). The other sheet piles experience too much reinforcement from the boundary conditions. The model is shown in Figure 78.

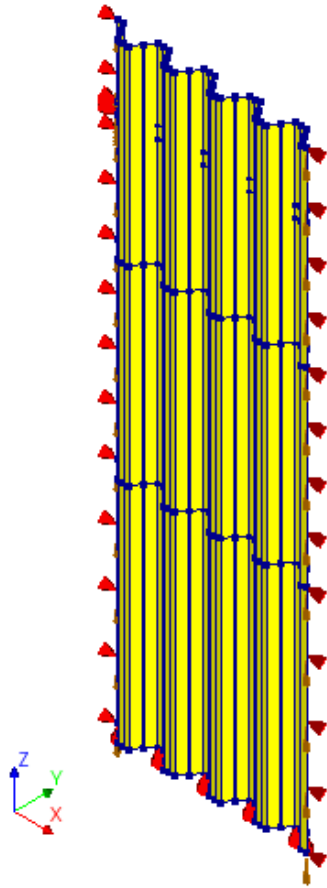


Figure 78: 3DSSI model for oblique bending

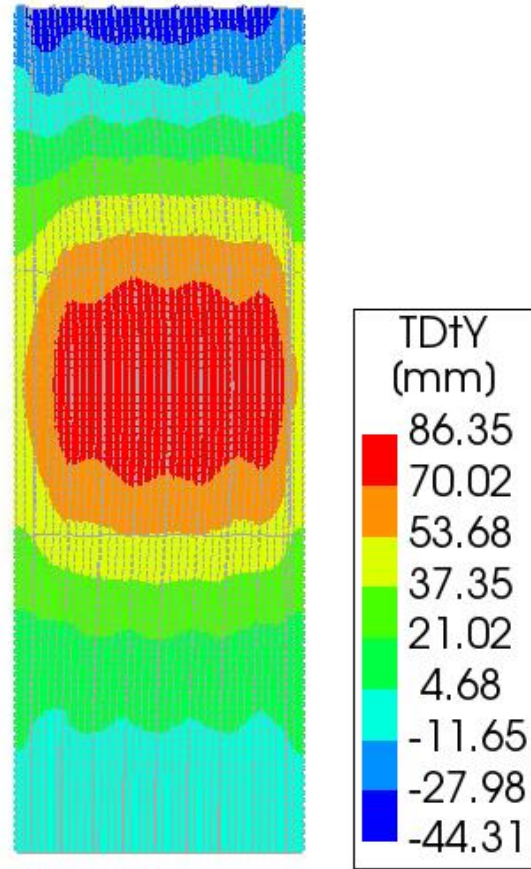


Figure 79: 3DSSI model for oblique bending with results

4.3.4. Material

Steel is defined in the model with nonlinear material properties. Plastic behaviour is captured with the von Mises plasticity model (equation 63). The steel is defined with a bilinear stress elongation diagram.

The Von Mises criteria:

$$\frac{1}{6}[(\sigma_1 - \sigma_2)^2 + (\sigma_2 - \sigma_3)^2 + (\sigma_3 - \sigma_1)^2] \leq \frac{1}{3} f_y^2 \quad (63)$$

4.3.5. Integration layers in thickness

The shell elements representing the web and flange are assigned the slenderness of the web and flange respectively. By default settings, the shell elements are divided into 3 layers in thickness. Then over the thickness, 3 integration points are considered. The integration layers can be increased. Using more integration layers has been studied to find the influence on the results. This is addressed in Appendix E. Using more integration layers does not influence the results and therefore with the default of 3 integration layers the study is proceeded.

4.3.6. Mesh (for situation without a hole)

The mesh for the situation without a hole is optimized especially around the location where the maximum bending moment and the maximum stresses occur. For each design, this location can be different. The mesh convergence study for the global behaviour is shown in Appendix E. From this figure, the mesh convergence starts from 100 mm. Larger mesh sizes show much irregularities. However, because of numerical stability for larger strains a mesh size of 50mm is chosen and at the maximum bending moment location, the mesh is refined with a mesh size of 20mm over a height of 2 meters. For design 1 of the parametric study discussed in chapter 5, this results in a mesh refinement of 20 mm from -5 m to -7 m.

Design 3, including oblique bending, is modelled with a refined mesh over a larger height, 4 meters, instead of 2 meters. This is due to the interface elements, requiring over the complete height of plasticity a smaller and consistent mesh for numerical stability and consistent plasticity results.

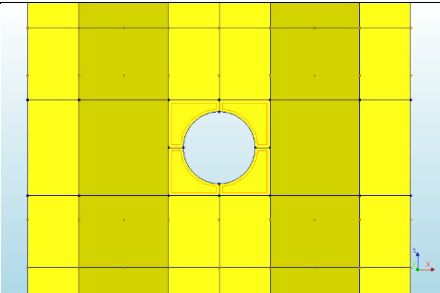
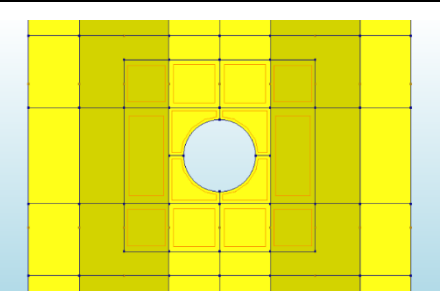
4.4. Numerical model: Hole weakening

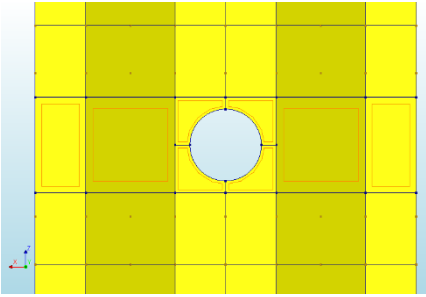
For the procedure of applying underwater anchors the first step is driving holes into the sheet pile. This hole weakening is studied and therefore modelled.

4.4.1. Redistribution load around hole

The nodal force produced by the springs at a location with large plasticity causes easily numerical errors and therefore the springs are replaced by a uniform distributed load over a height of 400 mm at the level of the hole. The soil is at the location of the hole always in active state and therefore the springs can be easily replaced by an uniform distributed load with the formula given for active earth pressure in chapter 2.4.2 equation 2 . Replacing the springs with a distributed load prevents local plasticity problems around the hole due to the nodal forces of the springs.

The earth pressure which normally acts on the steel at the location of the hole can be either neglected or redistributed around the hole. Several options are studied to determine the influence of this load around the hole and to study whether this small load influences the deformation and stresses/strains in the sheet pile significantly or whether it might can be neglected. The load of the soil acting at the location of the hole has to be redistributed around the hole. A study has been performed to study several options of redistributing the load around the hole These options are indicated in Figure 80, Figure 81 and Figure 82.

<p>Load distribution 1</p>	<p>Force is distributed over the width of the flange and a height of 400 mm around the hole.</p>	 <p>Figure 80: Load distribution around hole 1</p>
<p>Load distribution 2</p>	<p>Force is distributed around the hole within an area of 800x800 mm</p>	 <p>Figure 81: Load distribution around hole 2</p>

<p>Load distribution 3</p>	<p>Force is distributed over the width of the sheet pile over a height of 400 mm.</p>	 <p>Figure 82: Load distribution around hole 3</p>
----------------------------	---	--

The displacement curves are shown in Figure 83. Neglecting the earth pressure at the hole differs between load distribution 1 to 3 only 1 mm. However, neglecting the earth pressure at the hole is non-conservative and therefore, this option is not suitable. Load distribution 1 assumes the load to stay close to the hole. This option is used because it is not expected that the soil will redistribute over a large area. Moreover, Assuming the load to stay close to the hole is a conservative assumption. Therefore, the parametric study is proceeded with load distribution 1.

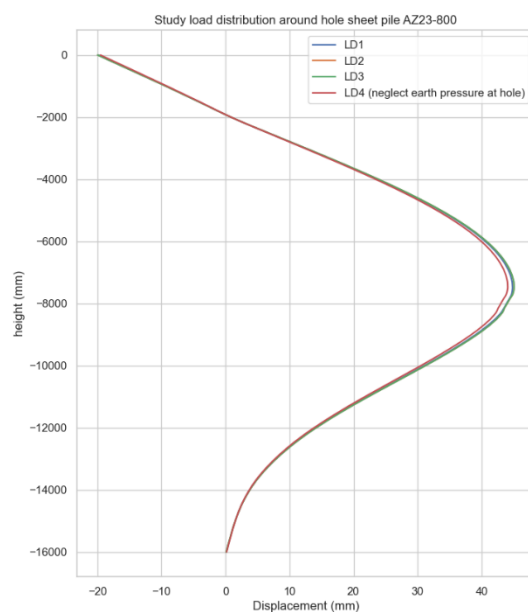


Figure 83: Displacement curve for different load distributions around the hole

4.4.2. Mesh for situation with a hole

The mesh around the hole is of large importance for the numerical stability of the model. Especially around the hole large plasticity occurs and mesh refinement is necessary. The mesh around the hole is designed according to the DIANA manual [41].

The mesh is refined around the hole and transferred to a larger mesh further from the hole. The mesh around the hole is over the height for which plasticity occurs modelled with a mesh of 10 mm. The mesh is above and below the hole transferred to a larger mesh. This is done by transition zones. The mesh is symmetric above and below the centre of the hole, i.e. the

transition zones are similar above and below the hole to transfer to a larger mesh. The mesh around the hole and the mesh transition are shown in respectively Figure 84 and Figure 85.

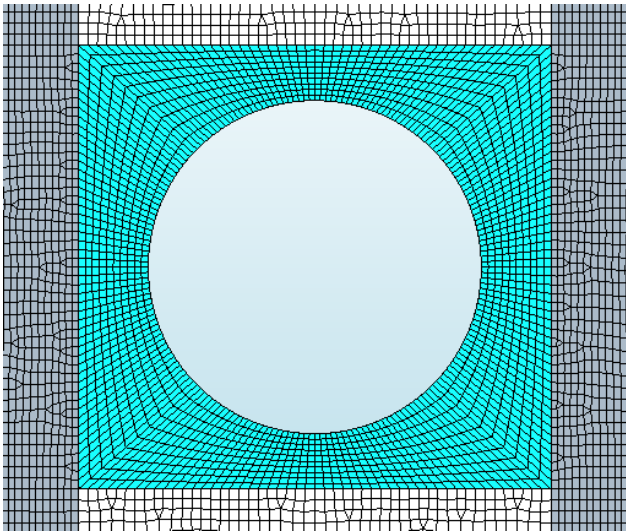


Figure 84: Mesh refinement around hole

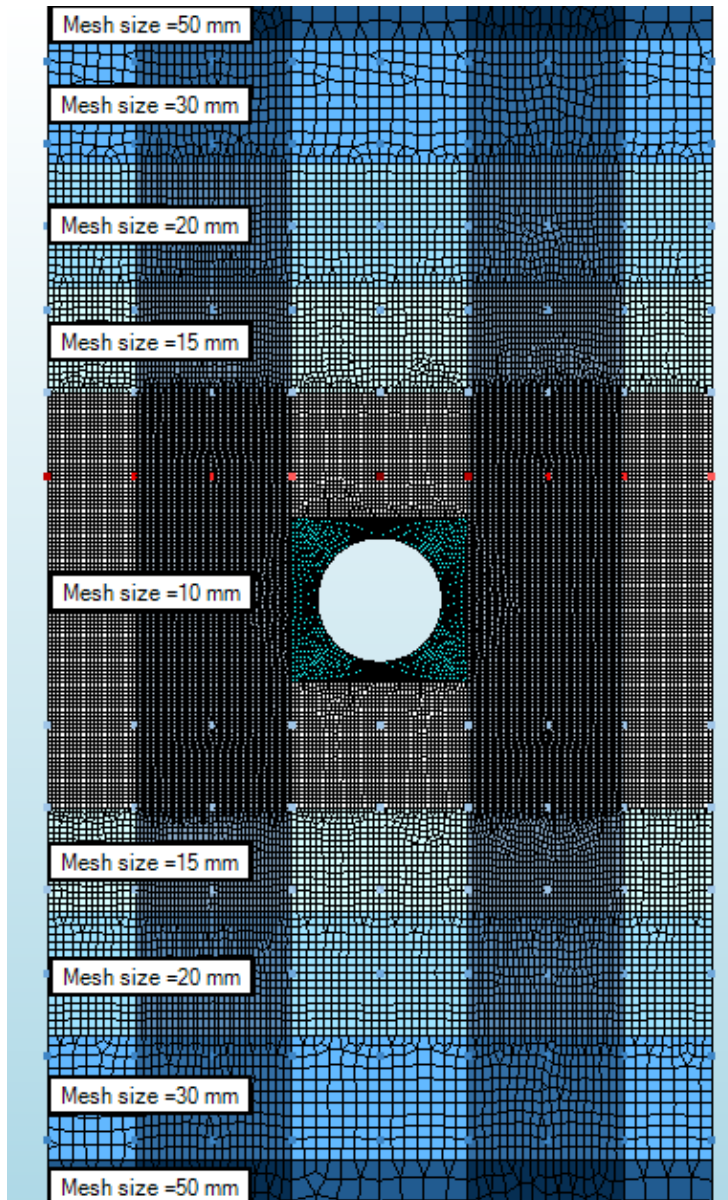


Figure 85: Overview mesh transition from fine to course

The mesh is 10 mm is extended over a height of 1m, thus 0.5m above the hole and 0.5m under the hole. The 15 mm mesh is applied over a height of 250mm, 20mm and 30 mm over a height of 300 mm. The course mesh used over the rest of the sheet pile is a mesh of 50mm

4.5. Numerical model: Finite Element Analysis characteristics

Analysis can be divided into linear and nonlinear analysis. Linear analysis consider linear elastic material and small displacements. Also, the boundary conditions remain unchanged while loading. This is also known as the infinitesimal strain theory. Nonlinear analysis are also applicable for large displacements and nonlinear materials. The stiffness matrix of a linear analysis remains constant, which is not the case for nonlinear analysis. For this study, a nonlinear analysis is of interest.

4.5.1. Nonlinear analysis

There are 3 types of nonlinearities in nonlinear analysis:

- Geometrical nonlinear: The geometrical nonlinearity includes large displacements and large rotations. The changes in geometry are considered in the calculation.
 - Material nonlinear: Nonlinear material includes nonlinear material behaviour of the material applied in the FE model. For steel, for example a bilinear steel diagram can be applied.
 - Geometrical nonlinear and material nonlinear: this analysis includes both geometrical nonlinearities and material nonlinearities.
- [42]

Geometrical nonlinear and material nonlinear analysis is of interest for this study. In general, material nonlinear properties are especially interest for cross section class 4 sections (chapter 3.2.1). Since hole weakening can change the behaviour, also geometrical nonlinear analysis for cross section class 1 till 3 are of interest to include local buckling behaviour in the model.

Considering the steel sheet pile, the material steel is used in the material nonlinear analysis. The theory used describing plasticity is the Von Mises yield model, with isotropic strain hardening. The von Mises criteria is highly applicable to ductile materials such as steel. The aspects which have to be prescribed are:

- Yielding: the stress rate when the material starts yielding
- Plastic flow: the plastic strain increments with reference to the stress increments
- Hardening: the hardening part gives the yielding during plastic flow

There are two types of hardening: isotropic hardening and kinematic hardening. Isotropic hardening means that the yield surface keeps the same shape. When increasing the stress, the yield surface expands. The kinematic hardening approach distinguishes itself from isotropic hardening in this phenomena. Kinematic hardening takes into account the Bauschinger effect. This effect contains the phenomena of increasing tensile strength occurring while reducing the compressive strength. The yield surface remains the same shape but translates in the stress space. Generally, there is no difference in the results using isotropic hardening or kinematic hardening, only when the material changes from tension to compression and vice versa. The hardening type is thus of interest for alternating loads. For this study, there is no difference in the results, and isotropic is inserted in the finite element program DIANA FEA.

For the geometrical nonlinear analysis, distinction is made between Total Lagrange and Updated Lagrange formulation. The Lagrangian formulation means that all particles are followed in the body in their motion and refers all static and kinematic variables to the initial configuration, thus the undeformed geometry, while Updated Lagrange formulation refers all static and kinematic variables to the last calculated configuration. This means that for the Updated Lagrange formulation, the strain and stress measures are based on an updated reference geometry. Therefore, the Updated Lagrange approach is more appropriate for problems with large strain and material nonlinear behaviour. For this study, the Updated Lagrange formulation is used. [42]

The detailed input in DIANA FEA can be found in Appendix B.

4.5.2. Load steps

The soil load is thus produced by the springs and therefore load steps cannot directly be included in the soil load. However, not using load steps and providing all the load at ones causes easily numerical errors. Therefore, to smoothen the calculation fictitious loads are included.

The loads are assigned to the nodes on which also the nodal springs representing the soil load are attached. The load is designed such that the sheet pile calculation starts from the equilibrium stage. To start from the equilibrium position of zero displacement, on both active and passive side of the sheet pile the springs should represent the neutral earth pressure. The load is designed such that the sheet pile starts from this equilibrium:

- Neutral earth pressure on passive side of the excavation height (level 0m – level -9m)
The load has to simulate neutral earth pressure over the excavation height. Therefore, on the nodal springs, a load is simulated depending on the height similar as the soil load equal to the neutral earth pressure as if there is no excavation (so similar to the neutral earth pressure on the active side which is included in the springs). This load is calculated according to equation 64.

$$F_{n1} = K_0 \cdot \gamma_{eff} \cdot z \cdot A_{spring} \quad (64)$$

With z from z=0 m to z=-9m and A_{spring} being the area represented by each spring, which is 200x200 mm².

- Neutral earth pressure on passive height (level -9m – level -16m)
Due to the excavation, different springs are presented at the active and passive side. To obtain equilibrium in the neutral earth pressure, the difference between the neutral earth pressure on active side and the neutral earth pressure on passive side is simulated with nodal loads. This is captured in equation 65.

$$F_{n2} = K_0 \cdot \gamma_{eff} \cdot (z_{active} - z_{passive}) \cdot A_{spring} \quad (65)$$

These loads are reduced from 1.0 (equilibrium, 0 displacement) to 0.0, the design and actual deformation shape of the sheet pile. The load steps in between 1.0 and 0.0 do not represent a real soil behaviour. However, it is thus only used to smoothen the calculation procedure and obtain the final deformation shape of the sheet pile including situations with large displacements and plastic strains.

For the sheet pile with a hole, after reducing the fictitious load (F_{n1} and F_{n2}) to zero, the distributed load around the hole (chapter 4.4.1) is applied, again in load steps, but then from 0 to 1.0, since this load is actually present and should be included in the results of the analysis. The sheet pile with the load F_{n1} and F_{n2} is shown in Figure 86.

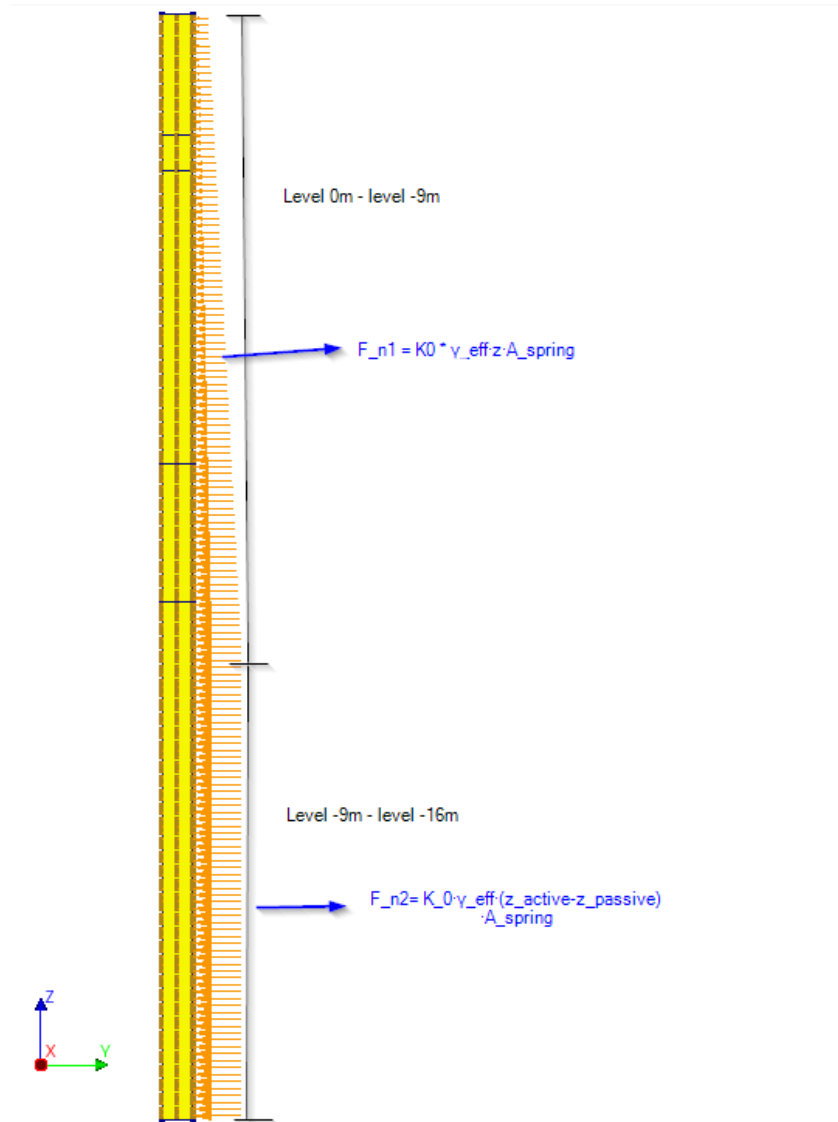


Figure 86: sheet pile with fictitious load for numerical purposes;
fictitious load is stepwise reduced to 0

4.6. Numerical model: Application

The numerical model is developed to find the behaviour of the sheet pile. The objectives of this thesis are to study the failure modes for steel sheet piles subjected to hole weakening and study the influence of hole weakening on the capacity and behaviour of the structure. To determine the failure of the sheet pile, the loading has to increase up till failure load, this is discussed in chapter 4.6.1.

4.6.1. Load increase

To study the sheet pile structural behaviour and failure load, a method to increase the soil load is developed. Therefore the soil behaviour keeps included in the study. The options which are found in practice are [4]:

- Increase retaining height by reducing passive height; excavating
- Increase load on active side of the sheet pile; for example terrain loads

Increasing retaining height

Increasing the retaining height causes large rotations at the toe of the sheet pile and the sensitivity to soil instability is large. For a large embedded sheet pile the displacement curves are shown in Figure 87. The sheet pile is 20 meters long with a retaining height of 9 meters. For a more realistic design with a length of 16 meters and a retaining height of 9 meters the D-sheetpiling results are given in Figure 88. Reducing the passive height by more than 2 meters (and thus a retaining height of 11 meters) the sheet pile becomes unstable. This is due to the soil becoming unstable. For the sheet pile, D-sheetpiling considers purely elastic behaviour. However, when the soil becomes fully active on the right side and fully passive on the left side, the maximum resistance of the soil is reached. Since this thesis aims to obtain the structural failure and not the geotechnical failure, this method of increasing the load is not desirable.

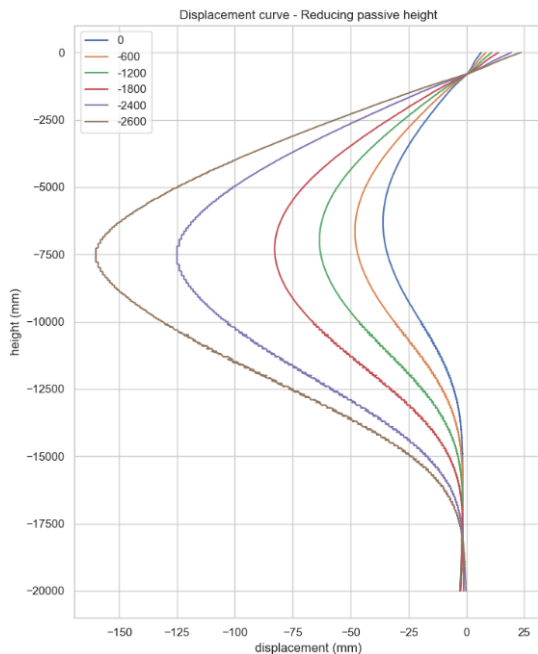


Figure 87: Displacement over height curves for increasing retaining height for an unrealistic long sheet pile

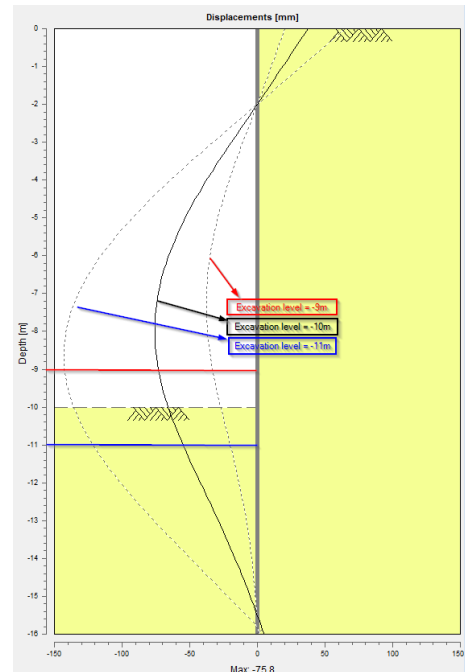


Figure 88: Displacement over height curves for increasing retaining height

Increasing load on active side

Increasing the load on the active side of the sheet pile by applying a uniform load (Figure 89) is a more stable solution for finding the structural failure of the sheet pile.

Similar as for reducing the passive height this is studied shortly using D-sheetpiling. The finite element model produced in this thesis models the soil with springs. The soil behaviour in the numerical model in DIANA are applicable for uniform loads and a horizontal surface. Therefore, the uniform load is applicable.

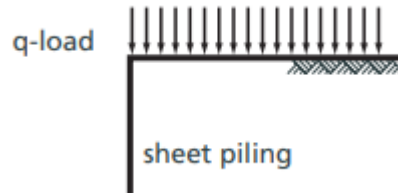


Figure 89: Uniform load on active side [22]

The uniform load results in different spring characteristics at the side of application of the uniform load, thus the active side. The load is indicated as a layer of sand in mm. The self-weight of sand is the uniform active load (kN/m^2). The theory of the changing spring characteristics is discussed in chapter 2.4.5.

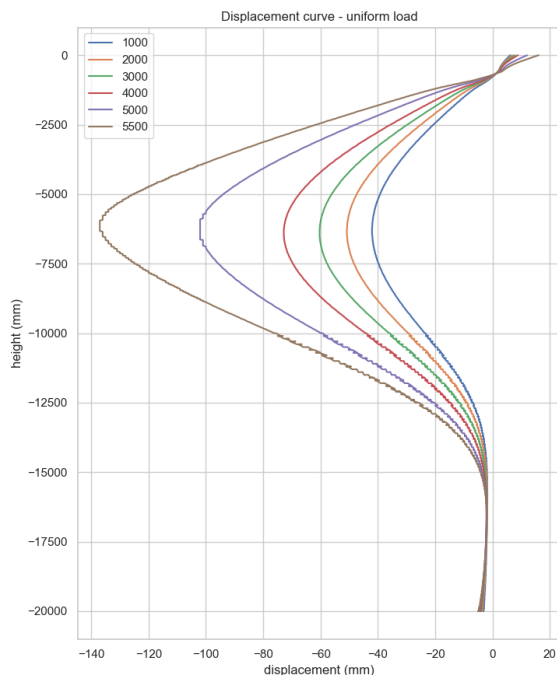


Figure 91: Displacement over height curves for increasing uniform surcharge load for an unrealistic long sheet pile

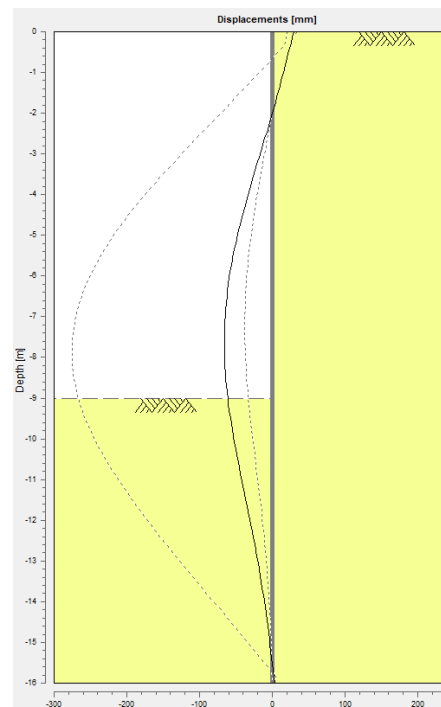


Figure 90: Displacement over height curves for increasing uniform surcharge load

The D-sheet result consider elastic behaviour and disregard the bending moment capacity of the sheet pile. However, it can be observed that the uniform load can reach much higher deformations without the becoming unstable regarding soil behaviour, as shown in Figure 90 and Figure 91.

Besides a uniform load, also a non-uniform surcharge load can be applied. This surcharge load can be applied over a certain length and differ in force over a certain length. However, the calculation procedure considering a surcharge load is in D-sheetpiling calculated with the method of Boussinesq (Figure 92). This theory is not further considered or used for this thesis since the interest is more in the capacity of the sheet pile than the soil behaviour. Therefore the limitation is that only uniform loads are applicable in the 3DSSI model.

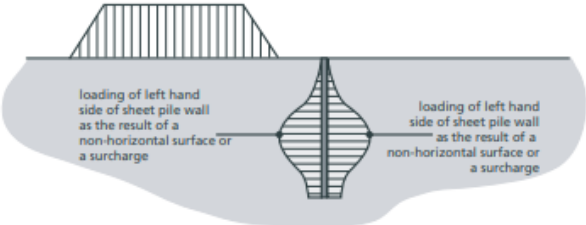


Figure 92: influence of a surcharge load according to the method of Boussinesq (source: Deltares)

With an increasing load on active side, the soil behaviour changes. This is shown in Figure 93. The active earth pressure increases with an increasing soil pressure. The passive sides shows also an increase in passive resistance needed to resist the active earth pressure. The soil on the passive side is over a larger height in passive state for larger uniform surcharge loads on active side. The change of the soil response has also influence on the sheet pile deformation shape.

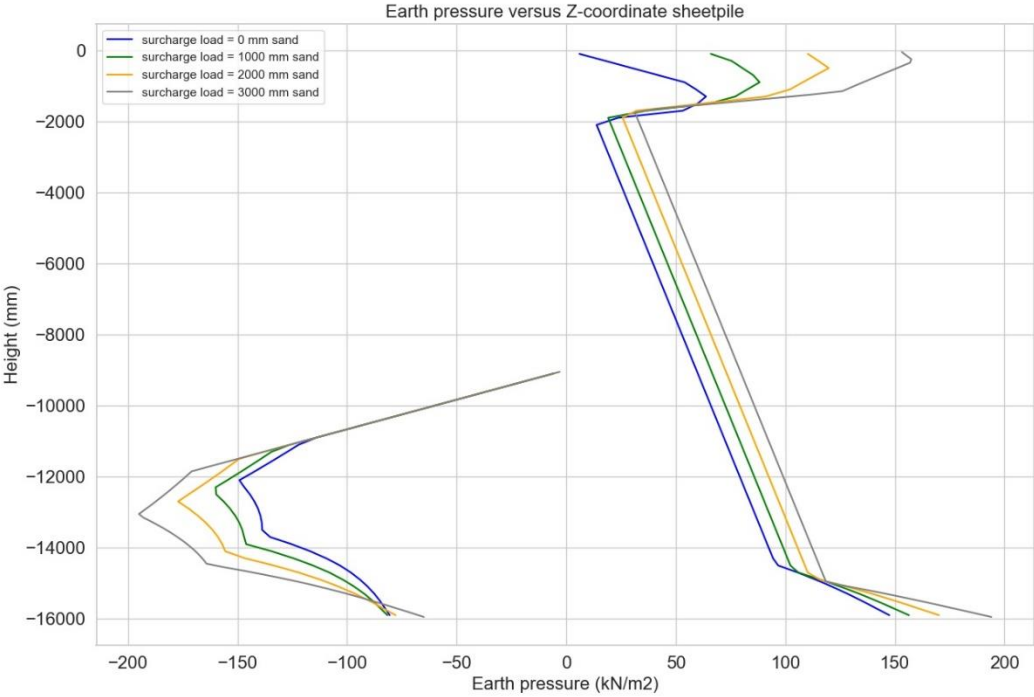


Figure 93: Earth pressure for different surcharge loads

4.6.2. Comparison 3DSSI model and D-sheetpiling

The 3DSSI model is based upon the soil theory used in D-sheet piling using uncoupled springs to model the soil. This is elaborated in chapter 4.2.1. Therefore, the model can be verified using D-sheet piling models. The main difference is the 3D behaviour which is included in the proposed model in DIANA and D-sheet piling considers the sheet piling as a elasto-plastic beam. For a normal case without a hole, the displacement over height curves can be compared. The displacement over height curves are given in Figure 94. The difference between the D-sheet piling deformation results and the results of the 3DSSI model is 2mm, on a sheet pile length of 16 m. The results of DIANA are conservative compared to the results of D-sheet piling. The 3DSSI model does not include corner radii and the additional material at the interlocks. This reduces the stiffness significantly. The stiffness is calculated manually to exclude the corner radii and additional materials in the interlocks, to give comparable stiffnesses of the sheet piles and thus comparable results for the soil behaviour and displacement graphs between D-sheetpiling and 3DSSI model. This shows thus that the soil-structure interaction is correctly captured with the 3DSSI model.

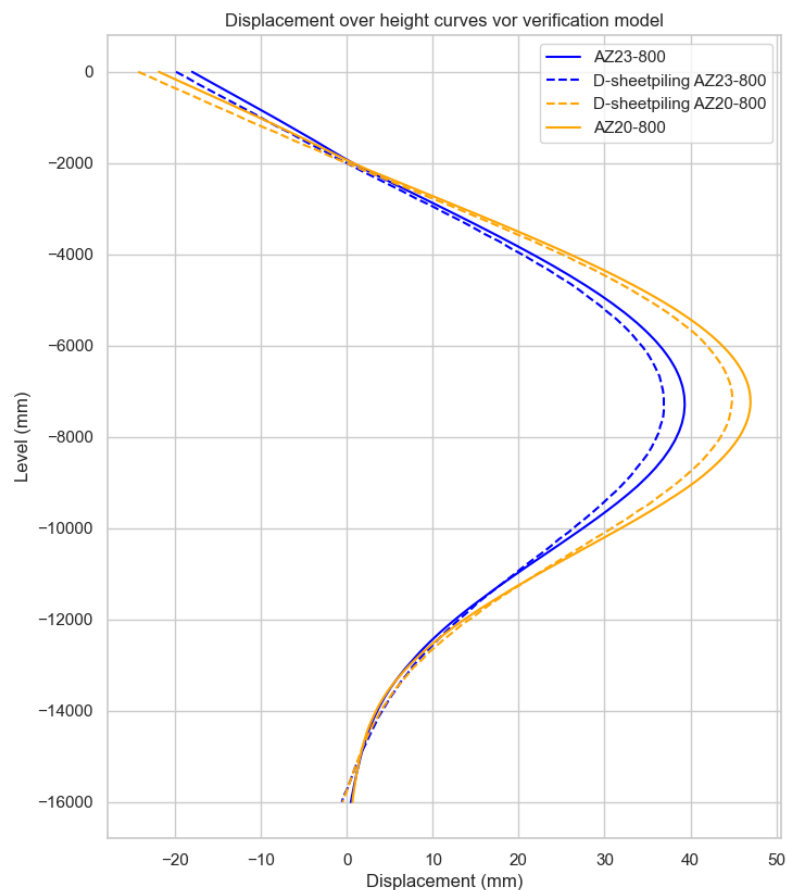


Figure 94: Verification of model with D-sheetpiling

Comparing D-sheetpiling with the developed 3DSSI model, the main difference is the 3D behaviour which is included in the 3DSSI model. D-sheetpiling models the sheetpiling as a beam with the corresponding stiffness, while the 3DSSI model draws the complete sheet pile with shell elements. For 3D problems such as hole weakening, connection of an anchor, oblique bending and more, the sheet pile behaviour and for example stress distribution can be

studied in detail. Therefore, the model can be used for much more purposes than hole weakening only. Nowadays, D-sheetpiling, or Plaxis 2D and 3D [43] models are used to study sheet pile behaviour. However, D-sheetpiling thus only gives 2D results and Plaxis focuses on the soil behaviour and not the detailed steel behaviour of the sheet pile. This new type of modelling is thus proposed to obtain insight into the steel behaviour of the sheet pile in detail in an efficient manner. Since as discussed in more detail in chapter 4.1.2, the springs provide accurate results regarding internal forces and deformations of the sheet pile and the calculation time is optimal compared to modelling the soil with the finite element method.

4.6.3. Verification model

The 3DSSI model is verified in chapter 4.6.2 with respect to the displacement over height with D-sheet piling. This shows that the soil-structure interaction is correctly captured in the model. However, verifying the failure mode of the 3DSSI model cannot be performed with D-sheet piling. This can for situations without a hole be verified by tests performed by Kort (2002). These tests are discussed in detail in the literature part, chapter 3.2. For the cases without a hole, test results are not available. Therefore, a displacement induced 4-point bending test is used to compare and verify the failure mode of the cases with a hole. The dimensioning of the 4-point bending test is based upon characteristics provided in the literature, the background report and research for EN 1993-1-5 (Sedlacek et al, 2001). These dimensions give the most accurate displacement shape approaching real sheet pile displacements and behaviour. These dimensions and characteristics are shown in detail in Appendix C and Figure 95. Summarizing, similar as the 3DSSI model, physical and geometrical nonlinear behaviour is included and the physical nonlinearity is included by bilinear elastic-plastic steel behaviour. The load is applied via stiffeners which help to introduce the load uniform over the width. The support forces are introduced in a similar manner. For more detailed sketches and description the reader is referred to Appendix C. The advantage of the 4-point bending test is the displacement-induced loading, which means that also behind the maximum load the sheet pile behaviour and resistance can be observed. However, soil behaviour is thus not included. The failure modes can be compared with the 3DSSI model as verification of the model. [30]



Figure 95: 4-point bending test designed by Sedlacek et al (2001) [30]

First, the reference case, the case without a hole, is discussed. Firstly, based on the 3DSSI model, the following failure mode is found: Local buckling in the flange, concentrated plastic kin, but plasticity over a larger area (Figure 98). The 4-point bending test (Figure 96) and 4-point bending model (Figure 97) show similar failure mode as the 3DSSI model, local buckling in the flange and plasticity with a plastic kink. A small difference is the buckling of the web in the 3DSSI model indicated with the red area in the webs in Figure 98. This is not observed for the test and 4-point bending model, but can be explained by the soil pressure included in the 3DSSI model on the location of the maximum bending moment which is not included in the 4-point bending test or 4-point bending model. The load-displacement curve for the 4-point bending test is given and discussed in Appendix C.

The 3DSSI model including oblique bending is also verified using 4-point bending models and literature. This is elaborated in Appendix D.



Figure 96: 4-point bending test up till failure of sheet pile [23]

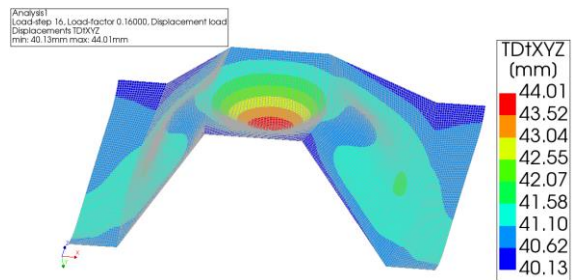


Figure 97: 4-point bending model: Displacements at ultimate load, no hole

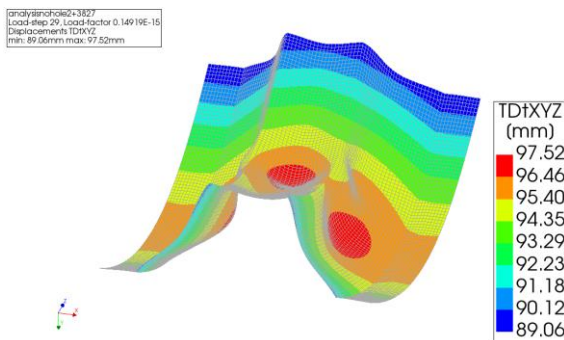


Figure 98: 3DSSI model: Displacements no hole at failure load

Then the basic case (defined in chapter 5), with a hole is loaded with the 4-point bending test. Again, the load-displacement curve is given in Appendix C. The failure modes of the 3DSSI model is given in Figure 100 and Figure 99 shows the failure mode of the 4-point bending test. For both situations, large plasticity around the hole, resulting in a deformed web outwards, is observed. For the 3DSSI model, the maximum stress due to the global bending moment is not exactly at the location of the hole. This explains the buckling of the web inwards, just above the hole at the location of the maximum bending moment.

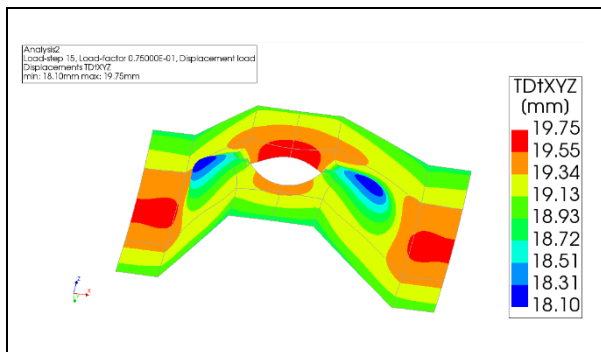


Figure 99: 4-point bending model: Displacements at ultimate limit, hole basic case

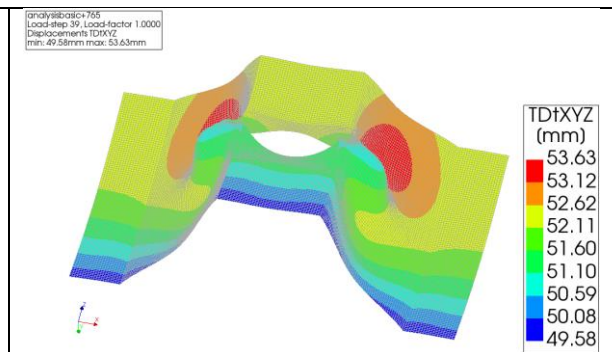


Figure 100: 3DSSI model: Displacements at ultimate load, basic case

Since similar failure modes are obtained for the 4-point bending model and the 3DSSI model, it can be assumed that the failure load and failure mode give the maximum load in the 3DSSI model.

4.7. Conclusion

The 3DSSI model answers the sub question: What are the characteristics of the numerical model to obtain understanding in the sheet pile resistance and behaviour regarding the effect of hole weakening?

The 3DSSI model combines several theories from the state of art in a manner which has not been performed in literature earlier. The soil is modelled with the subgrade reaction, providing accurate displacements and internal forces of the sheet pile. Until now, this theory has only been used in 2D calculations. In the 3DSSI model, the subgrade reaction model is extended to a 3D model. The sheet pile is therefore modelled with 2D shell elements. The 3DSSI model captures the 3D soil structure interaction, by modelling the soil with 1D springs and the sheet pile with 2D shell elements. Now, local behaviour, for example around the hole, can be calculated which is not possible with existing subgrade reaction models. For this model, numerical stability is also of importance. Therefore, the forces of the springs should be applied stepwise. A procedure is developed to compensate the spring force in the initial step, which is the neutral earth pressure. This compensating force is then reduced stepwise to zero to find the sheet pile deformation, internal forces and the soil-structure interaction. Also, around the hole, the springs have to be replaced by a uniform distributed load for numerical stability. This is equal to the active earth pressure in all cases and therefore not influencing the soil-structure interaction. For double U-profiles, with the 3DSSI model, the free interlock can be modelled by including the axial degree of freedom in the interlocks. Then oblique bending can be modelled and be studied. The load can be increased by increasing the uniform surcharge load on the active side of the sheet pile. Then the maximum load before structural failure can be obtained.

This model is thus developed for hole weakening, but more 3D behaviour can be studied in an efficient manner, such as oblique bending in more detail, physical and geometrical nonlinear behaviour, anchor connections and local behaviour. This is not all considered for this thesis, but this model can be used for these type of studies in further research.

5. Design of parameter study

The parameter study includes the different hole characteristics and sheet pile characteristics' influence on the hole weakening. First, the method developed to perform the parameter study is elaborated. Then the studied parameters are discussed in more detail.

5.1. Design of parameter study

The design of the parameter study is firstly discussed with respect to the research method. Then the design of the soil is discussed with respect to the parametric study and finally the different designs of the sheet piles.

5.1.1. Research method

The influence of the different hole characteristics on the sheet pile resistance and behaviour is obtained from the parameter study. Therefore, firstly a reference case is designed for a situation without a hole. This is a single – anchored sheet pile designed according to the existing design regulations discussed in chapter 3. A design with a unity check of approximately 0.6 with respect to the bending moment, which is the governing failure mode, is given. A unity check of 0.6 is not unrealistic for older existing sheet piles which are designed with Blum's method (chapter 2.4.4). Increasing the load captures than the initial design with Blum's method up till a more utilised design and the failure load.

To obtain the failure load, the uniform surcharge load on active side is increased failure of the sheet pile occurs. Besides the increasing surcharge load on active side, the soil characteristics remain constant (chapter 5.1.2). Discussion of this load increasement method can be found in chapter 4.6.1. The failure load is defined as the load for which the 3DSSI model cannot find convergence anymore and warns for a lack of capacity. Moreover, the slope of the load-displacement curve is low and decreased significantly compared to the stiffnesses before reaching the failure load which also indicated reaching the maximum capacity of the sheet pile. With the developed 3DSSI model (chapter 4) the deformations, stresses and strains and of the sheet pile can be obtained and the soil response.

The load-displacement curve is derived by exporting for each increment in uniform surcharge load the maximum displacement in y-direction of the sheet pile. Plotting this displacement against the uniform surcharge load gives the load-displacement curve. This is given in chapter 6.

For the parametric study, it is of importance that only one parameter varies per analysis. As discussed, first a general design without a hole is made, which is indicated as the reference case. Besides the reference case, also a basic case is designed. The basic case is the same sheet pile as the reference case, but then with a standard hole. In the parameter study differentiations are made based on the basic case, e.g. only hole diameter is changed and all other characteristics are kept constant with respect to the basic case. The parametric study thus considers firstly the reference case and the basic case. Since the aim is to study different hole characteristics, the basic case is adapted for each characteristic: Hole diameter, location hole (depth), location of the hole with respect to the flanges: hole in-pan or out-pan and the hole spacing.

Characteristics of the basic case are given in Table 2. The basic case is identified based upon practical desired hole characteristics. A hole of 300 mm is optimal for the desired equipment for drilling a hole, while the location of -8m is an optimal location regarding the maximum bending moment after excavating (chapter 5.2). Finally, a hole in compression zone makes sure that the anchor is not protruding from the sheet pile.

Table 2: Reference case and basic case characteristics

Reference case	No hole
Basic case	Hole diameter = 300 mm Location hole = - 8 m Hole in-pan or out-pan = in-pan (hole in compression zone) Hole spacing = Hole in each compression flange

Based on the literature of plastic design, discussed in chapter 3.2, the cross-section classification is also expected to influence the capacity of the sheet pile, including the hole weakening as well. Therefore, the reference case, basic case and the parametric study based on this basic case are performed twice, for a sheet pile of cross-section class 2 and a sheet pile of cross-section class 3. Also oblique bending will be studied, but in less detail. This is further elaborated in chapter 5.1.3.

The parameter study workflow can be summarized stepwise:

1. Based on the soil characteristics, the sheet pile profile of cross-section class 2 is designed with a unity check of approximately 0.6 based upon the bending moment resistance, using D-sheetpiling
2. The design is recreated with the developed 3DSSI model as described in chapter 4
3. Model is run for each increased uniform surcharge load until the failure load is found
4. For each run the displacements are exported
5. The maximum displacement (in y-direction) is plotted against the uniform surcharge load (reference curve)
6. The reference curve is adapted representing the basic case with the corresponding hole characteristics
7. Step 3 and 4 are repeated for the basic case
8. The maximum displacement is plotted against the uniform surcharge load (basic case)
9. One parameter, for example the hole diameter, is adapted, and step 3 and 4 can be repeated
10. The maximum displacement is plotted against the uniform surcharge load for the adapted parameter.

Step 9 and 10 are repeated, starting from the basic case and adapting one parameter, until all the proposed parameters are studied.

The same procedure is completely repeated for a sheet pile of cross-section class 3.

5.1.2. Soil characteristics

The soil characteristics are kept constant, except for the uniform surcharge load. The uniform surcharge load influences the springs as described in chapter 4.6.1. However, the soil material remains constant in all calculations, similar as the excavation height. The design is based on a realistic dimensions of a sheet pile design. However, the soil material is reduced to only one material instead of multiple layers, for simplicity. However, the internal forces such as bending moment and the displacement represent a realistic sheet pile design. The characteristics are summarized in Table 3:

Table 3: Soil characteristics

Material: γ_{eff}	Medium dense sand 20 kN/m ³
-----------------------------	---

Earth pressure coefficients (based on Müller-Breslau)	
K_a	0.33
K_0	0.5
K_p	3.0
Stiffness:	
$k_{h,1}$	20000
$k_{h,2}$	10000
$k_{h,3}$	5000

The existing top anchored is at a level of -2m.

5.1.3. Sheet pile characteristics

The sheet pile is thus as described in chapter 5.1.1 designed at a unity check of approximately 0.6. As discussed in chapter 3.2 the plastic resistance is also of importance considering the sheet pile resistance and behaviour. Therefore, two types of sheet piles are studied in the parameter study with a different cross-section classifications. Both are Z-profiles, to exclude oblique bending behaviour. Considering the available sheet piles, especially cross-section class cross 2 and cross-section class 3 profiles are available. Therefore, cross-section class 1 and cross-section class 4 are not studied. Cross-section 2 can be designed based on an elastic global analysis and the plastic bending moment capacity can be used. For cross-section class 3, there is no plastic capacity and the elastic bending moment capacity is the design bending moment resistance. For cross-section class 2 AZ23-800 is appropriate, while for cross-section class 3 a AZ20-800 with a higher steel grade is designed to obtain a unity check of approximately 0.6. The influence of a higher steel grade on the results is expected to be low, since for both steel grades comparable bi-linear steel diagrams are used and the unity check for both designs at initial stage are equal. Details are summarized in Table 4.

Table 4: Sheet pile characteristics

Design 1	AZ23-800 (S240)
Cross-section classification	2
Elastic bending moment resistance*	458 kNm
Plastic bending moment resistance*	525 kNm
Design 2	AZ 20-800 (S355)
Cross-section classification	3
Elastic bending moment resistance*	562 kNm
Design 3	PU22 (S355); including oblique bending
Cross-section classification	2
Elastic bending moment resistance*	672 kNm**

*The bending moment resistance of the sheet pile as modelled in DIANA FE excluding corner radii and additional material in the interlocks

**The elastic bending moment resistance excluding the influence of oblique bending

5.2. Parameters for hole weakening

The studied parameters are based on the hole characteristics and the characteristics which also influence the bending moment resistance.

- Location of the hole

With the location of the hole, the depth of the hole with respect to the active side’s soil surface is defined.

According to the study of Emarah and Seleem (2016), as discussed in chapter 2.2, the optimal location of the underwater anchor is between 0.6-0.7 of the retaining height. This means that the optimal location of the hole depends on the excavation and the new retaining height. Also, the location of the top anchor influences the optimal position of the underwater anchor. For this study, the findings of Emarah and Seleem are used and it is assumed that the location of the hole is approximately 0.65 of the increased retaining height. Also, a minimum of 1 meter above ground level is assumed, to have enough workspace for driving the hole and anchoring. This leads to the following hole positions (Table 5).

Table 5: Positions of the hole (m)

H_{hole} (m)	Excavation depth		
	1m	2m	3m
Retaining height			
8m	5.9	6.5 m	7.0
9m	6.5	7.2	7.8
10m	7.2	7.8	8.5
11m	7.8	8.5	9.1
12m	8.5	9.1	9.8

The optimal location of the hole and the underwater anchor is thus defined as (equation 66):

$$H_{hole} = 0.65 H \leq h - 1 \tag{ 66 }$$

H_{hole} is the depth of the location of the hole in meters measured from the active side’s soil surface

H is the new retaining height after excavating in meters.

h is the original retaining height before excavating in meters.

It is thus found that the optimal position of the hole depends on the new retaining height. Therefore the location of the hole with respect to the top of the sheet pile is studied as a parameter for determining the influence of the location of the hole on the bending moment resistance. Based upon the design case, the location of the hole is at the location of the maximum bending moment or lower. Since, due to excavating or uniform surcharge load, the new maximum bending moment will decrease in height and cannot be above the existing maximum moment this is also considered when determining the studied heights of the location of the hole.

For the parameter study, a retaining height of 9m is considered. In the original design the maximum bending moment is at a level of -7m. Based upon the reasoning above, the basic case is determined with a hole at a level of -8m. The other options considered are -7m and -7.5m.

- Hole diameter

The larger the hole diameter, the more steel is missing and it is expected that the reduction factor for the strength and stiffness will be larger for larger hole diameter. Based upon the equipment needed for drilling anchors, the basic case is defined with a hole of 300 mm. For

smaller anchors, smaller equipment can be used and therefore also a hole of 200 mm will be studied.

- Hole spacing

It is expected that the centre to centre distance (width) between the holes influences the strength and stiffness of the sheet pile and therefore this will be studied as well. For the basic case, the sheet pile is located in the compression flange and only one section of a sheet pile will be modelled, assuming that thus the hole is located each sheet. The other options studied is placing a hole while skipping one (compression) flange between each hole, thus a hole spacing of 2 sheets. For this parameter, the model is designed wider than for the other parameters, since the sheet pile spacing has to be captured. The model is shown in Figure 101 and Figure 102.

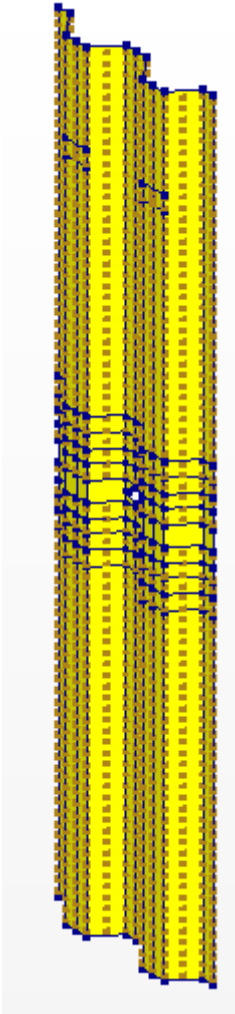


Figure 101: 3DSSSI model for hole spacing = 2 sheets (1)

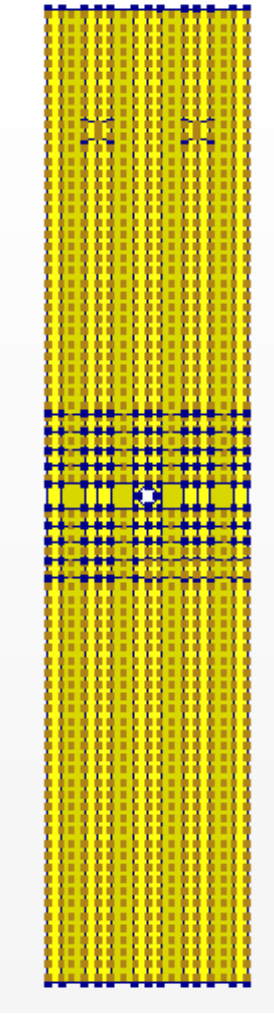


Figure 102: 3DSSSI model for hole spacing = 2 sheets (2)

- Location hole in-pan or out-pan

Whether the hole is located in-pan, which means in the compression zone of the sheet pile(at the soil side), or out-pan, in the tension zone (water side), could lead to different resistance of the sheet pile and different sheet pile behaviour. Therefore, both situations will be studied. Based on the desired location of the hole in-pan, in the compression zone, this is identified as the basic case.

- Cross-section classification

In the theory of plasticity it is found that the cross-section class, which depends on the web and flange slenderness influence the rotation bending moment capacity and therefore the bending moment capacity. It is expected that the hole reduces the bending moment capacity. Also at that location, there is less material in the flange and therefore the flange slenderness is locally changed. Therefore, it is expected that the cross-section classification influences the behaviour of the sheet pile regarding hole weakening. The most available sheet piles are from cross-section class 2 and 3 and these are both studied. Details on the slenderness and the boundaries for the cross-section classes are given in Table 6.

Table 6: Slenderness of studied sheet piles

Class 2 (Z-profile)	Class 3 (Z-profile)
Boundaries Cross Section Class 2	Boundaries Cross Section Class 3
$\frac{b/t_f}{\varepsilon} \leq 45$	$\frac{b/t_f}{\varepsilon} \leq 66$
Slenderness AZ23-800: 37.0	Slenderness AZ20-800: 55.6

- Oblique bending

Since oblique bending results in different bending behaviour (see chapter 3.3) the hole weakening is also studied for double U-profiles subjected to oblique bending. Since the design does not have a flange width of 300 mm and assuming the hole is only drilled in the flange, a hole of 200 mm is studied. Not all above mentioned parameters are studied for oblique bending since this would cost too much calculation time for the purpose of this thesis.

A summary of the studied parameters is given in Table 7.

Table 7: Parameters for hole weakening

Location of the hole	H = -8m (basic case), H=-7.5m, H=-7m
Hole diameter	D=300 (basic case), D=200
Hole spacing	1 sheet (basic case), 2 sheets
Location hole in-pan / out-pan	In-pan (basic case), out-pan
Cross-section classification	Class 2 and class 3
Oblique bending	No hole and a hole of D=200 is studied.

5.3. Overview parameter study

The complete parametric study is summarized in Figure 103. The parameter study exists thus of 3 different sheet pile designs, based upon the same soil and excavation depth. The 3 designs are design 1: AZ23-800, design 2: AZ20-800, design 3: PU22. Design 1 and design 2 address the difference between cross-section class 2 and cross-section class 3, while design 3 considers oblique bending of double U-sheet piles. Firstly focussing on design 1, reference curve for no hole, the basic case curve, and the curve for the studied parameters are made following the workflow discussed in chapter 5.1.1. Similar is performed for design 2 and design 3 will only consider the reference curve and a hole of 200 mm, as explained in chapter 5.1.1. A more elaborate overview of the complete parameter study is given in Appendix F.

Based on the results, an interesting difference in capacity and behaviour was found between the tension and compression cases. Therefore, for the parameter hole in tension, not only a hole of 300 mm is studied, but also a hole of 200 mm. This is further discussed in chapter 6.

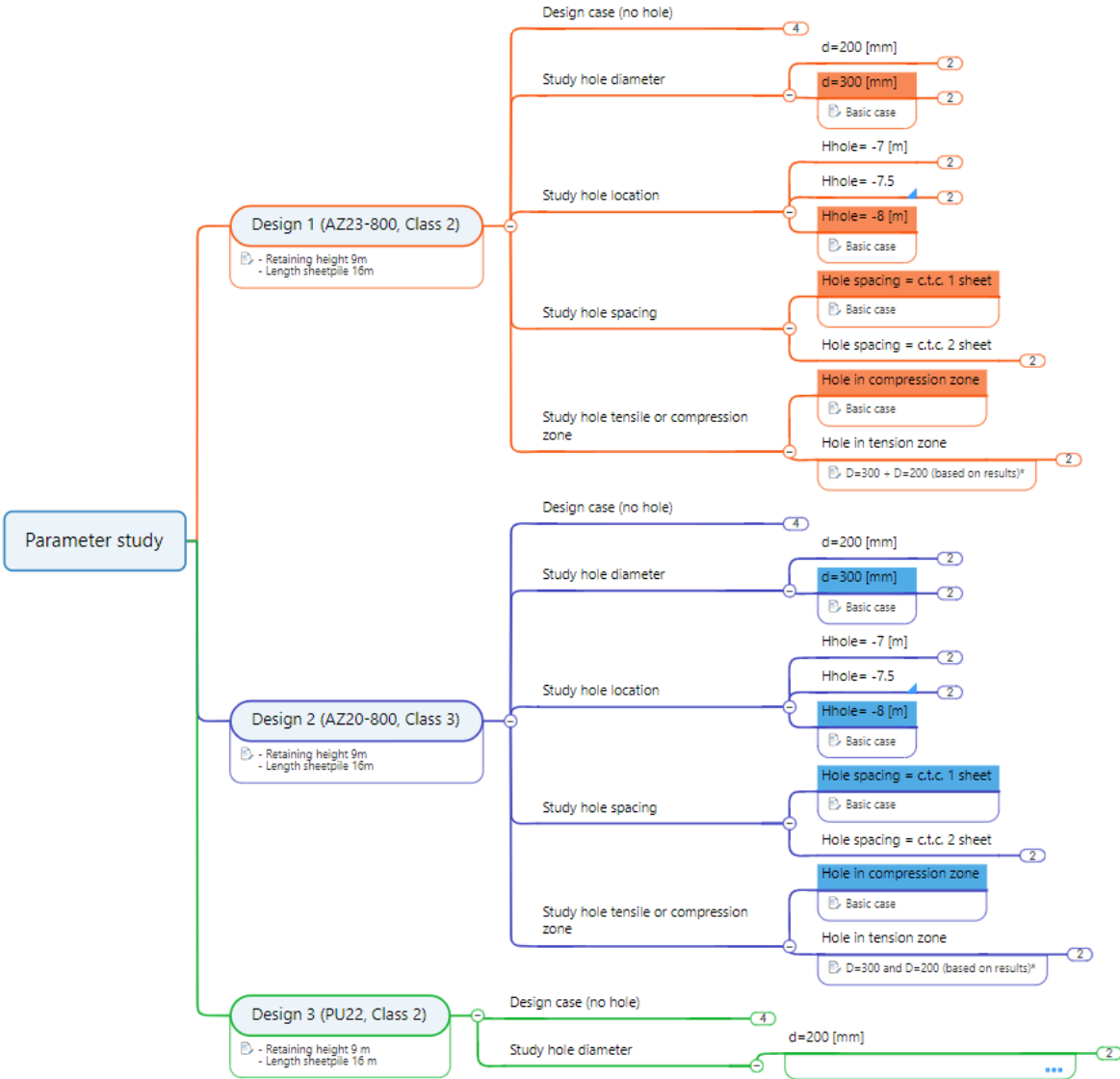


Figure 103: Parametric study overview

6. Results of parameter study

The results of the parameter study are analysed, considering load-displacements curves which result from the performed parameter study. The results for design 1 and 2, AZ23-800 cross-section class 2 and AZ20-800 cross-section class 3 respectively are presented, followed by design 3, PU22 cross-section class 2, including oblique bending.

The results followed from the parameter study contribute in answering the main research question:

What is the influence of hole weakening on the sheet pile's behaviour and resistance, before installing underwater anchors?

The complete procedure of answering this research question starts with the literature discussed in chapter 2 and 3. With this information, a model is developed which answers sub research question 1 and 2 and the main research question can be answered.

Sub research question 2 is repeated for completeness:

2. What is the influence of hole weakening on the resistance and behaviour of the sheet pile structure?
 - a. What phenomena will possibly have an influence on the sheet pile behaviour considering underwater anchors?
 - b. How do the hole characteristics influence the sheet pile resistance?
 - c. How do the hole characteristics influence the sheet pile stiffness?
 - d. Which variable should be considered in verification of the sheet pile structure with hole weakening?

With the sheet pile resistance, based on the load-displacement curves and the stiffness, also derived from the load-displacement curves and the 3D visualisation of plasticity and local behaviour from the 3DSSI model from DIANA FEA the influence of hole weakening on the resistance and behaviour of the sheet pile can be found regarding the steel behaviour. Despite that, the soil behaviour is included in these results. It is assumed that soil failure does not occur.

6.1. Result analysis procedure

The effect of hole weakening on the sheet pile behaviour and resistance is studied with respect to the failure load, failure mode and failure displacement firstly. Followed by a more thorough evaluation of the stiffness degradation over the sheet pile response.

6.1.1. Failure load and failure mode

To answer research question 2, the sheet pile resistance is studied. The failure load is assumed to be the load for which the 3DSSI model cannot find convergence. The lack of finding numerical convergence by the FE software suggest that the model cannot find an equilibrium stage. Which is in line with the expectations that a certain stiffness degradation leads to failure of the sheet pile.

This is accompanied by a decreased stiffness and obtaining a maximum at the load-displacement curve. Also, the failure mode is important to understand the sheet pile resistance and is studied at the failure load. The displacement at the failure load is of interest compared to the displacement at the initial stage. This provides insight into the behaviour of the sheet

pile, whether either sudden failure occurs or large displacements occur which can imply a warning before failure. The sheet pile resistance in the specific design case is thus defined by the failure load which is obtained by finding the maximum of the load-displacement curve.

To illustrate the difference between the maximum load of a case with a hole, and the no hole design resistance load (the maximum load which can be taken by the sheet pile without a hole), the load ratio is also plotted. The load ratio is defined in equation 67:

$$\text{load ratio} = \frac{\text{load } (y)}{\text{design resistance situation no hole}} \quad (67)$$

6.1.2. Stiffness

The sheet pile stiffness curve is derived from the load-displacement curve and therefore does also include the soil behaviour due to the increased uniform surcharge load. The behaviour of the soil load only is discussed in chapter 4.6.1. This means that not only one stiffness can be found but is changing for each load case due to the soil behaviour. However, it is possible to compare the stiffness curve of the original sheet pile without a hole (stiffness reference curve) with the studied cases with holes. The stiffness curve is derived with the following procedure: First, the load-displacement curves are derived for all the cases as described in chapter 5.1.1. With the results from 3DSSI model, a 6th order polynomial curve fit is performed using Python to find an analytical formula and curve for the load-displacement curve (Figure 104). The sheet pile stiffness is defined as the slope of the load-displacement curve: the uniform surcharge load in mm of sand / mm displacement. This is captured in equation 68.

$$\text{Stiffness (sheet pile)} = \frac{\Delta y \text{ load (mm uniform surcharge load)}}{\Delta x \text{ (mm displacement)}} \quad (68)$$

The stiffness can be easily calculated using the polynomial curve fit, as the derivative of this curve fit. The curve fit is used to determine the stiffness and not a numerical derivation from the 3DSSI model results, this is done to reduce the scatter in the stiffness results. The stiffness is plotted versus the uniform surcharge load. This compares the stiffness for similar loads, which is of interest for the design of a sheet piling and hole weakening as well. Now, the stiffnesses for similar soil loads can be compared, and also the 'stiffness ratio' with respect to no hole can be given. This 'stiffness ratio' captures the difference between the stiffness for the situation without a hole and the case with a hole, for similar soil loads. Both the soil behaviour and steel behaviour are included in the 'stiffness ratio'. The formula for the stiffness ratio is given in equation 69.

$$\text{Stiffness ratio} = \frac{\text{Stiffness case (at load } y)}{\text{Stiffness no hole (at load } y)} \quad (69)$$

With this method structural and soil behaviour are combined, at the same load level different global displacement shapes of the sheet piles are found. Therefore this method compares the total structure soil interaction response. This comparison will give a more insight into the difference that can be expected in a real design case.

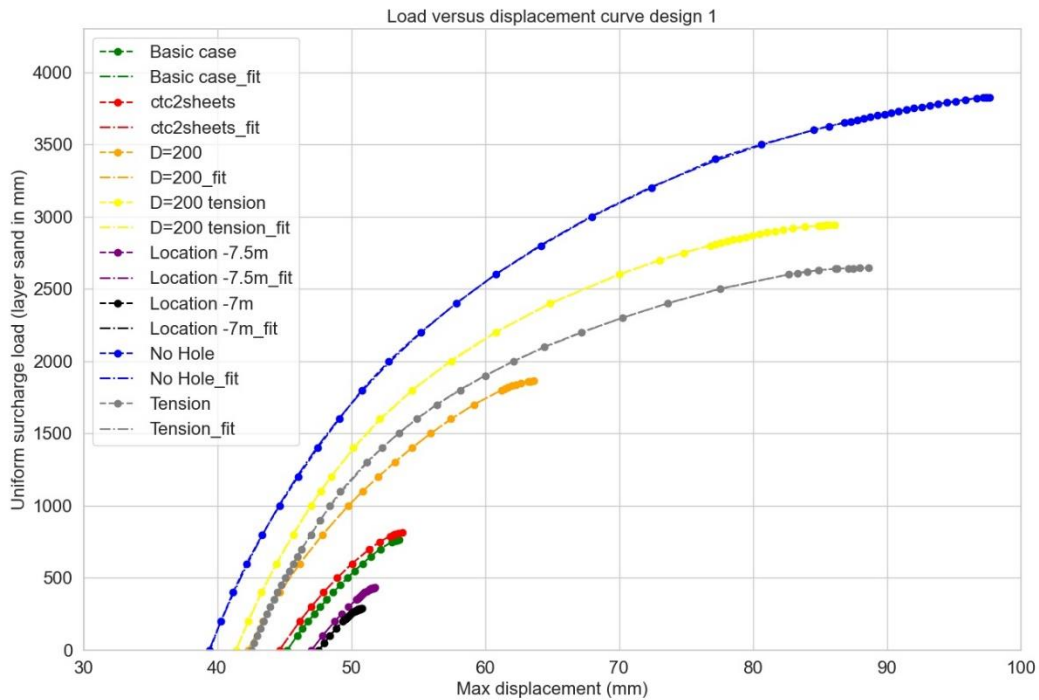


Figure 104: Load-displacement curve and curve-fit (design 1)

6.2. Results design 1

First the results of design 1 are compared for the studied cases. Design 1 is a sheet pile AZ23-800, cross-section class 2. The initial design has an unity check of 0.6. Then the surcharge load is increased as discussed in chapter 5.1. The studied hole parameters are discussed. Figure 105 shows for all cases the complete load-displacement curve. During the analysis, a large difference between the compression and tension cases occurred. Therefore, not only a D=300 mm hole diameter in tension is studied, but a hole D=200 mm is additionally studied. The load displacement curves are shown in Figure 105 for all cases.

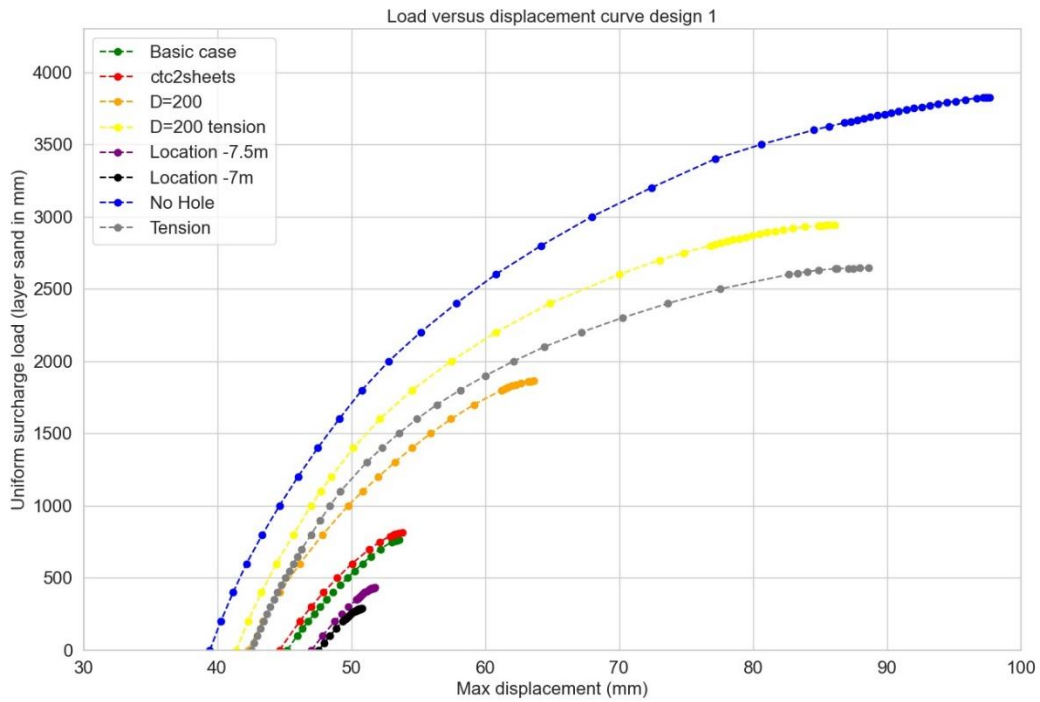


Figure 105: Load versus displacement graph for design 1, all cases

6.2.1. Failure load and failure mode

The failure load is determined as a percentage of the design load. For design 1, the bending moment resistance is reached for a surcharge load of 3500 mm of sand. Therefore, the y-axis is normalized to the (plastic) bending moment resistance. This is shown in Figure 106.

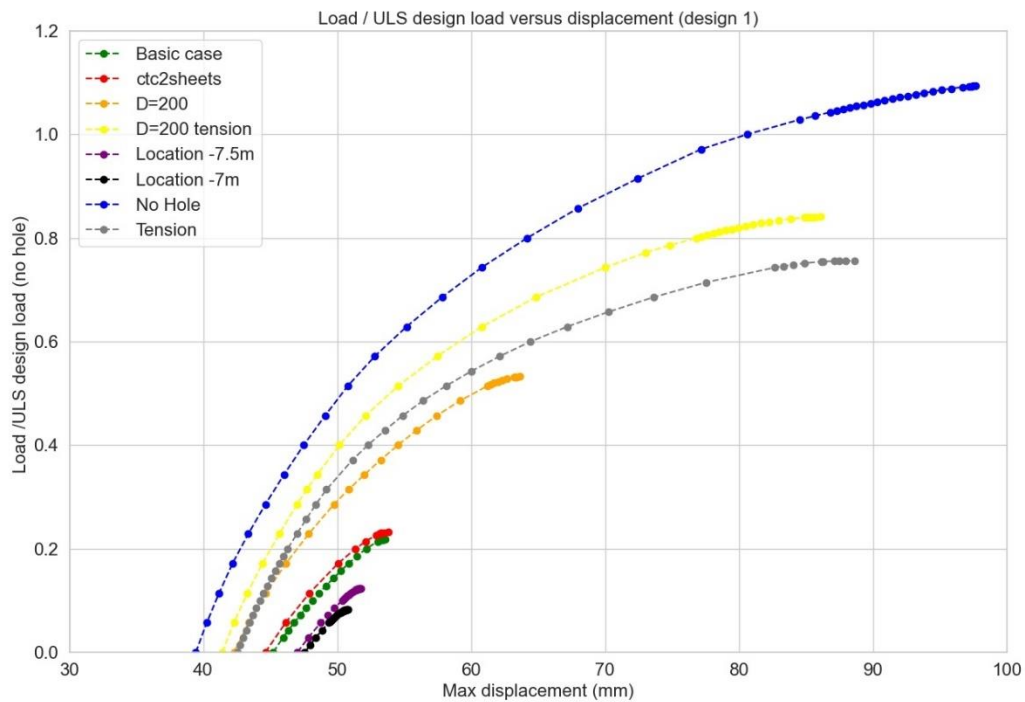


Figure 106: Load ratio versus displacement graph for design 1, all cases

Figure 105 shows the maximum failure load reached, while from Figure 106 the percentage reduction in failure load compared to the design load (ratio = 1.0) can be derived. The failure loads and ratio at failure load are given in Table 8. Also the displacements are considered, for both the initial stage (uniform surcharge load = 0) and at the failure load. This is given in Table 9.

Table 8: Failure loads design 1

Load case	Design 1 CC2 Ultimate load (mm sand uniform surcharge load)	Design 1 CC2 Ultimate load as percentage of design resistance (no hole)
No hole	3828	1.09
<i>D=300 compression (Basic case)</i>	765	0.22
D=200 compression	1863	0.53
<i>Location hole -8m (Basic case)</i>	765	0.22
Location hole -7.5m	433	0.12
Location hole -7m	289	0.08
<i>Hole spacing = 1 sheet (Basic case)</i>	765	0.22
Hole spacing = 2 sheets	815	0.23
D=300 tension	2646	0.75
D=200 tension	2943	0.84

Table 9: Displacement at initial stage and failure load

Load case	Design 1 CC2 Displacement at initial stage (mm)	Design 1 CC2 Displacement at failure load (mm)
No hole	39.4	97.7
<i>D=300 compression (Basic case)</i>	45.2	53.6
D=200 compression	42.3	63.6
<i>Location hole -8m (Basic case)</i>	45.2	53.6
Location hole -7.5m	47.0	51.8
Location hole -7m	47.6	50.8
<i>Hole spacing = 1 sheet (Basic case)</i>	45.2	53.6
Hole spacing = 2 sheets	44.6	53.8
D=300 tension	42.5	88.6
D=200 tension	41.4	86.1

From Figure 106 and Table 8 it shows that the cases including tension show much larger resistance than the cases in tension. Also, the location of the hole influences the results. The diameter of the hole also influences the resistance of the sheet pile, especially for compression. Clarification and reasoning for these observations will be discussed with the observed failure modes and can be found below.

Regarding the displacements, the tension cases show significant larger displacements at failure load than compression cases, but also a larger load at ultimate load. The initial displacement for the tension cases is lower than for compression cases.

No hole

The reference case, the original design case without a hole, can be loaded till the plastic bending moment resistance. According to the literature as discussed in chapter 3.2.2 and the 4-pointbending described by Kort (2002), the sheet pile fails after the design load due to local buckling. This is shown in Figure 49 and Figure 107 [23]. The failure of the sheet pile during a 4-pointbending test is characterised by the following phenomena:

- Increasing load results in increase deformation and increased local buckling
- Web deformation out of plane (in opposite direction of flange buckling)
- Concentrated plastic kink, but plasticity over a larger area

[23]

The plasticity and deformation at the failure load are shown in respectively Figure 109 and Figure 108. Comparing the literature with the results from the 3DSSI model, the following can be seen:

- At the failure load of the 3DSSI model, also an increasing load results in increase in deformation and local buckling.
- However, the buckling of the web and the flange are in similar direction, contrary to the 4-point bending test. This can be explained by the soil load pushing against the sheet pile, also at the location where local buckling occurs. This results in local buckling in the same direction as the soil load for both flange and web.
- Similar to the 4-pointbending test, a concentrated plastic kink occurs but plasticity occurs over a larger area.



Figure 107: 4-pointbending test up till failure of sheet pile [23]

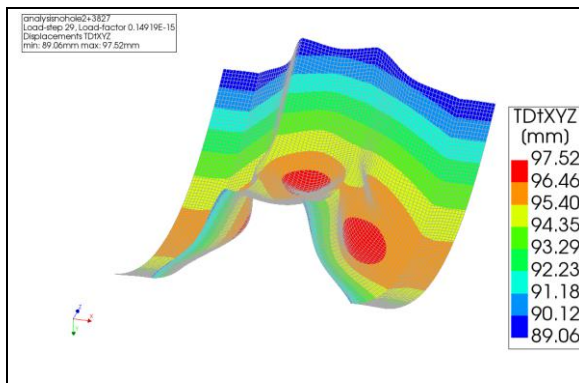


Figure 108: 3DSSSI model: Displacements no hole at failure load

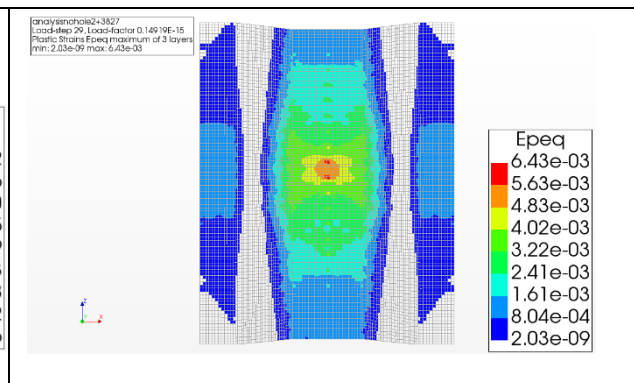


Figure 109: 3DSSSI model: Plastic strains no hole at failure load

At the initial stage the deformations are significantly lower. No plastic strains are present at the initial stage.

At plastic design resistance (uniform surcharge load = 3500 mm of sand) the deformations and plastic strains are given in Figure 110 and Figure 111.

The design resistance is close to the failure load. The start of the local buckling can be seen but the deformation is significantly lower than for the failure load. The strains are also lower.

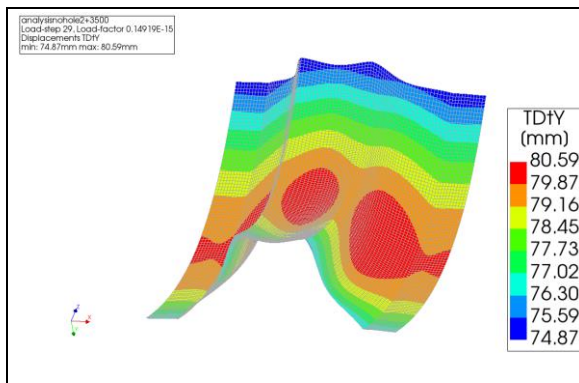


Figure 110: 3DSSSI model: Displacements (y-direction) no hole at plastic design resistance

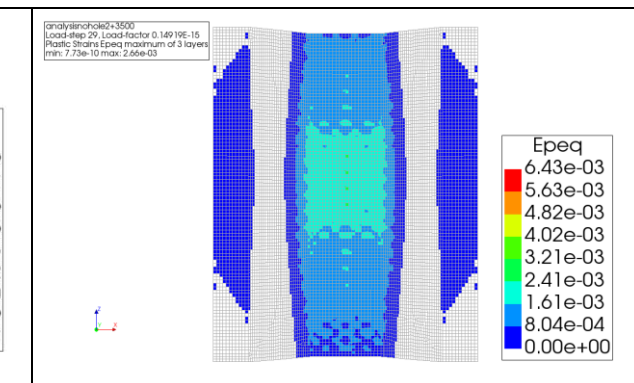


Figure 111: 3DSSSI model: Plastic strains no hole at plastic design resistance

Hole diameter

A sheet pile with a hole with a diameter of 200 mm ($D=200$) has a significantly larger resistance compared to a sheet pile with a hole diameter of 300 mm ($D=300$). This is shown in Figure 112. For $D=300$, the stresses in the webs are at a lower load (765 mm sand for $D=300$ and 1863 mm sand for $D=200$) on similar level as for $D=200$, approximately -250 N/mm^2 . Therefore, the web starts to buckle at a lower load for $D=300$ than for $D=200$. The failure mode is similar. Local buckling occurring in the webs and large plastic behaviour around the hole. The deformations and plastic strains at ultimate load are given in Figure 113 till Figure 116. Around the hole, where the plasticity is largest, the sheet pile is deforming outwards, while just above hole, the sheet pile is deforming inwards. The hole is deforming in the compression zone, resulting in a lower hole height and larger hole width, an oval shaped hole. The plasticity is centred around the hole. For $D=200$ some plasticity can be found above the hole as well. This plasticity is also found in the situation without a hole due to the bending moment.

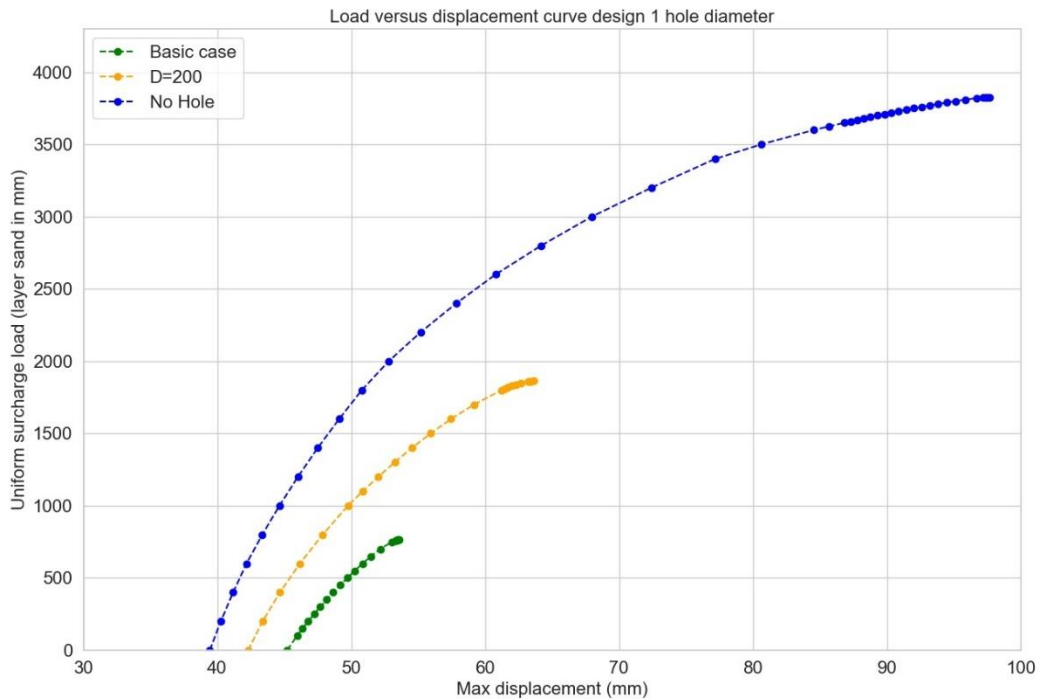


Figure 112: Load versus displacement graph for design 1, hole diameters

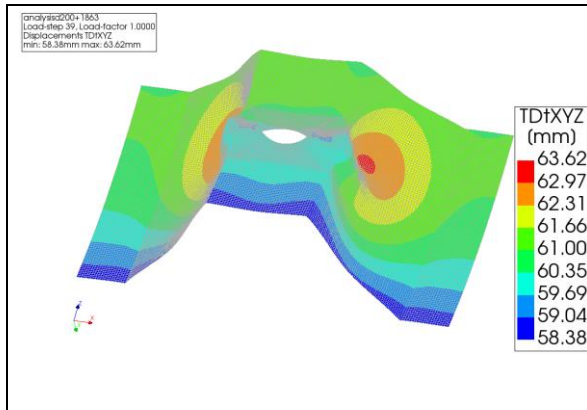


Figure 113: 3DSSI model: Displacements at failure load, hole diameter = 200 mm

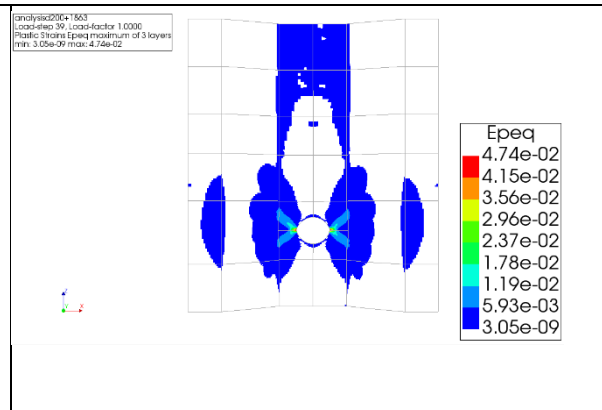


Figure 114: 3DSSI model: Plastic strains at failure load, hole diameter = 200 mm

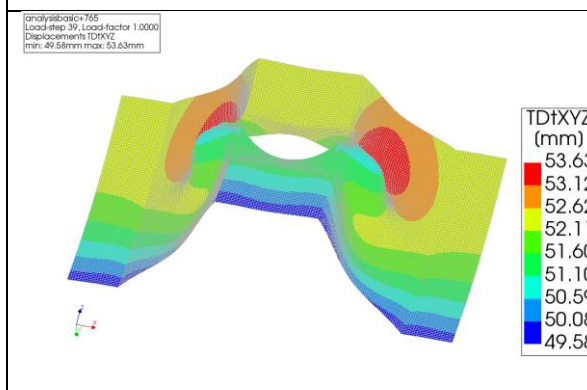


Figure 115: 3DSSI model: Displacements at failure load, hole diameter = 300 mm

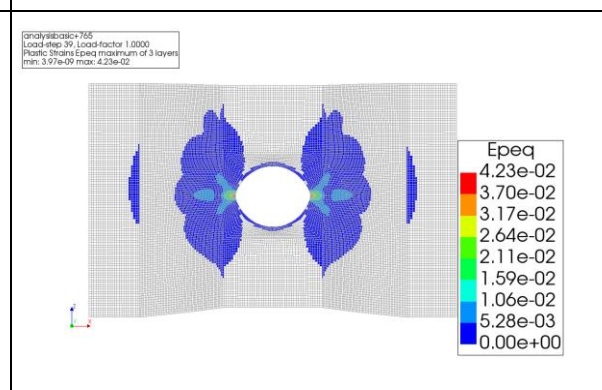


Figure 116: 3DSSI model: Plastic strains at failure load, hole diameter = 300 mm

Considering the initial stage of the designs D=200 and D=300 some differences can be seen. At the initial stage the plasticity around the hole is already present. Especially for a hole of 300 mm, the displacements around the hole are significant and the failure mode can already be observed in the initial stage. This is shown in Figure 117 up till Figure 120.

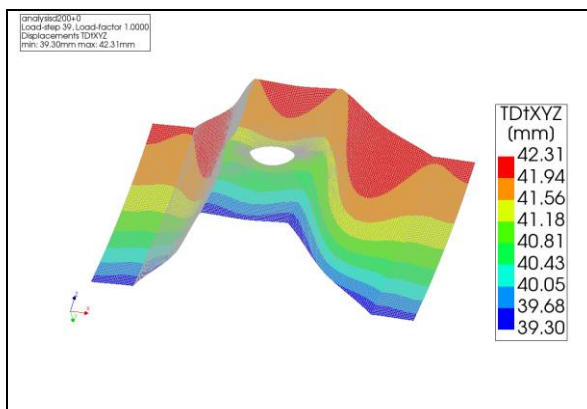


Figure 117: 3DSSI model: Displacements (y-direction) at initial load, hole diameter= 200 mm

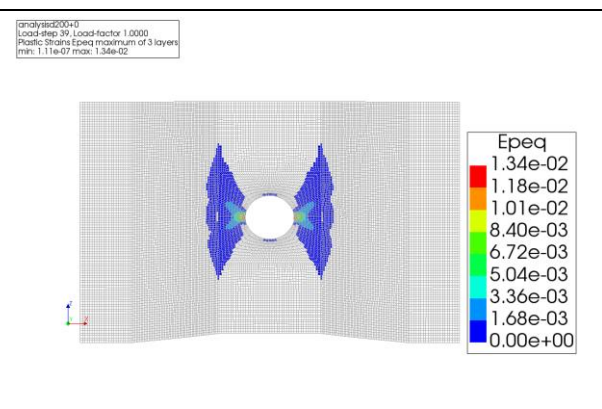
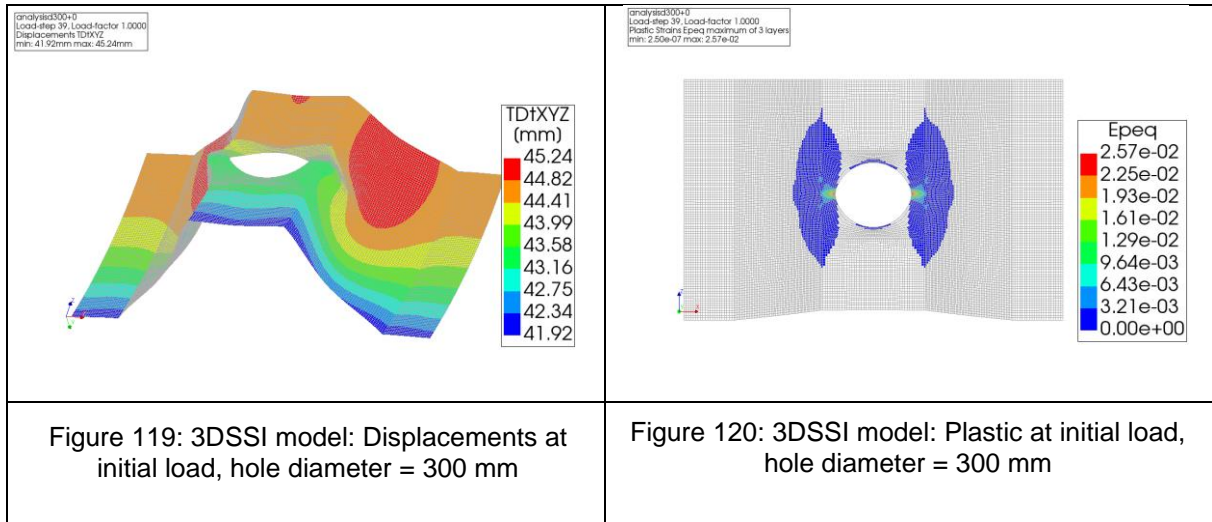


Figure 118: 3DSSI model: Plastic strains at initial load, hole diameter = 200 mm



Hole location

Three different hole locations have been studied: -8m, -7.5m and -7m. The case with -8m is the basic case and these figures can be found above (Figure 115, Figure 116, Figure 119 and Figure 120).

Considering the hole location of the sheet pile, main difference between the cases is the internal stresses at the location of the hole due to the location of the maximum bending moment. The load-displacement curves are given in Figure 121. The results of no hole, a hole on location -8m (basic case), location -7.5m and location -7m are shown.

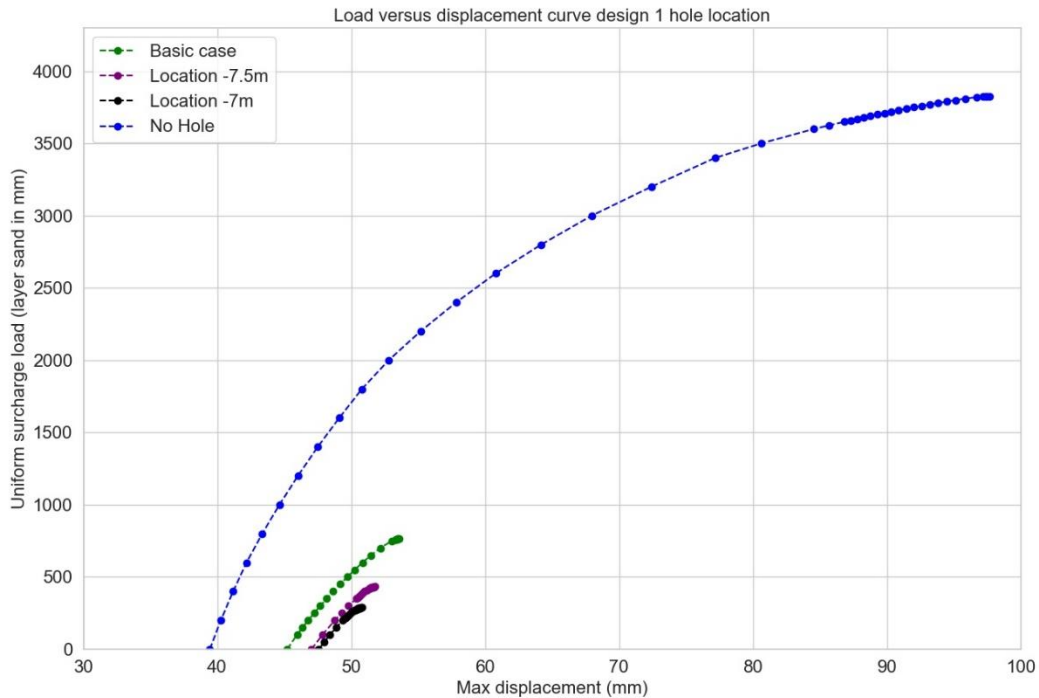
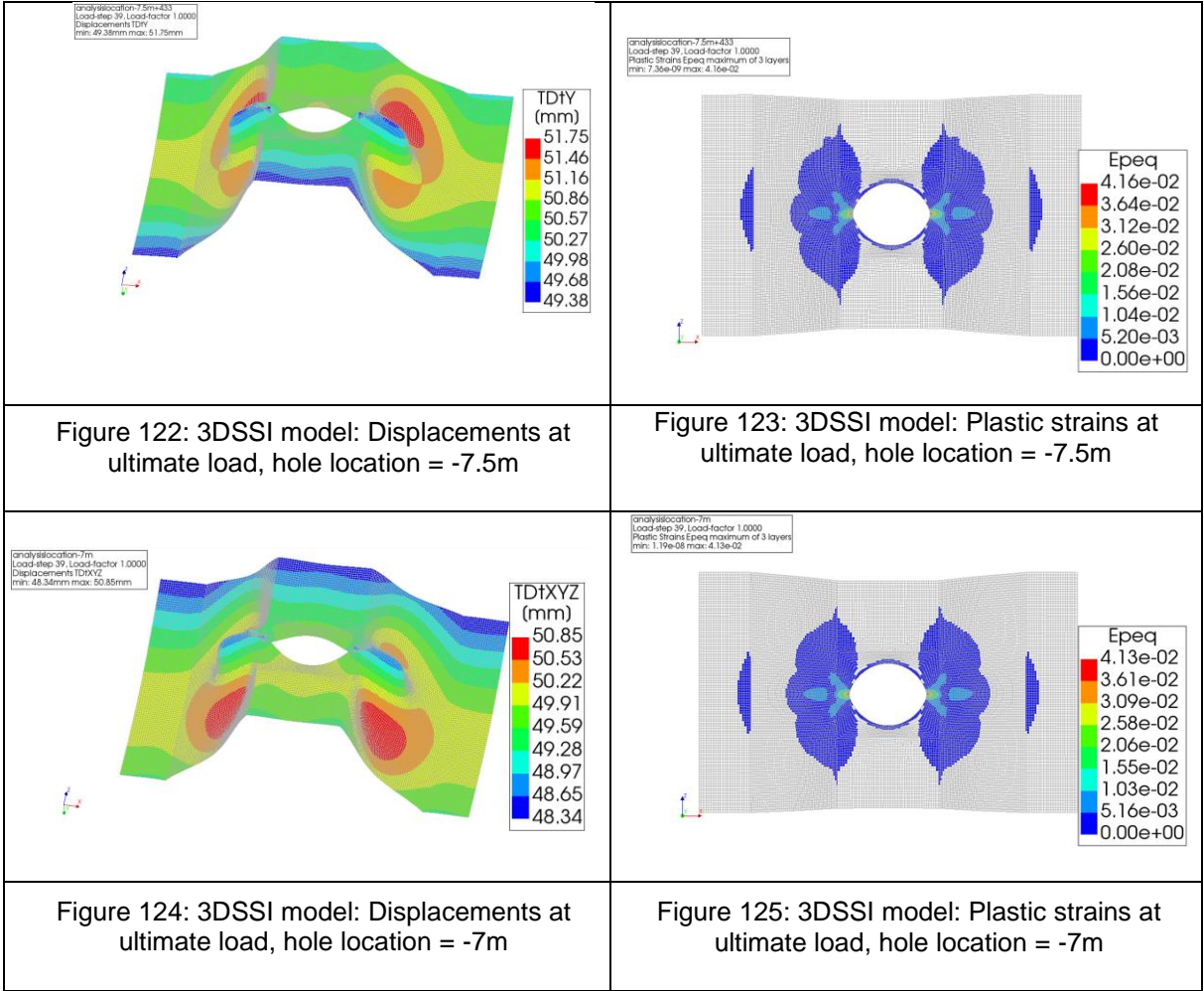


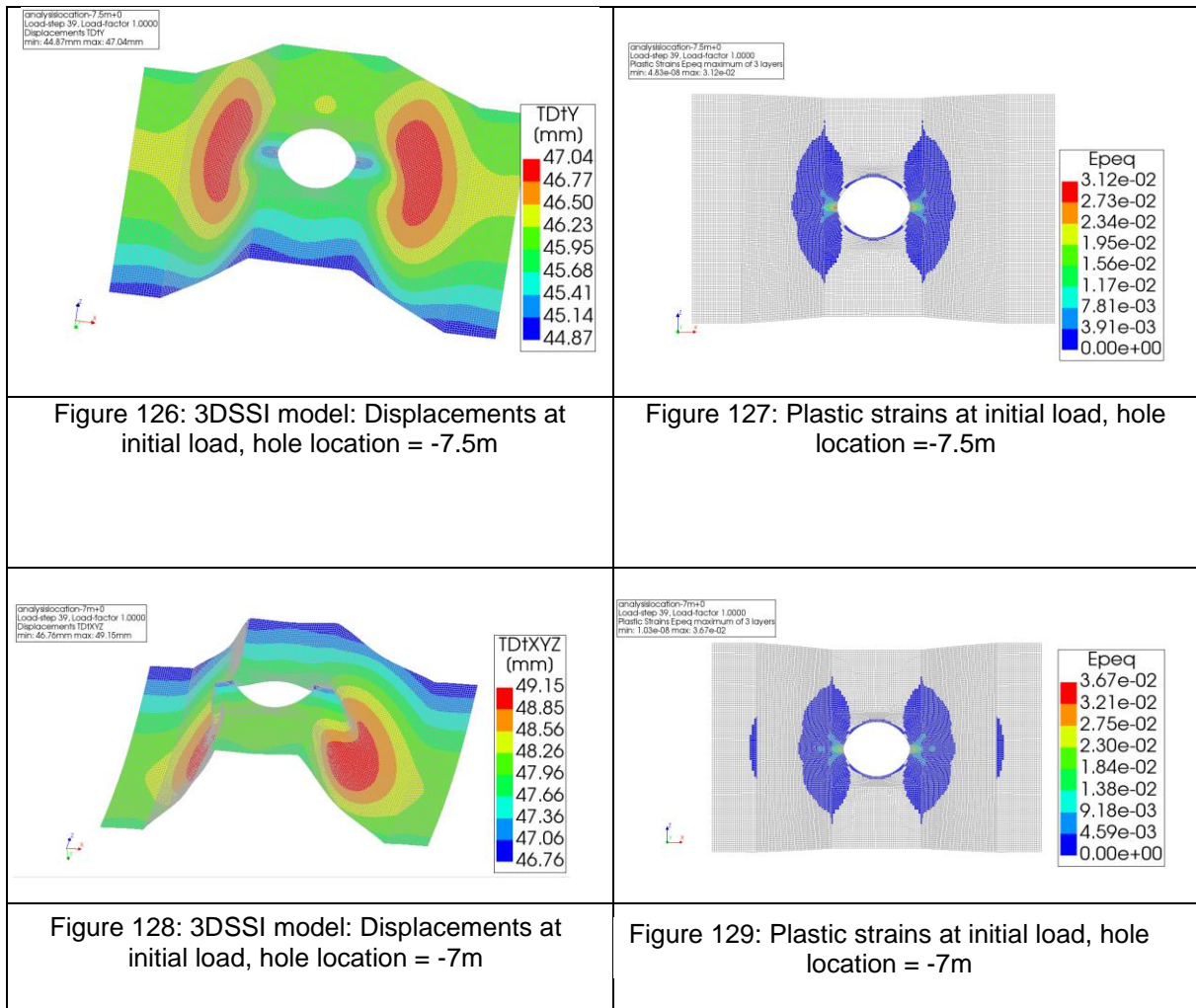
Figure 121: Load versus displacement graph for design 1, hole locations

For hole location -7m the web buckling is located underneath the hole, instead of above the hole as for the basic case. The web buckles near the hole where the stresses produced by the bending of the sheet pile are largest. This location is depending on the load, but around -7.5m. Therefore the web buckles above the hole for a hole location of -7m and below the hole for a

hole location of -8m. For the hole on -7.5m, buckling occurs in the webs above the hole, but also around the plasticity some additional local deformation is shown. The large plasticity on the level of the hole in the flange and web is similar for the different hole locations. The deformation and plasticity figures for -7.5m and -7m at ultimate load are shown in Figure 122 up till Figure 125.



Already at the initial stage, large plasticity and local buckling can be observed (Figure 126 up till Figure 129).



Hole spacing (c.t.c. distance hole)

A hole spacing of 1 sheet (basic case; Figure 115, Figure 116, Figure 119 and Figure 120) and 2 sheets (Figure 131 up till Figure 134) is studied. The load-displacement curve is given in Figure 130.

A larger centre to centre distance between the hole gives a very comparable load-displacement curve as the basic case. Similar failure mode as the basic case is observed: plasticity and local buckling near the hole. The failure mode occur locally around the hole, and therefore, using a larger hole spacing does not significantly benefit the results.

A limitation of the 3DSSI model considering hole spacing is the local failure determining the failure load of the model. It is expected that, when the sheet pile is local deforming and having large plastic strains around the hole, for a hole spacing of 2 sheets, more force will be transferred to the sheet pile without a hole, before the sheet pile completely fails. However, due to numerical limitations, this cannot be captured by the model. Therefore, the failure load is limited at the load resulting in local buckling and large plasticity near the hole. In practice, this is not a problem, since large deformations and plasticity around the hole will also determine the failure load. Large deformations near the hole are not desirable regarding the procedure of drilling an underwater anchor.

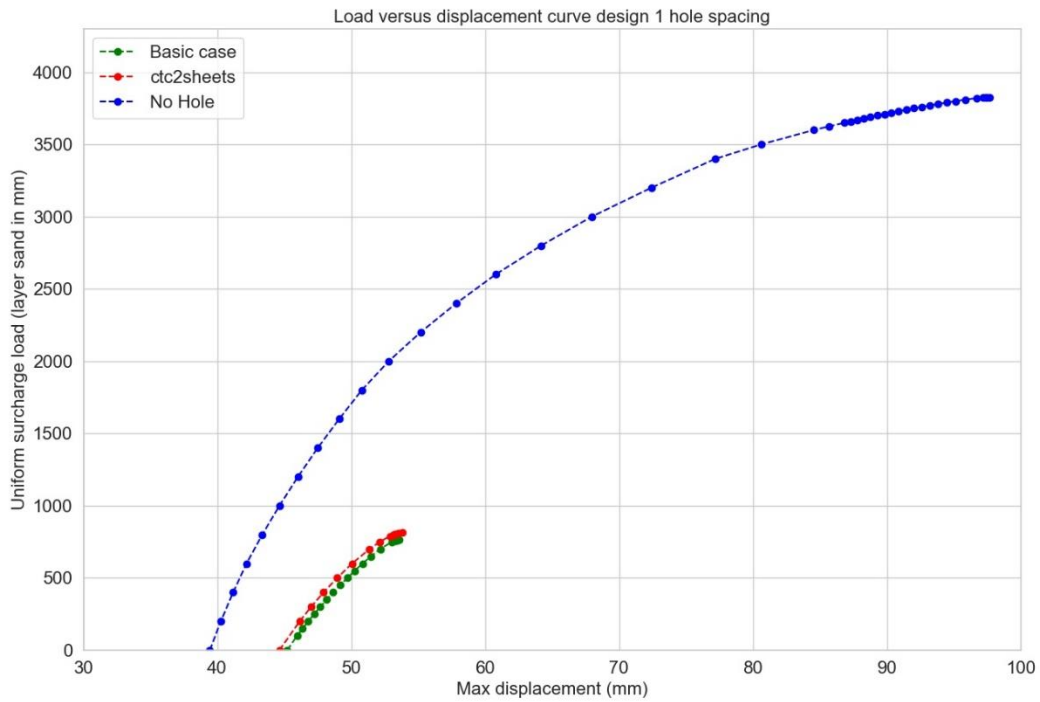
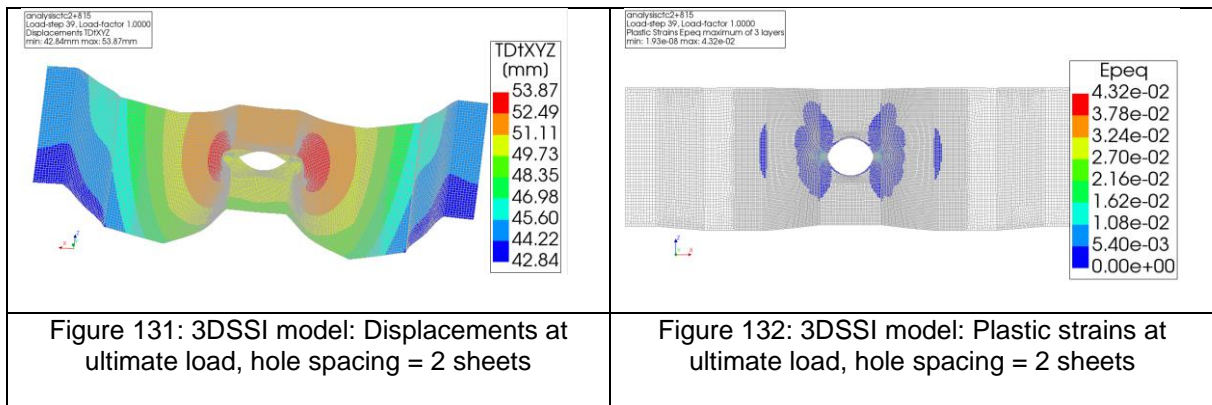
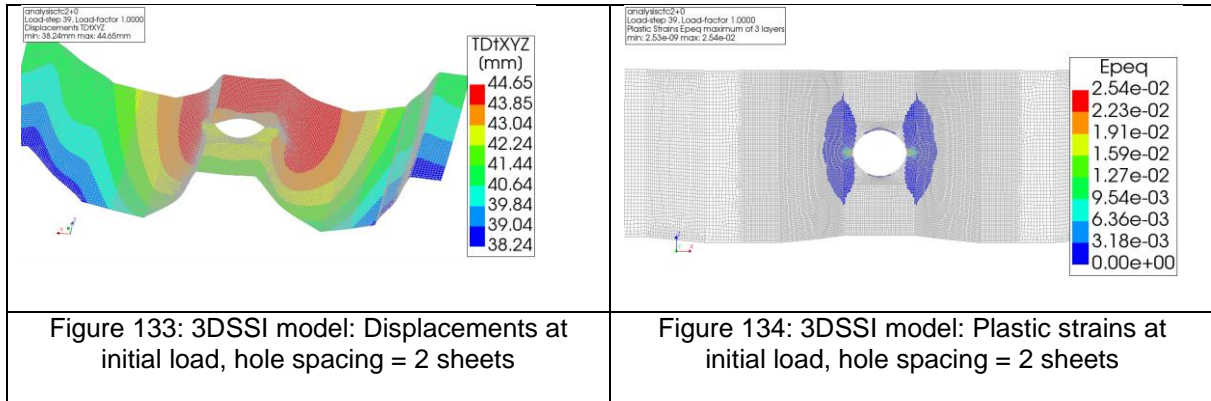


Figure 130: Load versus displacement graph for design 1, hole spacing



At initial load also already plasticity can be seen. Comparing the initial stage of the basic case and the hole spacing of 2 sheets, the plastic strains and displacements are almost equal (Figure 133 and Figure 134).



In-pan / out-pan (compression or tension zone)

The hole in-pan (compression zone) and out-pan (tension zone) showed different behaviour for the sheet pile. Therefore, not only the basic case (hole in-pan, D=300), but also a hole diameter D=200 is studied in tension and compression. The load versus displacement graph is shown in Figure 135. The in-pan deformation and plastic strains figures are given in Figure 113 up till Figure 120 and out-pan deformation and plastic strains in Figure 136 up till Figure 143.

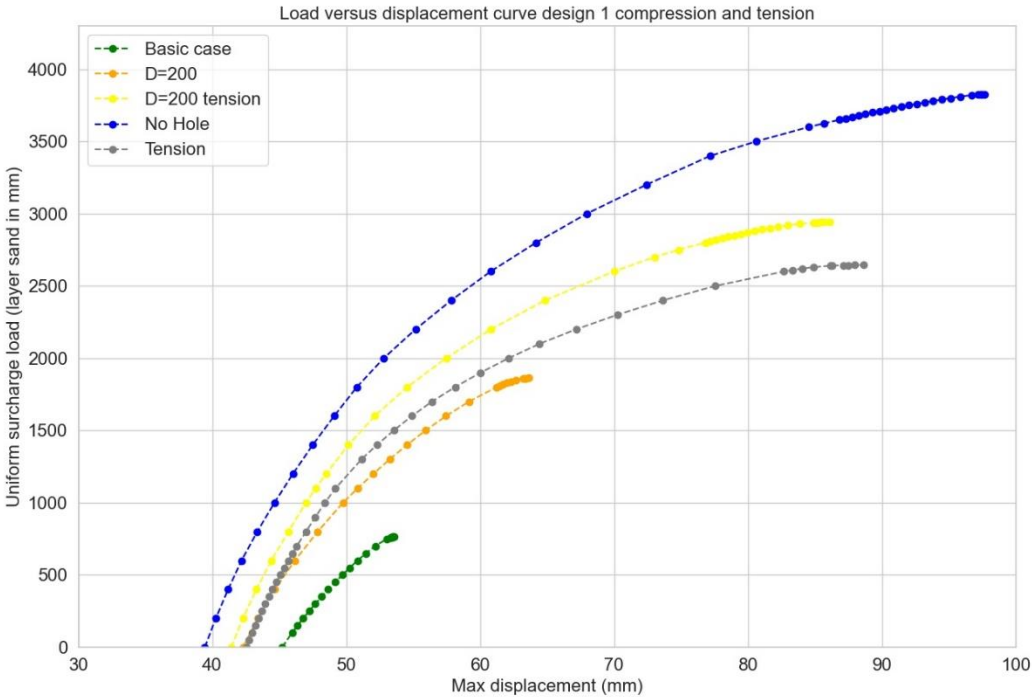


Figure 135: Load versus displacement graph for design 1, in-pan / out-pan

The location of the hole in-pan (compression zone) or out-pan (tension zone) significantly influences the results. Out-pan holes have a larger resistance and show larger displacements before failure occurs. Considering the failure modes, plasticity starts to occur over the complete cross-section, with larger plastic strains around the hole and locally in the compression flanges. The compression flange buckles locally, comparable with the no hole failure mode. The failure mode is similar for a hole in tension with a diameter of 200mm or 300mm.

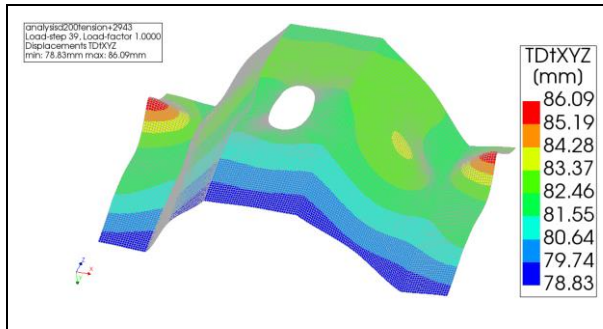


Figure 136: 3DSSI model: Displacements at ultimate load, hole out-pan, d=200

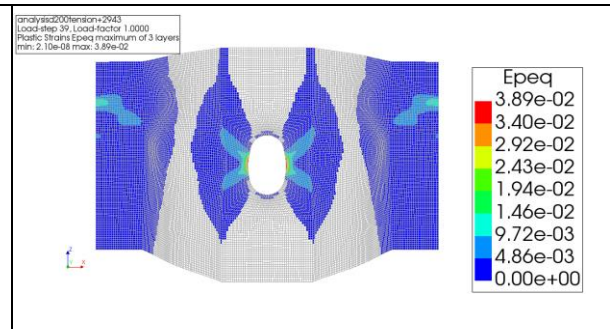


Figure 137: 3DSSI model: Plastic strains at ultimate load, hole out-pan, d=200

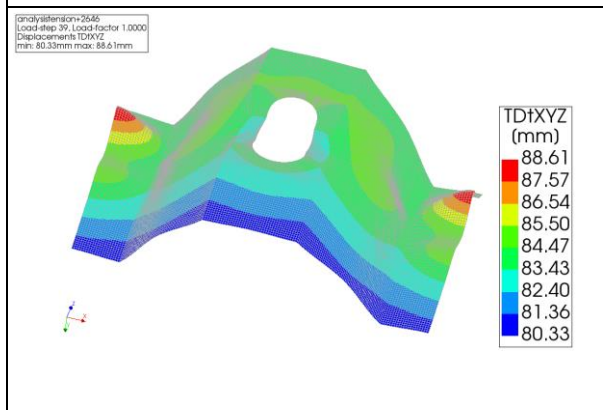


Figure 138: 3DSSI model: Displacements at ultimate load, hole out-pan, d=300

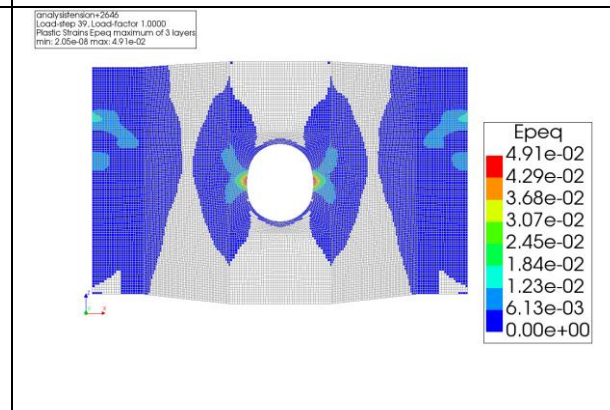


Figure 139: 3DSSI model: Plastic strains at ultimate load, hole out-pan, d=300

At the initial stage, the holes in tension do not show local buckling or irregular local displacements. However, some plasticity can be found around the hole (Figure 140 up till Figure 143).

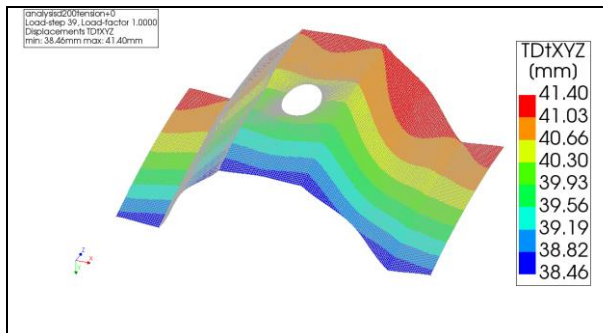


Figure 140: 3DSSI model: Displacements at initial load, hole out-pan, d=200

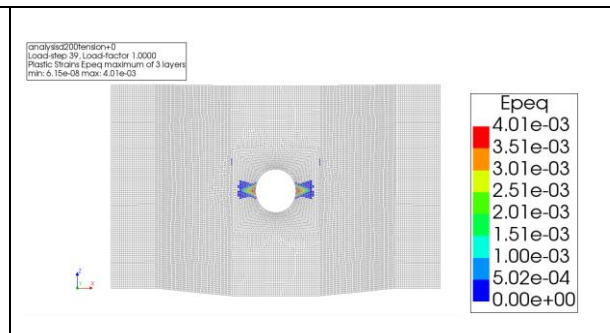
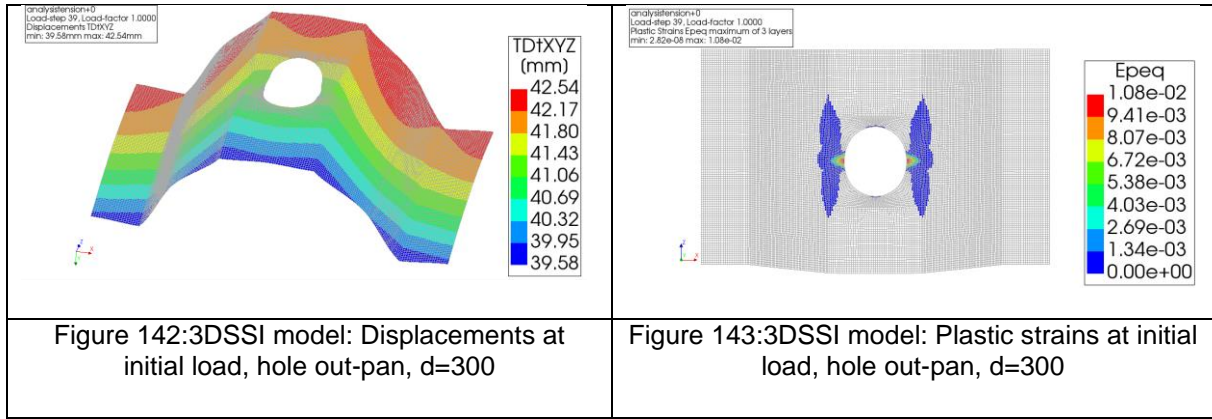
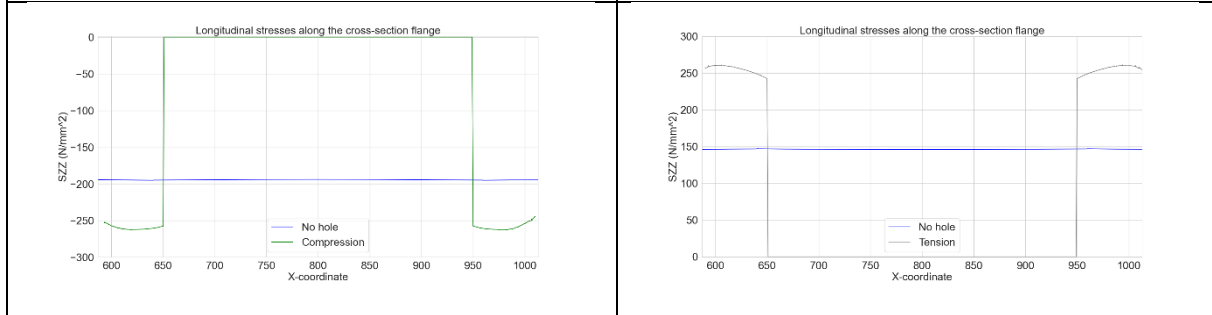
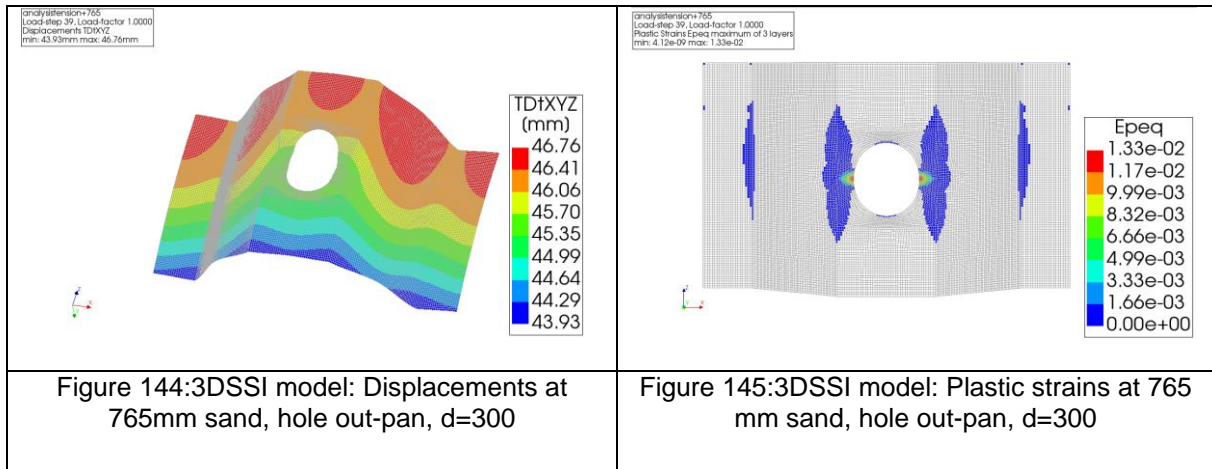


Figure 141: 3DSSI model: Plastic strains at initial load, hole out-pan, d=200



Comparing the tension and compression zone for a similar load case, the ultimate load for the basic case, the benefit from the tension case can be expressed. A hole $D=300$ in compression fails at a load of 765mm. The displacement and plasticity can be found in Figure 115 and Figure 116. At similar load for the hole in tension, the local buckling in the flange is not visible. Plasticity is occurring, but not over the complete cross-section. The maximum plastic strain for the compression case is 0.0432, while for the hole in tension is much lower, 0.0133. The longitudinal stresses, SZZ , are plotted for the load of 765 mm sand, as shown in Figure 146 and Figure 147 for respectively hole in compression and hole in tension. Also the stresses in the flange in case of no hole are plotted. The longitudinal stresses are higher for the compression case than the tension case without a hole, due to the vertical component of the anchor force. Due to the hole, larger forces occur near the hole in the flange for both compression and tension.



<p>Figure 146: Longitudinal stresses flange, hole in compression and no hole</p>	<p>Figure 147: Longitudinal stresses flange, hole in tension and no hole</p>
--	--

6.2.2. Stiffness

As explained in chapter 6.1.2, the stiffness is determined for all cases, including no hole. The stiffness includes both soil and steel behaviour. How the soil behaviour changes is discussed in chapter 4.6.1. The stiffness versus load curve and stiffness ratio (as defined in chapter 6.1.2) versus load curve are shown in respectively Figure 148 and Figure 149. The stiffness degradation appears for the no hole case as well for the tension cases to show a linear trend. For the compression cases an initial offset is present. Also a more severe decrease of the stiffness is observed.

Considering the stiffness ratio, a large offset in initial stiffness can be observed for the cases with a hole in compression; a 40-50% decrease in stiffness compared to no hole. More stiffness reduction with respect to no hole is observed until progressive degradation of stiffness resulting in failure is shown. For the tension cases different behaviour is observed. Almost similar initial stiffness is observed as for no hole followed by a gradual stiffness reduction until failure. A much larger resistance and stiffness is observed for the situations with a hole in tension compared to holes in compression.

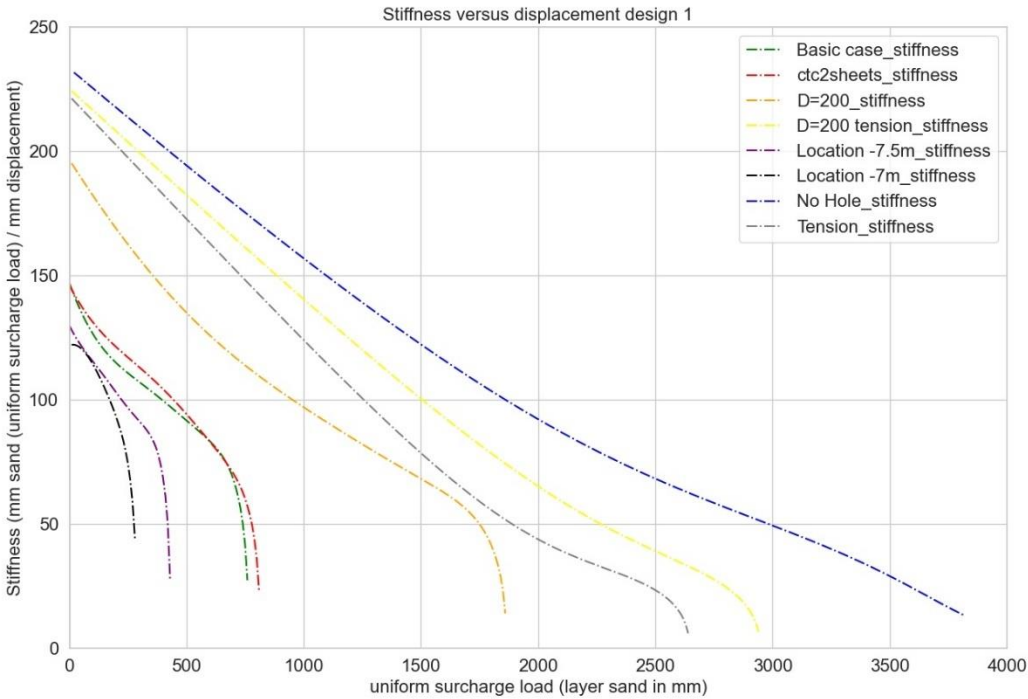


Figure 148:Stiffness versus load graph design 1

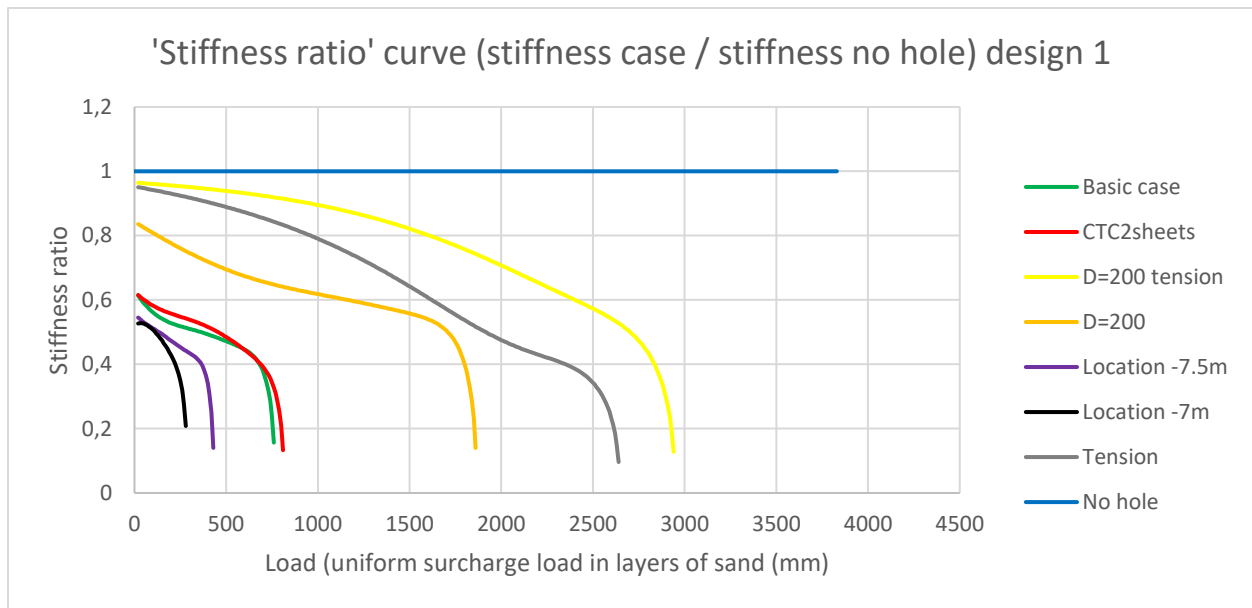


Figure 149: Stiffness ratio versus load design 1

6.2.3. Conclusion

From the load-displacement curve and stiffness curves several conclusions can be drawn. The first main difference is observed between the tension and compression cases. The tension cases show much larger capacity and deformation capacity, e.g. for case 'tension' 75% of the surcharge load, and the basic case (similar but with hole in compression) 22%. Plasticity occurs over a large area over the cross-section for tension cases and local buckling in the compression flange. For the compression cases, local buckling occurs in the webs near the hole and large plasticity is centred around the hole. For all compression cases, except D=200, the failure modes can be observed at the initial stage.

For different hole diameters, with the hole in compression, the hole diameter influences the resistance, but the failure modes are similar: local buckling in the webs and plasticity. Case 'D=200' can resist 31% more surcharge load than 'Basic case' (D=300). The hole location shows also similar failure modes, but the location of local buckling differs. The local buckling occurs at the location of the maximum stresses due to global bending, near the hole. The hole location resistance differs less than hole diameter and hole in-pan/out-pan, 14%. For a hole very close to the maximum stresses, the local buckling and plasticity is already observed from the initial stage. A different hole spacing shows similar plasticity and local buckling as the basic case. The failure mode is similar and the failure load is comparable as well.

Considering the stiffness compared to no hole, the compression cases show a reduction at initial stage of 40-50% which is increasing with an increasing load until progressive degradations are observed. For the tension cases, a very small stiffness reduction of 6-7% is observed at the initial stage. However, for increasing load, gradual stiffness reduction is observed until failure.

6.3. Results design 2

Similar as for design 1, the results of design 2 are compared for all cases. Design 2 is a sheet pile AZ20-800, cross-section class 3. The initial design starts again at a unity check of 0.6. The surcharge load increases until failure is observed. The studied hole diameters are discussed in chapter 6.3.1 and 6.3.2 and the results are shown in a load-displacement curve in Figure 150. Similar as for design 1, a large difference between the compression and tension case for a hole of 300 mm is observed, and therefore also a hole of 200mm is studied in tension zone.

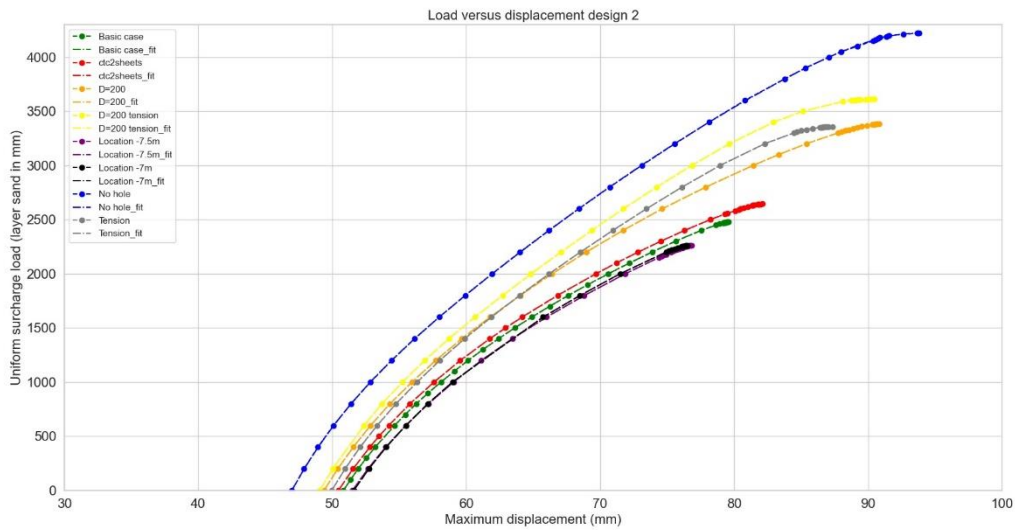


Figure 150: Load versus displacement graph for design 2, all cases, including curve fit

6.3.1. Failure load and failure mode

Similar as for design 1, the load ratio with respect to the design load for the sheet pile without a hole is given. The ultimate loads are given in Table 10 and displacements at initial stage and ultimate load in Table 11. the load ratio versus displacement curve is shown in Figure 151.

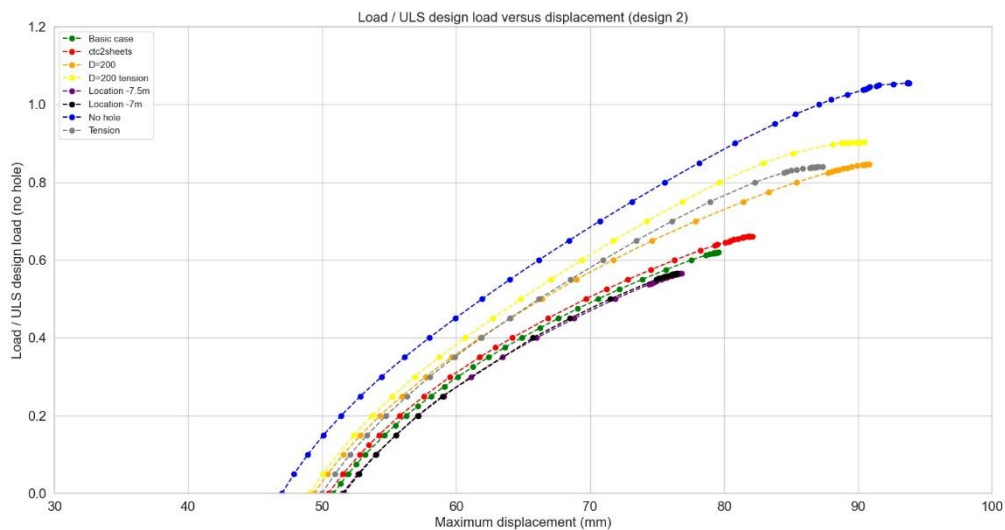


Figure 151: Load ratio versus displacement graph for design 2, all cases

Table 10: Failure loads design 2

Load case	Design 2 CC3 Ultimate load (mm sand uniform surcharge load)	Design 2 CC3 Ultimate load as percentage of design resistance (no hole)
No hole	4221	1.06
<i>D=300 compression (Basic case)</i>	2479	0.62
D=200 compression	3384	0.84
<i>Location hole -8m (Basic case)</i>	2479	0.62
Location hole -7.5m	2264	0.56
Location hole -7m	2261	0.56
<i>Hole spacing = 1 sheet (Basic case)</i>	2479	0.62
Hole spacing = 2 sheets	2645	0.66
D=300 tension	3359	0.84
D=200 tension	3613	0.90

Table 11: Displacements at initial stage and failure load design 2

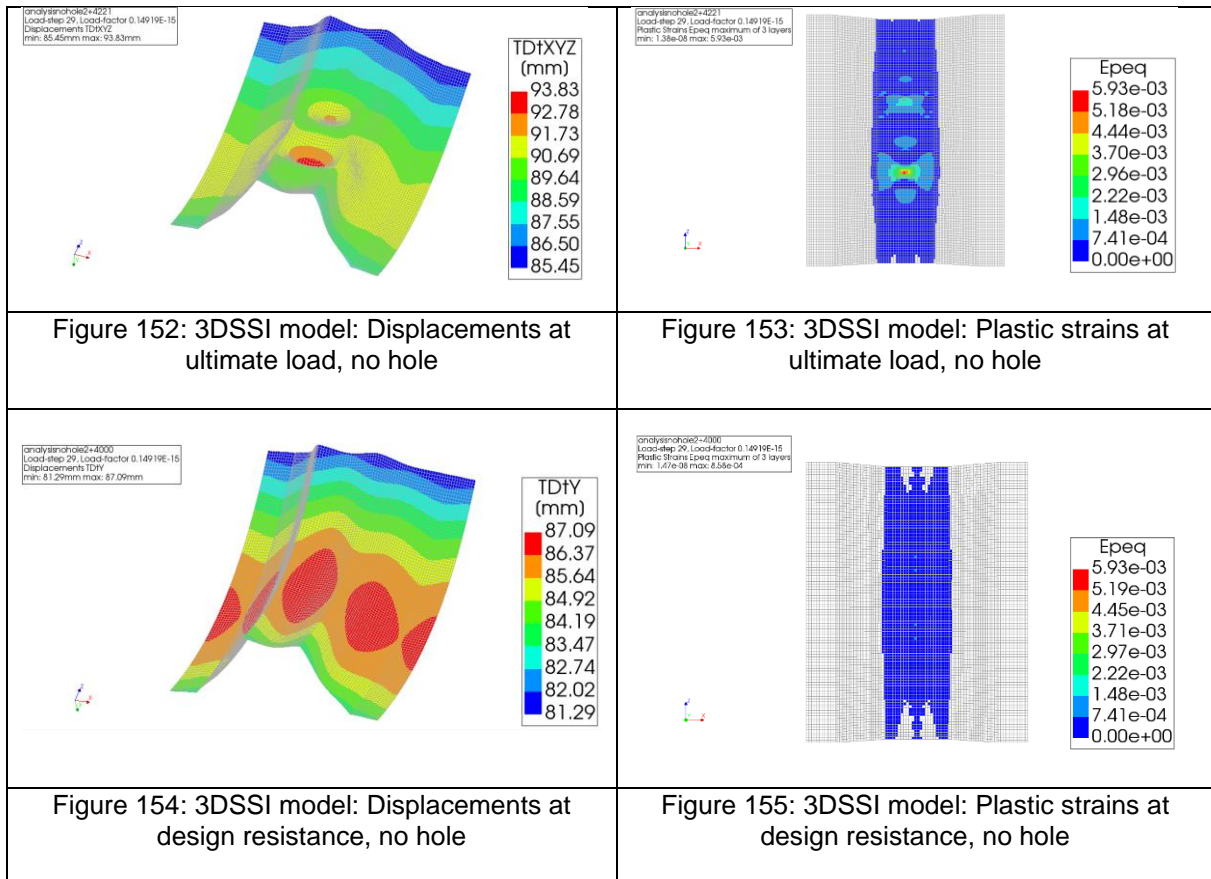
Load case	Design 2 CC3 Displacement at initial stage (mm)	Design 2 CC3 Displacement at failure load (mm)
No hole	47.0	93.8
<i>D=300 compression (Basic case)</i>	50.8	79.6
D=200 compression	49.4	90.8
<i>Location hole -8m (Basic case)</i>	50.8	79.6
Location hole -7.5m	51.5	76.8
Location hole -7m	51.6	76.5
<i>Hole spacing = 1 sheet (Basic case)</i>	50.8	79.6
Hole spacing = 2 sheets	50.5	82.1
D=300 tension	50	87.4
D=200 tension	49.1	90.4

Figure 150 and Table 10 show a larger resistance for the tension cases than the compression cases. The location of the hole does not significantly influence the resistance. The smaller diameter increases the resistance, especially for a hole in the compression zone.

The displacements at the initial load are for all cases with hole quite close to each 49-51 mm. The maximum displacements are between 79-91 mm.

No hole

For a sheet pile of cross-section class 3, it is expected that after reaching the elastic limit, local buckling will occur and no plastic capacity is left. This is based on the literature discussed in chapter 3.2.1. This is also found for the 3DSSI model without a hole (Figure 152 up till Figure 155). Local buckling in the compression flange is the governing failure mode. Plasticity is observed only in the compression zone. At the design resistance, very small plasticity is found. In theory, there should only be elastic behaviour at the elastic design resistance. However very small plastic strains are observed. This is partly due to the local forces of the springs, and the geometrical nonlinear behaviour which is starting to occur and eventually leads to local buckling.



Hole diameter

Similar as for design 1, a smaller hole diameter results in a larger resistance, as expected. Local buckling and plasticity is again the failure mode of the sheet piles with holes (Figure 157 up till Figure 160). For a hole diameter of 300 mm ($D=300$) the web on the same level of the hole is deforming more significant than for a hole diameter of 200 mm ($D=200$). For $D=200$ the web is deforming next to the hole, as indicated with the red area which is for $D=300$ more above the hole, in the webs. Looking at the stress distribution at the ultimate load, the compression stresses are largest next to the hole. For $D=300$, the plasticity is not only in the flange causing large deformations, but also in the webs. Then, local buckling of the web occurs not at the same place as this plasticity, but above the hole.

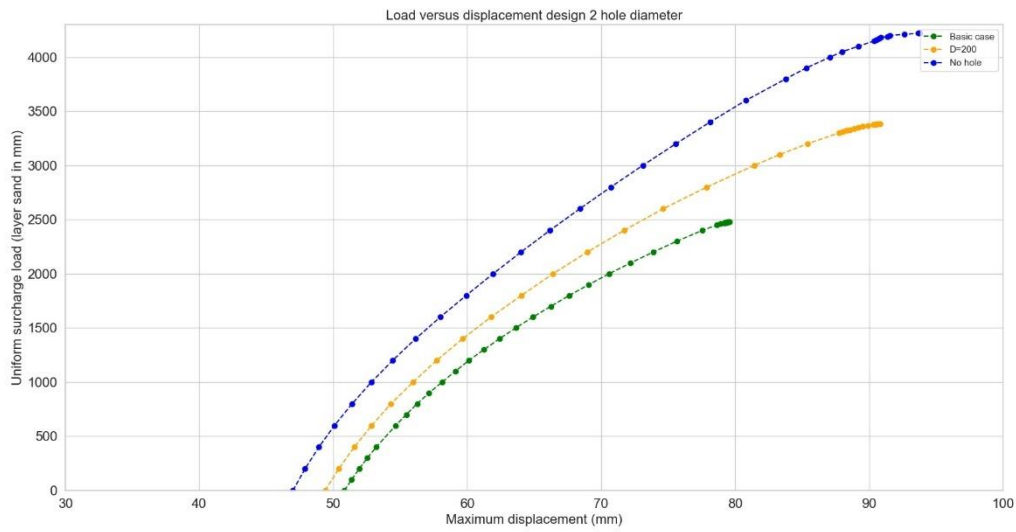
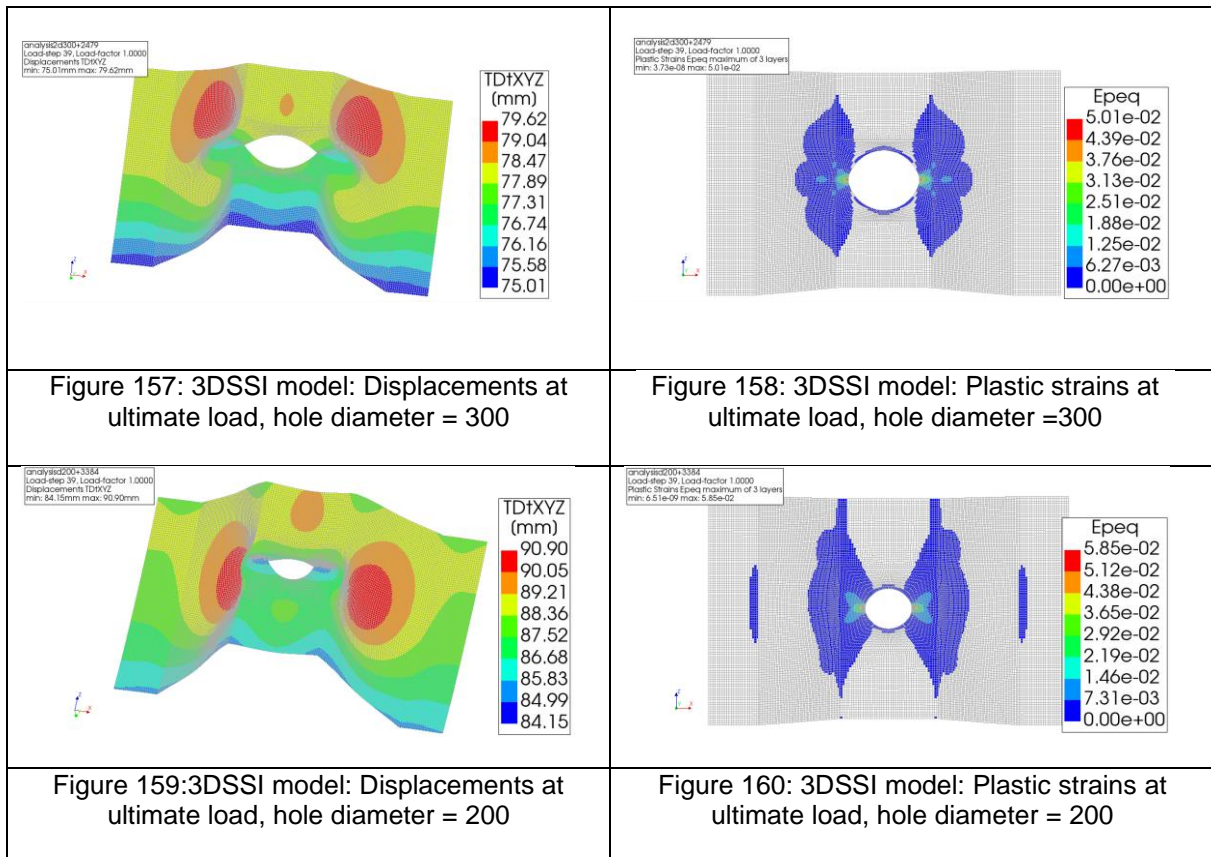
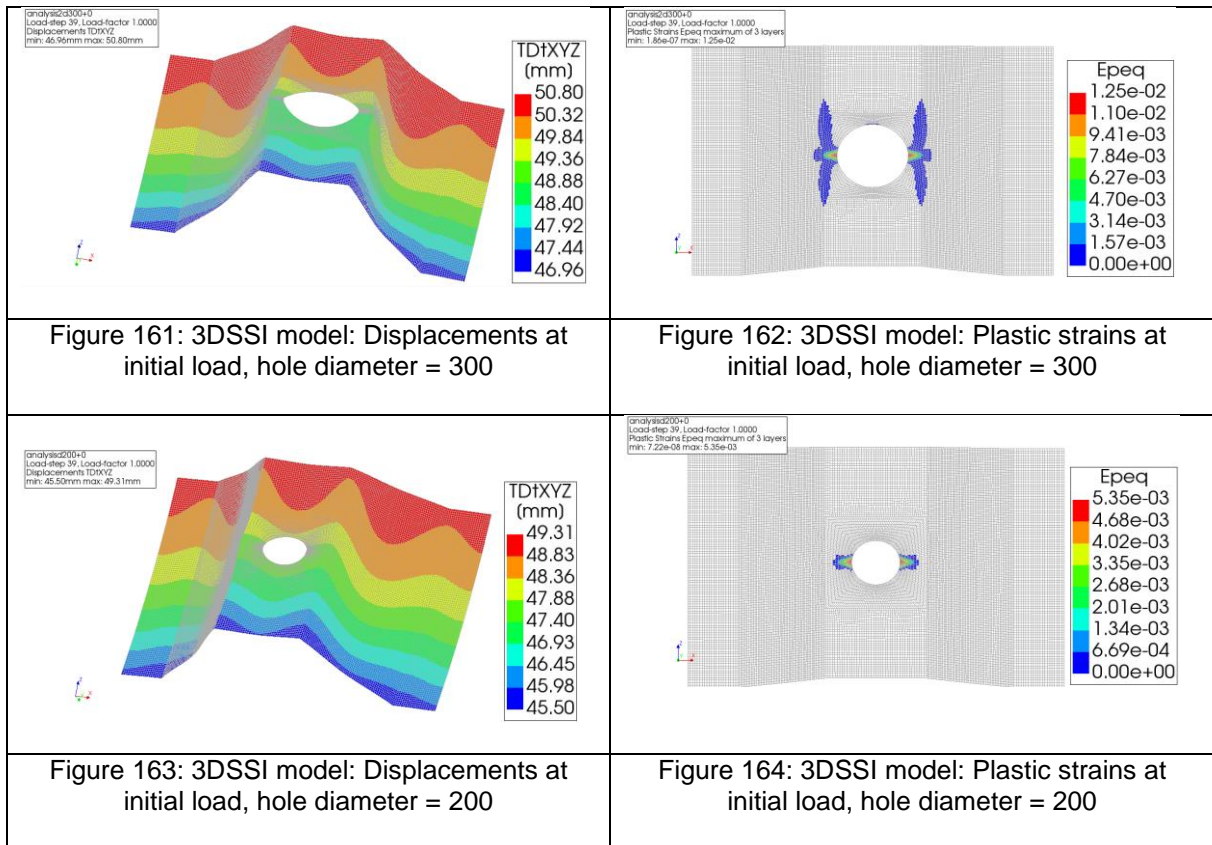


Figure 156: : Load versus displacement graph for design 2, hole diameters



In the initial stage, some plasticity is already present. However, local buckling is not noticeable (Figure 161 up till Figure 164). The difference between the plasticity for D=200 and D=300 is quite significant with a maximum plastic plasticity of respectively 0.54% and 1.25%.



Hole location

The influence of the hole location is considerably small. The difference in bending moment between the hole locations is also small. For the basic case, the web buckles above the hole, while for the location of -7.5m, the web buckling occurs around the hole. For a hole on location -7m, the web buckles below the hole. The web buckles near the hole where the stresses produced by the bending of the sheet pile are largest. The maximum bending moment is between -7m and -8m, but the difference between the maximum bending moment is small. The web seems to buckle at the location of the maximum bending moment, around the deformation caused by the hole. This is, together with the plasticity graphs, shown in Figure 166 up till Figure 169. The load-displacement curves are also very similar for the different hole locations (Figure 165).

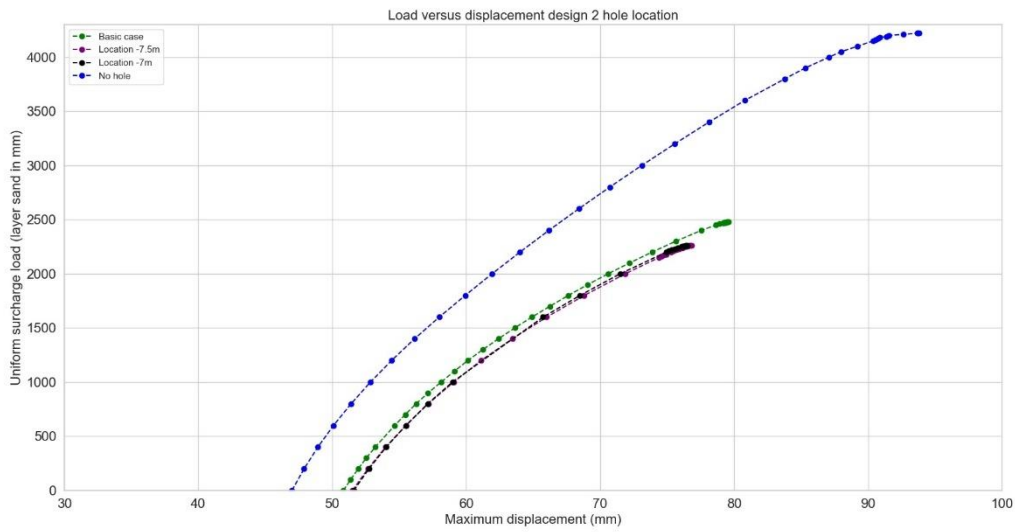


Figure 165: Load versus displacement graph for design 2, hole location

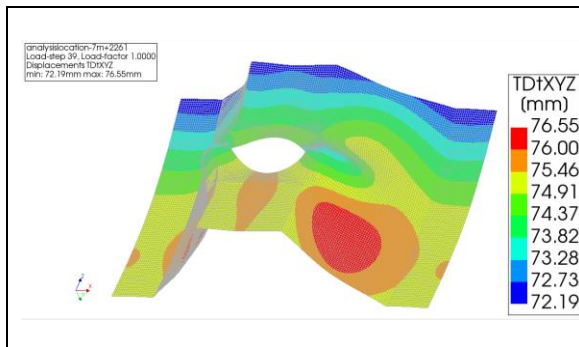


Figure 166: 3DSSI model: Displacements at ultimate load, hole location = -7m

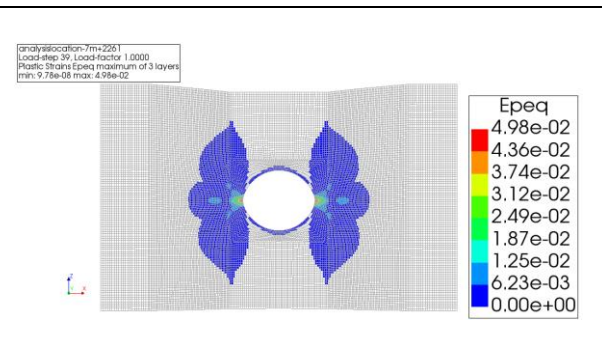


Figure 167: 3DSSI model: Plastic strains at ultimate load, hole location = -7m

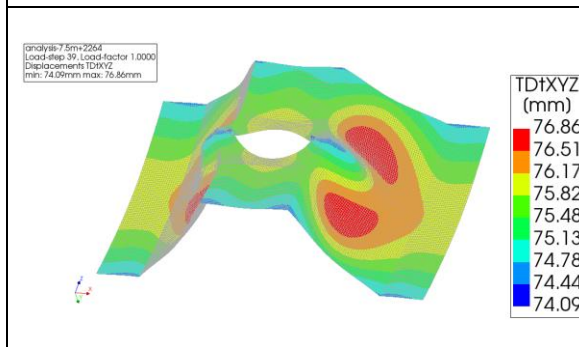


Figure 168: 3DSSI model: Displacements at ultimate load, hole location = -7.5 m

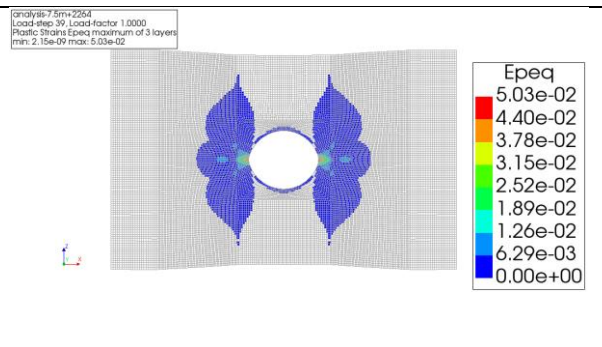
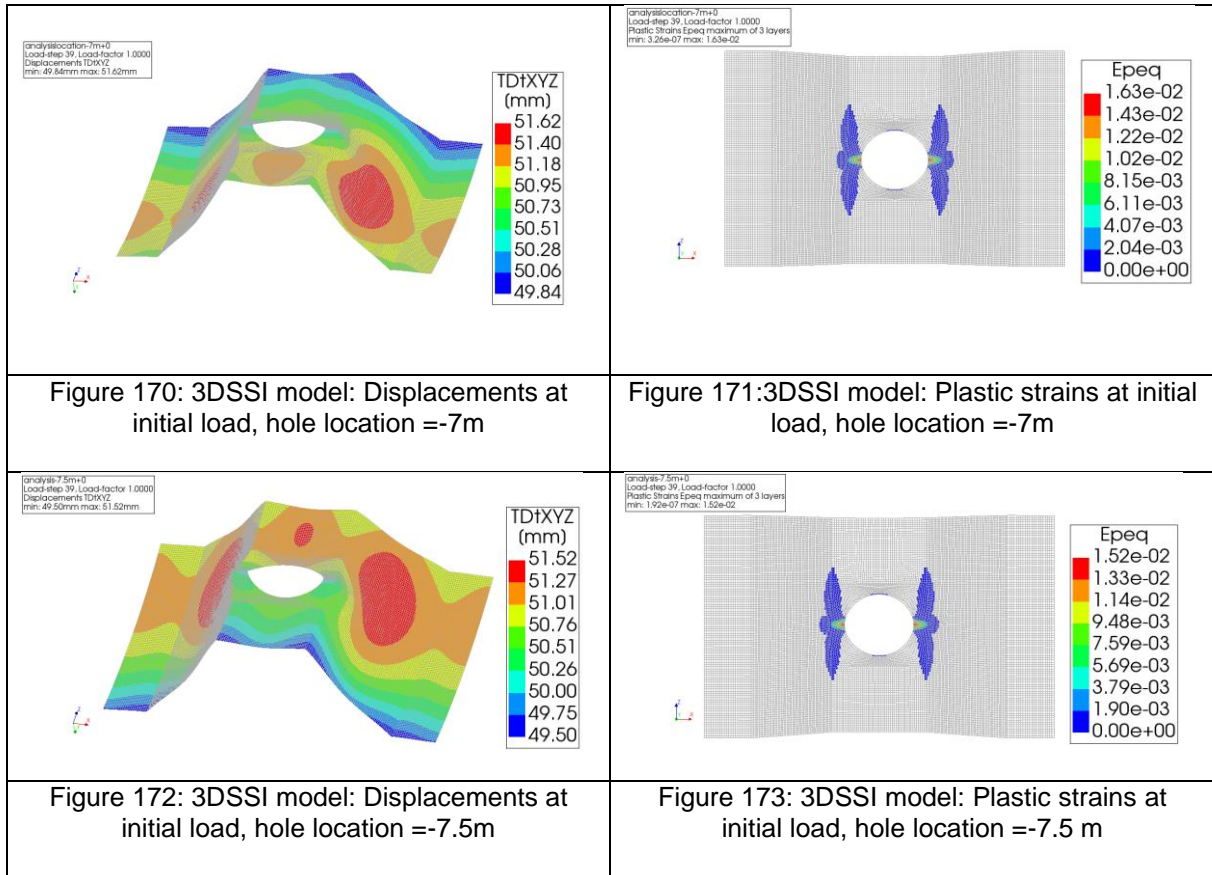


Figure 169: 3DSSI model: Plastic strains at ultimate load, hole location = -7.5 m

Already at the initial stage, significant plasticity and the failure modes can be observed. The local buckling is showing and the plastic deformation around the hole as well, as shown in Figure 170 up till Figure 173.



Hole spacing

The hole spacing does not significantly influence the resistance or behaviour of the sheet pile, as shown in Figure 174. Similar failure modes as for the basic case are governing for 'hole spacing = 2 sheets' case: plasticity around the hole and local buckling (Figure 175 and Figure 176).

The limitation of this model with respect to hole weakening is discussed in chapter 6.2.1.

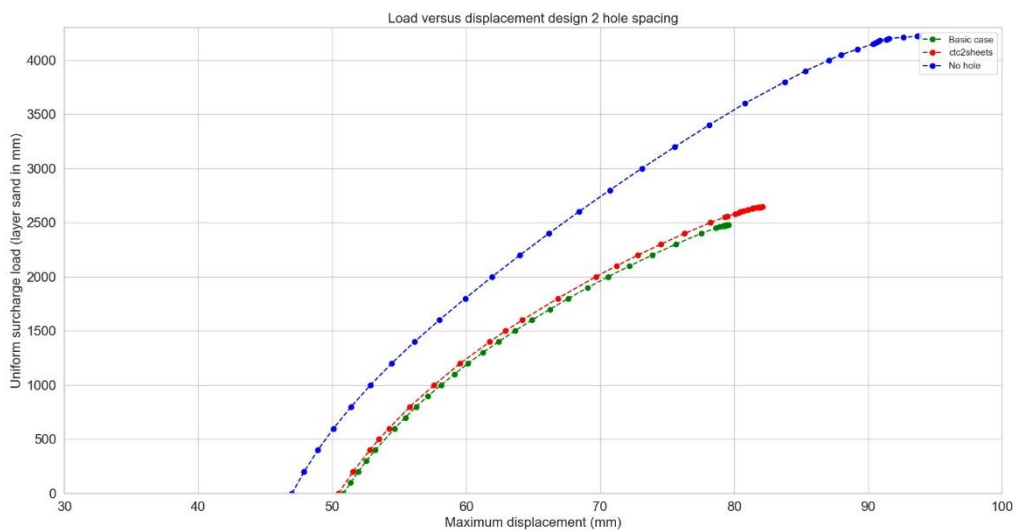
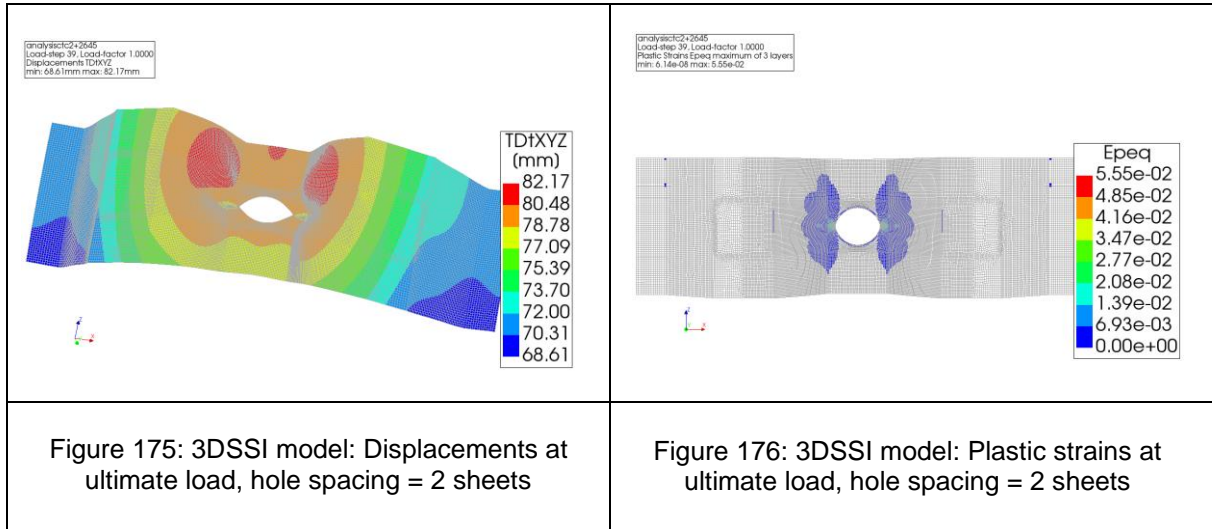
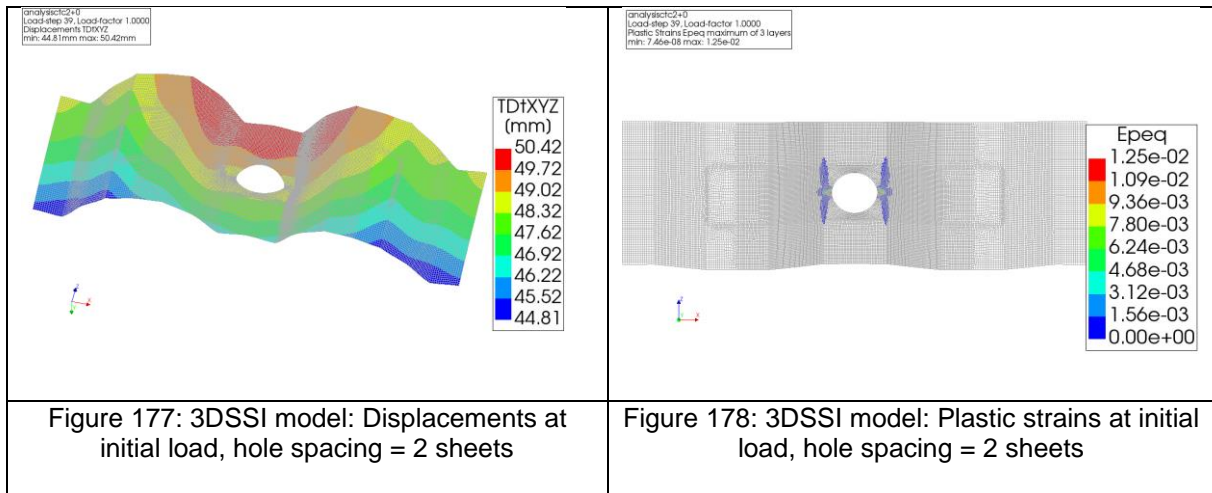


Figure 174: Load versus displacement graph for design 2, hole spacing



At the initial load, the local buckling is not present yet (Figure 177). Some plastic strains are visible around the hole (Figure 178).



In-pan / out-pan (compression or tension zone)

The resistance is larger for holes out-pan (in tension zone) than holes in-pan (in the compression zone). Also, for similar loads, the displacements are lower out-pan compared to in-pan. This is shown in the load-displacement curve in Figure 179.

The hole out-pan shows different deformations and failure loads, especially for a hole diameter of 300 mm. Also the failure mode is different. At the failure load, the compression flange (without a hole) starts to buckle. Plasticity around the hole in tension zone can be observed, resulting in larger deformations compared to the no hole situation (Figure 180 up till Figure 183). The hole is due to deformation and plasticity extended in length.

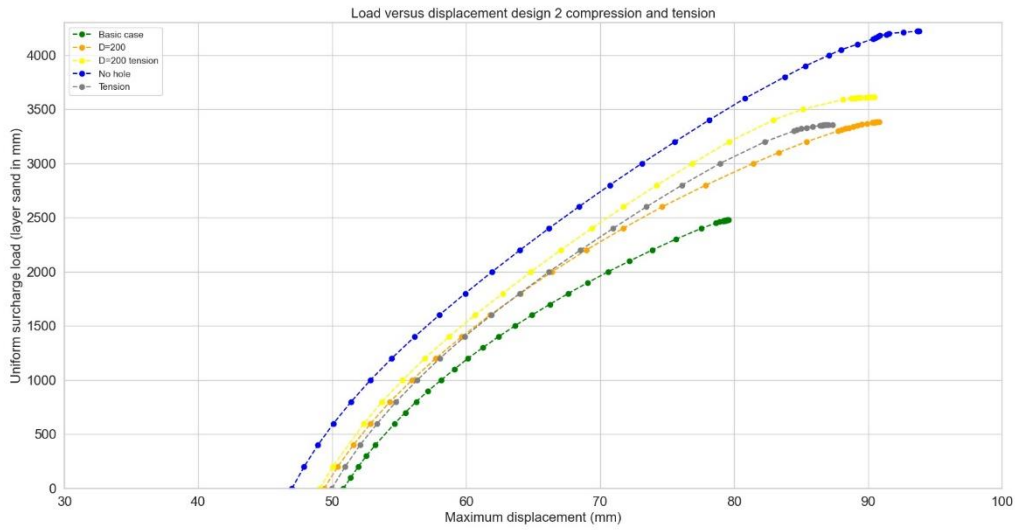
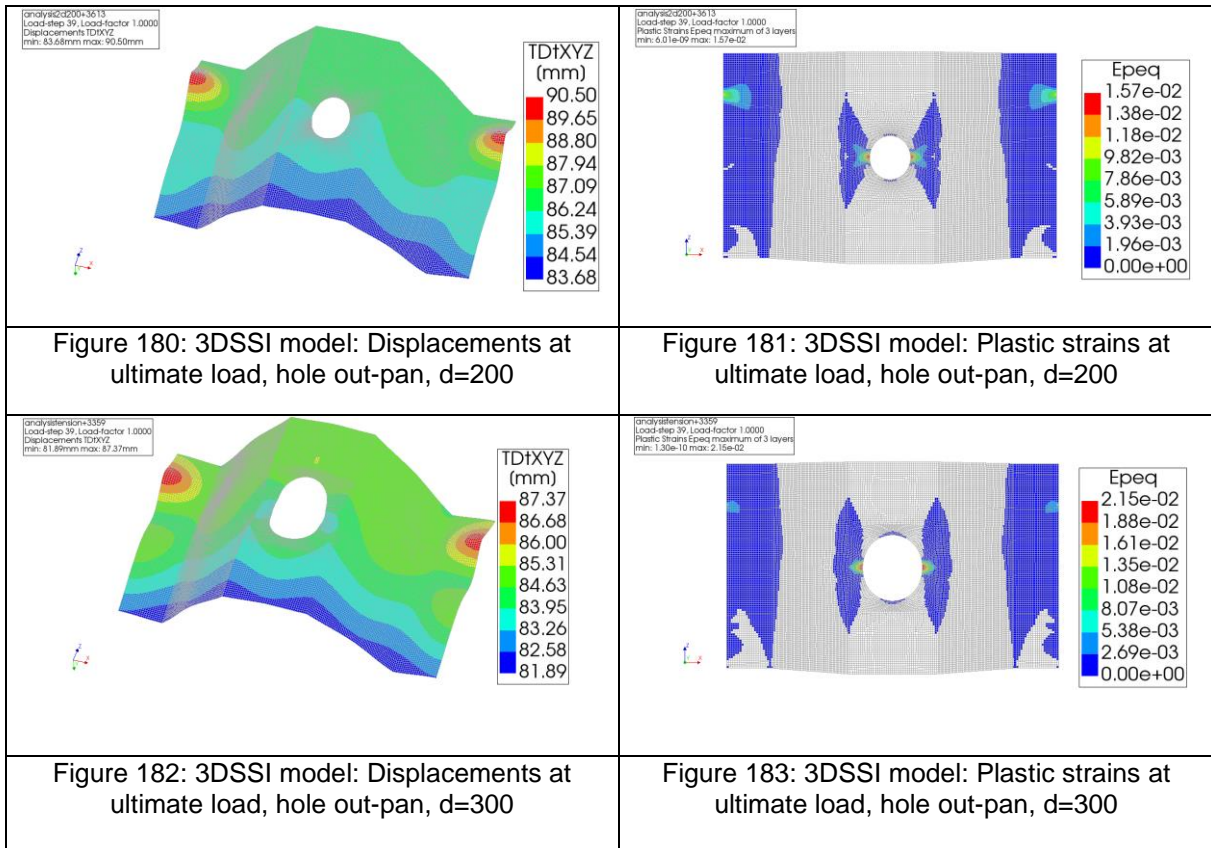
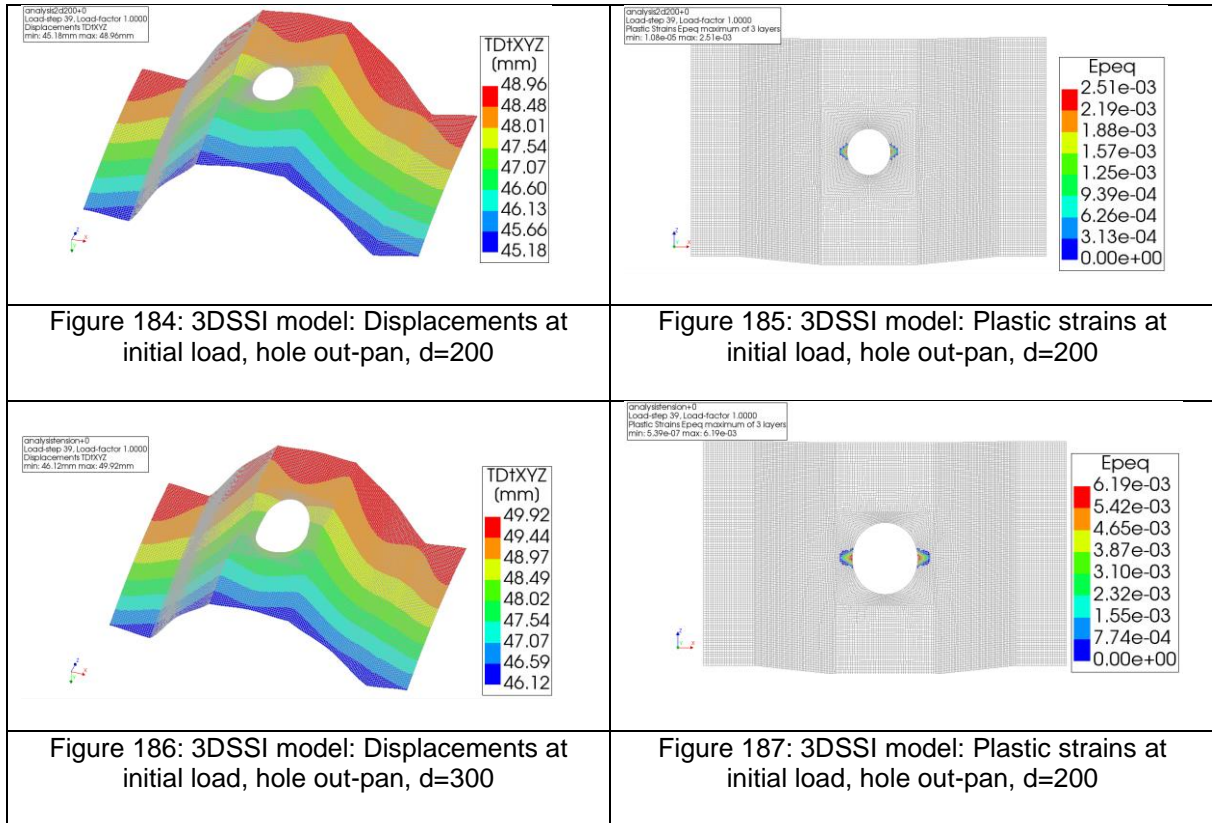


Figure 179: Load versus displacement graph for design 2, in-pan / out-pan



At the initial stage, only some plasticity can be observed near the hole (Figure 184 up till Figure 187).



6.3.2. Stiffness

The stiffness is determined for all cases, including no hole. The stiffness includes both soil and steel behaviour. The stiffness versus load curve and stiffness ratio (as defined in chapter 6.1.2) versus load curve are shown in Figure 188 and Figure 189 respectively. The stiffness curves show similar trends. The stiffness of the holes in tension perform better than holes in compression.

Considering the stiffness ratio, a offset in initial stiffness can be observed for the cases with a hole in compression; a 10-20% decrease in stiffness compared to no hole. The stiffness ratio is reducing even more when increasing the load. For the tension cases different behaviour is observed. A small reduction in initial stiffness of 7% is observed. Especially for a hole of 200 mm in tension, when increasing the load, the stiffness reduction remains approximately 7%, until failure starts to occur and rapid decrease in stiffness is observed from a surcharge load of 2800mm sand. Reduction occurs until failure. For a hole of 300 mm this reduction starts to decrease earlier at a load of 1800 mm. Then gradual stiffness decrease is observed up till also approximately a load of 2800 mm. Then similar behavior as for d=200 mm can be observed, but at a lower load.

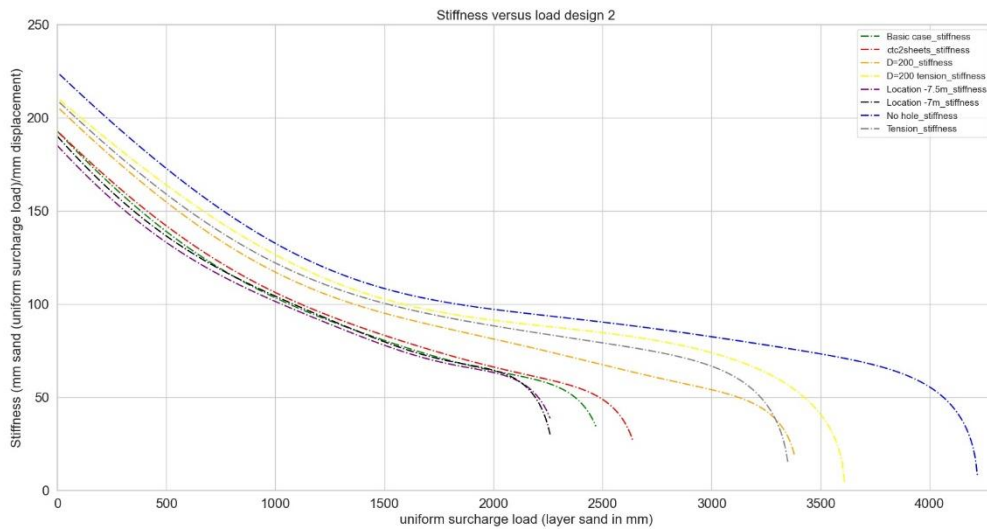


Figure 188: Stiffness versus load curve design 2

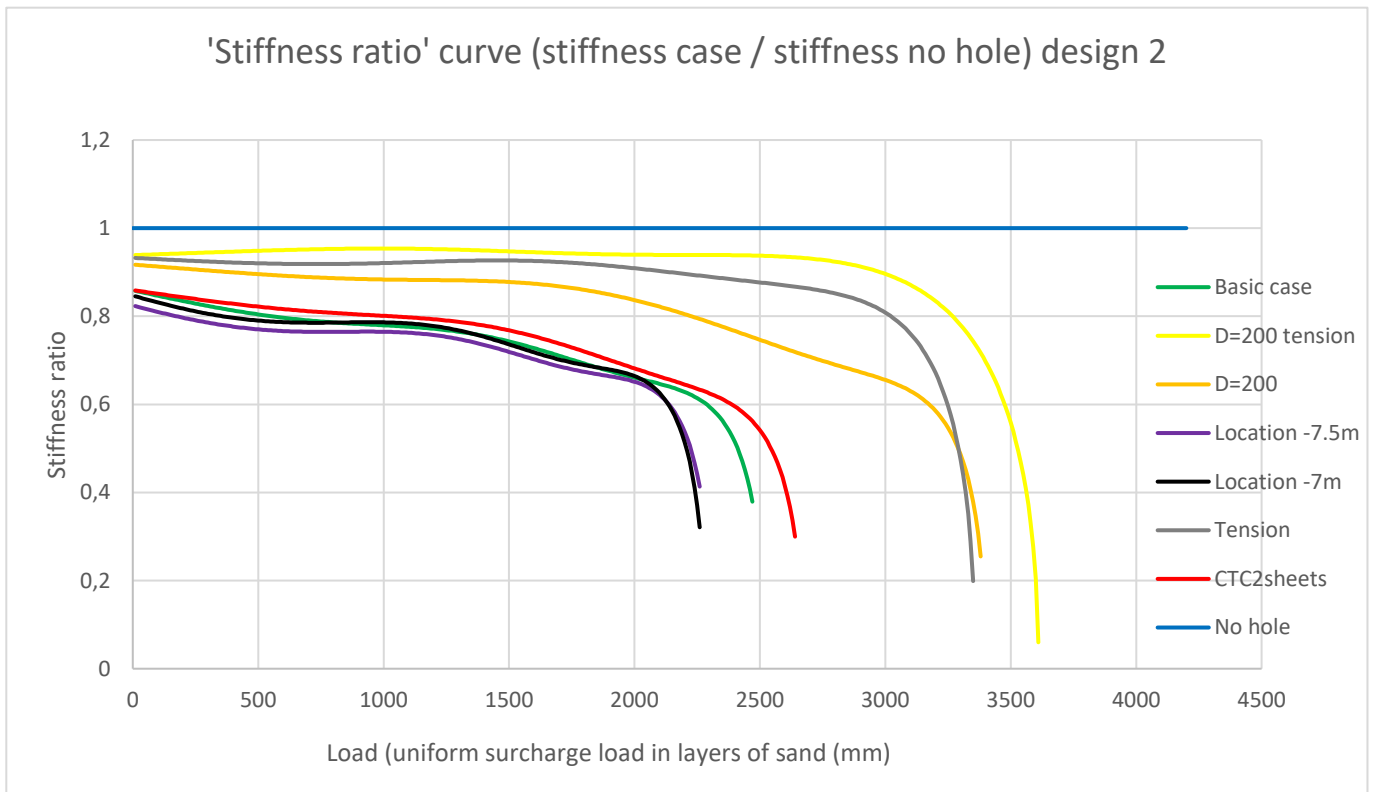


Figure 189: Stiffness ratio versus load curve

6.3.3. Conclusion

The results of design 2, including load-displacement curves and stiffness curves, result in the following conclusions.

Holes in tension cases show a larger resistance before failure than the cases with holes in compression zone. For case 'D=200' the difference of the uniform surcharge load capacity

between tension and compression is smaller than for basic case 'D=300'. The difference is respectively 8% and 22%. At failure load, the tension cases show more than the compression cases, which show only plasticity locally around the hole. Also the deformations when reaching the maximum failure load for tension cases is larger than for compression cases. The compression cases fail due to local buckling in the webs and local plasticity around the hole. Tension cases' failure modes is plasticity and local buckling of the compression flange (without a hole).

The hole diameter influences the resistance of the sheet pile, especially in compression case. For case hole diameter 'D=300' (basic case), the web buckles above the hole and the resistance is 62% of the uniform surcharge load, while for 'D=200' the web buckles next to the hole and the resistance is 84% of the uniform surcharge load. However, for the basic case, the plasticity is more severe around the hole in the webs. The hole location does not significantly influence the resistance, 6-7%, but the local buckling of the web is located differently with respect to the hole. The web buckles at the location of -7.5 mm around the hole, and for a location of -8 above the hole and for -7 below the hole. This is again explained due to the maximum bending moment occurring at the location where the web buckles. A different hole spacing shows similar failure mechanisms: plasticity around the hole and local buckling.

Considering the stiffness compared to no hole, an offset in initial stiffness for compression cases 10-20%. The stiffness ratio reduces when increasing the load. For tension cases, a smaller offset of the stiffness ratio is observed: 7%. For the tension cases, for an increasing load the stiffness ratio reduction remains equal, until gradual stiffness reduction starts to occur, followed by progressive failure.

6.4. Comparison design 1 and design 2

Design 1 is an AZ23-800 sheet pile, cross-section class 2, while design 2 is an AZ20-800 profile, cross-section class 3. The difference in cross-section class is expected to result in available plastic capacity for cross-section class 2, and only elastic capacity for cross-section class 3 (chapter 3.2). For the no hole situation, this is also found by the 3DSSI model. For design 1, the plastic design capacity can be reached and for design 2 the elastic design capacity determines the maximum loading of the sheet pile. Both designs show local buckling behaviour after passing the maximum load. However, for design 1 (CC2), the local buckling is accompanied by plasticity over almost the complete cross-section. For cross-section class 3, as expected by the literature, local buckling is governing the failure mode before reaching a plastic cross-section.

Since the designs exist of different cross-sections the characteristics of these designs should also be considered. The AZ20-800 has a lower moment of inertia, resulting in larger displacements.

Considering the cross-section characteristics more closely, the flange thickness, web thickness and the ratio between these differ. Since the hole is located in the flange, this is of interest. For a AZ23-800, more steel is removed in order to create a hole due to the thicker flange than for an AZ20-800 with hole. Therefore, the influence of a hole is expected to be larger for an AZ23-800 than for an AZ20-800. This is also observed comparing Table 8 and Table 10, where for the basic case in design 1, only 22% of the surcharge load can be applied, while for design 2, 62% can be applied.

With respect to the hole diameter, the reduction in resistance is significantly more for design 1 than for design 2. This is partly explained by, as elaborated above, the thicker flange which means more steel is removed. Also, the plastic capacity of the profile which can be used for the design with no hole, is not reached for the cases with hole. The elastic bending moment capacity of design 1 with hole is 48% of original plastic bending moment capacity at the location

of the hole. For design 2 the elastic bending moment capacity is 62% of the original bending moment capacity. However, the failure mode is equal for design 1 and 2: plasticity around the hole and local buckling in the webs.

Regarding the hole location, also similar failure modes are observed: plasticity and local buckling. The local buckling of the web depends on the location of the maximum stresses caused by the bending moment. The local buckling of the web is observed at the location of the maximum bending moment stresses, which is depending on the hole location, above or below the hole.

The hole spacing does for both designs not influence the failure mode or the failure load significantly. For both models the failure is determined by the local buckling of the web and large local plasticity. As elaborated in chapter 6.2.1, in practice it could be expected that the ultimate load will be larger for larger hole spacing. However, large deformations at the hole are in practice also not desirable due to the equipment needed for the underwater anchor and the force transferred from the coming underwater anchor to the sheet pile.

For the holes in tension, for design 1 and design 2, the behaviour is favourable compared to holes in compression. For holes in tension, the failure mode consists of plasticity around the hole in tension and local buckling in the compression flange (without a hole). However, for design 1 this benefit is larger than for design 2. For design 1 also larger plasticity can be observed at the maximum load. This is similar as for the comparison of no hole, depending on the cross-section classification.

The stiffness curves, including soil-structure interaction, show different shapes. For design 1, an almost linear curve is shown while for design 2, a nonlinear stiffness-curve is obtained for all cases. The compression cases show a faster decrease in stiffness than the tension cases. Considering the stiffness ratio, with respect to no hole, the tension cases show less reduction in stiffness than the compression cases for both designs. Also the stiffness degradation with respect to no hole is more severe for compression cases than for tension cases. This is similar for design 1 and design 2. The stiffness degradation is however larger for design 1 cases than for design 2 cases. This can, similarly as for the resistance, be explained by the larger reduction in cross-section, as explained above.

6.5. Results design 3

Design 3 includes oblique bending behaviour. Therefore this results are studied separately. The design is a sheet pile PU22, cross-section class 2. Due to the oblique bending, the stiffness and strength is significantly reduced. Again, the design starts at a unity check of approximately 0.6. For oblique bending only a hole in the tension flange, with a diameter of 200 mm on location -8m is studied. This design is chosen based upon the results of design 1 and 2, showing beneficial behaviour. The load-displacement curve is shown in Figure 190.

The transverse soil stiffness, as discussed in chapter 4.2.3, is neglected. Therefore, it is expected that the model and results are conservative and will differ more from the reality, especially for stiffer soils, due to neglecting transverse soil stiffness.

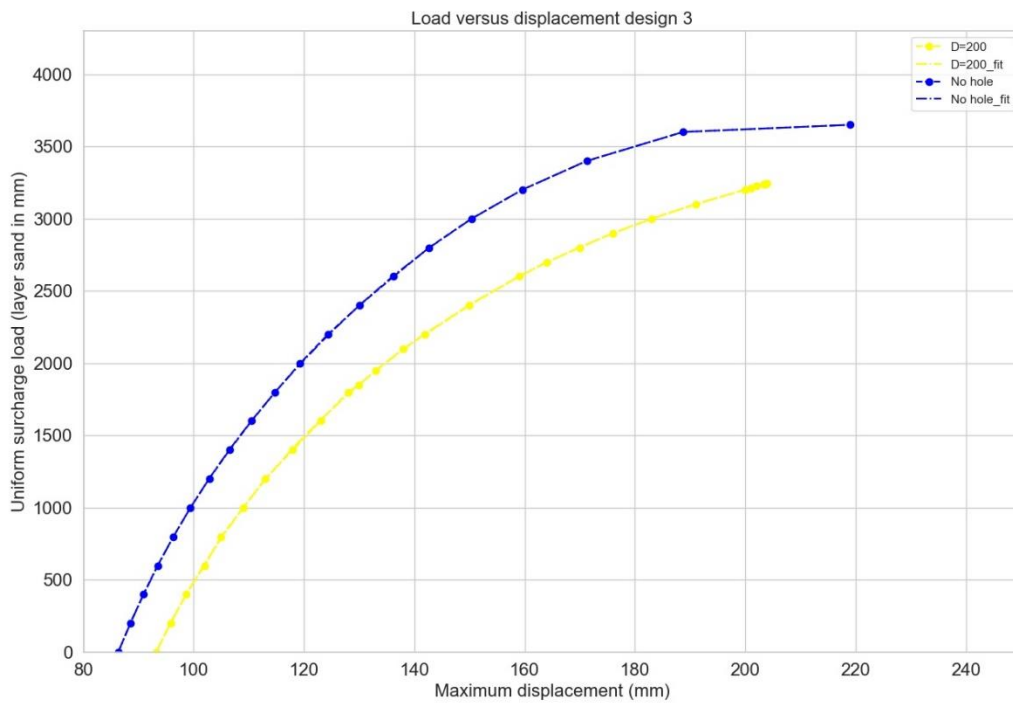


Figure 190: Load versus displacement graph design 3

The global oblique bending behaviour is shown for a situation with hole in Figure 191. The double bending with respect to the zero displacement sheet pile is shown by the 3DSSI model.

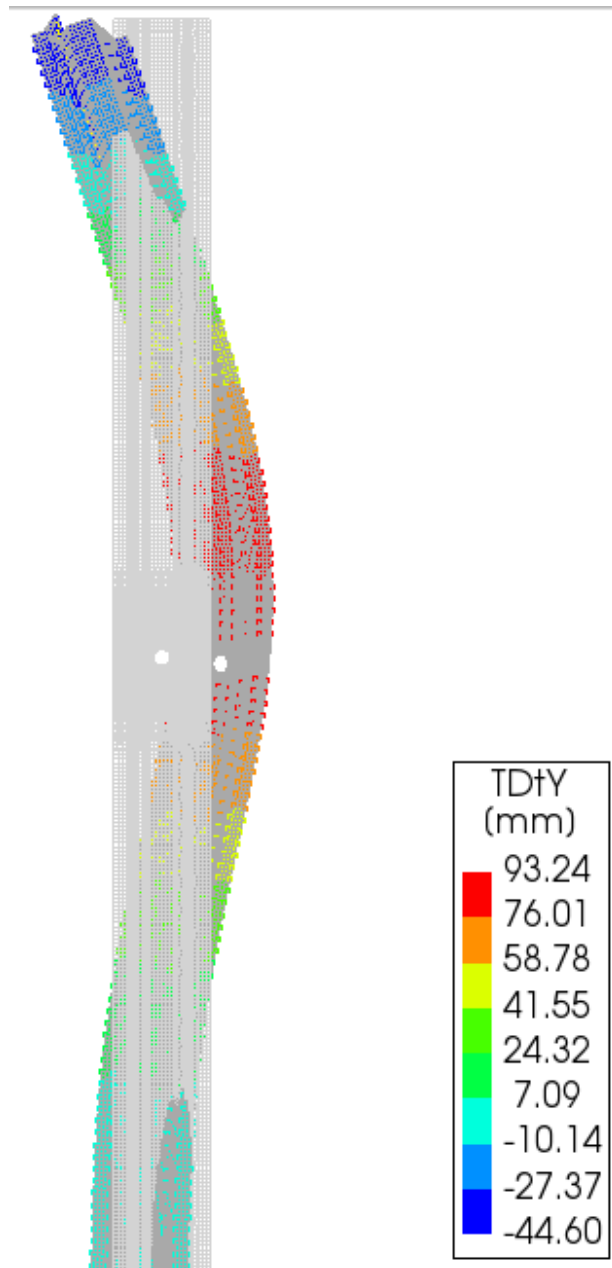


Figure 191: 3DSSSI model: oblique bending (with hole)

6.5.1. Failure load and failure mode

Similar as for design 1 and 2, the load ratio is determined (Figure 192), based upon the design resistance of design 3 without a hole, including oblique bending. The failure loads are given in Table 12.

Table 12: Failure loads design 3

Load case	Design 3 CC2 and oblique bending Ultimate load (mm sand uniform surcharge load)	Design 3 CC2 and oblique bending Ultimate load as percentage of design resistance (no hole)
No hole	3650	1.04
D=200 tension	3240	0.93

Also the displacements at initial stage and failure load are shown. The displacements are larger for the situations with a hole, and in general the displacements are larger than design 1 and design 2 due to oblique bending, reducing the stiffness of the cross-section. The displacements are given in Table 13.

Table 13: Displacements at initial stage and failure load

Load case	Design 3 CC2 and oblique bending Displacement at initial stage (mm)	Design 3 CC2 and oblique bending Displacement at failure load (mm)
No hole	86.3	219.0
D=200 tension	93.2	203.9

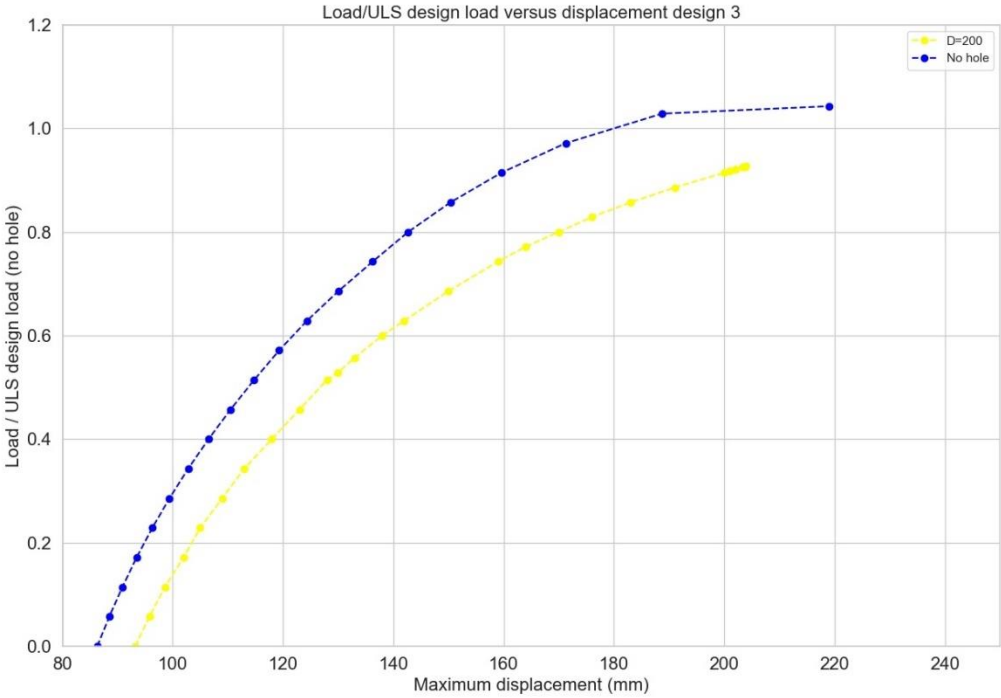
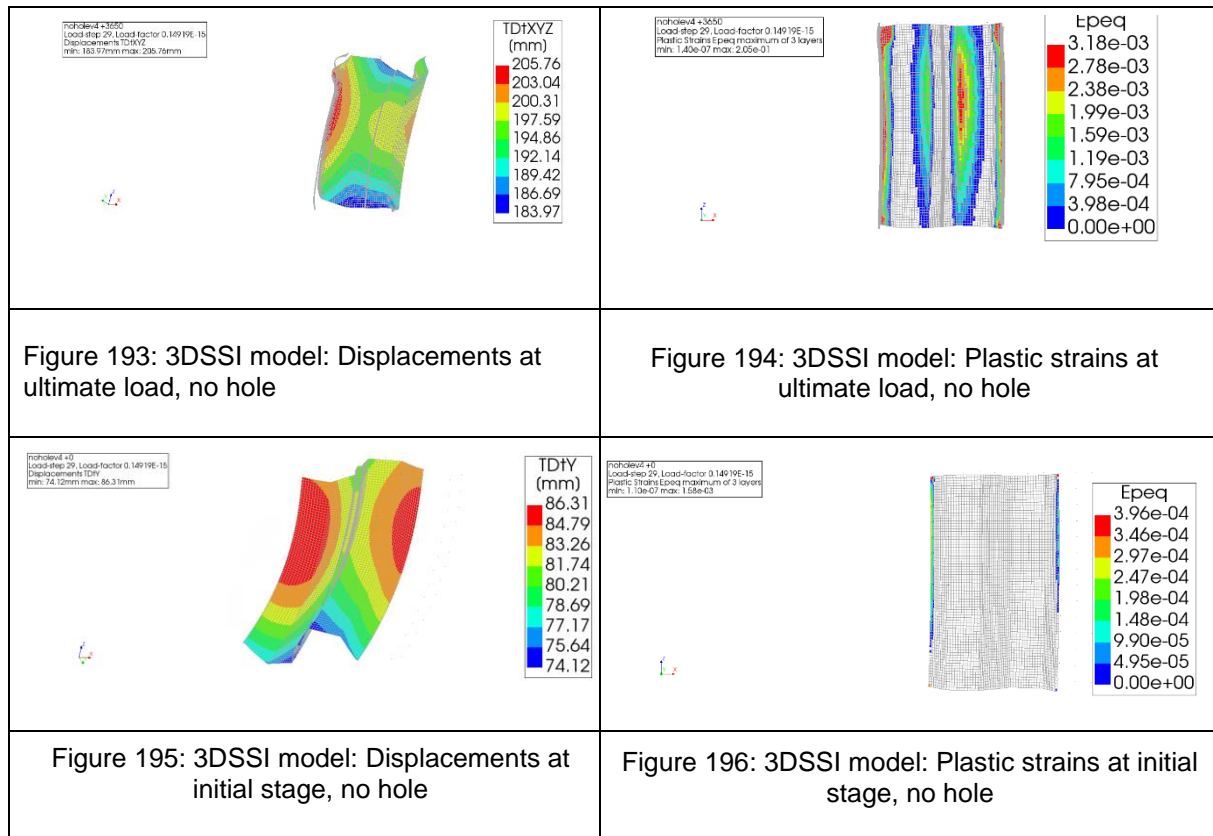


Figure 192: Load ratio versus displacement design 3

No hole:

At the ultimate load, locally large displacements occur. Almost the complete cross-section shows plasticity (Figure 194), with the largest strains in the webs. This can be explained by the inclined neutral axis due to oblique bending, resulting in largest stresses in the webs instead of the flanges. The deformations at ultimate load are given in Figure 193.

At the initial stage, the sheet pile shows oblique bending behaviour as shown in Figure 195. A double U-sheet pile is shown to include the complete oblique bending behaviour. Plastic strains can be observed only at the interface elements (Figure 196). Where different sheet pile shell elements connect, local stress concentrations occur. However, these are not representative for the sheet pile behaviour or failure.



D=200, hole out-pan

For a hole $D=200$, out-pan, the failure behaviour is different than for design 1 and 2. This is due to the oblique bending. As discussed in the literature part for oblique bending, chapter 3.3 and the verification model for oblique bending, Appendix D, the neutral axis is inclined. The model with the interface element is shown in Figure 197. This can also be observed from the plasticity distribution in the cross section, which is to the right of the hole (near the locked interlock), larger than left from the hole (near the free interlock), shown in Figure 199. The plasticity occurs over almost the complete cross-section resulting in large deformations. The webs show local buckling (Figure 198). In design 1 and design 2, the local buckling occurred in the flanges for cases with holes in tension. This can be explained by the inclined neutral axis causing compression over a larger area of the web. The tension and compression zones are shown in Figure 200 for a double U-sheet pile. Figure 201 is also showing global tension and compression stresses with the appropriate scale values.

At the initial stage, no local buckling of the webs is observed and only the oblique bending deformation of the cross-section is observed (Figure 202). Some plasticity is already present in the cross-section, especially near the free interlock and to the right side of the hole, where the stresses are larger than to the right of the hole, due to oblique bending (Figure 203).

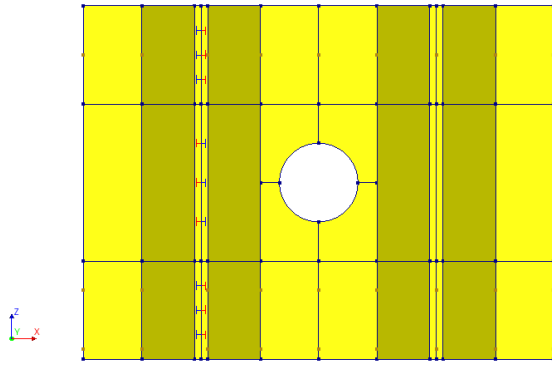


Figure 197: 3DSSI model: model with interface connection (free interlock) left from the hole

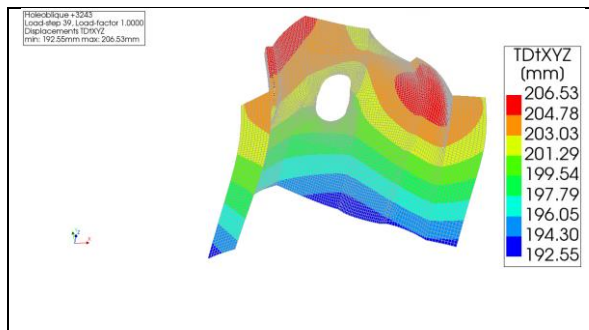


Figure 198: 3DSSI model: Displacements at ultimate load, hole out-pan, d=200

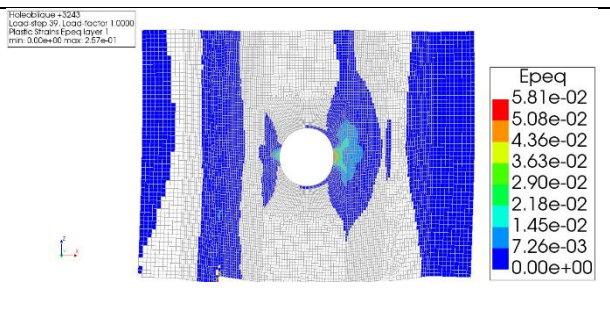


Figure 199: 3DSSI model: Plastic strains at ultimate load, hole out-pan, d=200

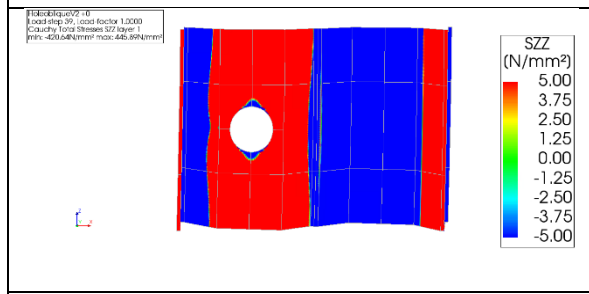


Figure 200: 3DSSI model: Indication of tension and compression zone double U-sheet pile, hole out-pan, d=200

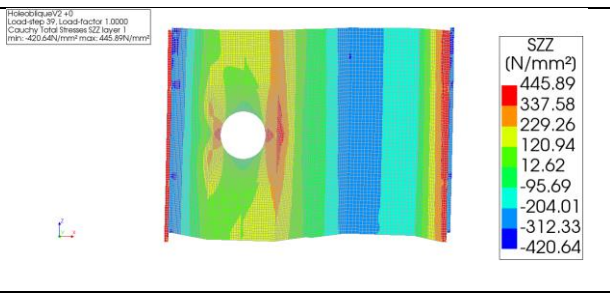


Figure 201: 3DSSI model: Stresses SZZ double U-sheet pile, hole out-pan d=200

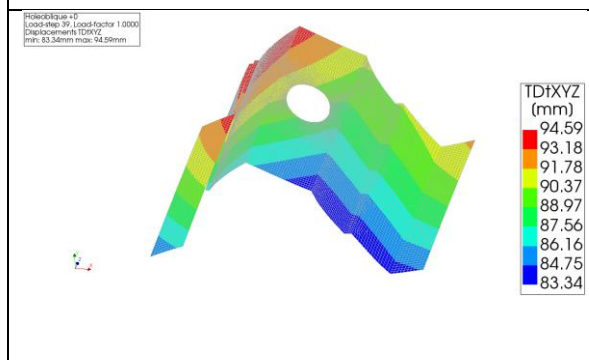


Figure 202: 3DSSI model: Displacements at initial load, hole out-pan, d=200

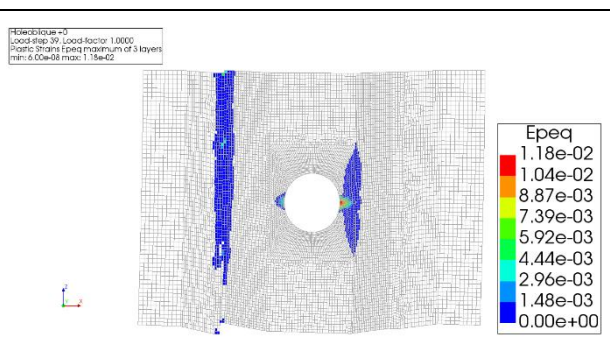


Figure 203: 3DSSI model: Plastic strains at initial load, hole out-pan, d=200

6.5.2. Stiffness

The stiffness is also plotted against the load (Figure 204). This plot again includes both soil and steel behaviour. The stiffness ratio (as defined in chapter 6.1.2) curve is shown in Figure 205. The stiffness is already from the initial design approximately 50% lower than for design 1 and design 2. This is due to oblique bending reducing the stiffness of the cross-section. The stiffness then decreases showing an almost linear trend. The case $d=200$, out-pan, shows similar trend, with a lower stiffness than the original design without a hole. This can also be seen in the stiffness ratio curve. From a load of 1200 mm sand, the tension case with hole the reduction in tension with respect to no hole starts to increase. However, this considers also a relatively low stiffness for the no hole situation, and therefore the results are also quite sensitive. The initial stiffness reduction is 18% with respect to no hole, which starts to increase from a load of 1200 mm and to a stiffness reduction of almost 50%.

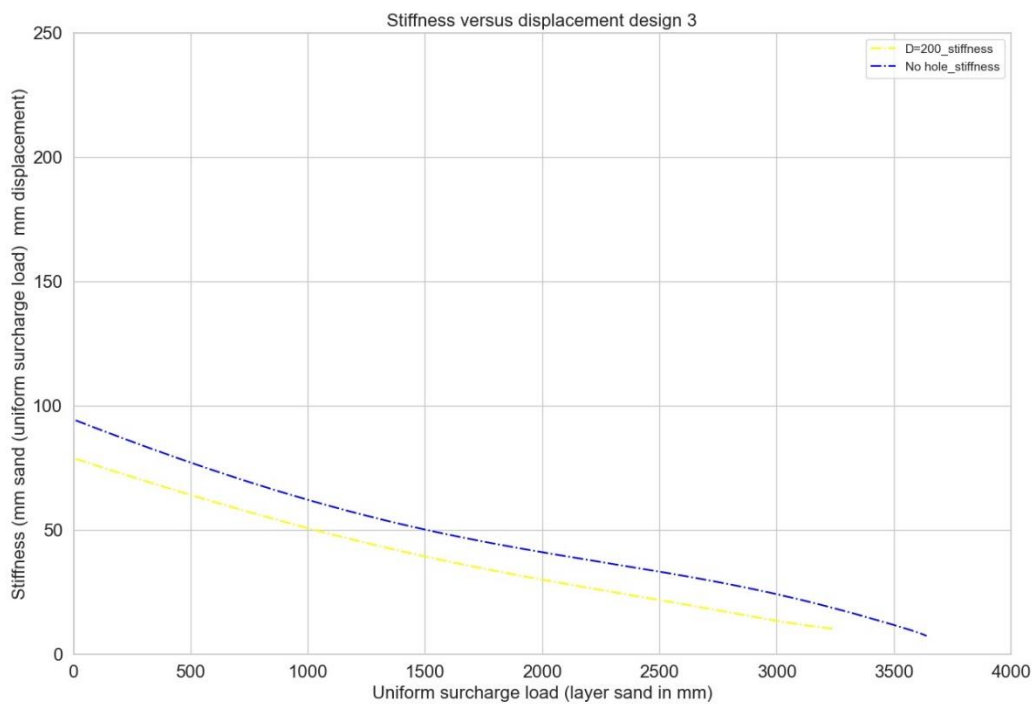


Figure 204: Stiffness versus load curve design 3

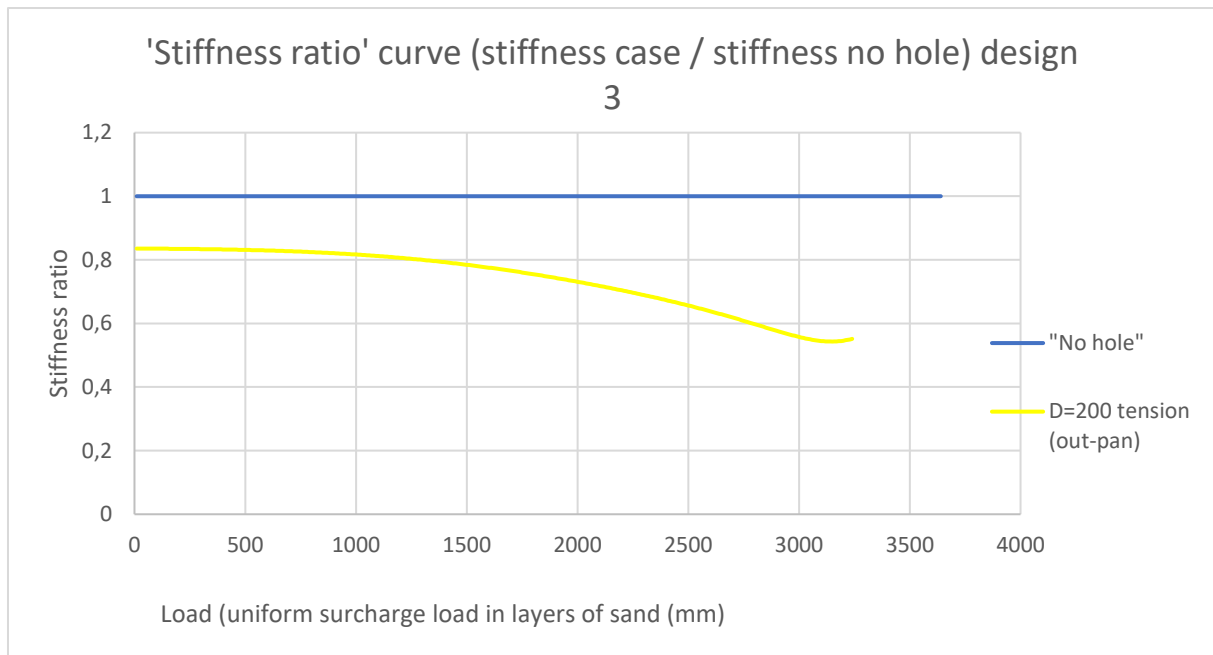


Figure 205: Stiffness ratio curve design 3

6.5.3. Conclusion

The load reduction due to a hole $D=200$ in tension is relatively small, only 7%. The oblique bending can be observed for the cases with and without the hole. For the case with hole, this results in different shapes of the cross-section around the hole compared to design 1 and design 2, and unequal plasticity distribution around the hole. The webs in compression show local buckling. The stiffness reduction due to a hole in tension is at the initial stage, up to a load of 1200 mm, approximately 18-20%. The stiffness for a situation with hole and without a hole show over a large area quite a similar trend. The stiffness is significantly lower than design 1 and design 2, due to oblique bending.

6.6. Conclusion

The phenomena having most influence on the sheet pile behaviour and resistance observed by the 3DSSI model is especially the in-pan or out-pan location, thus respectively in compression or tension zone of the sheet pile. Making a hole in tension shows preferable behaviour compared to holes in compression zone in both stiffness and resistance. For design 1, the tension cases show 30-50% better resistance than the compression cases, for design 2 8-22%. Therefore, it is recommended when making a hole to locate this in the tensile zone. A hole in tension shows plasticity around the hole and at the ultimate load failure in the compression flange starts to occur, while for a hole in compression local buckling in the webs is observed, and also plasticity around the hole. For a sheet pile of cross-section class 2, the plastic capacity is no longer observed for the situation with holes in compression zones. The second phenomena found having influence is the hole diameter. A smaller hole diameter significantly increases the sheet pile resistance and stiffness, e.g. for design 1, a hole diameter of 200 can take 53% of the surcharge load, while $d=300$ can take 22% of the surcharge load. The failure mode is similar: local buckling in the webs and plasticity around the hole. The hole location also shows some influence, but this effect is relatively small compared to hole in-pan/out-pan and hole diameter. The hole spacing shows for a spacing of 1 sheet and 2 sheets

very similar behaviour for the 3DSSI model; the failure load is determined by the local behaviour around the hole: plasticity and local buckling. Considering the sheet pile design, a sheet pile with a smaller flange/web ratio appears to show beneficial behaviour with respect to the no hole situation.

The stiffness is, with respect to no hole, for all cases reduced. Especially all cases with holes in compression show a significant stiffness degradation; for design 1 40-50%, for design 2 10-20%, while the tension cases show a stiffness reduction for design 1 and 2 of 6-7%. The stiffness starts to reduce significantly at a much lower load than the tension cases. Therefore, the tension cases cannot only resist larger loads, but also show larger displacements before failure occurs.

Considering oblique bending, the stiffness is already significantly reduced compared to design 1 and design 2. The case studied, a hole with a diameter of 200 mm in tension zone, shows a reduction in resistance of 7% and a stiffness reduction compared to no hole of 18-20%. However, the displacements are for all cases large due to oblique bending.

The hole weakening thus significantly influences the resistance and sheet pile behaviour. The influence on resistance and behaviour depends mainly on the hole location in-pan or out-pan, the hole diameter and the type sheet-pile; the flange and web thickness and cross-section classification.

From the results, it can be concluded that before making holes, running the developed 3DSSI model is necessary to obtain the specific resistance, failure mode and stiffness and displacement. The results have showed significant influence of hole weakening on the sheet pile resistance and behaviour for all cases.

7. Conclusion

This thesis aims to develop a model to study the influence of hole weakening on the resistance and behaviour of sheet piles and to identify the influence of hole weakening on the sheet pile resistance and behaviour. With the sub-research questions, the main research question is answered.

What are the characteristics of the numerical model to obtain understanding in the sheet pile behaviour regarding the effect of hole weakening?

Literature review showed that the soil behaviour can be best described with the subgrade reaction method for researching the hole weakening in sheet piles. The subgrade reaction model (spring model) is an efficient modelling technique and gives accurate displacements and internal forces. To include the behaviour of the sheet pile around the hole, the existing subgrade reaction method is extended by using it in combination with a 3D sheet pile modelled with shell elements in the finite element software DIANA FEA. Therefore, the developed model is a subgrade reaction model with 2D shell elements and captures the soil-structure interaction in 3D, named 3DSSI model. The model is developed for Dutch soils, trilinear spring characteristics based upon the Dutch soil model are incorporated. To study the sheet pile behaviour and resistance for hole weakening, physical and geometrical non-linear behaviour of the steel sheet pile have to be included. For numerical purposes, the loading caused by the springs should be applied stepwise until the full load case is present. The procedure developed is to compensate spring forces by modelling the neutral earth pressure on the spring nodes as a load. By reducing this load stepwise, there will be no numerical errors. Around the hole, the springs are replaced by a distributed load to create a numerical stable model. The soil load within the hole should be redistributed over the flange width and over a height of approximately 2 times the diameter. When double U-profiles are used it is necessary to include axial degree of freedom in the interlocks, allowing for double bending.

To research the influence of hole weakening a load displacement graph should be determined, where the soil-structure interaction is incorporated. A convenient method to obtain those results is by application of a uniform surcharge load that will be increased step by step. By plotting the uniform surcharge load versus the maximum displacement the behaviour and resistance can be determined. A more in dept analysis also allows for determining the stiffness and stiffness reduction to the initial case.

What is the influence of hole weakening on the resistance and behaviour of the sheet pile structure?

The parameters included in this research are based on current knowledge found in literature. The most important parameters are analysed: hole diameter, hole location, hole spacing, hole in-pan / out-pan, sheet-pile cross-section classification and oblique bending. These parameters give the influence on the resistance and behaviour of the sheet pile structure.

The sheet pile resistance is influenced by the hole, especially the location of the hole in-pan (compression zone) or out-pan (tension zone). Hole weakening out-pan shows larger resistance than in-pan. Especially for the a AZ23-800 cross-section class 2 (design 1) sheet pile with larger diameter, the out-pan/tension case (hole in tension; $D=300$) showed 53% more surcharge load capacity compared with the basic case (hole in compression/in-pan; $D=300$). For a AZ20-800 cross-section class 3 (design 2) the increase in resistance for the similar case is 22%. The failure mode given by 3DSSI is also different: for all cases in-pan, the failure mode is plasticity around the hole and local buckling in the web. For out-pan cases, the failure mode

is plasticity around the hole and local buckling in the compression flange. These failure modes occurs at a later stage than for compression cases. The hole diameter also significantly influences the resistance. The difference between 'D=200' and 'basic case' (D=300) in compression, is for design 1 and design 2 respectively 31% and 22%. The influence of hole location is relatively small up to 14-6% for design 1 and design 2 respectively. Hole spacing (c.t.c. distance between the holes in width) does not influence the failure mode or resistance. The plastic capacity which is available for cross-section class 2 cases is not observed any longer for the cases with holes in compression. Design 3, including oblique bending, shows significant larger displacements. For the case "D=200" in tension zone, the strength reduction is small, 7%, but the failure mode is different compared to design 1. The neutral axis has inclined, resulting in local buckling of the web.

The hole characteristics also influence the sheet pile stiffness. The stiffness is reduced, especially for compression cases. The tension cases show a much lower stiffness reduction than the compression cases. For design 1, the tension cases show a stiffness reduction of 6-7% and the compression cases 40-50%. Design 2 shows also less stiffness reduction for tension cases, 7% than compression cases, 10-20%. Design 3 shows also a stiffness reduction in tension of 7%. For compression cases, the stiffness reduction also shows fast, progressive reduction in stiffness, for tension cases this progressive reduction in stiffness occurs much later, resulting in larger displacements and larger loads before reaching the maximum load.

Main research question:

What is the influence of hole weakening on the sheet pile's behaviour and resistance, before installing underwater anchors?

To predict a realistic influence of hole weakening on the sheet pile behaviour and resistance, a soil-structure interaction model is necessary. The characteristic of the developed 3DSSI model is a soil-structure interaction model; by modelling the soil with the subgrade reaction model and the steel sheet pile with 2D shell elements. This type of modelling allows for the 3D behaviour of the sheet pile and local behaviour can be observed, also near the hole. The 3DSSI model is able to study the influence of hole weakening on the sheet pile behaviour and resistance and can include oblique bending for double U-sheet piles. The main parameters influencing the resistance and stiffness, are the hole in-pan or out-pan, the hole diameter and the sheet pile type; web and flange thickness and cross-section classification. The resistance and stiffness of the sheet pile is reduced due to hole weakening. For design purposes for underwater anchors, based on these findings, it is beneficial to locate the hole out-pan and to keep the diameter as small as possible. Based on the different results found, it can be concluded that for each design, running a 3DSSI model to obtain the resistance, failure mode and sheet pile behaviour for the specific practical case is necessary. So, the hypothesis: hole weakening of the sheet pile will reduce the sheet pile resistance and stiffness for the hole diameter, is partially accepted. The research has shown that the in- and out-pan location also contributes to the resistance and stiffness of the sheet pile.

Discussion

The 3DSSI model is a model based on the subgrade reaction model. The subgrade reaction model idealises and simplifies the soil behaviour with trilinear springs. However, in practice soil shows a much more complex behaviour. This could especially be of interest around the hole. However, this is not included in this model due to lack of knowledge in this soil behaviour near a local weakening of the structure. Phenomena such as soil arching is an example of this more complex soil behaviour which is not included in the model. Soil arching could reduce the load on the sheet pile near the hole, neglecting this phenomena is therefore conservative. Ideal soil behaviour as in the subgrade reaction method is as within the state of art.

The 3DSSI model neglects wall friction. All vertical forces are transferred to the toe of the sheet pile. However, in practice this will not be the case. This is a conservative assumption. However, the 3DSSI model cannot verify the vertical force balance of the sheet pile. A different calculation program, such as D-sheet piling can be used for this calculation.

The shear resistance is neglected as well. This is especially of influence on the results with oblique bending. However, as discussed in chapter 3.3, this influence is relatively small, 5-10% and for Dutch, non-stiff soils, even lower than 5%. Neglecting the shear resistance of the soil is conservative.

Considering the steel modelling of the 3DSSI model, the interlocks and corner radii are neglected. This additional steel is expected to increase the resistance and it is therefore conservative to neglect this steel. Especially for U-sheet piles with holes, the web will be reinforced by the interlock in the middle of the web, where the web buckling now occurs. It is therefore expected that due to the interlock web buckling will occur later than in the 3DSSI model. The 3DSSI model can be improved by modelling the interlocks and corner radii.

The existing top anchor is modelled as a stiff spring. This assumes that the design of the top anchor also suffices and is stiff, resulting in a zero displacement at the location of the spring. In practice, this should be verified since this can significantly influence the stresses and displacements of the sheet pile. A solution in case the existing top anchor does not suffice, could be an additional anchor near the top of the sheet pile.

The 3DSSI model is now used for studying the hole weakening of the sheet piles. However, the model can be used for more research, especially with interest to 3D behaviour of the sheet pile. Detailed soil studies cannot be captured with the 3DSSI model, but structural behaviour such as oblique bending can be studied in an efficient manner. Also other 3D behaviour of the sheet pile, such as the anchor connection of for example the underwater anchor, or the reinforcement necessary in case hole weakening reduces the resistance of the sheet pile too much, could be studied. This is not captured in this thesis but could be studied with the 3DSSI in further research. The advantage of using this model is then the limited calculation time with respect to 3D solid soil elements, but still soil-structure interaction is included.

A limitation of this model is the load-induced force method. Since the loading is performed by the soil, which is modelled with springs, not the complete load-displacement curve can be obtained. Past the maximum load, the model cannot find equilibrium and cannot give results. Therefore, post failure behaviour cannot be observed.

The accuracy of the model is difficult to predict. The model is verified with D-sheetpiling and 4-pointbending tests, but to determine the accuracy of the model, field measurements could be a good solution. Then, with measurement devices, the accurate displacements, also locally around the hole, can be measured and compared with the 3DSSI model.

Bibliography

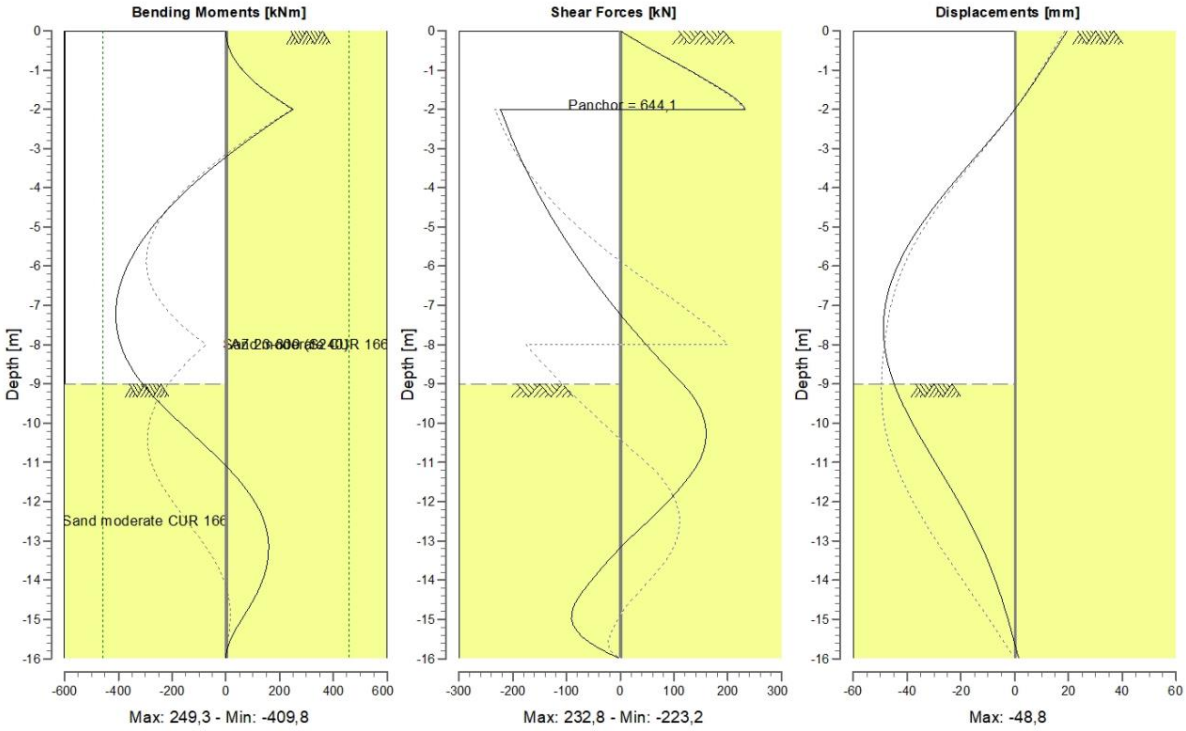
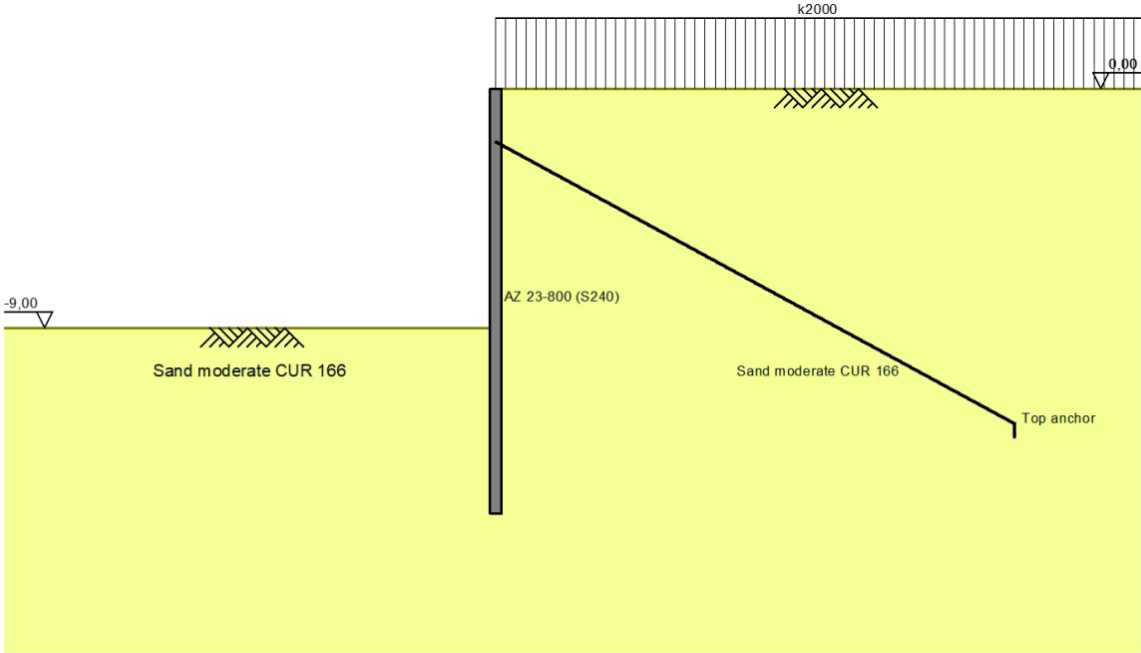
- [1] Van Leeuwen Verankeringen en Funderingssystemen BV, "Materieel." <https://www.vanleeuwenbv.nl/materieel> (accessed May 30, 2022).
- [2] ArcelorMittal, "Tie back / anchoring system," 2020. <https://sheetpiling.arcelormittal.com/products-services/production-range/anchors-struts/> (accessed May 30, 2022).
- [3] A. Roubos, "Enhancing reliability-based assessments of quay walls," TU Delft, 2019. doi: 10.4233/uuid.
- [4] RoyalHaskoningDHV, "Ontwikkeltraject onderwaterankers." Rotterdam, 2020.
- [5] M. Douairi and J. De Gijt, "Upgrading techniques for quay walls," 2013.
- [6] Ö. Bilgin, "Lateral Earth Pressure Coefficients for Anchored Sheet Pile Walls," *Int. J. Geomech.*, vol. 12, no. 5, pp. 584–595, 2012, doi: 10.1061/(asce)gm.1943-5622.0000154.
- [7] M. Korff, "Reader Deep Excavations." Delft University of Technology, Delft, 2018.
- [8] Port of Rotterdam, "Proeftuin voor verdiepen kademuren met onderwaterankers," 2020. <https://www.portofrotterdam.com/nl/nieuws-en-persberichten/proeftuin-voor-verdiepen-kademuren-met-onderwaterankers> (accessed May 10, 2021).
- [9] D. A. Emarah and S. A. Seleem, "Comparison Between Single and Double Anchored Sheet Piles With Simplified Approaches To Solve the Statically Indeterminate Systems," *JES. J. Eng. Sci.*, vol. 44, no. 6, pp. 659–674, 2016, doi: 10.21608/jesaun.2016.117622.
- [10] P. Ritthiruth, "Flexural behavior of cold-formed and hot-rolled steel sheet piling subjected to simulated soil pressure," 2020.
- [11] ArcelorMittal, "Cold formed steel sheet piles," 2020. <https://sheetpiling.arcelormittal.com/products-services/production-range/cold-formed/> (accessed Jul. 07, 2020).
- [12] W. F. Molenaar and M. Z. Voorendt, *Manual Hydraulic Structures*. 2016.
- [13] V. Van Delft, "Global buckling of sheet piles," Delft University of Technology, 2020. [Online]. Available: <http://repository.tudelft.nl/>
- [14] United States Steel, "Steel sheet piling design manual," 1984.
- [15] E. Gammeljord and M. S. Gronholdt, "Numerical Analyses of the Behaviour of a Sheet Pile Wall," Aalborg university, 2017.
- [16] C. R. I. Clayton, R. I. Woods, A. J. Bond, and J. Milititsky, *Earth pressure and earth retaining structures*, 3rd ed., vol. 3. Boca Raton: CRC Press, 2013.
- [17] A. Verruijt, *Grondmechanica*, 1st ed. Delft University Press, 2010.
- [18] NEN 6740, "Geotechniek TGB 1993 Basiseisen en belastingen." 2006.
- [19] T. S. Ingold, "Some simplifications of Coulomb's active earth pressure theory," *Gr. Eng.*, pp. 23–25, 1978.
- [20] G. Gedeon, *Design Of Sheet Pile Walls*. Woodcliff Lake, 1994.
- [21] K. J. Bakker, *Soil retaining structures*. Rotterdam: A.A. Balkema, 2000.
- [22] Deltares, "D-sheetpiling," Delft, 2020.
- [23] D. A. Kort, "Steel sheet pile walls in soft soil," Delft University of Technology, 2002.
- [24] CUR Civieltechnisch Centrum Uitvoering Research en Regelgeving, *Damwandconstructies*. 2008.
- [25] A. Karamperidou, "Parametric Analysis of Quay Walls with Relieving Platform, by means of Elastic Supported Beam and Finite Element Method," Delft University of Technology, 2008.
- [26] A. Simone, "An introduction to the analysis of slender structures." Delft University of Technology, p. 9, 2011.
- [27] J. G. de Gijt and M. L. Broeken, *Quay walls*, 2nd ed. Rotterdam: CRC Press/Balkema, 2014.
- [28] D. A. Kort, "The transfer matrix method applied to steel sheet pile walls," *Int. J. Numer.*

- Anal. Methods Geomech.*, vol. 27, no. 6, pp. 453–472, 2003, doi: 10.1002/nag.281.
- [29] S. Krabbenhoft and R. Christensen, “Design of anchored sheet pile walls in cohesionless soil,” *Numer. methods Geotech. Eng. IX*, 2019, doi: 10.1201/9781351003629-144.
- [30] G. Sedlacek, R. Hartmann-Linden, F. van Tol, A. Kort, A. Schmitt, and M. Meyrer, “Development of unified design rules for steel sheet piles for introduction into Eurocode 3, part 5,” Luxembourg, 2001.
- [31] E. Meijer, “Comparative analysis of design recommendations for quay walls,” *Delft Univ. Technol.*, 2006.
- [32] CEN European Committee for Standardization, “Eurocode 3: Design of steel structures - Part 5: piling.” 2008.
- [33] P. J. Bourne-Webb, D. M. Potts, and D. Rowbottom, “Plastic bending of steel sheet piles,” *Proc. Inst. Civ. Eng. Geotech. Eng.*, vol. 160, no. 3, pp. 129–140, 2007, doi: 10.1680/geng.2007.160.3.129.
- [34] ArcelorMittal, *Piling Handbook*, 9th ed. Luxembourg: ArcelorMittal Commercial RPS, 2016.
- [35] M. P. Doubrovsky and G. N. Meshcheryakov, “Physical modeling of sheet piles behavior to improve their numerical modeling and design,” *Soils Found.*, vol. 55, no. 4, pp. 691–702, 2015, doi: 10.1016/j.sandf.2015.06.003.
- [36] J.-F. Vanden Berge, A. Holeyman, E. Juaristi, and A. Schmitt, “interlock friction in a sheet pile wall: laboratory tests,” *Online Libr. Int. Soc. Soil Mech. Geotech. Eng.*, pp. 1273–1276, 2001.
- [37] J. A. W. Hockx, “Methods to Reduce Oblique Bending in a Steel Sheet Pile Wall,” 1998.
- [38] D. A. Kort, “Interlock friction in steel sheet piling,” *Int. Soc. soil Mech. Geotech. Eng.*, pp. 845–851, 2006, doi: 10.1007/978-3-319-73568-9_174.
- [39] E. J. Aukema and A. G. Joling, “A 3D Numerical Simulation of Oblique Bending in a Steel Sheet Pile Wall,” Delft University of Technology, 1997.
- [40] ArcelorMittal, “U-type sections.” <https://sheetpiling.arcelormittal.com/products/pu-22-3/> (accessed Jun. 06, 2022).
- [41] DIANA FEA, *User’s Manual - Release 10.5*, 1st ed. Delft: DIANA FEA bv, 2021. [Online]. Available: <https://dianafea.com/manuals/d105/Diana.html>
- [42] K. J. Bathe, *Finite Element Procedures*, 2nd ed. Watertown: Prentice hall, pearson education, inc., 2016. [Online]. Available: <http://www.amazon.com/Finite-Element-Procedures-Part-1-2/dp/0133014584>
- [43] Bentley Systems, “Plaxis 3D.” 2022.
- [44] ArcelorMittal, “AZ sections.” <https://sheetpiling.arcelormittal.com/products/az-23-800-2/> (accessed Jun. 06, 2022).

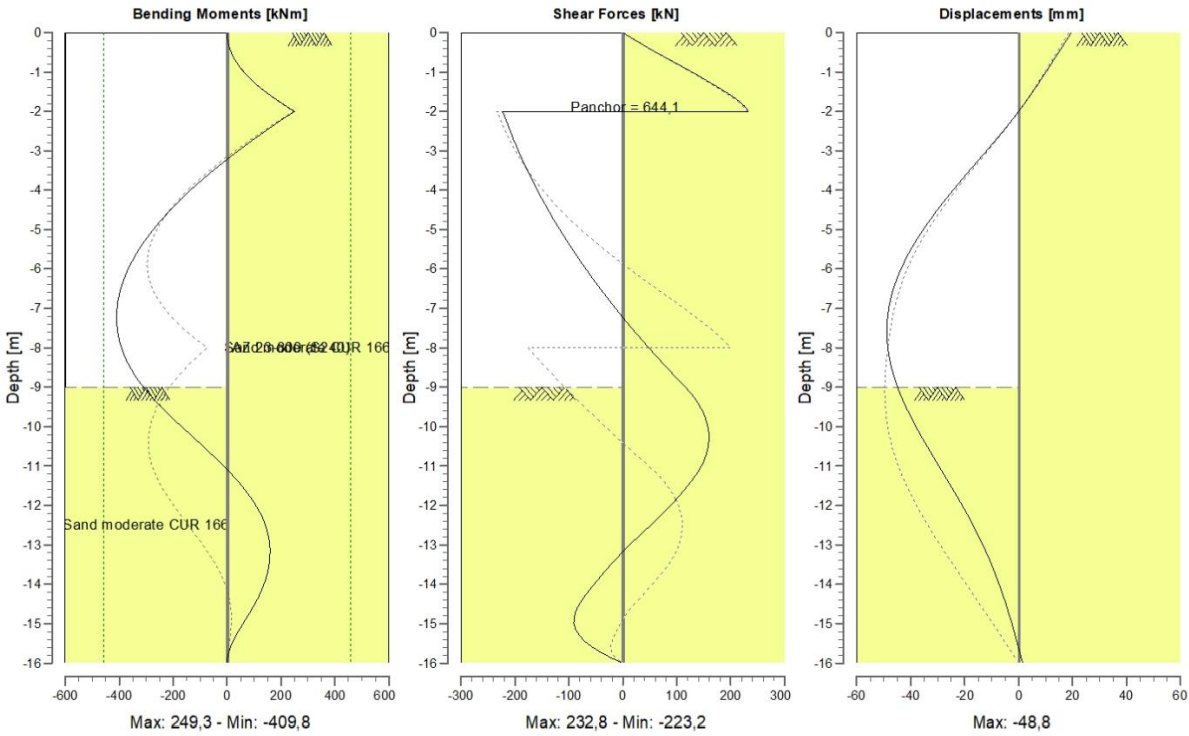
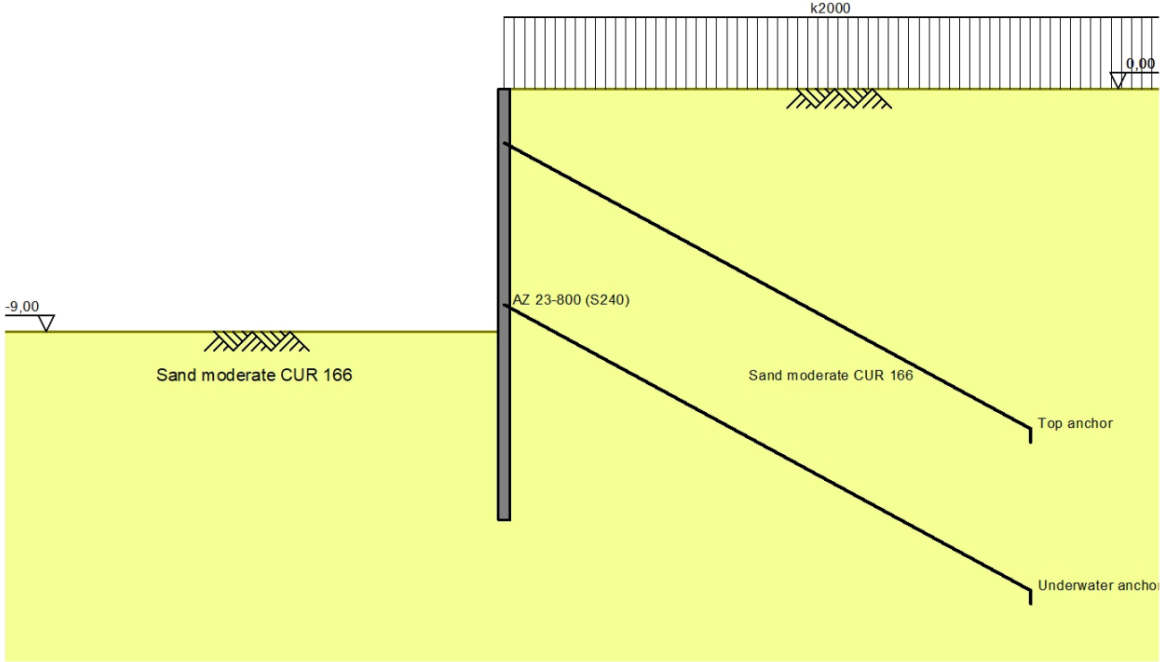
Appendix A: D-sheet piling underwater anchor procedure

The bending moment, shear force and deformation line of a single anchored sheet pile and the process of adding an underwater anchor and excavating the harbour.

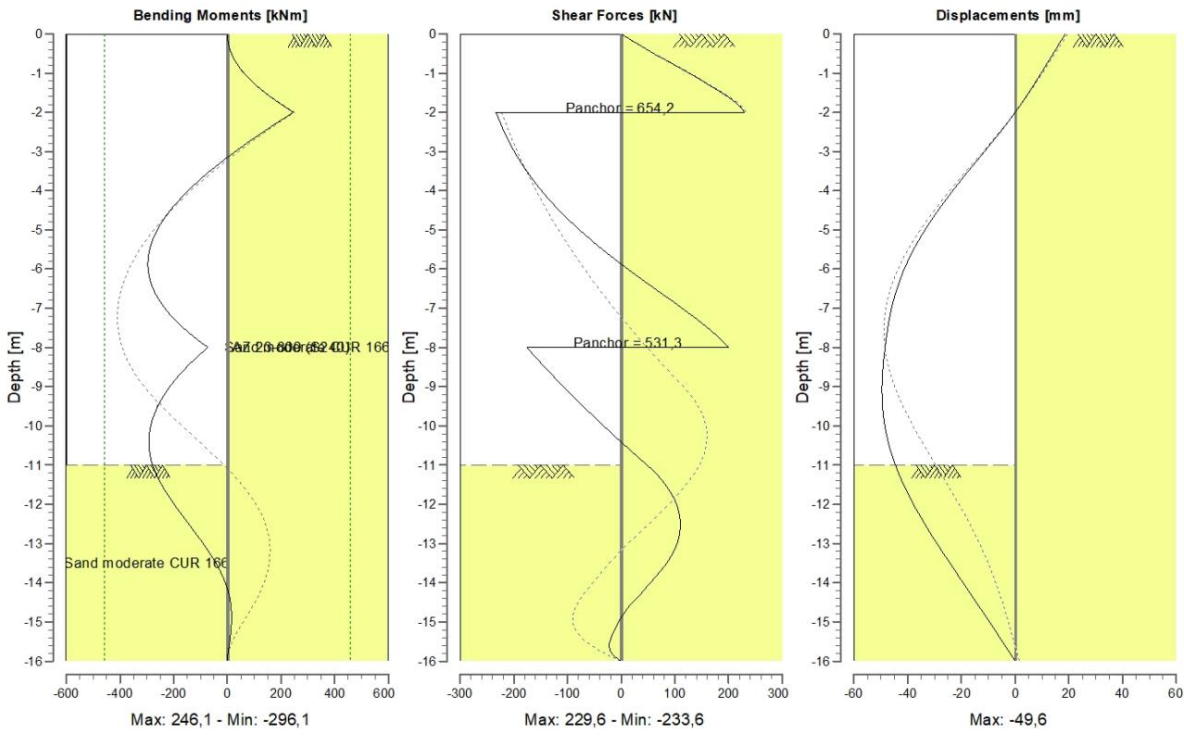
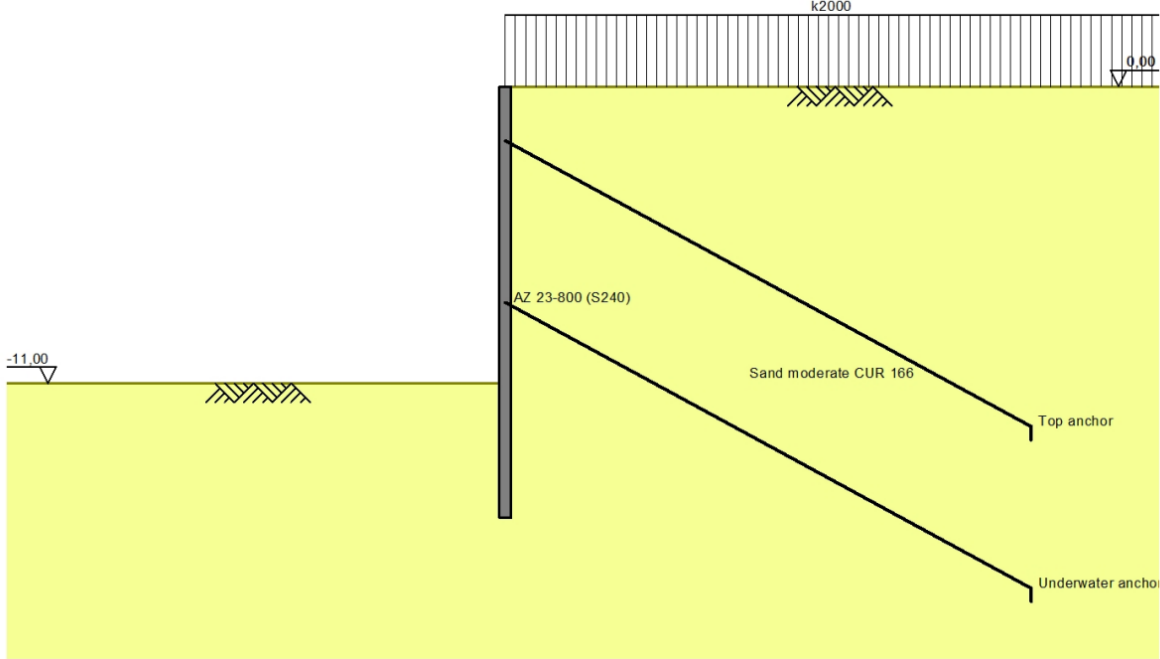
Initial stage example: single-anchored sheet pile



Initial stage with underwater anchor:

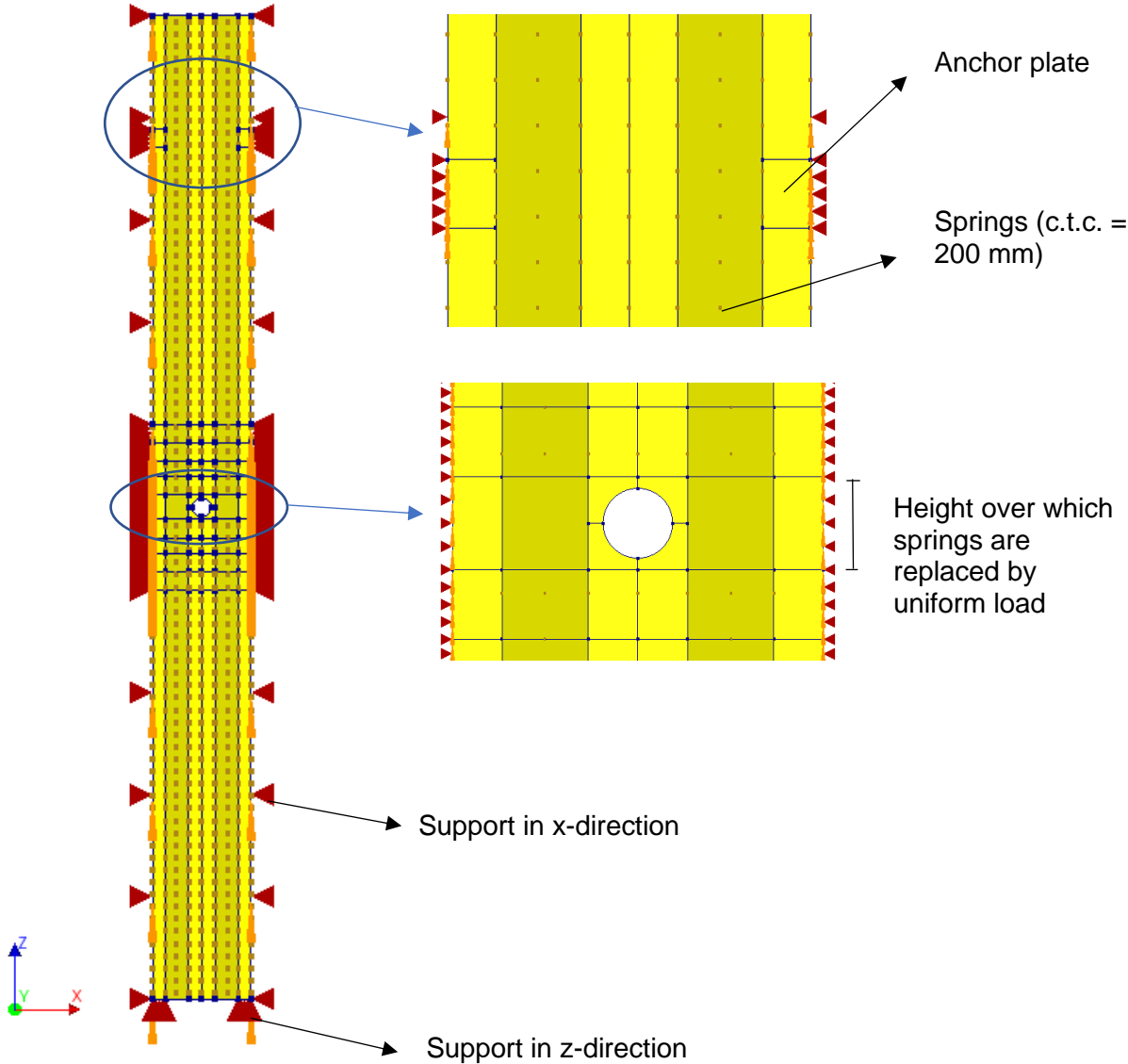


Excavation after placing underwater anchor:

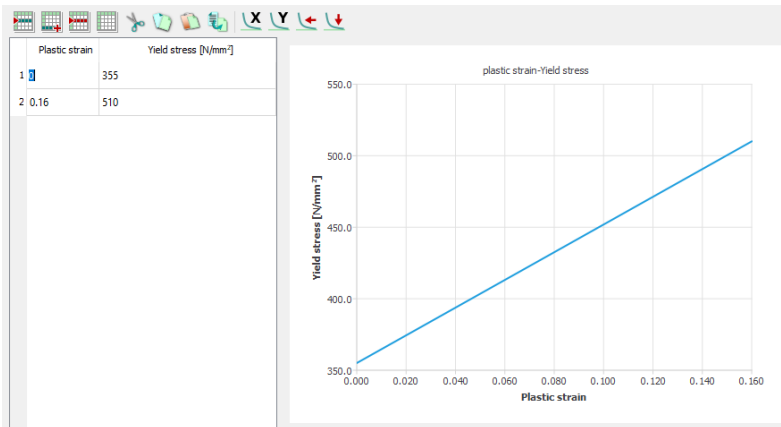


Appendix B: Numerical model in DIANA FEA

3DSSI model: Detailed DIANA figures.



Non-linear steel input: (plastic strain-yield stress diagram)



Name: steel

Aspects to include

- Thermal effects
- Damping
- Additional dynamic surface mass
- Additional dynamic 3D line mass

Linear material properties

Von Mises and Tresca plasticity

Plasticity model: Von Mises plasticity

Hardening function: Plastic strain-yield stress

Hardening hypothesis: Strain hardening

plastic strain-yield stress*: 0.00000 355.000 0.160000 510.000

Hardening type: Isotropic hardening

Linear steel input: (for anchor plate)

Name: Steel linear

Aspects to include

- Thermal effects
- Damping
- Woehler diagram
- Design check parameters
- Additional dynamic surface mass
- Additional dynamic 3D line mass

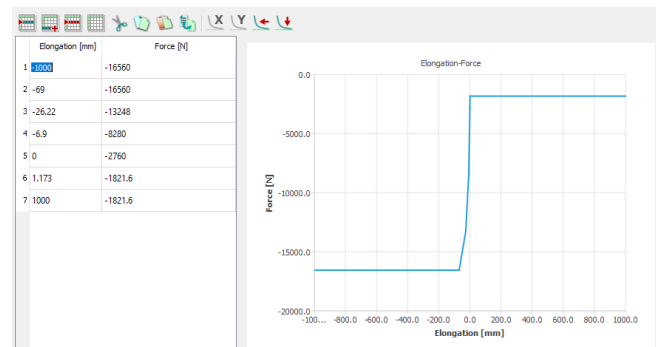
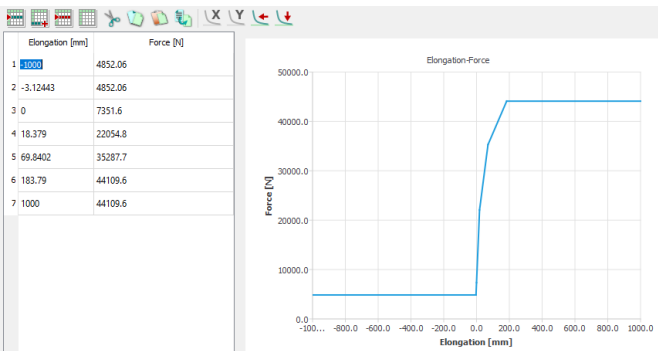
Linear material properties

Young's modulus*: 210000 N/mm²

Poisson's ratio*: 0.3

Mass density: T/mm³

Active spring characteristics level -15.9m: Passive spring characteristics on level -15.9m



Edit geometry

Name: spring active

Working direction*: 0 -1.0

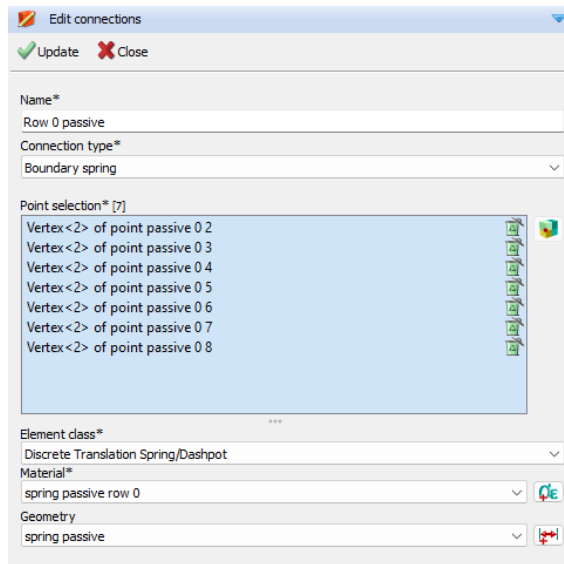
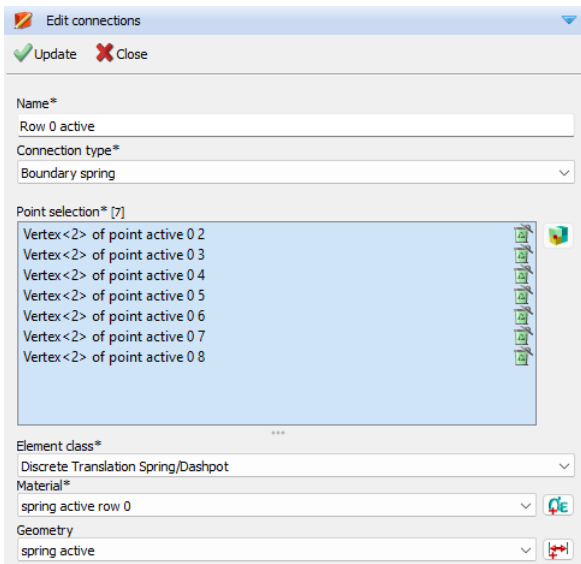
Close Help

Edit geometry

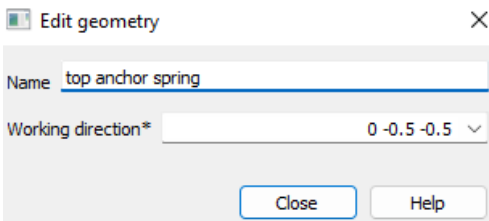
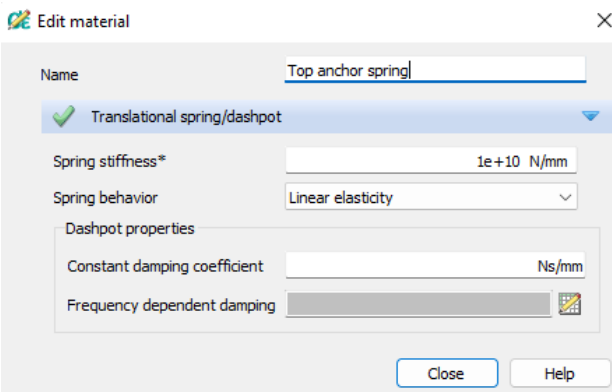
Name: spring passive

Working direction*: 0 -1.0

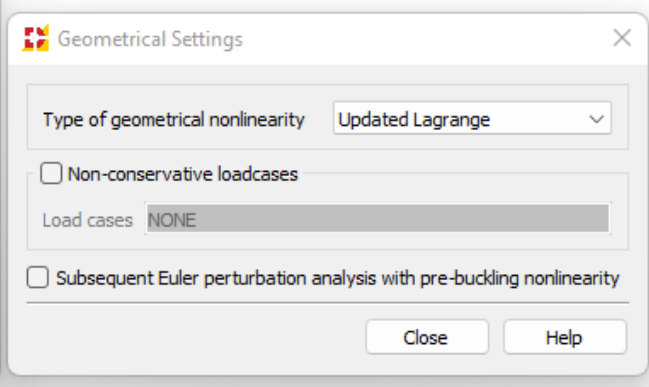
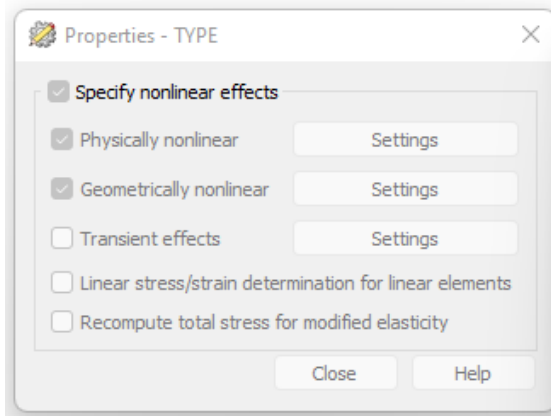
Close Help

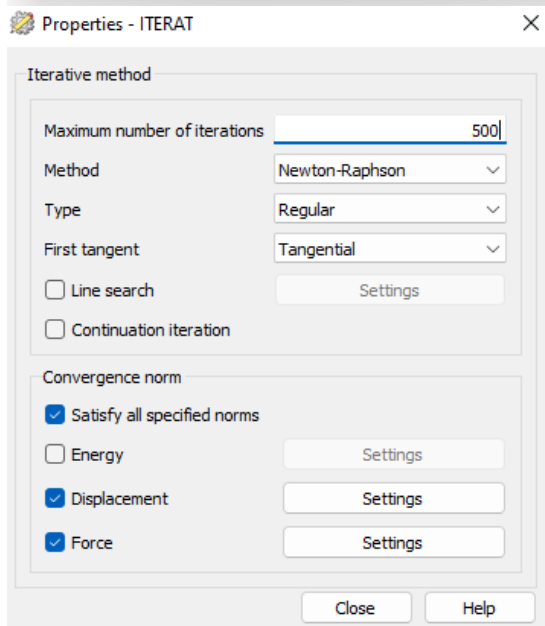
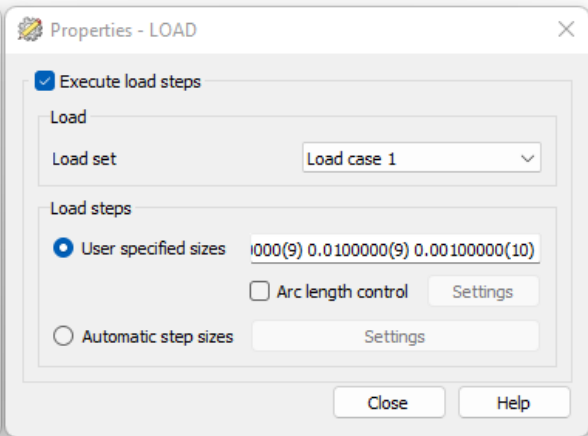
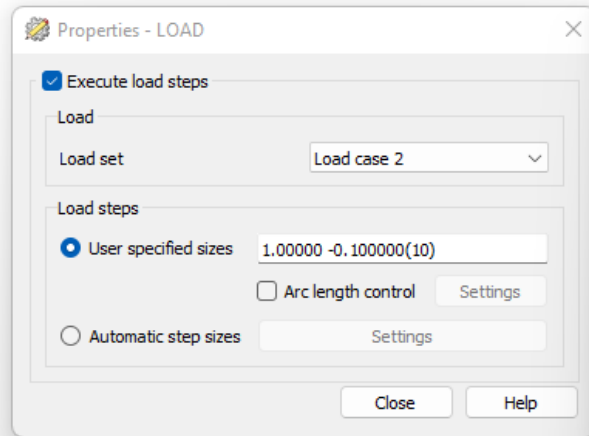


Top anchor spring:

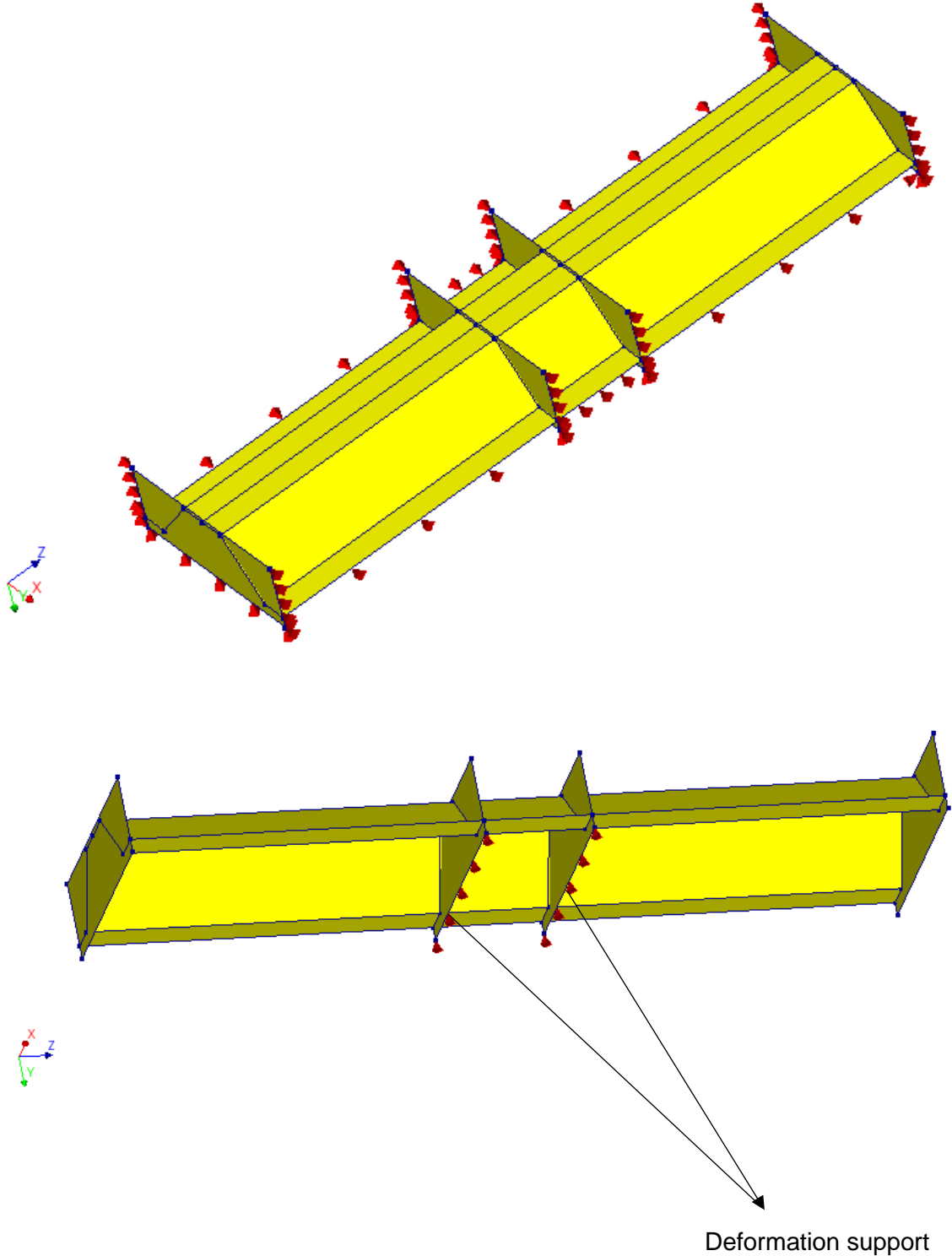


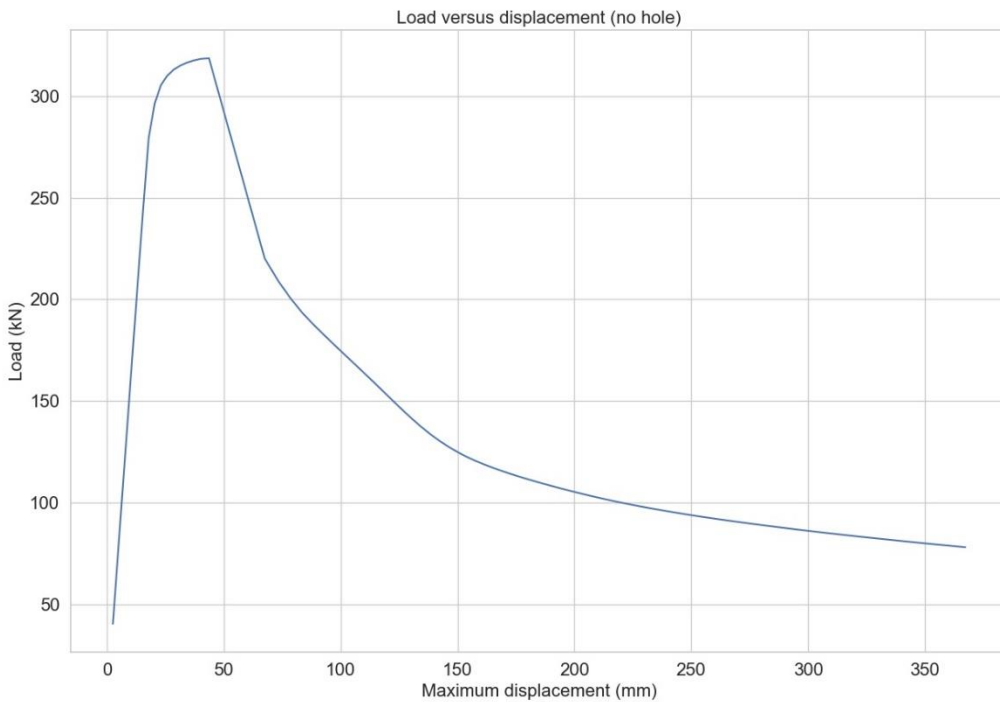
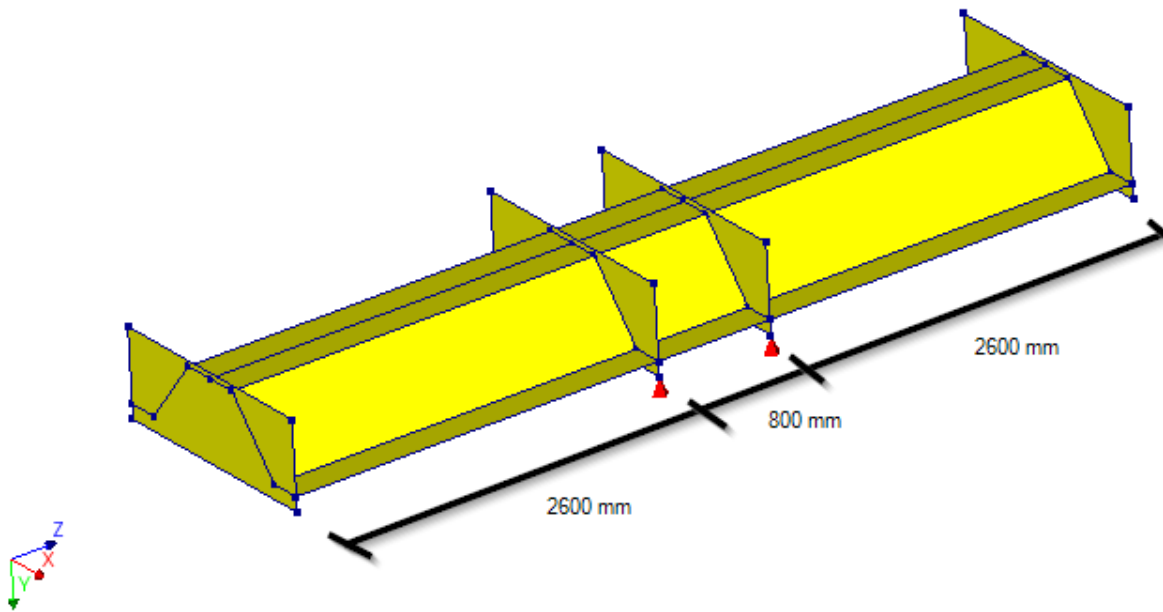
Analysis details:



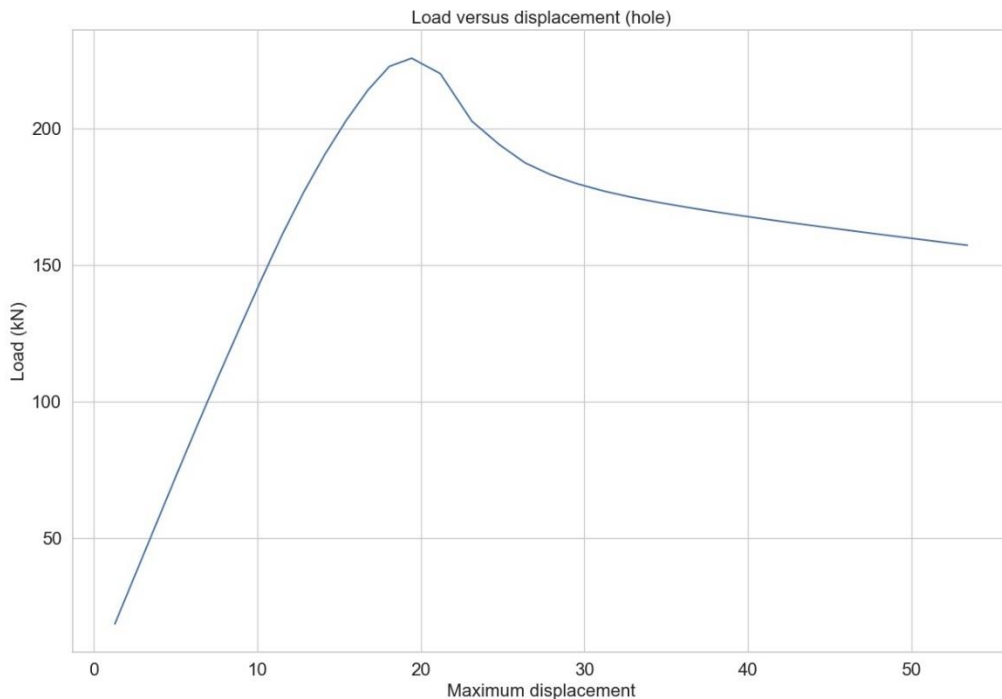
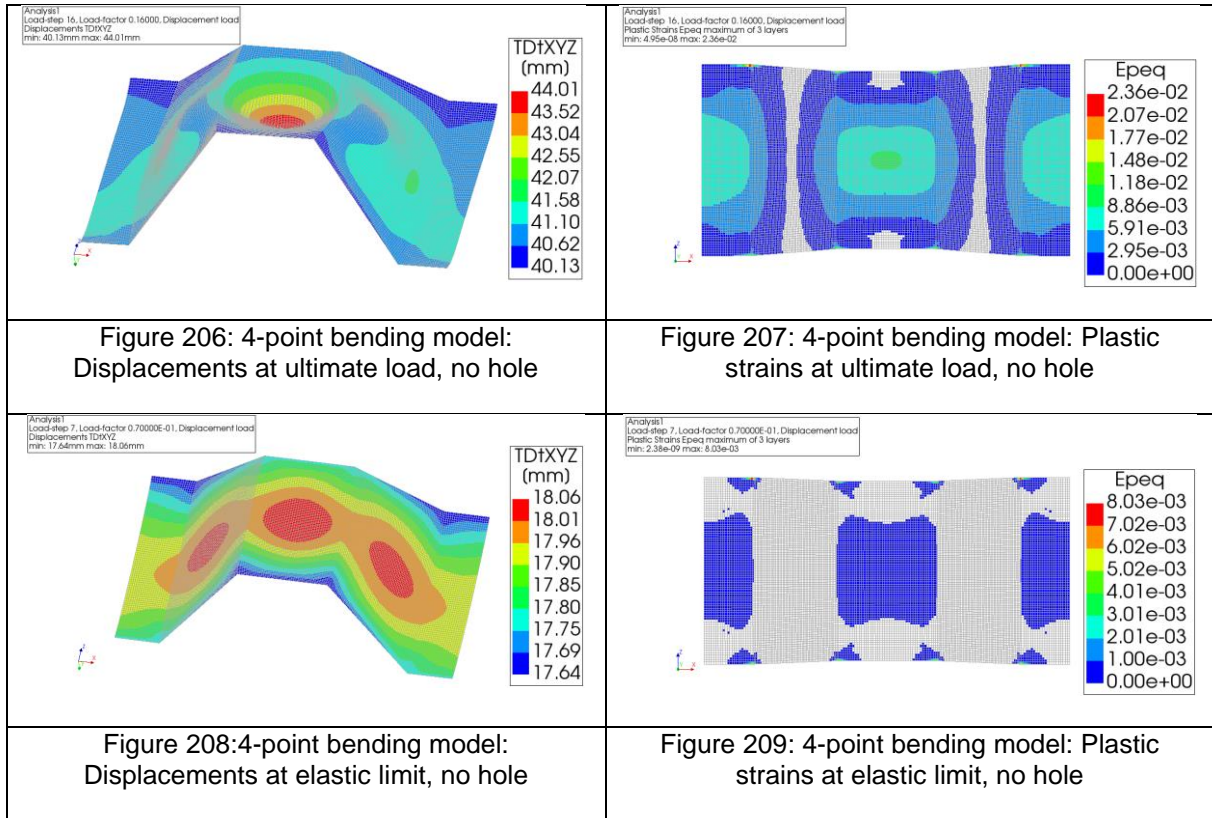


Appendix C: Verification model (4-point bending model)





The maximum load is found at a prescribed displacement in the 4-point bending test of 40 mm on the load plates. The deformation pictures similar as for the 3DSSI model are given below. The linear part of the 4-point bending test is up to a prescribed displacement of 17.5 mm. The deformation pictures of the end of the linear part are also given. Since the soil-behaviour is not included, linear behaviour and the elastic limit can be easily distinguished.



Similar as for the 3DSSI model, a lower resistance and a lower stiffness is observed. The failure load is found at a maximum displacement of 19.4 mm. The failure modes are shown.

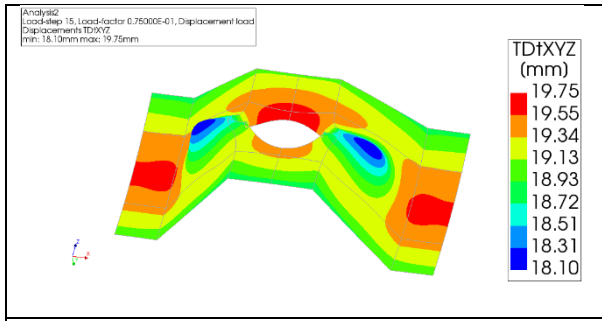


Figure 210: 4-point bending model: Displacements at ultimate limit, hole basic case

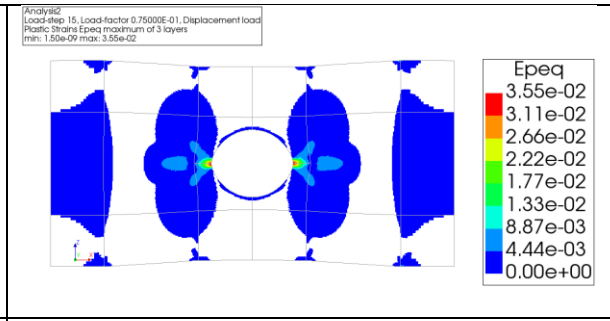


Figure 211: 4-point bending model: Plastic strains at ultimate load, hole basic case

Appendix D: Oblique bending verification

The theory of oblique bending is discussed in chapter 3.3. Before studying oblique bending with soil models, 4-point bending tests have been performed and modelled to study the behaviour of double U-sheet piles. These tests are performed by Sedlacek et al [30] and modelled with FEM by Aukema and Joling [39]. Kort (2002) [23] has modelled the oblique bending with the subgrade reaction model.

In this thesis, the oblique bending is also considered with respect to the design of a sheet pile and the influence of hole weakening on the resistance of the sheet pile. To verify the finite element approach used in this thesis to model the oblique bending, the 4-point bending test is reproduced and the results of the tests and models from the paper are compared to the results of the model in DIANA FEA.

The test consists of the set-up shown in Figure 212, also shown in chapter 3.3. For the purpose of this thesis, two double U-sheet piles are modelled. This gives more insight into the behaviour including the free interfaces in DIANA FEA. Therefore, two load introduction stiffeners are modelled which are disconnected with the tool 'DISCONNECT' in DIANA FEA. This prevents the stiffening plates to strengthen the sheet pile via the stiffening plates. In practice, the load stiffeners are also not connected to each other (Figure 213).

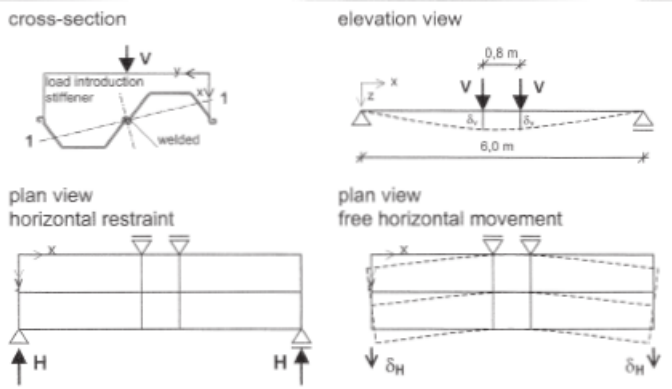


Figure 212: 4-point bending test to study oblique bending [30]

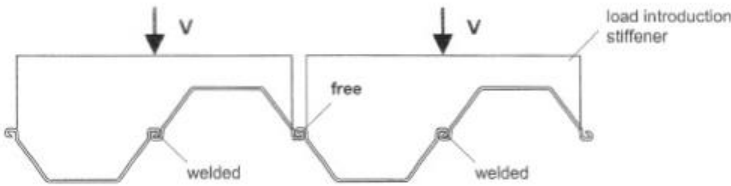


Figure 213: Load introduction on two double U-sheet piles [30]

The 4-point bending test is thus reproduced in DIANA FEA. The free interlocks are modelled with interface elements. The interface elements are prescribed a zero shear force stiffness in axial direction. This means that in axial direction, no shear forces are transferred and the sheet pile can move freely with respect to each other in that direction. In lateral and transverse direction the sheet piles are still connected. The stiffening plates are modelled and disconnected, to make sure that these do not disable the oblique bending.

The deflections found by DIANA are close to the deflections found by the tests, which were for restrained and unrestrained bending respectively 39 and 73 mm.

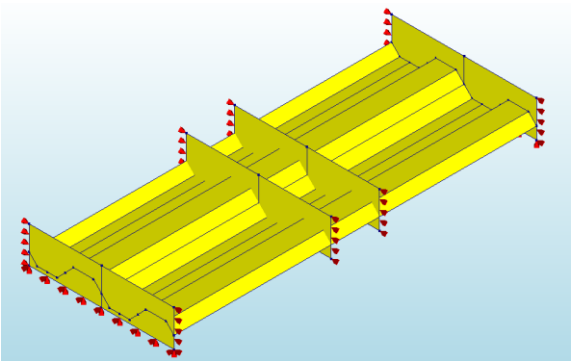


Figure 215: 4-point bending model; restrained oblique bending(DIANA)

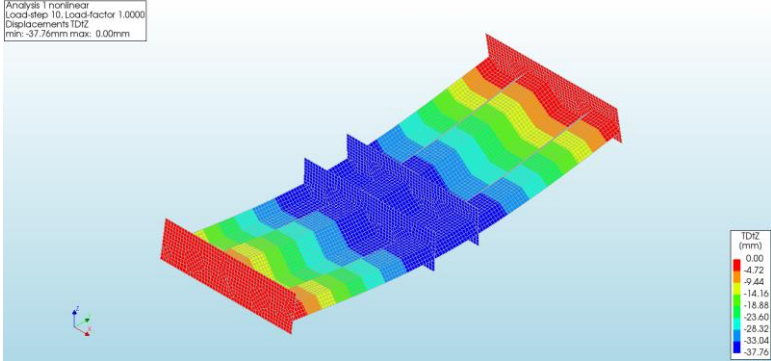


Figure 214: deflection for restrained oblique bending (mm)
Max. displacement = 37.76 mm

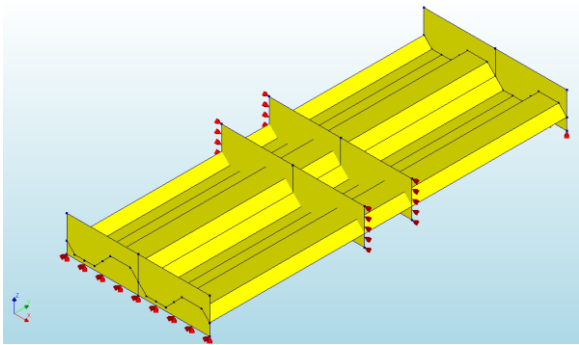


Figure 217: 4-point bending model; unrestrained oblique bending (DIANA)

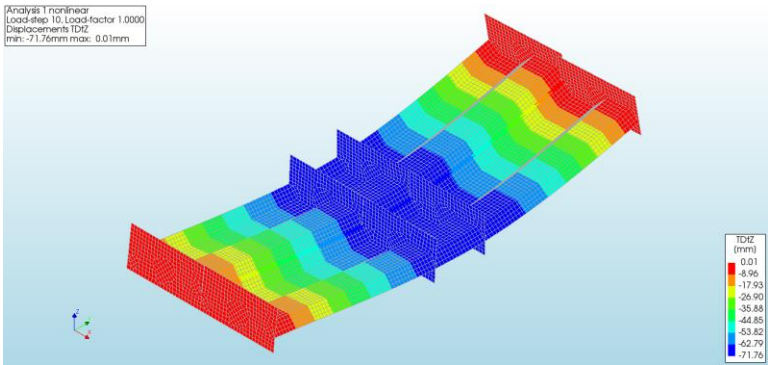


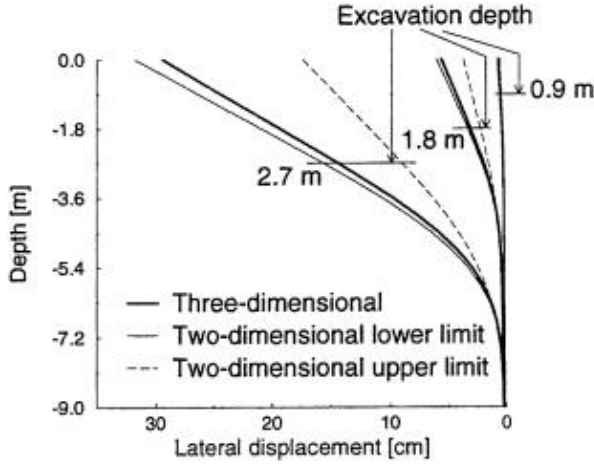
Figure 216: deflection for unrestrained oblique bending (mm)
Max. displacement = 71.76 mm

From the 4-point bending test it can be obtained that the interface elements used in DIANA FEA are consistent with the free translational degree in the interlocks in axial direction and give the expected result. This interface element is applied in the 3DSSI model which is designed in this thesis, using the soil spring model to model the soil and shell elements for the steel sheet pile. This model is thus extended for oblique bending with an interface element in the free interlocks with a zero shear stiffness in z-direction.

The oblique bending model is also verified with the model used by Aukema and Joling [39] who studies modelling oblique bending with a 3D finite element model. A cantilever sheet pile wall is studied and Aukema and Joling also compare 3D and 2D analysis (Figure 218). The PU8 profile is loaded with sand with an effective unit weight of 10 kN/m³. The upper limit describes a sheet pile wall in which oblique bending is completely prohibited. The lower limit describes the deformation of the sheet pile wall, including oblique bending. In general, due to the factors influencing and restraining oblique bending as described in chapter 3.3, the actual deformation will be in between the upper and lower limit.

The oblique bending model for an excavation of 2.7 meters is reproduced in DIANA FEA. With this DIANA FEA model the subgrade reaction model and gives similar results as the study performed by Aukema and Joling (Figure 219). Also, the inclination of the neutral axis found in the DIANA FEA model is plotted and consistent with the theory of the inclination of the neutral axis for a double U-sheet pile. This inclined neutral axis is found by filtering the coordinates for which the stress SZZ is near zero (between +10 N/mm² and -10 N/mm²).

Between these coordinates a line is interpolated which illustrates then the neutral axis (Figure 220).



(a)

Figure 218: Lower and Upper limit of oblique bending [39]

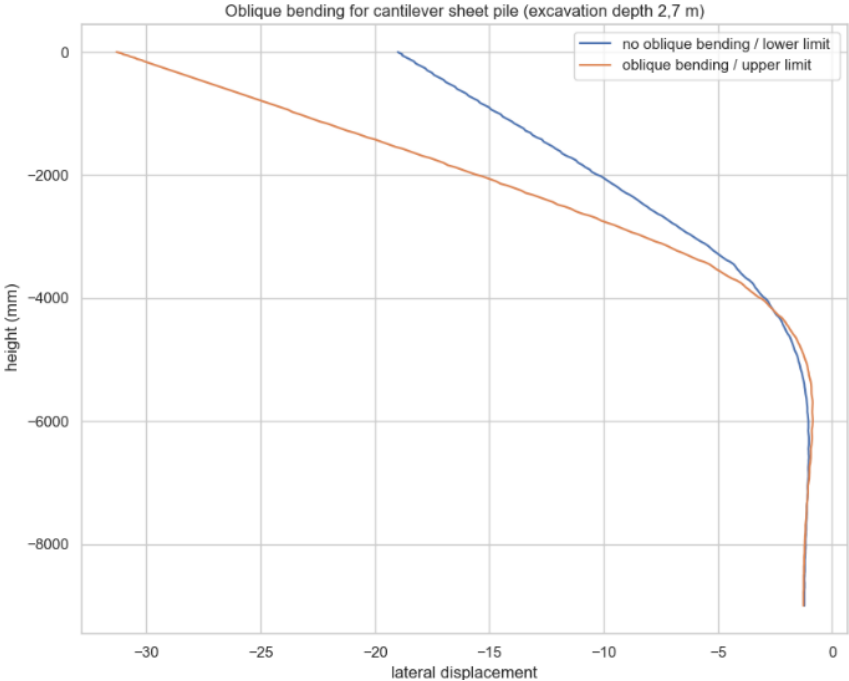


Figure 219: Reproduced oblique bending model in DIANA

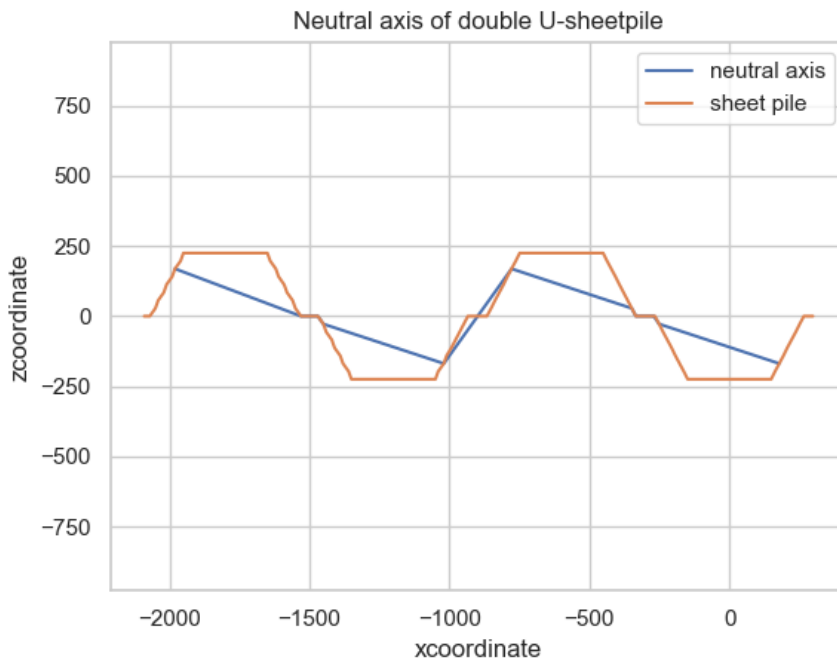


Figure 220: Neutral axis of sheet pile PU8 with oblique bending

Finally, the oblique bending for a single-anchored sheet pile is compared to the reduction factors prescribed in CUR 166 and the reference document of the CUR regarding oblique bending: Steel sheet piles in soft soil (Kort, 2002) [23].

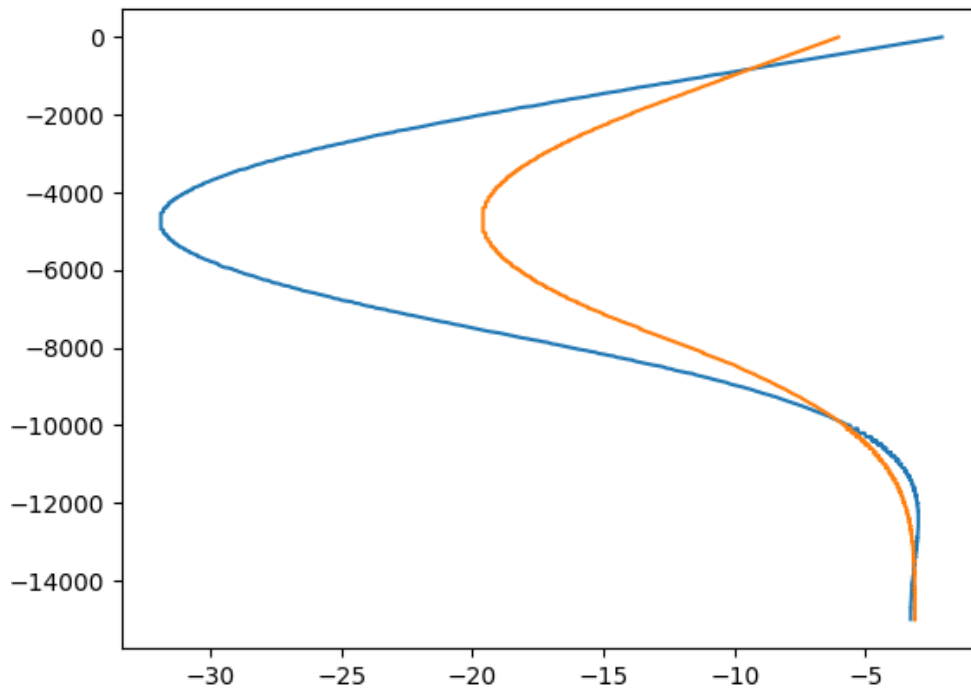


Figure 221: Comparison oblique bending and restrained oblique bending for a single anchored sheet pile

The reduction factor for oblique bending is defined for the deformation (stiffness of the sheet pile) with the following formula:

$$\beta_I = \frac{w_{y,max;normal}}{w_{y,max;oblique}}$$

For the lower limit, disregarding all factors possible which could restrain oblique bending, the reduction factor β_I is defined as:

- CUR 166: single anchored sheet piles: $\beta_I = 0.55$
- Steel sheet piles in soft soil: $\beta_I = 0.60$

The reduction factor found with the 3DSSI model is :

$$\beta_I = \frac{19.3 \text{ mm}}{31.8 \text{ mm}} = 0.61$$

The results are therefore found to be consistent with the results found by Kort 2002 and the calculation rules described in CUR 166 for oblique bending.

Appendix E: Convergence studies

To verify the numerical model, several convergence studies are performed: the convergence study for the c.t.c. distance of the springs, the mesh convergence study and the study of the convergence of integration layers of the shell elements.

- Studie convergence springspacing

Different centre to centre distances between the springs are studied to find the optimal spring spacing for which the results are accurate but not an infinite amount of springs are needed. The springspacing is defined as the centre to centre distance between the springs in vertical and horizontal direction. Each spring thus represents a squared area of soil. The springspacings studied are 600mm, 400mm, 200 mm and 100mm. Figure 222 shows the displacement curve of the complete sheet pile. Especially at the location of maximum bending and at the top and toe of the sheet pile the differences between the studied springspacing is visible . From a springspacing of 200 mm and smaller the results are similar and therefore a springspacing of 200 mm is used. A smaller springspacing could ofcourse also be used, however this takes more calculation time and therefore the optimization of a springspacing of 200 mm is used.

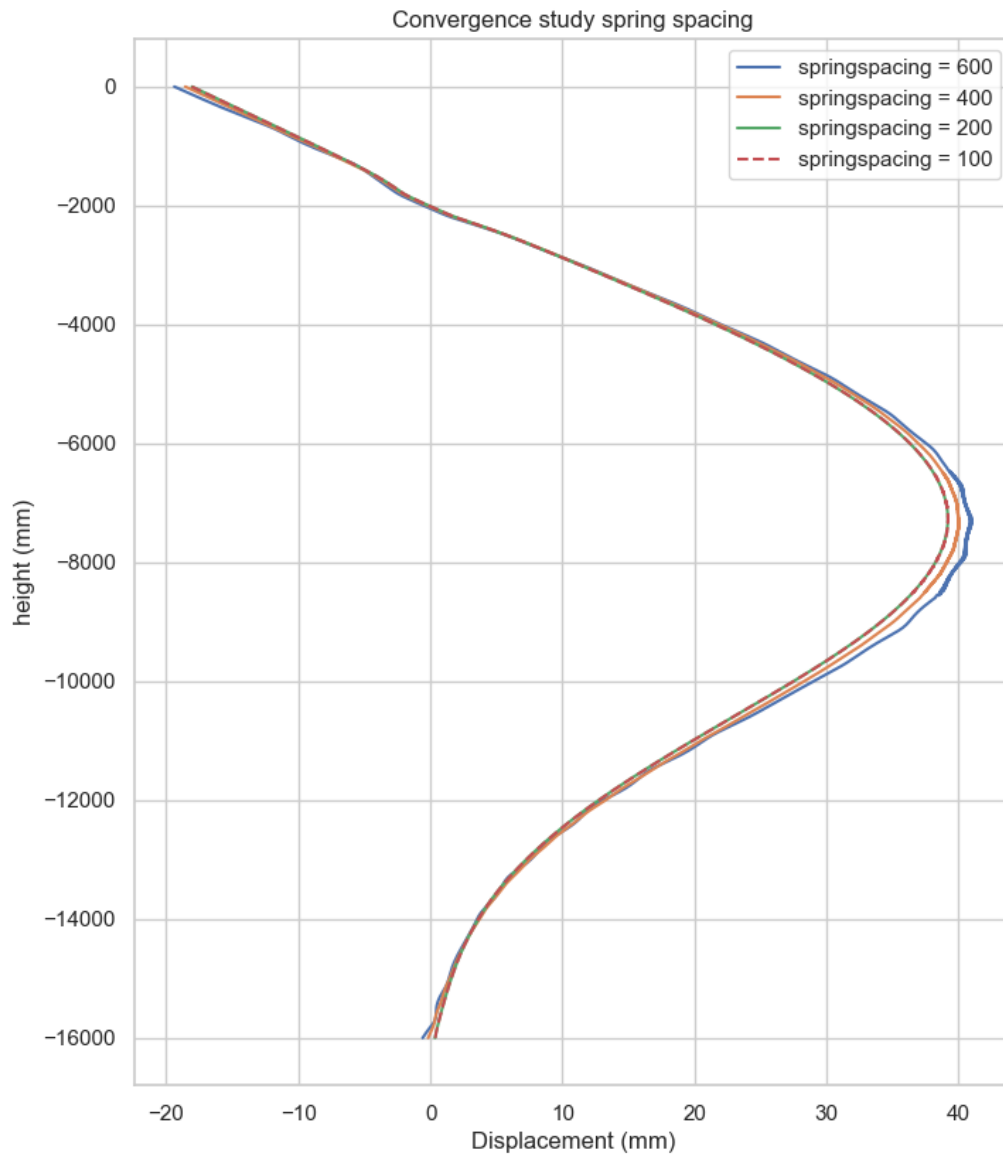


Figure 222: Displacement over height curves for springspacing of 600mm, 400mm, 200mm and 100 mm

- Study mesh convergence

The mesh convergence study is discussed in chapter 4.3.6. The displacement over height graph is given in Figure 223 and Figure 224.

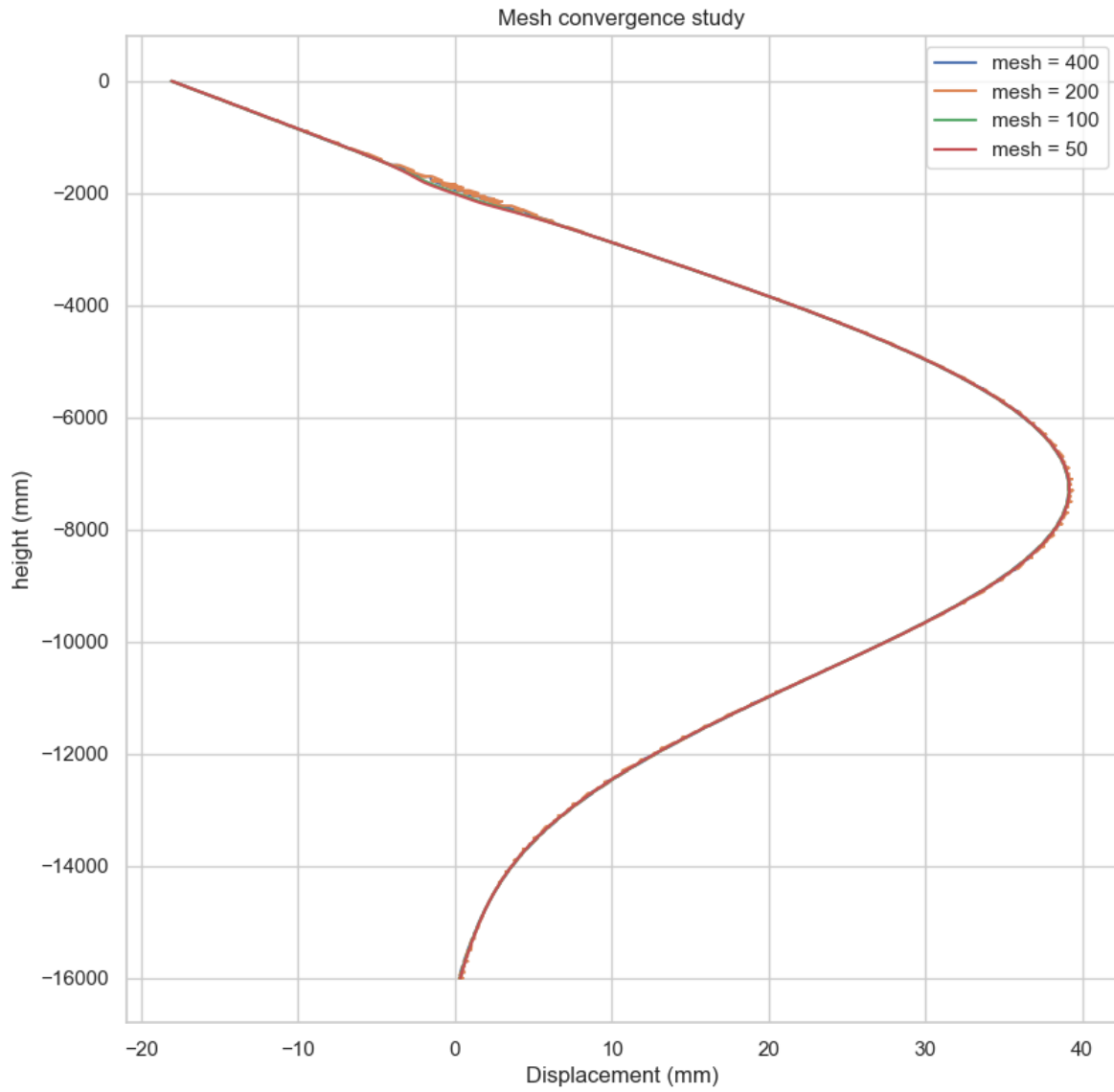


Figure 223: Mesh convergence study

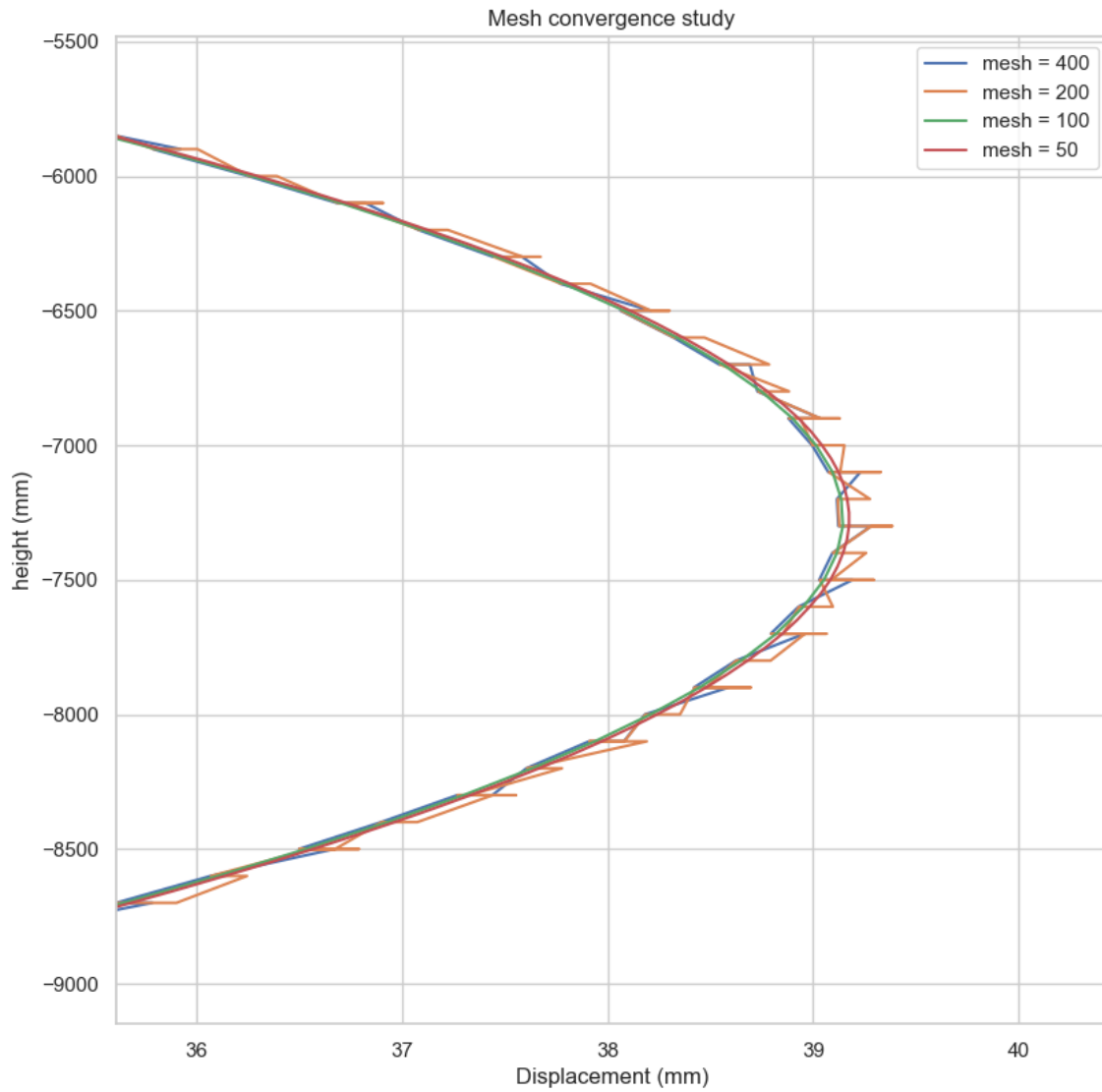


Figure 224: Mesh convergence study detailed at location of maximum displacement

- Study integration layer convergence

The influence of the number of integration layers is studied to determine the optimal number of integration layers. The more integration layers are used, the more accurate the results are expected to be.

The shell elements are divided by default in 3 layers in thickness. For the elastic zone, there is no difference found in displacement and stresses using 3, 5 or 7 layers. The comparison for 3 and 7 layers is shown in Figure 225 and Figure 226. Also for the stress plots over the height, there is no difference between 3,5 or 7 layers. This is studied for a sheet pile in elastic state and in plastic state (Figure 225 and Figure 226).

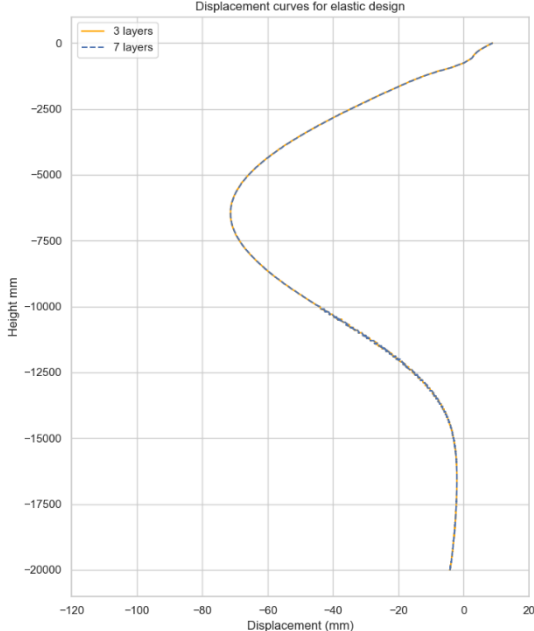


Figure 225: Displacement curve for 3 and 7 integration layers for sheet pile in elastic state

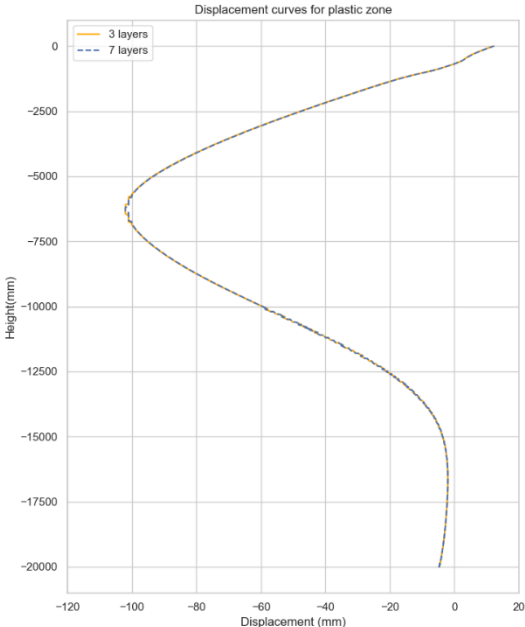


Figure 226: Displacement curve for 3 and 7 integration layers for sheet pile in plastic state

For the stress curves, there is also no difference found between 3 layers or more layers in thickness (Figure 227). The irregularities at location -750 mm are due to the anchor at the anchor plate.

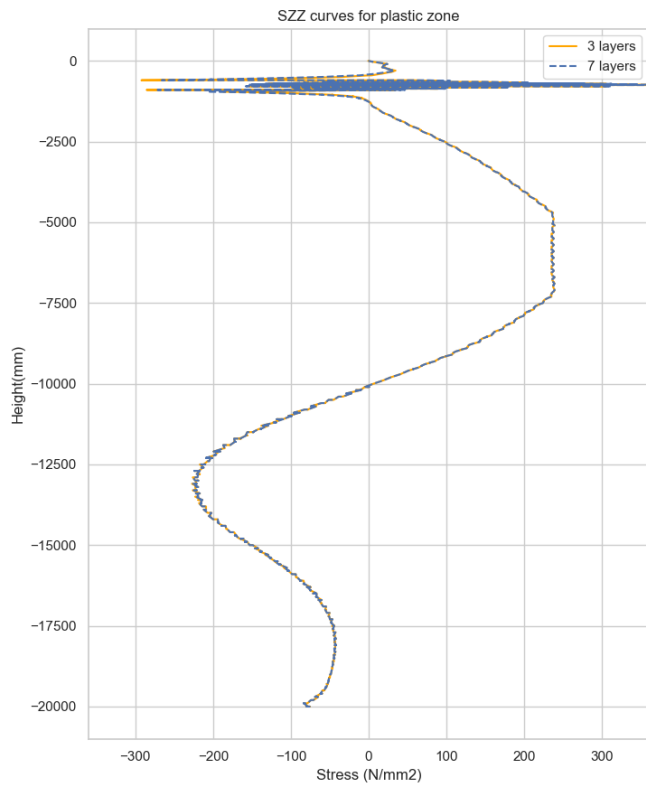


Figure 227: Stress curve for 3 and 7 integration layers for sheet pile in plastic state

Appendix F: Parameter study

A complete overview of the parameter study is given. The approach is summarized in the flow chart.

